Thesis Outline

Elucidating the mechanism by which nerve endings can achieve quantal release of neurotransmitters into the synaptic cleft is of fundamental importance. Release occurs via Ca^{2+}-regulated exocytosis which involves a highly complex series of steps. It is dependent on the membrane excitability of the nerve endings controlled by voltage-sensitive cation channels, and can also be modulated by way of pre-synaptic receptors. Naturally-occurring neurotoxins from diverse sources such as snakes and micro-organisms have been found to facilitate or inhibit transmitter release and, in doing so, helped the identification of pre-synaptic proteins responsible for neuro-exocytosis and its regulation. Both over- and under-active transmitter release cause significant clinical symptoms and, therefore, compounds that restore normal function would be of great value as therapeutics for such conditions (Dolly, 2005). The work described in this thesis relates to the regulation of exocytosis; both overactive (Section A) and underactive (Section B).

Botulinum neurotoxins (BoNTs) produced by *Clostridium botulinum*, are very specific blockers of acetylcholine release from peripheral nerve endings. This action has been exploited to explore the process of regulated exosytosis including the vital part played by the target of these toxins, SNARE proteins, leading to their use as theraputic agents for disorders due to over-active skeletal muscle. BoNT complex (serotype A) is used for treating dystonias and spasticity and has also been proved useful for smooth muscle disorders (Dolly, 2005). Interestingly, it has been observed that the toxin alleviates pain associated with various conditions with or without accompanying excess muscle contractions (Aoki, 2001). These anti-nociceptive effects have been demonstrated in a number of applications including the treatment of tension-associated headaches, and chronic pain, active areas of research (Aoki, 2001). As early indications suggest that the toxin is effective in the treatment of refractory joint pain associated with chronic arthritis (Mahowald et al., 2006), Section A of this thesis explores its possible mechanism of action in this application.

In contrast to the blocking activity of BoNTs, dendrotoxins isolated from the venoms of the green and black mamba snakes, facilitate acetylcholine (Ach) release at the neuromuscular junction due to a potent and selective inhibition of some members of the Kv1 family of voltage-activated K^+ channels. Blockade of their outward hyper-polarising current increases transmitter efflux leading to repetitive firing and even some epileptic-like activity. Through selective inhibition of channel subtypes, their specific roles in neurons can be better understood (Dolly, 2005). Dysfunction of Kv1 channel subtypes underlie several human diseases including Episodic Ataxia I and some types of epilepsies (Lehmann-Horn and Jurkat-Rott, 1999; Manganas et al., 2001; Zuberi et al., 1999) and their blockade in experimental models of multiple sclerosis has been shown to improve inefficient nerve impulse conduction (Smith et al., 2000). Specific blockers of K^+ channels could act as potential therapeutics for certain conditions, returning under-active neurotransmitter release back up to normal levels. Understanding the interactions of a range of Kv1 channel blockers with heteromultimeric Kv1 channels mimicking those found in mammalian brain is the focus of Section B of this thesis.

Section A

An exploration of the possible mechanism of action of BOTOX® in the treatment of chronic pain and inflammation resulting from arthritis

Chapter 1

1.1 Introduction

1.1.1 Pathogenesis of rheumatoid arthritis

Rheumatoid arthritis (RA) is the most common auto-immune disease (Nishimoto and Kishimoto, 2004), affecting 1% of the population (McInnes and Schett, 2007). Despite this, there is no evidence yet for a specific auto-antigen (Fox, 1997) and the etiopathogenesis (cause and development) of the disease remains far from clear (McInnes and Liew, 1998). Without doubt though, this is a chronic inflammatory condition (Beeton et al., 2003; Keeble and Brain, 2004; McInnes and Liew, 1998; McInnes and Schett, 2007) typically affecting distal synovial joints, characterised by "flare ups" and periods of remission (Keeble and Brain, 2004; McInnes and Schett, 2007), where dysregulation of the cellular immune system and cytokine network results in severe pain (Beeton et al., 2003; Keeble and Brain, 2004). This, coupled with associated extra-articular disease, significantly impacts morbidity and mortality (Beeton et al., 2003; McInnes and Schett, 2007). Synoviocytes (cells of the synovial membrane) proliferating uncontrollably attach to the surface of the joint causing infiltration of mononuclear cells (e.g. lymphocytes, dendritic cells, macrophages) which produce pro-inflammatory cytokines. These cytokines induce further synoviocyte propagation and activation resulting in the formation of invasive and destructive pannus. Eventually oedema forms in the joint, the pannus invades the joint and along with chondrocytes (cells of the cartilage), produce proteolytic enzymes causing destruction of adjacent cartilage and release of more pro-inflammatory cytokines (Kay and Calabrese, 2004). The function of osteoclasts (responsible for bone resorption) is also dysregulated, altering the balance of normal bone turnover and resulting in overall resorption (Kay and Calabrese, 2004; McInnes et al., 2003). These processes lead to the classical symptoms of RA: swollen, painful joints with loss of mobility leading ultimately to joint erosion and deformity. Hence, there is loss of movement and further pain as well as systemic effects [caused by release of cytokines from inflamed joints (McInnes and Schett, 2007)] such as inflammation of the lining of organs (Kay and Calabrese, 2004).

1.1.2 The role of inflammatory mediators

As a specific auto-antigen trigger or alternative cause of RA remain unknown, potential therapeutics have tended to focus on the increased levels of pro-inflammatory cytokines in affected joints, and the immune cells responsible for their production. Cytokines play a role in every stage of the pathogenesis of RA from contributing to auto-immunity, to maintaining chronic inflammation in joints, to the destruction of cartilage and bone (McInnes and Schett, 2007). However, as there are many cytokines over-expressed in affected joints including interleukin (IL)-1β, IL-6, IL-15 and tumour necrosis factor alpha (TNFα) (McInnes and Schett, 2007), elucidating which are the most important was imperative (Feldmann et al., 2005). TNFα is crucial in controlling inflammatory and immune reactions resulting from disease and IL-1β [the secreted form of IL-1 typically considered more important as it acts on neighbouring cells (Kay and Calabrese, 2004)] is implicated in conditions that result in chronic inflammation (Kaneyama et al., 2005). IL-1 and TNFα are involved in the communication between cells in affected joints and, importantly, each cytokine up-regulates production of the other (Kay and Calabrese, 2004). Examination of cytokine interactions in cultured synovial cells from rheumatoid joints found that blockade of TNFα reduced not only the synthesis of IL-1 but all pro-inflammatory cytokines found in diseased joints (Feldmann et al., 2005), thereby, revealing a central role for TNFα in the regulation of synovial inflammation (McInnes and Liew, 1998) and, therefore, the pathogenesis of RA (Grimsholm et al., 2005). The streptococcal cell wall arthritis model in IL-1 and TNFα-deficient mice has gone some way to distinguishing the roles of these 2 cytokines revealing TNFα to be important in the inflammatory process and implicating IL-1 in pathways that result in joint damage (Kay and Calabrese, 2004). IL-6 is another cytokine over-expressed in rheumatoid joints (McInnes and Schett, 2007) that has a pivotal role in the disease pathogenesis (Nishimoto and Kishimoto, 2004). It is produced by a variety of cell types and regulates immune plus inflammatory responses to infection or injury (Kaneyama et al., 2005; Nishimoto and Kishimoto, 2004). Despite the array of factors implicated in RA, the crucial functions of these 3 cytokines have not only been demonstrated *in vitro* but also *in vivo*. Various therapies attenuating the actions of these cytokines are in widespread clinical use; TNFα (Feldmann et al., 2005; McInnes and Schett, 2007), licensed for clinical use; IL-1 (Kay and

Calabrese, 2004; McInnes and Schett, 2007), and in late stage clinical trials; IL-6 (McInnes and Schett, 2007; Nishimoto and Kishimoto, 2004).

1.1.3 Immune cells and rheumatoid arthritis

Given the undeniable importance of cytokines in RA, the cells that produce them as a means of communication (Kay and Calabrese, 2004) are also under scrutiny. The role of T-cells was once thought to be central to disease pathogenesis given not only their presence in large numbers in diseased joints (Fox, 1997; McInnes and Schett, 2007), but the fact that specific subsets accumulate (Fox, 1997). A possible genetic involvement in RA involving specific class II MHC (major histocompatibility complex) alleles implies that CD4 T-cells responding to specific antigens are necessary for development of the disease. Onset of arthritic symptoms in animal models has also been shown to depend on T-cells (Fox, 1997; McInnes and Schett, 2007). However, disappointing results with therapeutics aimed at decreasing T-cell numbers have called into question their central role (Beeton et al., 2003; McInnes and Schett, 2007). Additionally, neutrophils are implicated in inflammatory and immune events; in RA, once activated (Kontny et al., 2002), they infiltrate affected joints accounting for 90% of the cells found in the synovial fluid (SF) (Beeton et al., 2003; Kay and Calabrese, 2004). They are concentrated at sites of erosion (Beeton et al., 2003) and destroy connective tissue via release of proteolytic enzymes and oxygen free radicals (Kontny et al., 2002). When neutrophils are activated they release hypochlorous acid (which contributes to the destruction of bacteria). Taurine is a dominant free amino acid in the cytoplasm of neutrophils and is a scavenger for hypochlorous acid. The two compounds react together to form taurine chloramine, which has potent anti-inflammatory activity. In neutrophils from patients with RA the formation of taurine chloramine is impaired (Kontny et al., 2002). Furthermore, the normally short life-span of these cells is extended from hours to days once they enter the site of inflammation (Beeton et al., 2003; Kay and Calabrese, 2004). This is coupled with the release of inflammatory mediators including IL-1β, TNFα and IL-6 (Beeton et al., 2003; Kasama et al., 2000; Kontny et al., 2002; McInnes and Schett, 2007). Despite this, studies on possible RA therapies that would target these cells are lacking (Beeton et al., 2003). B-cells produce auto-antibodies and immunoglobulins that can form complexes which trigger not only local inflammation, but

also release of IL-1 and TNFα by macrophages (see below) (Kay and Calabrese, 2004; McInnes and Schett, 2007). They are a further source of the pro-inflammatory cytokines key in the arthritic diseased state: Il-1β, TNFα and IL-6. Hence, the use of B-cell depleting therapies have produced some significant and sometimes long-term positive results (McInnes and Schett, 2007). Arguably the primary source of inflammatory mediators in affected joints [including among many others Il-1β, TNFα and IL-6 (McInnes and Schett, 2007)] is macrophages (Kay and Calabrese, 2004). These are found in close proximity to T-cells and may act as antigen presenting cells and, in doing so, continue the immune response (Kay and Calabrese, 2004). While other cell types are involved in cartilage and bone erosion, they are less important in the production of the inflammatory factors described here.

1.1.4 The neural influence

While the immune system undoubtedly has a huge role to play in the development and continuation of RA, there is evidence for involvement of the nervous system. Inflammation of symmetrical joints suggests a neural influence and neurogenic inflammation, which is involved in the onset and progression of joint disease, has been shown by several groups to be involved in RA (Keeble and Brain, 2004). Stimulation of sensory nerves and a subsequent release of neuropeptides, mediates this type of inflammation which is characterised by oedema formation, increased blood flow, extravasation and inflammatory cell recruitment (Grimsholm et al., 2005; Keeble and Brain, 2004). It was, therefore, important to identify the neuropeptide(s) responsible. Substance P (SP) is the best characterised and evidence for its role in RA is plentiful. Following release from sensory neurons, and subsequent binding to the neurokinin 1 (NK_1) receptor, SP exerts its pro-inflammatory effects; increased microvascular permeability leading to inflammatory swelling as well as inflammatory cell accumulation resulting in vasodilation (Keeble and Brain, 2004). Levels of SP are increased in SF from RA affected joints, where it is responsible for increased synoviocyte proliferation, enhanced release of pro-inflammatory mediators and destructive enzymes including collagenase, presumably due to the presence of NK_1 receptors on rheumatoid synoviocytes (Grimsholm et al., 2005). Not only are SP-positive nerve fibres found in rheumatoid synovium and SP-sensitive cells occur on blood

vessels in the joint (contributing to vasodilation and inflammatory cell accumulation), but SP-containing neurons in the bone marrow communicate with the synovium (Keeble and Brain, 2004). As well as a pro-inflammatory role, SP is also involved in central pain pathways as a chief mediator in "wind up" which leads to central sensitisation, a feature of chronic pain conditions. Neurons in the dorsal horn of the spinal chord develop increased sensitivity and enlarged receptive fields (Keeble and Brain, 2004) as a result of peripheral inflammation (Ji et al., 2003). Indeed, spinal NK_1 receptors are vital for the persistence of arthritic pain (Keeble and Brain, 2004). Calcitonin gene related peptide (CGRP) is another neuropeptide involved in pain signalling and occurs at elevated levels in SF from RA joints (Grimsholm et al., 2005). Like SP, it also causes neurogenic inflammation (Helyes et al., 2006).

1.1.5 Interactions between the immune and nervous systems

The immune controlled reactions in RA do not work in isolation from the neural processes. The nervous and immune systems are known to interact in a reciprocal fashion (Freidin and Kessler, 1991) not only by secretion of neuropeptides at the site of inflammation during immune responses but via the production of these mediators by immune cells (Grimsholm et al., 2005). Conversely, cytokines can function as growth and differentiation factors in the nervous as well as the immune system (Shadiack et al., 1993). Some studies have found correlations between SF levels of SP and various pro-inflammatory cytokines such as IL-6 and TNFα in long-standing (greater than 1 year) RA as well as a correlation between SP levels and joint inflammation (Grimsholm et al., 2005). However, there are claims that serum levels of SP do not correlate with disease activity (Keeble and Brain, 2004). Undoubtedly though, IL-1β induces SP expression in cultures of superior cervical ganglionic neurons (SCGN) and SP increases IL-1 production in B-cells (Freidin and Kessler, 1991) and modulates release of IL-1, TNFα and IL-6 from blood monocytes (macrophage precursors) (Grimsholm et al., 2005).

Another cytokine with a role in the "cross-talk" between the nervous and immune systems is leukaemia inhibitory factor (LIF). It is an IL-6 type cytokine named for its ability to induce terminal differentiation in myeloid leukaemia cells. It also has several other functions including regulating blood cell development and T-cell maturation in the immune

system, and gene expression and neuronal response to injury in the nervous system (Patterson, 1994). Levels are increased in inflammatory conditions such as RA (and osteoarthritis) although the source is not clear (Patterson, 1994). However, LIF has been shown to be produced by IL-1β, and the former acts to induce the production of SP (Shadiack et al., 1993) in SCGN cultures; this process is dependent on the presence of non-neuronal cells in the cultures, implying that glial cells are the source of LIF not only in events concerning solely the nervous system but those involving the immune system also (Patterson, 1994; Shadiack et al., 1993). So inflammation (and the presence of inflammatory mediators) induces LIF which, in turn, triggers production of neuropeptides (including SP and CGRP) in sensory neurons that do not usually express them, and through the induction of neurogenic inflammation, these neuronal mediators contribute directly to the inflammatory process (Patterson, 1994).

1.1.6 Osteoarthritis

Osteoarthritis (OA), the most common joint disease, chiefly affects the hands, spine, hips and knees. Changes in bone below the cartilage and loss of cartilage in the joint lead to pain and disability. It is thought that various processes, with a variety of causes or origins, potentially coupled with existing pre-dispositions, result in this joint disease. Cartilage integrity, vital for healthy joints, is maintained by the balance between cytokine-controlled anabolic and catabolic processes. However, the contribution of cytokines to joint destruction is not as well understood in OA as it is in RA. Despite this, it seems that the cytokine profile of SF from OA patients is the same as that of RA, although individual factors are present at lower concentrations. It is thought, therefore, that either OA joints are more sensitive to cytokines and damage occurs at lower concentrations or the cytokines themselves are not responsible for joint damage (Westacott and Sharif, 1996).

Joint cartilage is composed of collagen, water and proteoglycan (PG). IL-1 is an inducer of cartilage degradation acting by suppressing production of collagen, increasing destructive enzyme levels and interfering with the ability of chondrocytes to produce PG. Despite this, IL-1 in the SF of OA joints cannot always be detected. An increase in the number of IL-1α and β secreting macrophages in OA compared to non-arthritic joints demonstrates that diseased areas can produce IL-1. Furthermore IL-1 receptor numbers are increased on OA

chondrocytes suggesting that cartilage in these joints could be more sensitive to damage by IL-1 compared to healthy joint cartilage. TNFα also degrades cartilage although less potently than IL-1 and, similarly, its detection in OA SF is not consistent. Interestingly, there is no correlation between IL-1 and TNFα levels demonstrating that in OA, at least, these cytokines are not produced by the same cells in response to a common stimulus (the opposite is thought to be the case in RA). Like IL-1, there are increased TNFα receptor levels on OA chondrocytes, perhaps conferring increased sensitivity of cartilage to this cytokine thereby enhancing destruction. High levels of IL-6 in diseased joints have been hypothesised to indicate disease activity. Both IL-1 and TNFα induce IL-6 production which is necessary for IL-1 mediated inhibition of PG synthesis, a contributing factor to cartilage damage (Westacott and Sharif, 1996). As well as a role in RA, LIF has also been found in SF from OA patients (Patterson, 1994; Westacott and Sharif, 1996). It is thought to be involved in the degradation of joint cartilage, possibly by stimulating the loss of PG (Westacott and Sharif, 1996). However, a role for LIF in immune and nervous system communication in OA joints has not been investigated.

1.1.7 Botulinum neurotoxins and their mechanism of inhibition of SNARE-mediated exocytosis

There are seven distinct serotypes of BoNT (A-G) which are produced by the bacterium *Clostridium botulinum*. The disease caused by these toxins, botulism, is characterised by flaccid paralysis caused by inhibition of synaptic transmission resulting from blockade of Ach release at peripheral nerve endings (Dolly and Aoki, 2006; Humeau et al., 2000). The toxin is produced as a single chain, 150 kDa polypeptide, but cleavage one-third of the way from the N-terminus into a 100 kDa heavy chain and 50 kDa light chain is necessary for full biological activity. However, the 2 resultant chains remain connected by a disulphide bridge and non-covalent interactions. Following binding of the toxin to high affinity sites on pre-synaptic motor nerve endings, acceptor-mediator endocytosis results in internalisation followed by reduction of the inter-chain bridge and the light chain is released into the cytoplasm (Humeau et al., 2000). BoNT light chains have zinc-dependent protease activity and cleave SNARE proteins, with serotypes targeting only specific SNAREs (Dolly and Aoki, 2006; Humeau et al., 2000). SNARE (soluble NSF (N-

ethylmaleimide sensitive factor) attachment protein receptor)-mediated exocytosis is required for Ach release and SNARE cleavage by BoNTs prevents this process (Humeau et al., 2000). For exocytosis to occur, vesicles containing Ach must contact the target membrane (i.e. the plasma membrane) through docking. The vesicle membrane is then integrated completely into the target membrane in a multi-step process - priming and fusion (Rizo and Sudhof, 1998). This is dependent on the interaction of SNARE proteins on the vesicle and target membranes, v-SNAREs and t-SNAREs, resulting in the formation of a 4-helix bundle and fusion of the two membranes. The energy released from the formation of the very stable SNARE complex is thought to be sufficient to fuse the membranes allowing efflux of the vesicle contents (Jahn and Scheller, 2006; Rizo and Sudhof, 1998). At the neuromuscular junction, the v-SNARE is vesicle-associated membrane protein (VAMP) and the t-SNAREs are SNAP-25 (synaptosomal-associated protein, with molecular mass 25 kDa) and syntaxin (Dolly and Aoki, 2006; Rizo and Sudhof, 1998). VAMP is cleaved by BoNTs /B, /D, /F and /G, SNAP-25 by BoNTs /A, /C1 and /E and syntaxin by BoNT/C1 (Dolly and Aoki, 2006; Humeau et al., 2000). Many homologues of these proteins exist in various tissues and some are cleaved by the BoNTs. Cleavage can also be species specific. In almost all cases, alterations in toxin potency on various homologues/species are due to mutations in amino acid sequence of the SNAREs in question although occasionally it is due to an absence of receptors to a given BoNT serotype in a particular species (Humeau et al., 2000).

1.1.8 Aims of the study

BOTOX®, a pharmaceutical preparation containing BoNT/A complexed with haemagglutinin (Dolly and Aoki, 2006), has proved successful in the treatment of severe, chronic pain associated with joints affected by both RA and OA (Mahowald et al., 2006). BoNT/A can inhibit SNARE-mediated exocytosis of neuropeptides from sensory nerves – C and Aδ fibres – preventing "wind-up" and central sensitisation (Aoki, 2001; Dolly and Aoki, 2006), processes that have been shown to be involved in RA (Keeble and Brain, 2004) (see above). Notably, LIF in the pancreas has been shown to cause an alteration in the phenotype of sympathetic neurons; the transmitter released changes from norepinephrine to Ach – an affect that can be replicated in cultured sensory neurons (Patterson, 1994;

Shadiack et al., 1993). Given that the toxin has a high affinity for cholinergic neurons, conferred by receptors present at nerve endings (Aoki, 2001; Dolly and Aoki, 2006), perhaps, the presence of LIF in arthritic joints can influence the phenotype of the innervating neurons resulting in heightened toxin sensitivity. Furthermore, there is much evidence that the release of cytokines implicated in the pathogenesis of these diseases is SNARE-mediated (Chai et al., 2006; Martin-Martin et al., 2000; Mollinedo et al., 1999; Murray et al., 2005b; Pagan et al., 2003), and provided the cells can mediate their uptake, BoNTs could selectively cleave these proteins preventing exocytosis of the inflammatory mediators. It is, therefore, reasonable to hypothesise that the mechanism of action of BOTOX in the treatment of chronic pain is related to SNARE inactivation in cytokine-releasing cells. Demonstrating reduction by BoNTs of neuropeptide and cytokine release and associated SNARE cleavage in cells would confirm the ability of BoNTs to act directly on immune cells. Substantiating this hypothesis is a crucial step in defining the action of BOTOX® and, hence, characterising the target(s) of this therapeutic in the treatment of arthritis.

1.2 Materials and Methods

1.2.1 Materials

SF samples were provided by Dr. M. Mahowald, Minnesota Medical School, MN, USA. The Bioresources Unit at Dublin City University provided Sprague-Dawley rat pups. BoNT/B, /C1, /D, /E and /F were purchased from Metabiologics. List Laboratories provided BoNT/A in fully active di-chain form. Anti-syntaxin antibody (HPC-1, demonstrated in house to react with mouse, rat and human proteins) as well as alkaline phosphatase (AP) and horseradish peroxidase (HRP) conjugated secondary antibodies were purchased from Sigma. SMI-81 antibody (anti-SNAP-25, reactive with mammalian protein) was bought from Sternberger Monoclonals. Anti-VAMP-2 and anti-SNAP-23 antibodies (both reactive with human, rat and mouse proteins) were from Synaptic Systems. The pan VAMP antibody (HV62, reactive with mammalian proteins) was produced in-house. Fluorescently conjugated secondary antibodies were bought from Molecular Probes [Alexa Fluor (AF) 488] and Jackson Immunoresearch [Indocarbocyanine 3 dye (Cy3)]. SuperSignal West Pico Luminol/Enhancer solution was from Pierce. ELISA kits for TNFα, IL-1β, IL-6, LIF and SP, and CGRP were purchased from R&D Systems and SPIbio, respectively. Leibovitz's (L15) medium, trypan blue, RPMI-1640 medium (RPMI), L-glutamate, phosphate buffered saline (PBS) used for tissue culture and antibiotic/antimicotic (ab/am) solution were from Gibco. Other tissue culture reagents and all other chemicals were sourced from Sigma.

1.2.2 Details of synovial fluid donors and sample preparation for analysis

As part of a double blind, randomised, placebo-controlled clinical trial, SF samples were taken from arthritic patients before and after intra-articular (IA) injection with BOTOX® or placebo as detailed in **Table 1.1** and stored at -80°C until used. In preparation for ELISA analysis, samples were thawed on ice and sonicated.

1.2.3 ELISA of synovial fluid samples and cell supernatants of botulinum neurotoxin-treated macrophages

ELISAs were carried out using kits, according to the manufacturers' instructions. For all factors tested, levels in test samples were calculated from standard curves produced from absorbance readings of wells containing known concentrations of standard solutions.

1.2.3a TNFα, IL-1β, IL-6 Samples and standards were incubated overnight at 4°C in 96-well plates pre-coated with the relevant capture antibody. After thorough washing, plates were incubated with a second biotinylated antibody for 2 h at room temperature. Following another washing step, plates were incubated with streptavidin-HRP for 20 min at room temperature in the dark, washed, and substrate added for 20 min in the dark. Stop solution was then applied and the plate read using a microplate reader set to 450 nm with a reference wavelength of 570 nm.

1.2.3b LIF Standards and samples were reacted overnight at 4°C in 96-well plates pre-coated with a monoclonal antibody against LIF. After thorough washing, plates were incubated with a second antibody conjugated to HRP for 2 h at room temperature. Plates were developed with substrate solution for 20 min, in the dark, at room temperature, and after the addition of stop solution, read using a microplate reader as above.

1.2.3c Substance P SP levels in test samples were determined using a competitive enzyme immuno-assay. Samples, standards and controls were placed in a 96-well plate pre-coated with a polyclonal antibody. Primary antibody (for SP) solution and SP conjugated to HRP were added to the wells and the plate was incubated overnight at 4°C. After washing, substrate solution was added to the wells and the plate incubated for 30 min, at room temperature, in the dark. Following the addition of stop solution, the absorbance at 450 nm of each well was determined using a microplate reader, with a reference wavelength as before.

1.2.3d CGRP A 96-well plate pre-coated with a monoclonal antibody for CGRP was rinsed with wash buffer. Samples, standards and controls were placed into the plate; an anti-CGRP tracer was added and the plate incubated overnight at 4°C. The plate was washed again and incubated with Ellman's reagent [5, 5'-dithiobis-(2-nitrobenzoic acid)] in the dark, at room

temperature for 30 min. Absorbance of wells at 405 nm was determined using a microplate reader.

1.2.4 Isolation and culture of superior cervical ganglionic neurons; treatment with LIF and quantification of SNARE cleavage by botulinum neurotoxins

Culturing of SCGNs was performed as discussed in (Mahanthappa and Patterson, 1998). Rat pups (1–3 day old) were killed with a lethal injection of Dolethal (50 mg/kg body weight). The animals were then placed on their backs and pinned through the front paws and snout. Using a dissection microscope, the trachea was exposed and cut through to reveal the oesophagus. Once the latter and the tongue were removed, the carotid artery was visible and ganglion (found at the artery branch) could be dissected out. Dispersal of ganglia was achieved with 1 mg/ml collagenase in L15 buffered for a 5% CO_2 atmosphere (L15-CO_2), for 30 min, with periodic agitation. Following trituration with a glass pipette, centrifugation, and resuspension in L15-CO_2 to remove the collagenase, neurons were plated in wells previously coated with rat tail collagen. Typically, 10 ganglia were used per 48-well plate. The following day, the antimitotic agent cytosine arabinoside (AraC), was added to the medium to prevent proliferation of non-neuronal cells. AraC was removed at day 2 after plating and replaced again on day 3. At this stage LIF (10 ng/ml) was added to some of the cells. Next day, AraC was removed but LIF was retained in test cultures. Medium (with and without LIF) was changed on day 9 after plating. Cells cultured for 12 days were exposed to toxins (BoNT/A, /B, /C1 and /E), diluted in L15-CO_2 to the concentrations detailed in **Fig. 1.2** and **1.3**, with 2 wells used for each concentration. The following day, the toxin containing medium was removed and cells harvested in lithium dodecyl sulphate (LDS) sample buffer, with pooling of wells for each concentration. After samples were heated to >80°C for 5 min, they were run on NuPAGE 12% Bis-Tris gels in MOPS buffer (50 mM Tris, 50 mM MOPS, 0.1% SDS, 1 mM EDTA, pH 7.7) for 2 h at 175 volts. Gels were layered onto nitrocellulose membranes, sandwiched between several sheets of blotting paper, all previously soaked with transfer buffer [25 mM Tris, 192 mM glycine, 30% (v/v) methanol]. Wet transfer was carried out for 2 h at 25 volts. The resultant membranes were blocked with 3% TBS-T (20 mM Tris, 300 mM NaCl and 0.1% Tween 20, pH 7.5)/milk for 1 h at room temperature. After blocking, membranes were incubated with

mouse HPC-1 (1:2000), mouse SMI-81 (1:4000) and rabbit anti-VAMP-2 (1:200) diluted with 3% TBS-T/milk. After 1 h, three 10 min washes were performed with TBS-T and the membranes incubated for 1 h with the anti-mouse and anti-rabbit secondary antibodies conjugated to AP, made up in 3% TBS-T/milk. Membranes were washed twice for 10 min with TBS-T and once with AP buffer (200 mM Tris, 200 mM NaCl, 20 mM $MgCl_2$, pH 9.5) before addition of substrate solution (40 mM BCIP/10 mM NBT in AP buffer). This was left for 5 – 30 min depending on colour development before a TBS-T wash and, finally, a rinse with TBS-T containing EDTA (20 mM) to stop the enzymic reaction. Band densitometric analysis was performed using GeneTools software to determine the amount of intact relative to cleaved protein. Where cleavage products were not detectable by antibodies, densities of the diminishing intact protein band were compared to that of an internal standard i.e. VAMP-2 was compared to syntaxin-1.

1.2.5 Culture of lymphocytes and macrophages

DG75 (an Epstein-Barr Virus-negative B cell line from a patient with Burkitt's lymphoma) cell line was cultured in RPMI medium supplemented with 10% foetal calf serum (FCS), L-glutamate and ab/am solution. Cells were maintained in flasks as suspension cultures and grown to a density of $1x10^6$ cells/ml before harvesting by centrifugation in a sterile tube at 1000 g, for 5 min, at room temperature. When further cell propagation was required, a suitable volume of cells was returned to a culture flask containing fresh medium.

Murine macrophages (J774 cell line) were also grown in RPMI supplemented with 10% FCS. Once confluent, they were detached from the base of the flask that they loosely attach to, by tapping the sides. Medium containing the cells was collected and cells were pelleted by centrifugation at 200 g for 5 min at room temperature. For continuation of cultures, cells were resuspended in 7 ml of fresh medium and 1 ml was used to seed a 75 cm^2 flask containing 14 ml of RPMI. Cells were maintained for 3-4 days before splitting again.

1.2.6 Treatment of murine macrophages with botulinum neurotoxins

Macrophages cultured as previously described were plated in 6-well plates at a density of 4 million cells/well. Medium was removed the following day and replaced with one containing 1 or 10 nM of BoNT/A, /B (1 nM only), /D, /E or /F in both the presence and

absence of 1 µg/ml lipopolysaccharide (LPS). After 24 h incubation, supernatants were collected and analysed using ELISAs.

1.2.7 SNARE profiling of membranes prepared from cultured lymphocytes and macrophages

Cells previously pelleted (at least $1x10^8$ cells) were resuspended in ice-cold PBS and centrifuged at 200 g for 5 min; this was repeated twice before the cells were resuspended in 5 ml of ice-cold distilled H_2O. At this stage, a protease inhibitor cocktail was added at a 1:1000 dilution (according to manufacture's instructions, Sigma). Cells were then lysed by three freeze/thaw cycles; the tube containing cells was alternated between a beaker containing -80°C IMS and water at 37°C. The lysate was passed through a pre-cooled 25 gauge needle 10 times, adjusted to 0.32 M sucrose and centrifuged at 1000 g for 10 min at 4°C. The resultant supernatant was centrifuged at 105,000 g for 1 h at 4°C, the pellet solubilised in LDS sample buffer and heated to >80°C for 5 minutes once it had been passed through another 25 gauge needle. SDS-PAGE and Western blotting were performed as described previously. Antibodies used were as in section 1.2.4 with the inclusion of rabbit anti-SNAP-23 (diluted 1:1000), and in this case a HRP-conjugated secondary antibody. For development, three ten min washes with TBS-T were performed after the secondary antibody incubation, before substrate solution (SuperSignal West Pico Luminol/Enhancer solution) was added. After an appropriate incubation, according to the manufacturer's instructions, excess liquid was removed and the membrane covered with a plastic sheet. Visualisation was with a G:BOX (Syngene) gel documentation system.

1.2.8 Isolation of neutrophils from whole blood

Human heparinized whole blood (30 ml) was separated into 4 tubes and diluted 1:2 with Hank's balanced salt solution (HBSS). Each aliquot of diluted blood was layered over 10 ml of ficoll-paque and centrifuged at 400 g for 30 min at room temperature. The plasma and ficoll-paque were aspirated off leaving a red blood cell pellet containing the neutrophils. The pellet was resuspended in 15 ml HBSS (twice the original volume of whole blood) and 6% dextran (w/v in 0.85% NaCl solution) added to a final concentration of 1%. Red blood cells were left to settle out for 1 h at room temperature. The neutrophil-rich supernatant was

removed, diluted 1:2 with HBSS and centrifuged at 600 g for 10 min. Sometimes, red blood cell contamination was still present in the resultant pellet so, on these occasions, the red blood cells were briefly lysed with 2 ml ammonium chloride lysing buffer (168 mM NH_4Cl, 7.2 mM $KHCO_3$, 1 mM EDTA, pH 7.3). HBSS (20 ml) was then added and another centrifugation step (at 600 g for 10 min) performed. The neutrophil pellet was resuspended in RPMI and cell number/viability ascertained using trypan blue and a haemocytometer. Typically in the region of 3 million cells were collected, with greater than 98% viability.

1.2.9 Immuno-staining of isolated neutrophils

All steps were performed with cells in suspension, as described in (Tapper et al., 2002). Neutrophils were pelleted out of RPMI and fixed in 1.5% paraformaldehyde (PFA) for 30 min at 4°C then 1 h at room temperature, washed twice by centrifuging (at 1000 g for 3 min) and resuspending in 50 µl PBS. Following fixation, cells were permeabilised with 0.1% Triton-X 100 (TX-100) for 5 min before being washed again. Cells were then resuspened in 25 µl of rabbit anti-SNAP-23 or guinea pig HV62 made up in 5% FCS/PBS for 2 h at room temperature, with constant agitation to avoid settling. Following another wash step, cells were incubated with 25 µl of the appropriate, fluorescently-conjugated, secondary antibody (anti-rabbit AF 488 or anti-guinea pig Cy3), for 1 h at room temperature, in the dark, again with agitation. After washing, cells were incubated with 30 µl 4',6-diamidino-2-phenylindole (DAPI) stain for 10 min, washed a final time, and resuspended in 15 µl of PBS. Glycerol (45 µl of 100%) was added and the cells resuspended. This mixture was then placed onto a slide (taking care not to form bubbles). A coverslip was placed on top, and nail varnish used to seal the edges, once all excess liquid was removed with tissue. After the nail varnish had hardened, slides were stored overnight at 4°C before being examined with a fluorescent microscope, using the appropriate filter sets.

In some experiments, permeabilised neutrophils were intoxicated with tetanus toxin (TeTX) light chain before and after fixation. In such instances, cells were incubated in HEPES buffer (50 mM HEPES-NaOH (pH 7.4), 2 mM dithioreitol (DTT), 0.2 mg/ml bovine serum albumin (BSA), 50 µM $ZnCl_2$) containing 400 nM toxin light chain for 1 h at 37°C, washed, then stained as described above.

1.3 Results

1.3.1 Comparison of cytokine profiles of arthritic patients pre- and post- BOTOX® administration failed to reveal a trend that can be attributed to this treatment

As part of a clinical trial involving patients suffering from chronic pain associated with RA or OA, SF samples were taken pre- and at various times post-IA injection with BOTOX® or placebo (**Table 1.1**). Samples were analysed for levels of various inflammatory cytokines (TNFα, IL-1β and IL-6), as well as the neuropeptides SP and CGRP and, also, LIF. Despite its key role in the pathogenesis of RA (Grimsholm et al., 2005), TNFα was only detectable in 1 of the 2 RA patients tested (**Fig. 1.1a**). Where TNFα was present in RA patient RFS (**Fig. 1.1a inset**), there was no substantial decrease 1 month after IA BOTOX®. However, 3 months post the 2nd BOTOX® treatment, the patient's SF cytokine concentration had nearly tripled compared with initial baseline levels before any toxin was administered. In line with previous studies (Westacott and Sharif, 1996), TNFα was detectable in 3 out of 4 SF samples from OA patients (**Fig. 1.1a**). TNFα-containing sample sets were not available to track the effect of BOTOX® on cytokine levels within the expected duration of action of the treatment. Instead, SF was only taken when a patient presented for another BOTOX® injection, presumably once the effects of the previous dose had worn off. In this instance, there were similarities between RA and OA patients (RFS and CMO) in that TNFα concentrations had again nearly tripled compared with baseline (**Fig. 1.1a**). Cytokine levels were unchanged in samples from patients who received a placebo. Despite the fact that in RA TNFα and IL-1β upregulate each other (Kay and Calabrese, 2004) and are produced by the same cells, presumably in response to the same stimulus (Westacott and Sharif, 1996), IL-1β was measurable in one RA patient's SF, TAH, where no TNFα was detected (**Fig. 1.1b**). In the other RA patient, RFS, differences in concentrations of both factors over time were consistent (**Fig. 1.1a,b** and **insets**). Where TNFα was detected in OA SF, IL-1β was also present (**Fig. 1.1b**). However, TNFα concentration changes in patient CMO were not mirrored in IL-1β levels.

Patient	Diagnosis	Patient ID	Knee	Study Visit	Treatment
TBB	OA	TBB #1	left	Baseline - pre IA placebo	placebo
		TBB #2	left	1 mo blind - after IA placebo	placebo
		TBB #3	left	1 mo OL - after IA BOTOX®	BOTOX®
		TBB #4	left	3 mo OL - after IA BOTOX®	
		TBB #5	left	6 mo OL - after IA BOTOX®	
CMO	OA	CMO #1	left	Baseline - pre IA BOTOX®	BOTOX®
		CMO #2	left	6 mo OL - after second IA BOTOX®	
RJO	OA	RJO #1	left	Baseline - pre IA placebo	placebo
		RJO #2	left	1 mo blind - after IA placebo	placebo
MCS	OA	MCS #1	right	Baseline - pre IA placebo	placebo
		MCS #2	right	1 mo blind - after IA Placebo	placebo
TAH	RA	TAH #1	right	Baseline - pre IA BOTOX®	BOTOX®
		TAH #2	right	1 mo blind - after IA BOTOX®	BOTOX®
RFS	RA	RFS #1	left	Baseline - pre IA BOTOX®	BOTOX®
		RFS #2	left	1 mo blind - after IA BOTOX®	BOTOX®
		RFS #3	left	3 mo OL - after second IA BOTOX®	BOTOX®

Table 1.1 | Details of SF samples taken from patients involved in a clinical trial assessing the effect of BOTOX® for the treatment of refractory joint pain associated with arthritic joints. Information relates to the patients, their treatments and time course of sample collection. (OA – osteoarthritis, RA – rheumatoid arthritis, IA – intra-articular injection, OL – open label, mo – month)

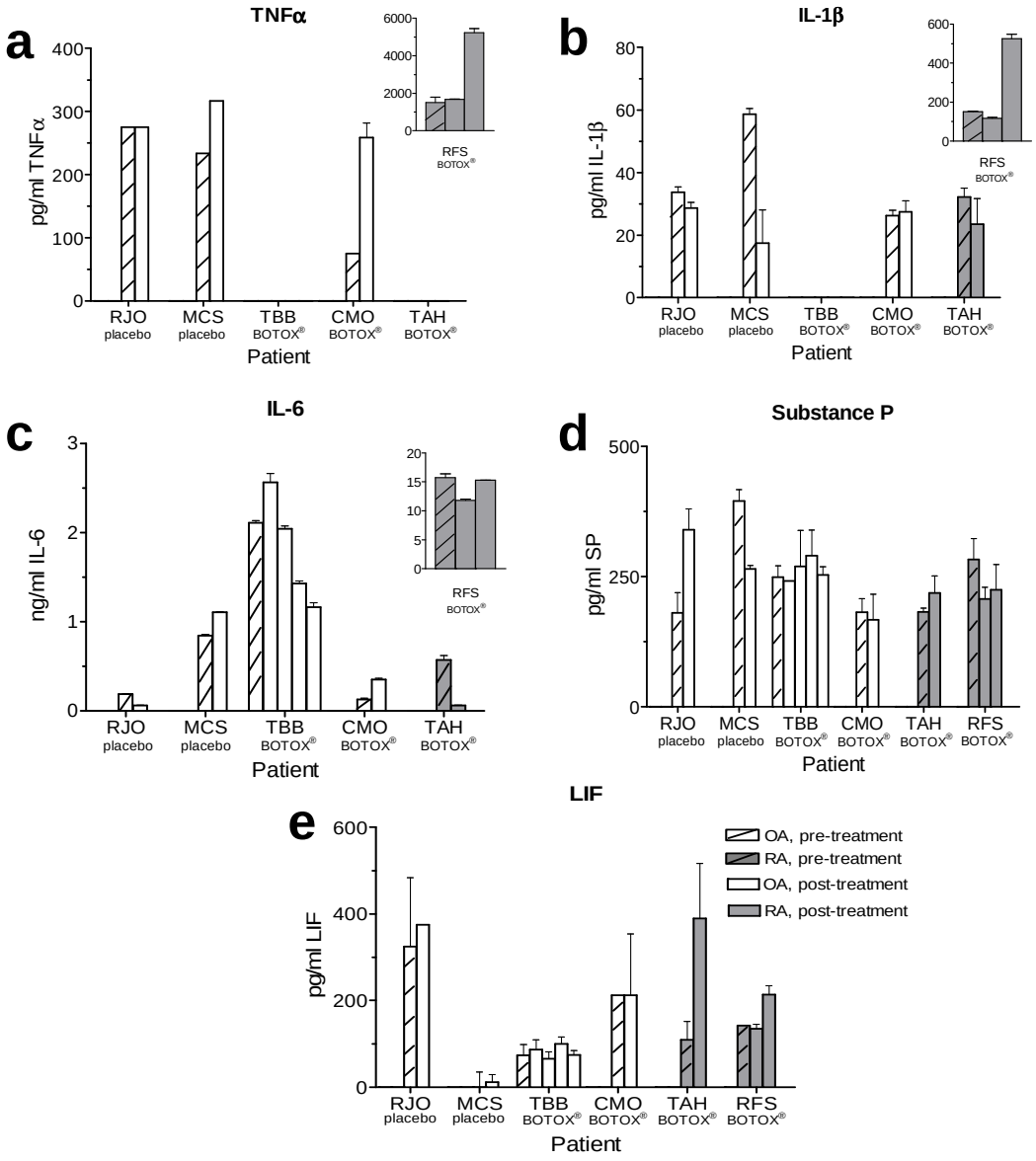

Figure 1.1│ Effect of BOTOX® on cytokine levels in SF samples from arthritic patients. Graphs show cytokine profiles of SF taken from patients with OA and RA before and after treatment with BOTOX® or a placebo. SF was taken at various time points and individual cytokine concentrations (**a-e**) were determined by ELISA. Samples were grouped according to patient; with each bar representing a different SF sample, plotted chronologically. Sample details are given in **Table 1.1**. Patient "RFS" shows inflammatory cytokine levels approximately 10 times higher (**insets**) than others. Results are averages (± S.D.) from ELISAs performed (n=4) on at least 2 different days. Error bars are sometimes encompassed by the bars.

Surprisingly, a greater than 50% drop in IL-1β was observed in patient MCS following treatment with a placebo. Consistent with the proposed correlation of IL-6 with disease activity in both RA (Nishimoto and Kishimoto, 2004) and OA (Westacott and Sharif, 1996), this cytokine was detected in all SF samples (**Fig. 1.1c**). Furthermore, where appropriate samples were available, in all patients treated with BOTOX® a decrease (albeit minimal in some cases) in cytokine concentration was observed (TBB, TAH and RFS). Levels increased again some months after BOTOX® administration in some patients (CMO 6 months and RFS 3 months – **Table 1.1**) corresponding to the expected duration of action of the treatment. The neuropeptide SP was also present in all the samples tested (**Fig. 1.1d**). Disappointingly, the concentration of SP in SF appeared unaffected by BOTOX® treatment, while placebo treatment appeared to alter SP levels; both an increase and decrease were observed. LIF was also present in SF from both OA and RA joints (**Fig. 1.1e**). Interestingly, RA patient TAH had an appreciable increase in SF LIF following IA BOTOX®. In contrast with results from other studies (Grimsholm et al., 2005), CGRP was undetectable not only in OA SF but RA samples also (data not shown). For all the factors measured, there were no obvious concentration differences between the RA and OA samples. While patient RFS had appreciably higher levels of inflammatory cytokines than the others (**Fig. 1.1a,b,c insets**), this was the only trend seen between individuals.

1.3.2 LIF enhanced botulinum-neurotoxin mediated SNARE cleavage in superior cervical ganglia neurons

BoNT cleavage of SNARE proteins in cultured SCGNs, in the presence and absence of LIF, was quantified by SDS-PAGE, Western blotting and band densitometric analysis. Cleavage of SNAP-25 by BoNT serotypes /A, /C1 and /E, and VAMP-2 proteolysis by BoNT/B were analysed. BoNT/C1 also has proteolytic activity against syntaxin-1 but it was not analysed. Membranes resulting from Western blotting appeared to show enhanced cleavage of SNARE proteins in neurons cultured with 10 ng/ml LIF (**Fig. 1.2**). Thus, cleavage products of SNAP-25 were visible in LIF-treated cells where lower doses of BoNT/A, /E or/C1 had been administered. In the case of BoNT/B cleavage of VAMP-2, the intact VAMP band was reduced at lower concentrations of toxin compared with neurons cultured in the absence of LIF.

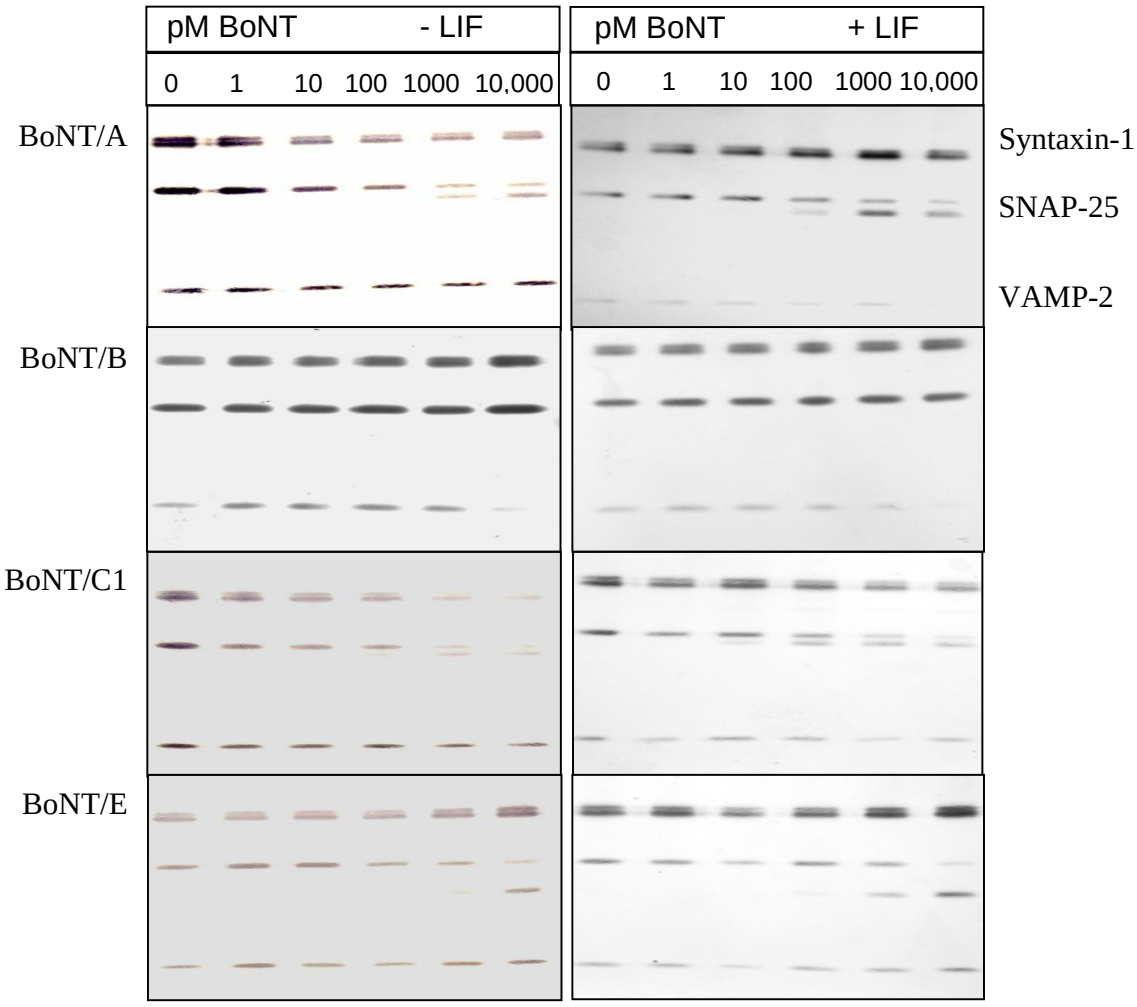

Figure 1.2 │Botulinum neurotoxin-mediated SNARE cleavage in superior cervical ganglia neurons – visualisation. The effect of 12 days of 10 ng/ml LIF treatment on cleavage of SNARE proteins in SCGNs by various BoNT serotypes. SCGNs, cultured for 12 days with and without LIF were exposed to BoNT/A, /B, /C1 or /E (1 – 10,000 pM) for 24 h, SNARE cleavage was then revealed by SDS-PAGE and Western blotting. Membranes were probed with antibodies against syntaxin-1 (HPC-1), SNAP-25 [including BoNT/A, /C1 and /E cleavage products] (SMI-81) and VAMP-2, developed with AP and photographed with a G:BOX documentation system.

Densitometry analysis of the protein bands revealed by AP development of the Western blots, performed as described in the figure legend (**Fig. 1.3**), confirmed the visualised effect of LIF treatment, i.e. that it resulted in more extensive SNARE cleavage with lower doses of toxin (**Fig. 1.3**). Repetition of these experiments will be necessary in order to ascertain the significance of cleavage differences.

1.3.3 SNARE protein profiles in immune cells

Membranes were prepared from cultures of human lymphocyte and murine macrophage cell lines and subjected to Western blotting using antibodies against the SNARE proteins syntaxin-1, VAMP-2, SNAP-25 and SNAP-23. Rat brain membranes were also included to provide positive controls for the neuronal SNAREs (**Table 1.2**, **Fig. 1.4**). Neither syntaxin-1 nor SNAP-25 were detectable in either of the membrane preparations but were found in the brain membranes, as expected. VAMP-2 was visualised in murine macrophages but not in human lymphocytes which both contained SNAP-23. The detected molecular mass for the latter, though greater than 23 kDa, corresponds with the 29 kDa size previously reported and estimated for both human and mouse SNAP-23 respectively (Martin-Martin et al., 2000).

Neutrophils were isolated from human heparinized whole blood and immuno-staining was performed to determine the SNARE profile of these non-neuronal cells (**Table 1.2**). SNAP-23 was identified (**Fig. 1.5a**) but, as human SNAP-23 is resistant to cleavage by all serotypes of BoNT, cleavage assays were not attempted.

	Neuronal tissue ***(BoNT sensitivities)***	**Non-neuronal tissue** ***(BoNT sensitivities)***
v-SNAREs	VAMP 1 *(/B, /D, /F, /G)*	VAMP 3 *(/B, /D, /F, /G)*
	VAMP 2 *(/B, /D, /F, /G)*	
t-SNAREs	SNAP-25 *(/A, /E)*	SNAP-23 *(none)*
	syntaxin 1A, 1B *(/C1)*	syntaxin 2, 3, 5, 6 *(/C1*)*
		syntaxin 4 *(none)*

Table 1.2│ Human SNAREs – location and toxin sensitivities. Adapted from (Humeau et al., 2000). ** expected*

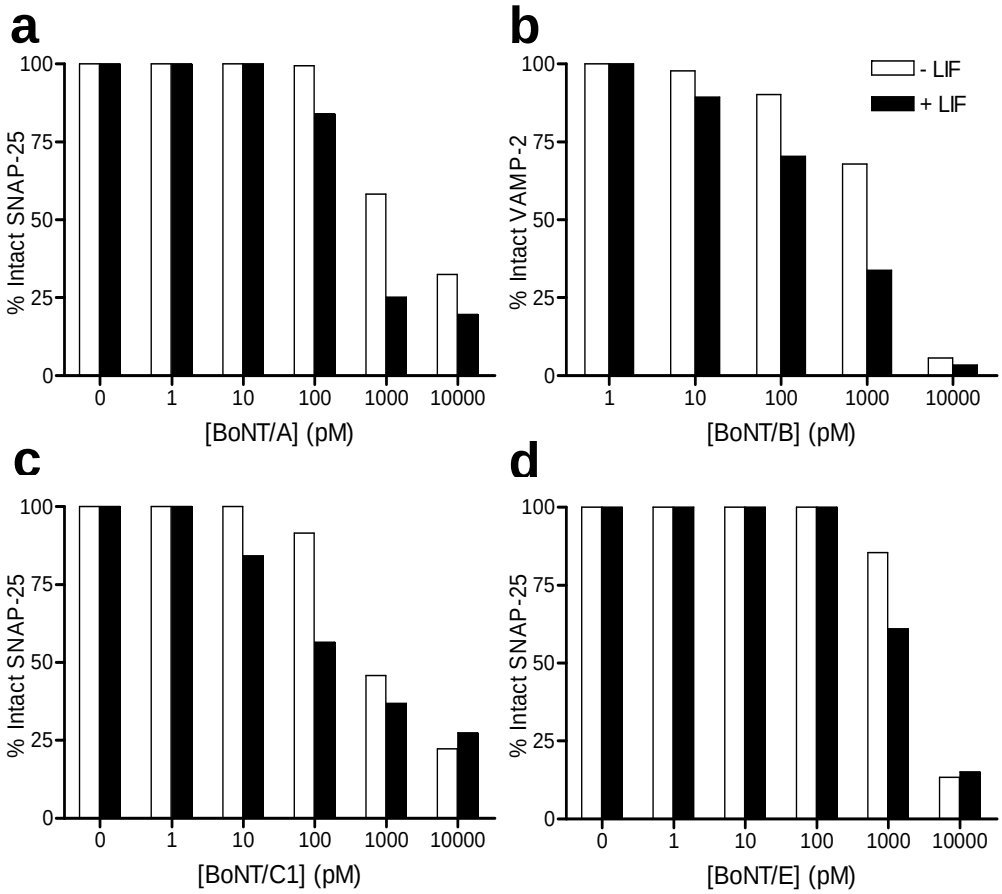

Figure 1.3| Botulinum neurotoxin-mediated SNARE cleavage in superior cervical ganglia neurons – quantitation. Analysis of SNARE cleavage by BoNT serotypes /A, /B, /C1 or /E in SCGNs with and without LIF treatment. Densitometric analysis of protein bands was performed on AP developed Western blots (**Fig. 1.2**) using GeneTools software. In the case of SNAP-25 (**a, b, c**), the density of the intact protein band in each lane was expressed as a % of the total (intact and cleaved). For VAMP-2 (**d**) where the cleavage product was not visualised, band density was compared to the syntaxin band as it is not cleaved by BoNT/B and served as an internal control for the amount of protein in each lane.

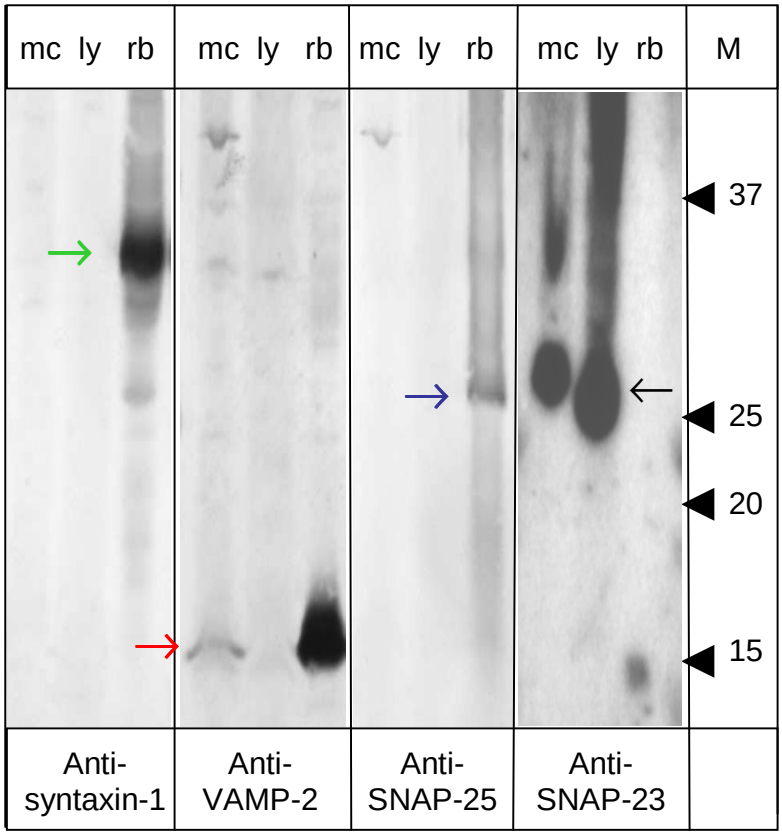

Figure 1.4 | SNARE proteins of lymphocytes and macrophages. Membranes prepared from human lymphocyte (ly) and murine macrophage (mc) cell lines were subjected to SDS-PAGE and Western blotting (AP conjugated secondary antibodies were used for syntaxin-1, VAMP-2 and SNAP-25 and HRP for SNAP-23) and their SNARE profiles determined. Rat brain membranes (rb) were included as a positive control for neuronal SNAREs. Syntaxin-1 (→) and SNAP-25 (→) were only found in the rat brain membranes, VAMP-2 was present in murine macrophages and rat brain membranes (→) and SNAP-23 only in the immune cells (→). M, (◀) denotes mobilities of standard proteins (kDa). The apparent molecular weight of SNAP-23 was as expected from previous studies – see section 1.3.3.

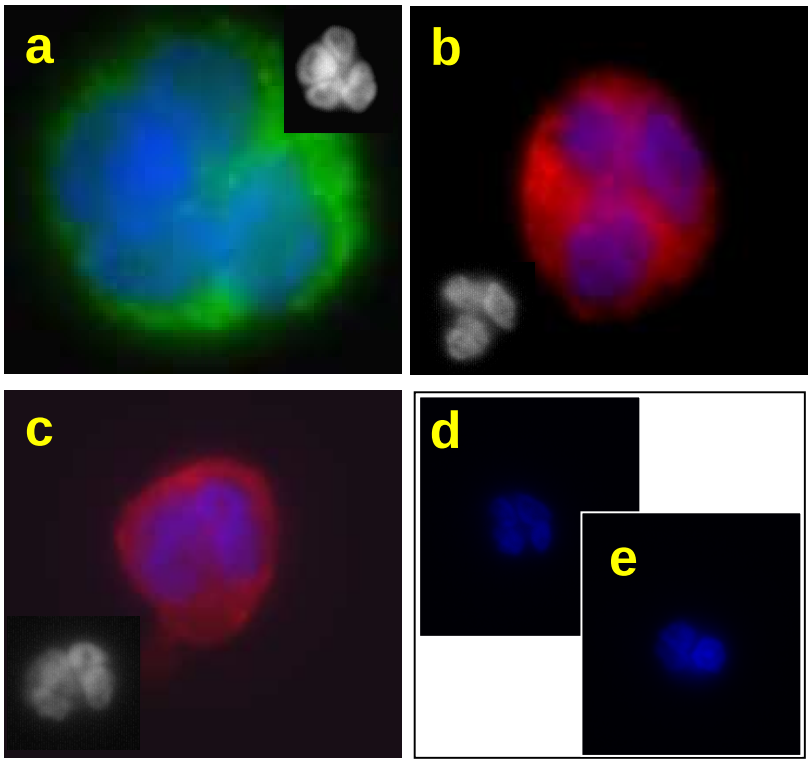

Figure 1.5| SNARE profile of neutrophils. These cells were isolated from human heparinized whole blood and SNAREs fluorescently labelled. **a**, SNAP-23 (rabbit anti-SNAP-23 and anti-rabbit AF 488); **b**, VAMP (guinea pig HV62 and anti-guinea pig Cy3). DAPI staining revealed distinct multi-lobed nuclei of neutrophils (insets). Incubation with 400 nM TeTX light chain (**c**) did not attenuate the VAMP signal (**b** compared with **c**) in fixed and permeabilised cells. Permeabilised, toxin treated, un-fixed neutrophils disintegrated during processing and could not be assessed. Omission of the primary antibody, with DAPI included to demonstrate the presence of cells, gave only background fluorescence: **d**, AF 488 and **e**, Cy3.

The HV62 antibody which recognises VAMPs -1, -2 and -3 labelled these cells (**Fig. 1.5b**). Omission of either of the primary antibodies resulted in only background signals (**Fig. 1.5d,e**). VAMP proteins are cleaved by BoNT/B, /D, /F and /G and also by TeTX. For safety reasons and for ease of working, cleavage of VAMP in neutrophils was attempted by incubation with TeTX light chain rather than with a VAMP-cleaving BoNT serotype (**Fig. 1.5c**). However, the fluorescent signal was not eliminated when fixed neutrophils were treated with TeTX light chain and labelled with HV62. Attempts were made to cleave protein in permeabilised, unfixed samples but due to the very delicate nature of the cells and their inability to survive outside the body for more than a few hours, neutrophils disintegrated before the staining process could be completed. Therefore, cleavage of VAMP and demonstration of the presence of toxin-sensitive VAMP in these immune cells could not be confirmed within the confines of working with such delicate cells (**Fig. 1.5b,c**).

1.3.4 Various serotypes of botulinum neurotoxin act on LPS-activated macrophages to reduce release of inflammatory cytokines

Murine macrophages were treated with different serotypes of BoNT (/A, /B, /D, /E or /F) overnight, in the presence and absence of LPS. After 24 h, cell supernatants were collected and inflammatory cytokine compositions analysed by ELISA. In the absence of LPS, BoNTs /B, /E and /F caused a small but significant increase in the release of IL-1β from the macrophages at 1 nM (**Fig. 1.6a**) ($p=0.0447$, 0.0025 and 0.0276 respectively). At a higher concentration (10 nM), BoNTs /E and /F continued to exert this significant effect with $p<0.0001$ in both cases (BoNT/B wasn't tested at the higher concentration). In the presence of LPS some toxin serotypes reduced IL-1β release; /A, /B and /E having significant effects at the concentrations tested. BoNT/D only reduced IL-1β release significantly ($p=0.0091$) when 10 nM was applied to the LPS treated cells. In the case of TNFα, BoNT/A, /B, /E and /F significantly increased release in the absence of LPS at 1 nM, with an even greater response from 10 nM BoNT/E and especially BoNT/F. Conversely, the higher dose of BoNT/A did not result in a significant increase in TNFα release from non-activated cells (**Fig. 1.6b**). BoNT/D, which did not affect cytokine release in the absence of LPS, was able to reduce TNFα levels in its presence, but not significantly and only at the lower dose of 1 nM. IL-6 release from LPS-activated macrophages was not significantly suppressed by any

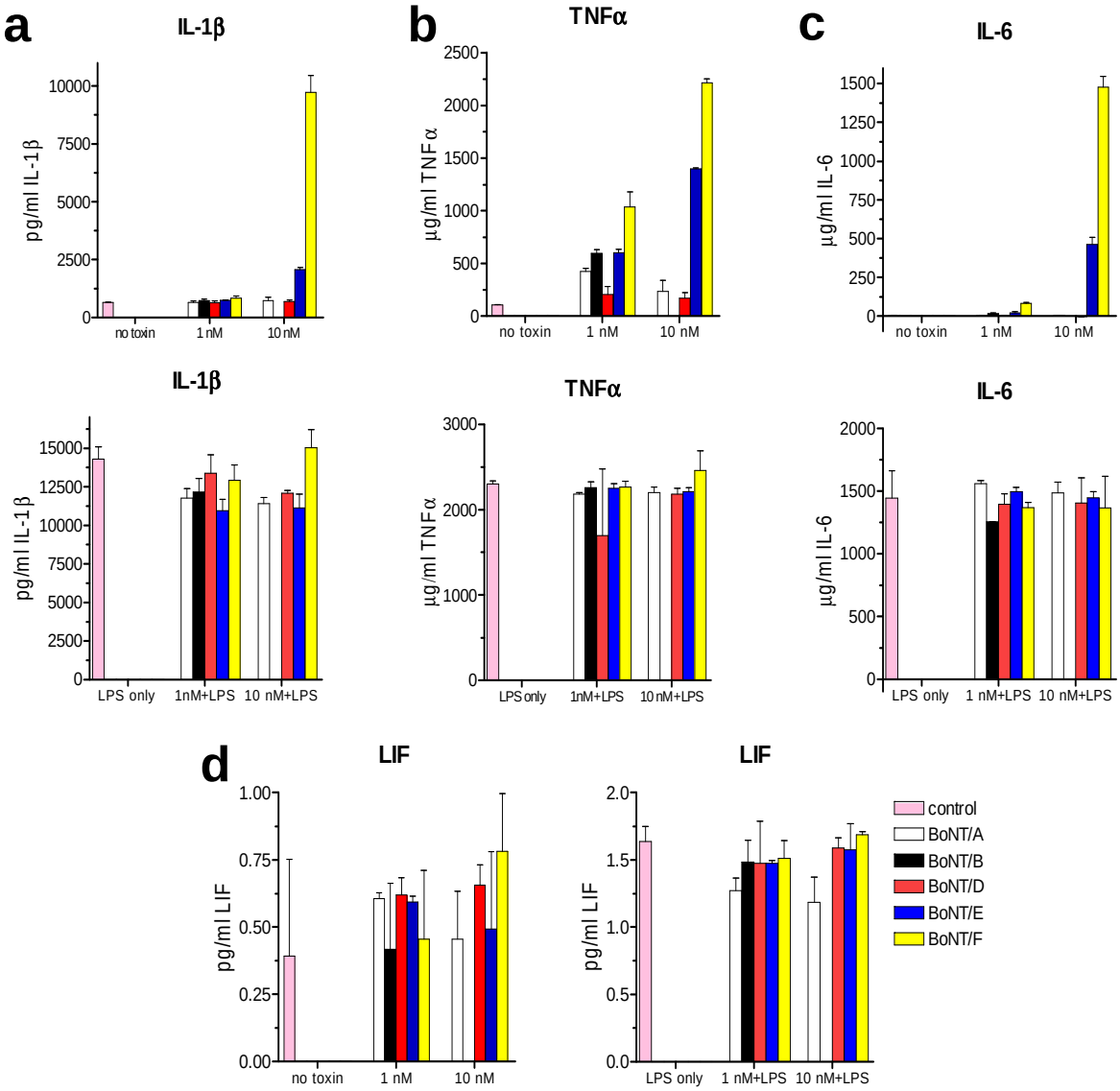

Figure 1.6| Cytokine release from botulinum neurotoxin-treated macrophages. Some serotypes of BoNT can attenuate the release of various cytokines from LPS-treated murine macrophages. Macrophages were treated with 1 or 10 nM toxin for 24 h in the absence (**a-c** upper panels and **d** left hand panel) and presence (**a-c** lower panels and **d** right hand panel) of LPS (1 µg/ml) before cell supernatants were collected and cytokine levels measured by ELISA. Control supernatants from cells not exposed to toxin, with and without LPS, were similarly analysed. Data is plotted as mean (n=3) ± S.D. Significance values refered to in the text were calculated using unpaired t-tests, where control release was compared individually, to that in the presence of the various serotypes tested.

of the BoNT serotypes tested regardless of concentration (**Fig. 1.6c**), but 1 nM of /B ($p=0.0233$), /E ($p=0.0311$) and /F ($p<0.001$) cause significantly increased levels in the absence of LPS, an effect that was increased by a higher dose of BoNT/E and especially BoNT/F ($p<0.0001$) as seen with other cytokines where 10 nM BoNT/F causes release in the non-activated macrophages similar to that seen in the LPS-treated control. Given that LIF is produced by cells in arthritic joints, the affect of BoNTs on its release were also studied (**Fig. 1.6d**). Treatment with both 1 and 10 nM of the BoNT serotypes did not significantly increase or decrease LIF release from macrophages which had not been exposed to LPS. Only BoNT/A significantly attenuated LIF levels, and at both concentrations tested (1 nM, $p=0.0129$; 10 nM, $p=0.0235$). In summary, BoNT treatment had differing effects on the various cytokines examined. While increased (compared to control) release was usually the case when toxin was added to non-activated cells, this did not seem to have any bearing on results from LPS-treated cells, with the exception of BoNT/F which not only triggered cytokine release in the absence of LPS but also failed to reduce release in its presence.

1.4 Discussion

Despite the success of BOTOX® IA injections in treating the chronic pain associated with both RA and OA (Mahowald et al., 2006), the mechanism of action of the toxin in this application has yet to be deciphered. This preliminary study was designed to begin to investigate potential targets for BOTOX® in the arthritic joint and the possible actions of other BoNT serotypes in such a condition, taking into account both the neural and inflammatory contributors. The first step in this exploration was to analyse SF taken from arthritic joints before and after BOTOX® treatment, administered during a clinical study. It was hoped that changes in the concentrations of various inflammatory mediators would reveal the potential site(s) of action of this treatment.

In the SF samples investigated, from both RA and OA joints, only IL-6 levels consistently appeared to be affected by BOTOX® treatment, with levels reducing post treatment and increasing again when further treatments were required, which would be expected given the role IL-6 is thought to play in indicating disease activity in both conditions (Nishimoto and Kishimoto, 2004; Westacott and Sharif, 1996). However, a correlation between SP and IL-6 levels in RA previously demonstrated was not revealed here (Grimsholm et al., 2005), nor was there a relationship between the other inflammatory cytokines tested and SP, as might be expected given previous observations (Grimsholm et al., 2005). Furthermore, a link between TNFα and IL-6 SF concentrations which have been seen in SF samples from patients with temporo-mandibular joint disorders including OA (Kaneyama et al., 2005) were not revealed in this study. While it is unwise to draw too many conclusions from such a small sample, some of the discrepancies between the results obtained in this study and others could be due to the well documented lack of reproducibility between such measurements made with various assay systems (Westacott and Sharif, 1996) in different Institutions (Kaneyama et al., 2005). So it is necessary to primarily compare results only within individual studies.

Despite this, there is value in this investigation if limitations in both SF samples and factors analysed are addressed. Firstly, there were a very small number of samples available with

insufficient time points post BOTOX® administration. Age and disease stage matching would also be important in a more comprehensive study as well as information on the clinical outcomes for treated patients. Since SF volume can distort outcomes (Kaneyama et al., 2005), it is important to ensure that aspirated infusions are consistent in volume between patients. In this initial exploration, the number of factors investigated was limited. Assuming sufficient SF volume, it would be interesting to compare inflammatory mediators and their soluble receptors which act as antagonists (Grimsholm et al., 2005) as an excess of cytokine compared to such receptors is necessary (Kaneyama et al., 2005) for a factor to exert its effect. Where large excesses of inflammatory cytokines or alterations in their levels following treatment are not found, investigating anti-inflammatory cytokines could reveal whether an imbalance between the 2 groups is indicative of symptoms, or, deficiencies in compounds capable of counteracting inflammation are causal. Monitoring other factors more directly implicated in joint destruction such as receptor activator of nuclear factor-κB (RANK) ligand (RANKL) which is important for osteoclast differentiation (McInnes and Schett, 2007) could also reveal further information.

LIF, a cytokine with many functions, has been found in SF from both RA and OA joints both in this study and elsewhere (Patterson, 1994). While it is thought to have a destructive role in the joint (Westacott and Sharif, 1996), it can also induce a cholinergic phenotype in neurons *in vitro* and *in vivo* (Patterson, 1994; Shadiack et al., 1993). Given the high affinity of BoNT serotypes for ecto-acceptors on cholinergic nerve endings (Aoki, 2001; Dolly and Aoki, 2006), experiments were performed to test the hypothesis that the presence of LIF enhances the sensitivity of sensory nerve endings in arthritic joints to BOTOX®. To this end SNARE cleavage by various serotypes of BoNTs was quantified in control and LIF-treated cultured SCGNs. Incubation with LIF gave evidence of SNARE cleavage at lower toxin doses not just in the case of BoNT/A, the serotype used clinically, but for BoNT/B, /C1 and /E also. It is worth noting that LIF-treated cultures often appeared to be somewhat sparser with fewer processes. This corresponded to weaker bands on blots developed under the same conditions as control cultures, an effect particularly clear when analysing the already quite faint VAMP-2 bands. This made densitometry analysis of this protein somewhat more challenging; furthermore, as cultures were plated on collagen, protein

quantitation of samples before analysis was not possible. While this result is certainly promising, it is unwise to assume that such enhancements in SNARE cleavage would result in altered exocytosis of neuropeptides. A pertinent next step would be to compare the exocytosis of factors such as SP from cultures grown with and without LIF and to attempt a correlation of SNARE cleavage and release. This may also provide confirmation of the individual proteins contributing to the SNARE complex in the exocytosis of neuropeptides from these cells.

Many studies have been performed to establish the SNARE proteins present in a variety of immune cells. A few examples include (Chai et al., 2006; Feng et al., 2001; Martin-Martin et al., 2000; Mollinedo et al., 1999; Murray et al., 2005a; Murray et al., 2005b; Pagan et al., 2003; Pitzurra et al., 1996), some of which have established that exocytosis mediated by these SNAREs is the mechanism of release of the pro-inflammatory cytokines IL-1β and TNFα from immune cells (Chai et al., 2006; Murray et al., 2005a; Murray et al., 2005b; Pagan et al., 2003). It is, therefore, very plausible that BOTOX® injected into arthritic joints is acting on such cells, and that clinical benefits of this treatment, are at least in part, due to a reduction in inflammatory factors due to BOTOX®-mediated SNARE cleavage resulting in attenuation of their release. While BoNT/D has been shown to prevent release of TNFα from human monocytes (macrophage pre-cursors) activated by LPS (Imamura et al., 1989), the substrate for the toxin was not identified; therefore, no evidence of BoNT-mediated SNARE cleavage was sought. Conversely, where SNARE cleavage has been demonstrated in these cells, it was either by micro-injection or in permeabilised cells. VAMP proteins were cleaved by TeTX micro-injected into neutrophils (Mollinedo et al., 1999); likewise, the same toxin cleaved VAMP in macrophages following a perforation procedure (Pitzurra et al., 1996). As TeTX shares the same cleavage site as BoNT/B on VAMP (Humeau et al., 2000), it is reasonable to hypothesise that at a minimum, VAMP in immune cells will be sensitive to BoNT/B if not other VAMP cleaving serotypes. In identifying SNARE proteins in immune cells in this study, the aim was to then cleave those proteins following application of the toxin in intact cells, one step further in demonstrating that BoNTs can target immune cells.

In contrast to their abundance in neurons, SNARE proteins are present in much smaller amounts in immune cells, especially in cell lines (like the lymphocyte and macrophage lines used here). Therefore, it was necessary to grow many flasks of cells and prepare membranes before Western blot analysis could be attempted. Although identification of SNAREs was possible, the number of cells and consequently the volume of culture medium that toxin would have to be applied to before cleavage experiments were attempted made this approach unworkable. The decision was then made to label SNARE proteins in isolated neutrophils, the benefit being that work was being conducted with native tissues. Due to limitations in the volume of blood available for extracting of such cells, immuno-fluorescence rather than Western blotting was employed to identify SNAREs. While this was successful, the frailty of the neutrophils made cleavage experiments very difficult. Attempts were made to treat unfixed, permeabilised neutrophils with TeTX light chain (used rather than BoNT as it is much safer and, therefore, easier to work with) but, unfortunately, the cells disintegrated and immuno-staining could not be completed. TeTX was applied to fixed cells but no alteration in the fluorescent signal of labelled VAMP was observed. This is likely due to the fact that the target protein was fixed. So the low levels of SNARE proteins expressed in immune cells and the frailty of neutrophils made cleavage experiments very difficult.

Even without demonstrating BoNT ability to cleave target proteins in immune cells, the effect of toxins on exocytosis from such cells was investigated. Control and LPS-activated macrophages were treated with BoNT/A, /B, /D, /E or /F and effects on the release of arthritis-pertinent cytokines measured. While taking into account that these experiments were performed *in vitro*, it is promising that cytokine release was affected by BoNT application. In the case of non-activated cells it is not surprising that, in some instances, toxins elicited cytokine release greater than that of control cells given that BoNT is a protein foreign to these cells. It is noteworthy that exposure to different serotypes resulted in release of different cytokines from non-activated cells but, in the main, BoNT/F triggered release greater than that from control cells and BoNT/B did not. More striking effects were seen from the LPS-activated macrophages, which more closely mimic the state of the cells as they would be in the arthritic joint. Again, attenuation of cytokine release

differed between the various serotypes tested indicating a specificity in response, perhaps a result of the many different combinations of SNARE proteins responsible for exocytosis from immune cells (Chai et al., 2006; Martin-Martin et al., 2000; Murray et al., 2005a; Murray et al., 2005b; Pagan et al., 2003). SNAP-25 cleaving BoNT/A, and BoNT/D which cleaves VAMP were most effective in this study. As BoNT/A is the serotype present in BOTOX®, it is encouraging that it was able to reduce IL-1β release. Furthermore, as IL-1β and TNFα up-regulate each other (Kay and Calabrese, 2004) and IL-1β increases SP release in neurons (Freidin and Kessler, 1991), attenuating release of just one factor could have several knock-on effects. However, while human SNAP-23, the non-neuronal homologue of the BoNT/A target SNAP-25, is insensitive to all BoNTs, the murine form is cleaved by BoNT/E and to a lesser extent by BoNT/A (Humeau et al., 2000). Therefore, actions seen in this murine *in vitro* model may not be replicated in the human joint. Despite this, BoNT/A was most effective at 1 nM and this dose may not be strong enough to overcome the reduced susceptibility of SNAP-23 to this toxin. Perhaps, though unlikely, there is as yet unidentified SNAP-25 in these cells, or the toxin is acting on a different target.

In a search for the mechanism of action for IA administration of BOTOX® for the treatment of chronic pain in arthritic joints, there is some evidence from a small number of SF samples that IL-6 levels are reduced after toxin treatment. Evidence has been gathered that suggests that culturing neurons in the presence of LIF increases the sensitivity of SNARE proteins to cleavage by BoNT, although whether this would in turn alter neuropeptide release from such cells remains to be established. Although SNARE cleavage in immune cells could not be demonstrated, evidence was obtained that various BoNT serotypes, including the clinically-used BoNT/A, can alter SNARE-mediated cytokine release from activated macrophages. To take this study further it will be necessary to repeat the experiments measuring the effect of LIF treatment on SCGN SNARE cleavage by various serotypes of BoNTs. This will the establish the significance of the data achieved thus far as well as provide an opportunity to investigate the effect of both LIF and BoNT treatment on the release of SP from the cultured neurons thereby establishing if enhanced SNARE cleavage does result in reduced exocytosis from the SCGNs. It would also be appropriate to look for cholinergic markers in the neurons cultured with LIF to add weight to the

hypothesis that LIF causes a cholinergic phenotype which in turn leads to enhanced SNARE cleavage. As visualisation of cleaved SNAREs in cultured immune cells is challenging, fluorescence-activated cell sorting (FACS) could be employed to examine any effects of BoNT serotypes on the surface markers of cultured macrophages and thus demonstrate a direct action of BoNTs on these cells. Lastly an animal arthritis model e.g. rat adjuvant or rat and mouse type II collagen RA models could be employed to provide tissue and fluids from diseased, BOTOX® treated and untreated joints. Synovial membranes could be analysed for SNARE cleavage and SF for alterations in cytokine levels (assuming sufficient volume, therefore the larger the animal used the better). While there are still questions to be answered, this preliminary study has certainly yielded areas for further exploration and demonstrated the value in this line of approach.

Section B

Defining the pharmacology of heteromeric Kv1 channels mimicking those in mammalian brain

Chapter 2
Introduction

2.1 K^+ currents and K^+ channels

Neuronal action potentials are electrochemical signals that transmit information from one end of a cell to the other, triggering neurotransmitter release at synapses, resulting in cell to cell communication. These impulses are initiated and propagated by the movement of charged ions across usually impermeable cell membranes, through ion conducting channels (Li et al., 2006). K^+ currents are responsible for returning the membrane potential to a resting state, thereby governing the resting membrane potential of a cell (Li et al., 2006). These currents vary in many respects including kinetics, voltage dependency and pharmacology. Various types of currents can be found in the same cell and similar currents arise in different cells indicating that diversity is not due to cell type. Single channel recordings have shown that the observed current diversity is likely to be due to different types of K^+ channel. In fact, K^+ channels are the largest and most prevalent group of ion channels, and are present in almost all eukaryotic cells (Rudy, 1988). In non-excitable cells they have roles in hormone secretion, cell proliferation, cell volume regulation and lymphocyte differentiation (Xu et al., 1995). While the number of K^+ channel genes is large, the diversity of current phenotypes that exists across excitable cells is greater as alternative splicing, post-translational modifications and heterologous assembly of pore-forming subunits into tetramers all contribute to the functional diversity of K^+ channel gene products (Li et al., 2006). Co-assembly with accessory subunits enhances this multiplicity resulting in channels with altered properties including assembly, trafficking, gating and conduction (Li et al., 2006). There are many types of K^+ channel including Ca^{2+}-activated (K_{Ca}), inward-rectifying (K_{IR}) and two-pore (K_{2P}) but the voltage-gated (Kv) family is the biggest consisting of several sub-families (Gutman et al., 2003a).

2.2 The voltage-gated, Kv, family of K^+ channels

The lack of discovery of a K^+ channel rich tissue hampered early research (pre-1980s) in the K^+ channel field. Studying the genetics of *Drosophila melanogaster* provided an

alternative approach. Flies were isolated due to a mutation that caused their legs to shake when anaesthetized with ether. From 1983-87, voltage-clamp experiments in pupal and larval muscle showed that this "*Shaker*" mutation affects a K^+ current. The fact that other currents are not affected suggested that the *Shaker* gene encodes a structural component of the current i.e. the channel (Papazian et al., 1987). Next, in 1987-88, protein sequences from 2 cDNAs of the *Shaker* gene complex were shown to have properties of integral membrane proteins containing 6 identical, potentially membrane-spanning segments as well as a topology and amino acid sequence very similar to vertebrate voltage-dependent Na^+ channels (Pongs et al., 1988). Such channels were known to have 4 internal repeats, but this was not the case for the *Shaker* proteins leading to the hypothesis that 4 *Shaker* products aggregate to form a channel (Pongs et al., 1988).

Using information gained from cloning the *Shaker* gene, 3 further K^+ channel genes were isolated based on their similarity to *Shaker* viz. *Shab*, *Shaw* and *Shal* (Jan and Jan, 1992). All 4 members of this gene family encode peptides with conserved organisation, suggesting common function (Wei et al., 1990). While voltage-gating and K^+ selectivity are features shared by the family, their kinetic and voltage sensitivities differ. Variations in lengths of domains at the N and C termini result in differences in size of the peptides: *Shaker* ~71 kDa, *Shab* ~100 kDa, *Shaw* ~56.5 kDa and *Shal* ~56 kDa. Despite this, there is a conserved core region encompassing the 6 potentially membrane spanning domains, which varies little (Wei et al., 1990), resulting in about 40% amino acid identity between any pair of genes (Jan and Jan, 1992).

The 4 members of the Drosophila gene family, *Shaker*, *Shab*, *Shaw* and *Shal*, have 1 or more mammalian homologues and therefore each defines a subfamily (Kv1 – 4) of K^+ channel genes (Jan and Jan, 1992; Wei et al., 1990): Shaker-related, Kv1; Shab-related, Kv2; Shaw-related, Kv3 and Shal-related, Kv4 (Gutman et al., 2003a; Gutman et al., 2005). These mammalian and *Drosophila* proteins are more closely related (regardless of species) than the subfamily members of a single species, sharing roughly 70% amino acid identity in the core region (Jan and Jan, 1992; Wei et al., 1990) [compared with 40% between subfamilies (Xu et al., 1995)]. This demonstrates that the individual structural features of the subfamilies evolved before vertebrate/invertebrate separation (Wei et al., 1990). Despite the similarity in products from the gene subfamilies, heteromultimerisation of subunits into

channels is family specific. N terminal domains control this assembly ensuring that cells maintain several distinct K^+ current systems (Xu et al., 1995).

2.3 The structure of Kv1 channels

Kv1 channels are large (Mr ~ 400 kDa) sialoglycoprotein complexes (Parcej et al., 1992) composed of 4 pore-forming α subunits (Kv1.1-1.6) and 4 auxiliary, cytoplasmically-associated β subunits (Dolly and Parcej, 1996; Orlova et al., 2003; Parcej et al., 1992; Rettig et al., 1994; Scott et al., 1994a).

2.3.1 The α subunits The α subunits have several conserved features including 6 putative membrane-spanning segments (α helices S1-S6) and with both the N and C termini located intracellularly (**Fig. 2.1a,b**). A functional channel consists of 4 α subunits arranged around a central axis forming the ion conduction pathway (**Fig. 2.1c**). α helices S1-4 are responsible for voltage sensing, and wrap around the pore of the adjacent subunit (Long et al., 2005b) (**Fig. 2.1c**). The S4 helix contains a positively charged amino acid (arginine) at every third residue, interspersed with hydrophobic residues, and is generally thought to function as the main voltage-sensor (see below) (Jan and Jan, 1992). The ion conduction pore consists of S5, the S5-S6 loop and S6 (Long et al., 2005b).The S5-S6 loop contains a conserved sequence which acts as a K^+ selectivity filter (see below) (Li et al., 2006). The S4-S5 linker connects the pore and voltage sensing components of the α subunits (Long et al., 2005a).

2.3.2 The T1 domain Preceding S1, the first membrane spanning helix of an α subunit, the N-terminus forms the T1 domain (within the cell). These domains (1 from each α subunit) form a tetrameric complex at the intracellular membrane providing a docking platform for β subunits (Long et al., 2005a) (**Fig. 2.2a**). The T1-S1 linker maintains separation between the pore of the channel and the intracellular regions. A wide space between the T1 domain and pore is achieved by the radial direction of the linkers, allowing the inner pore helices to undergo large movements during pore opening (see below) without interference (**Fig. 2.2a**). This also results in diffusion pathways, called side portals, between the cytoplasm and pore entrance which provide a means for communication and allows the flow of K^+. The 4 side portals of a complete channel attract cations due to negatively charged amino acids on their

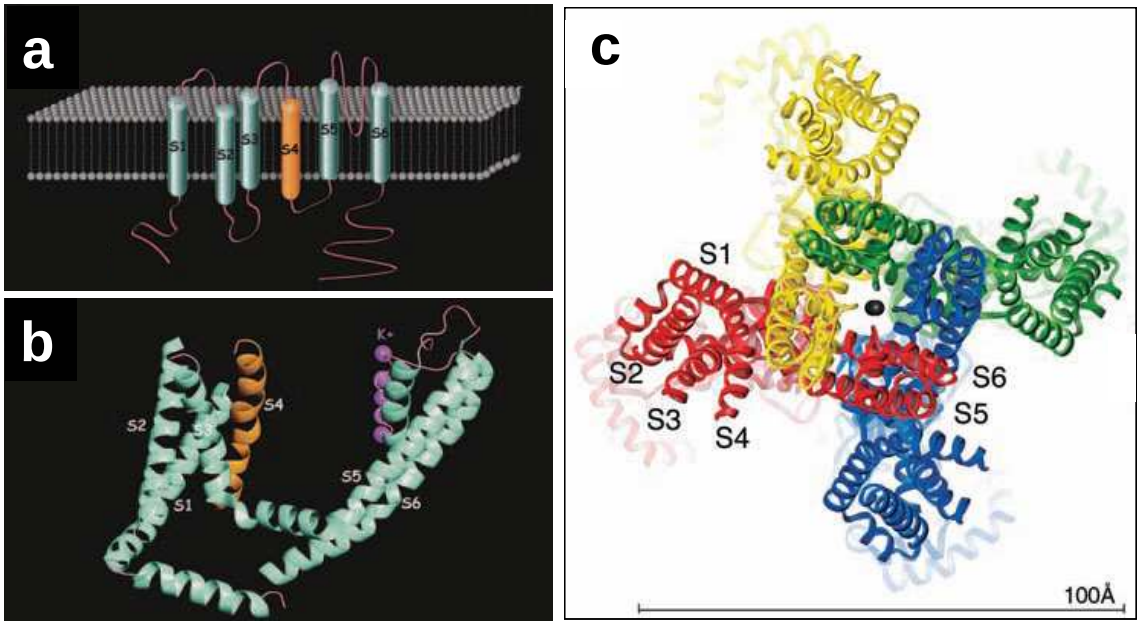

Figure 2.1 | Kv channel α subunit arrangement and structural model. **a**, A simple topographical model common to all Kv channels predicted by amino acid sequence. There are six membrane spanning segments (cylinders, S1-S6) with N- and C-termini arranged intracellularly. The fourth membrane spanning segment contains evenly spaced charged residues and comprises the membrane voltage-sensor. **b**, Side view of ribbon diagram of one subunit of Kv1.2 based on crystal structure (Long et al., 2005a). K^+ ions are shown as purple spheres. Transmembrane helices are labelled. The fourth transmembrane segment is shown in gold. **c**, Tetrameric arrangement of Kv1.2 as viewed above from the extracellular surface. The 4 subunits are coloured differently. Taken from (Li et al., 2006) (**a,b**) and (Long et al., 2005a) (**c**).

rims and surface (**Fig 2.2c**). They also have a role in inactivation (see below) (Long et al., 2005a).

2.3.3 The β subunits β subunits act as accessory proteins, mainly for Kv1 channels (Li et al., 2006; Parcej et al., 1992), and interact with them via the T1 domain (Long et al., 2005a) (**Fig. 2.2a,b**). There are several Kvβ family members with well conserved C-termini but differing N-termini (Leicher et al., 1998; Li et al., 2006; Scott et al., 1994b). These subunits also form tetramers, and are related to the aldo-keto reductase enzymes having both catalytic and substrate binding domains (Li et al., 2006). The active site contains an $NADP^+$ cofactor and catalytic residues for hydride transfer but the function of this is as yet undeciphered. It has been suggested that the enzyme may act as a sensor for Kv1 channels in such a way that the redox state of the cell could have an influence on electrical activity at the membrane (Long et al., 2005a). Through their N-terminal domain, β1 subunits confer fast inactivation when co-expressed with Kv1 α subunits that usually produce non-inactivating channels (Rettig et al., 1994) (see below). As other β subunits do not share this property it is likely they have other functions. Enhanced surface expression of channels co-expressed with β subunits indicates a possible role as channel chaperones (Manganas and Trimmer, 2000).

2.4 The pore-forming region of Kv1 α subunits.

All K^+ channels share a highly conserved pore region encoded by a critical amino acid sequence called the K^+ signature sequence from which the structural elements of the pore are formed (Doyle et al., 1998; MacKinnon, 2003). In Kv1 α subunits, this is a short stretch of amino acids between the S5 and S6 transmembrane domains. This pore region consists of the turret, pore helix and selectivity filter (Doyle et al., 1998). In a fully assembled channel, 4 pore regions, 1 from each of the α subunits, assemble together to form an ion conduction pathway (MacKinnon, 2003), with 4-fold symmetry around the pore. The "turrets" from each monomer jut into the extracellular solution above the centrally-located pore entrance (Imredy and MacKinnon, 2000) (**Fig. 2.3a**). The transmembrane α helices are tilted with respect to the membrane resulting in a broad vestibule at the entrance of the pore (Doyle et al., 1998), which dips into the membrane and tapers into the selectivity filter at the centre of the vestibule (Hopkins et al., 1996).

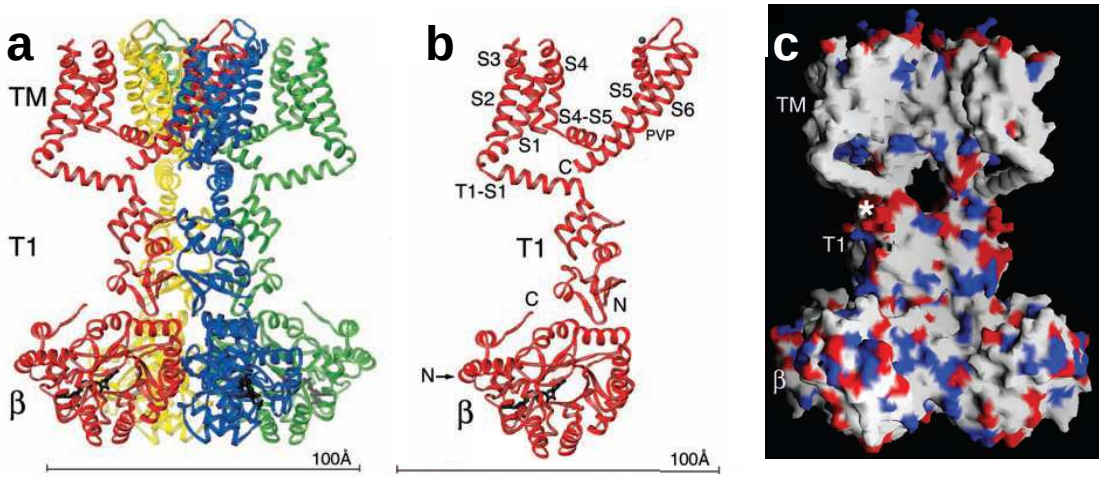

Figure 2.2 | Views of a Kv1.2-β2 subunit complex. **a**, Ribbon representation with the extracellular solution above and the intracellular solution below. Each α subunit, including the T1 domain and its associated β subunit, is coloured differently. TM indicates the membrane component of the channel. **b**, A single α and β subunit of the channel viewed from the side. The transmembrane S1-S6 helices, proline-valine-proline (PVP) sequence of S6, and the N and C termini of the Kv1.2 and β2 subunit are labelled. The N terminus of the β subunit is on the side furthest from the viewer. **c**, Surface representation of the Kv1.2-β2 complex. Negatively charged glutamate and aspartate residues are coloured red and positively charged arginine and lysine residues in blue. The large hole above the T1 domain depicts the side portal which connects the cytoplasm to the pore. Taken from (Long et al., 2005a).

2.4.1 Ion selectivity The selectivity filter is responsible not only for the 1000-fold greater selectivity of these channels for K^+ over Na^+ but, also, allows rapid diffusion through the pore. The selectivity filter separates the cavity of the channel from the extracellular solution. It is so narrow that it causes K^+ to shed its hydrating water molecules in order to enter (Doyle et al., 1998). A single layer of threonine hydroxyl oxygen atoms and 4 evenly spaced layers of carbonyl oxygen atoms from the K^+ signature sequence create 4 K^+ binding sites along the selectivity filter numbered 1 to 4 from the extra to intracellular side (**Fig. 2.3b,c**). Dehydrated K^+ binds to these sites taking 8 carbonyl oxygen atoms, 4 from above and 4 below the ion, which act like surrogate water taking the place of water oxygen atoms and in doing so compensate for the energetic cost of dehydration (Doyle et al., 1998; MacKinnon, 2003). In this way, a queue of K^+ binding sites is formed and the ions can diffuse from water into the selectivity filter (MacKinnon, 2003). Na^+ has a smaller radius than K^+ meaning that it cannot get close enough to the carbonyl oxygen atoms to compensate for the energetic cost of dehydration. This prevents them from passing through the channel, thereby, ensuring such impressive K^+ selectivity (Doyle et al., 1998). At most times, there are 2 ions in the selectivity filter. The repulsion between them overcomes the affinity that each has for its binding site so they are not too tightly bound, resulting in rapid diffusion through the pore. If the internal K^+ concentration is too low, only 1 ion occupies the selectivity filter and, hence, binds too tightly preventing the flow of ions (MacKinnon, 2003).

2.5 Gating of Kv1 channels

Ion channels gate (open and close) in response to external signals. Kv1 channels (as well as all voltage-gated K^+, Na^+ and Ca^+ channels) open (activate) in a voltage dependent manner in response to membrane depolarization, i.e. changes in voltage across the cell membrane, and then spontaneously shut (inactivate), usually independently of voltage (Long et al., 2005b; MacKinnon, 1991). The membrane electrical field exerts a force on charged amino acids (arginines in the S4 helix), called the gating charges, which move through the membrane, ultimately altering channel conformation. The gating charge is very large, resulting in channels that are very sensitive to small voltage changes (Long et al., 2005b). The gating charge of a Kv channel is the equivalent of almost 14 electrons moving across

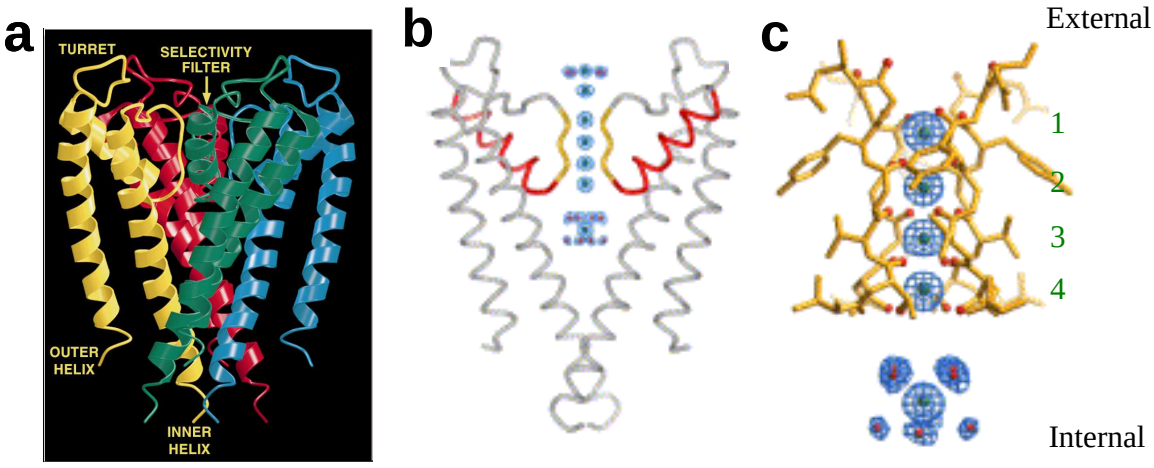

Figure 2.3 | The ion conduction pore of K^+ channels. This is a representation of a KcsA channel from *Streptomyces lividans.* While each subunit consists only of 2 helices as opposed to the 6 found in eukaryotic Kv1 channels, it shares close sequence homology in the pore region. **a**, View of a tetrameric channel, each subunit being distinguished by a different colour. **b**, Two of the four subunits of the pore are shown with the extracellular side on top (Zhou et al., 2001). The selectivity filter is depicted in gold. The blue mesh illustrates the electron densities of K^+ and water along the pore. **c**, Close-up view of the selectivity filter with dehydrated K^+ at positions 1 through 4 (external to internal) inside the filter and a hydrated K^+ in the central cavity below the filter. This figure was taken from (Doyle et al., 1998) (**a**) and (MacKinnon, 2003) (**b,c**).

the transmembrane voltage difference. These charges are attributed to 4 arginine residues per α subunit – resulting in a total of 16, with each arginine residue having approximately 1 electron charge (MacKinnon, 2003). The membrane electric field works on the charged residues, pushing them outwards when the inside of the membrane is positive, and pulling them inwards when the inside of the membrane is negative (Long et al., 2005b). S6 helices (1 from each subunit of a tetrameric channel) line the pore on the intracellular side of the selectivity filter, forming the inner helix bundle – an expandable constriction for opening and closing the pore. It is called the activation gate. The S6 helices have a conserved proline-X-proline (Pro-X-Pro) sequence (where X is any amino acid; valine in Kv1.2), which curves them so they run almost parallel to the membrane near the intracellular surface (Long et al., 2005a) (**Fig. 2.2b**). The S4-S5 linker (which connects the voltage sensing and pore channel components) runs parallel to the membrane inside the cell, crosses over the top of the S6 helix and forms amino acid contacts with it. The curved nature of S6, imbued by the conserved Pro-X-Pro sequence, enables it to act as a platform for the linker. Hence, the movement of the voltage sensor domain is transmitted to the activation gate, via the S4-S5 linker, resulting in the mechanical opening and closing of the pore (Long et al., 2005b).

2.5.1 Inactivation Diversity of Kv channels is based mainly on differences in the kinetics of activation and inactivation (Pongs, 1992). Indeed, the firing pattern and wave forms of action potentials in a neuron is determined to a large extent by the inactivation properties of the K^+ channels present in that particular cell (Jan and Jan, 1992). A refractory period follows inactivation when, through a series of conformational changes, the channel returns to its resting state. Channel inactivation can occur at the intra or extracellular entrance of the pore, and be imbued by the N or C terminus, respectively. Channels inactivated at the extracellular entrance to the pore reactivate rapidly compared with the slow reactivation resulting from intracellular inactivation (Pongs, 1992).

Fast inactivation of Kv1 channels is mediated by the N-terminus, resulting in spontaneous closure of channels which occurs over tens of milliseconds (MacKinnon, 1991). The process occurs in some members of the Kv1 family, e.g. Kv1.4. The N terminus “inactivation gate” of the α subunit of these channels enters the side portals, blocking access of the intracellular K^+ ions to the pore, thereby inactivating the channel. A very

specific N terminus sequence is required to produce an N terminal inactivation gate: approximately 10 hydrophobic amino acids followed by a mixture of hydrophilic and positively charged residues. The hydrophobic stretch enters the side portal, and reaches into the inner pore which is lined with hydrophobic amino acids. Positively charged amino acids from the hydrophilic sequence make electrostatic interactions with the negatively charged amino acids on the surface of the T1 domain and linkers to S1 (**Fig. 2.4**) (Long et al., 2005a). The N terminus of the β1 subunit also has inactivation gate properties, with 70 extra N terminal amino acids compared with other β subunit family members. This extra length allows the inactivation gate to reach to the side portal of the α subunit. Co-expression of β1 subunits with Kv1 channels other than Kv1.4, confers them with N-type inactivation (Rettig et al., 1994).

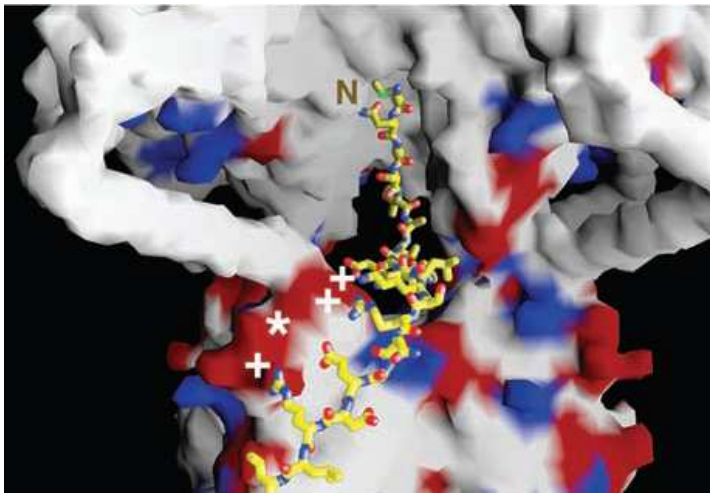

Figure 2.4 | Hypothetical model for the binding of an inactivation peptide to the Kv1.2-β2 channel. A portion of the T1 and transmembrane components are shown. The inactivation peptide is modeled on the 22 N terminal residues of β1. Three positive residues (+) at positions 13, 15 and 20 from the N terminus were placed at the site of interaction with negatively charged residues on T1 (*) and the hydrophobic residues at the N terminus were placed at the inner pore where they are known to bind and block the flow of K^+ ions. Taken from (Long et al., 2005a).

C-type inactivation is slower than N-type and is sensitive to external cations and the amino acid composition of the K^+ channel pore as all 4 α subunits of the channel participate co-operatively. The mechanism for inactivation is not as clear though it is likely that the outer mouth of the channel constricts, decreasing the inter-subunit distance across the outer vestibule of the channel pore (Panyi et al., 1995).

2.6 The toxin approach to studying the biochemistry of K^+ channels

While studying the genetics of a *Drosophila* mutant was very successful for identifying Kv channel genes, the simultaneous discovery of Kv channel blockers in the early 1980s lead to isolation and characterisation of K^+ channel proteins (Black et al., 1988; Rehm and Lazdunski, 1988). Several neurotoxins isolated from the venom of *Dendroaspis angusticeps* and *polylepis* (green and black mamba snakes, respectively) were found to facilitate neurotransmitter release at both peripheral and central synapses, an effect that was explained by the toxins' blockade of voltage-sensitive K^+ currents in these neurons (Dolly and Parcej, 1996; Halliwell et al., 1986). Toxin binding and affinity chromatography resulted in the purification of a subset of Kv channels from mammalian brain, revealed by cloning to be from the Kv1 family, identifying the dendrotoxins (DTXs) as blockers of some members of this set of proteins (Dolly and Parcej, 1996). Similarly, Noxiustoxin (NxTX) isolated from the venom of the Mexican scorpion *Centruroides noxius* (Carbone et al., 1982), was shown to increase neurotransmitter release from synaptosomes by decreasing K^+ permeability (Sitges et al., 1986). This and other toxins isolated from scorpion venoms proved to be high affinity selective probes for K^+ channels including those from the Kv1 subfamily and as such were, like DTXs, used to purify channels from native tissues [for example (Koschak et al., 1998)]. Despite the success of molecular cloning techniques, the subunit compositions of channels in native tissues was unknown. Importantly, the use of DTX to purify channels from native tissue resulted in the discovery of the β subunit and the α(4) β(4) stoichiometry of Kv1 channels (Parcej et al., 1992). In addition, scorpion toxins were used to identify the pore region of the *Shaker* channel, determine the tetrameric composition of K^+ channels and investigate the role of Kv1 channels in T cell function (Garcia et al., 2001; Garcia et al., 1998). Crucially, both DTXs and scorpion toxins were employed to define the subunit compositions of Kv1 channels in

native mammalian brain tissue (Koch et al., 1997; Koschak et al., 1998; Scott et al., 1994a; Wang et al., 1999b).

2.7 Kv1 inhibition by peptide toxins

2.7.1 Dendrotoxins DTXs are isolated from mamba venoms; αDTX, βDTX, γDTX and δDTX from *Dendroaspis angusticeps*, DTX_I and DTX_k from *D. polylepis* and DV14 from *D. viridis* (Benishin et al., 1988; Dolly, 1992; Hopkins et al., 1996). The toxins for which sequence data is available can be placed into 2 subfamilies (**Table 2.1**) which show approximately 60% amino acid identity. βDTX and γDTX have only been partially sequenced and while they are members of the DTX family, it is not clear to which subfamily they belong (Harvey, 1997; Hopkins et al., 1996).

	1 10 20 30 40 50
δDTX	AAKYCKLP VRYGPCKKKI PSFYYKWKAK QCLPFDYSGC GGNANRFKTI EECRRTCVG
DTX_k	AAKYCKLP LRIGPCKRKI PSFYYKWKAK QCLPFDYSGC GGNANRFKTI EECRRTCVG
DV14	AAKYCKLP VRYGPCKKKI PSFYYKWKAK QCYPFDYSGC GGNANRFKTI EECRRTCVG
	1 10 20 30 40 50
αDTX	pEPRRKLCILH RDPGRCYDKI PAPYYNQKKK QCERFDWSGC GGNSNRFKTI EECRRTCIG
DTX_I	pEP IRKLCILH RDPGRCYQKI PAFYYNQKKK QCEGFTWSGC GGNSNRFKTI EECRRTCIRK
	1 10 20 30 40 50
BPTI	RPDFCLEP PYTGPCKARI IRYFYNAKAG ICQTFVYGGC RAKRNNFKSA EDCMRTCGGA

Table 2.1 | Sequences of dendrotoxin subfamilies, and a homologous protease inhibitor. The single letter amino acid code is: A=alanine, R=arginine, N=asparagine, D=aspartic acid, C=cysteine, Q=glutamine, E=glutamic acid, G=glycine, H=histidine, I=isoleucine, L=leucine, K=lysine, M=methionine, F=phenylalanine, P=proline, S=serine, T=threonine, W=tryptophan, Y=tyrosine, V=valine, pE=pyroglutamate. Taken from (Hopkins et al., 1996), (Katoh et al., 2000) and (Swaminathan et al., 1996).

After initial findings that they facilitated neurotransmitter release at the neuromuscular junction, it was determined that DTXs act by blocking Kv channels (Halliwell et al., 1986). DTXs are arguably the most specific of venom peptide toxins, with activity against only a few of the Kv1 α subunits. As a group they inhibit Kv1.1, 1.2 and 1.6 (Hopkins et al., 1996) but the specificities of individual homologues differ as detailed in **Table 2.2**. They are single chain polypeptides of low molecular weight (around 7 kDa), 57 – 60 residues long with 3 conserved disulphide bonds (**Fig. 2.5b**). Specifically, DTX_k consists of a 3_{10}-helix (residues 3–7), a β-hairpin (residues 18-35) and an α helix (residues 47-56) (Smith et al., 1997) (**Fig. 2.6a**). The DTXs also have sequence homology to Kunitz serine protease inhibitors such as bovine pancreatic trypsin inhibitor (BPTI) (**Table 2.1**), but the most potent toxins have negligible protease inhibitor activity and the inhibitors do not block K^+ channels (Dolly and Parcej, 1996; Harvey, 1997).

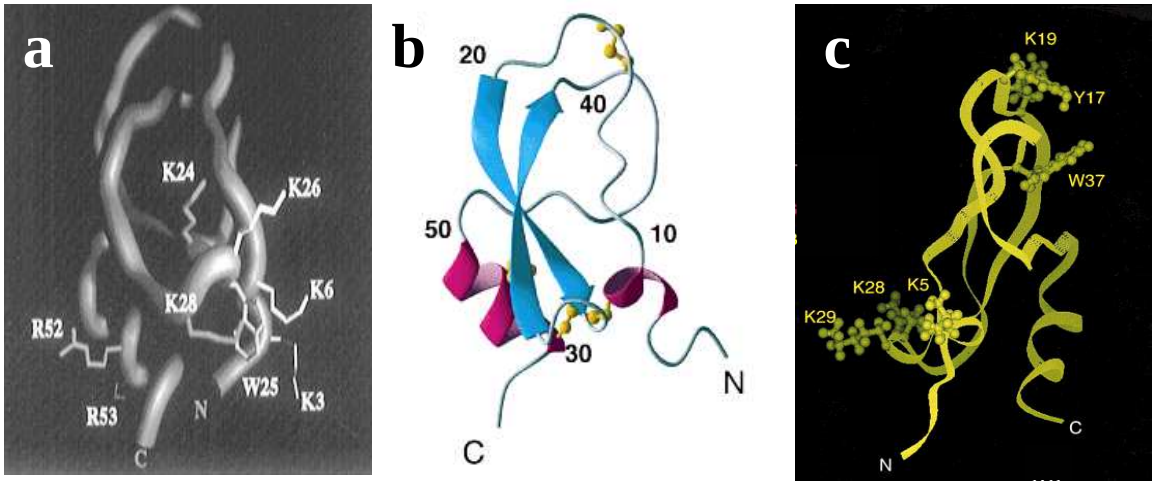

Figure 2.5 | Three-dimensional models of dendrotoxin$_k$ and dendrotoxin$_I$. **a**, main chain folding of DTX_k side-chain positions of some the residues vital for Kv1.1 channel binding affinity. **b**, ribbon structure of DTX_I with the three disulphide bonds, highly conserved among the DTXs, shown as yellow ball and stick models. **c**, positions of the two putative K^+ channel binding triads on DTX_I. Taken from (Smith et al., 1997) and (Katoh et al., 2000).

However, conserved patterns of disulphide bridging result in similar backbones of the DTXs and serine protease inhibitors, though there are differences in the detailed structures (Smith et al., 1997). Comparison of the 2 groups of homologues suggested that conserved lysine residues in the DTXs may be responsible for their channel blocking ability (Harvey, 1997). These positively charged amino acids are concentrated in the lower part of the structure, the cationic domain, formed by the N- and C-terminal regions and residues 27-30 of the β-turn (Katoh et al., 2000). In fact, studies involving site-directed mutagenesis of DTX_k revealed the areas of the toxin that interact with Kv1.1 channels [the specific target of the toxin (**Table 2.2)**] both in synaptic plasma membranes from rat cerebral cortex and recombinantly expressed in *Xenopus* oocytes (Smith et al., 1997; Wang et al., 1999a). Mutants were chosen on the basis that a positively charged region of DTX_k (the cationic domain) interacts with a negatively charged area on the channel (negatively charged amino acids in the S5-S6 domain). The multiple lysines and/or arginines (positive) conserved on DTX_k as well as other channel blocking homologues, coupled with the fact that removing glutamate (negative) from the toxin binding domains of α subunits decreases DTX affinity, provided evidence for the theory. Furthermore, it was shown that for scorpion toxins interacting with Kv1.3 channels, there are electrostatic interactions between the toxin residues (similar to those on DTXs) and acidic (negative) amino acids in the channel mouth (Smith et al., 1997). Altering positively charged lysine residues (K24, 26 and 28) to alanine in the β hairpin decreased the binding affinity with the K26 mutant giving the largest decrease. Mutating a tryptophan residue (W25) to the less hydrophobic alanine also reduced binding affinity demonstrating that both positively charged and hydrophobic residues in the β-hairpin are important for toxin/channel interaction. Altering residues K3 and 6 in the 3_{10}-helix also reduced toxin binding affinity, thus also demonstrating the importance of this region (**Fig. 2.5a**). Interestingly, mutating positively charged amino acids in the C terminal α helix did not influence binding, highlighting the selectivity of the identified residues. The studies concluded, therefore, that the 3_{10}-helix and β-hairpin domains are important for channel interaction with alterations of some residues in these structural elements reducing binding affinity (Smith et al., 1997; Wang et al., 1999a). A later study of DTX_I comfirmed that residues in the N-terminal half of the molecule are mainly responsible for binding of the toxin although there was evidence that

Toxin	Abbre-viation	Source Organism	Animal	Channels known to be sensitive	Refs.
Agitoxin-1	**AgiTX -1**	*Leiurus quinquestriatus var. herbraeus*	Scorpion	Kv1.1, 1.3, 1.6	(Garcia et al., 1994; Suarez-Kurtz et al., 1999)
Agitoxin-2	**AgiTX -2**	*Leiurus quinquestriatus var. herbraeus*	Scorpion	Kv1.1, 1.3, 1.6	(Garcia et al., 1994; Suarez-Kurtz et al., 1999) (Cayabyab et al., 2000)
Agitoxin-3	**AgiTX -3**	*Leiurus quinquestriatus var. herbraeus*	Scorpion	Kv1.3	(Garcia et al., 1994)
Charybdo-toxin	**ChTX**	*Leiurus quinquestriatus var. herbraeus*	Scorpion	Kv1.2, 1.3	(Grissmer et al., 1994)
αDendrotoxin	**αDTX**	*Dendroaspis angusticeps*	Snake	Kv1.1, 1.2, 1.6	(Grissmer et al., 1994; Grupe et al., 1990)
βDendrotoxin	**βDTX**	*Dendroaspis angusticeps*	Snake	Kv1.1, 1.2	(Hopkins et al., 1996)
γDendrotoxin	**γDTX**	*Dendroaspis angusticeps*	Snake	Kv1.1, 1.2	(Hopkins et al., 1996)
δDendrotoxin	**δDTX**	*Dendroaspis angusticeps*	Snake	Kv1.1, 1.6	(Hopkins, 1998; Imredy et al., 1998)
Dendrotoxin I	**DTX_I**	*Dendroaspis polylepis*	Snake	Kv1.1, 1.2	(Hopkins, 1998)
Dendrotoxin K	**DTX_k**	*Dendroaspis polylepis*	Snake	Kv1.1	(Shamotienko et al., 1997)
Hongotoxin	**HgTX**	*Centruroides limbatus*	Scorpion	Kv1.1, 1.2, 1.3, 1.6	(Koschak et al., 1998)
Kaliotoxin	**KTX**	*Androctonus australis*	Scorpion	Kv1.1, 1.3	(Grissmer et al., 1994)
Margatoxin	**MgTX**	*Centruroides margaritatus*	Scorpion	Kv1.1, 1.2, 1.3	(Garcia-Calvo et al., 1993) (Suarez-Kurtz et al., 1999)
Mast Cell Degranulating Peptide	**MCD**	*Apis mellifera*	Bee	Kv1.1, 1.2, 1.6	(Grissmer et al., 1994; Grupe et al., 1990; Stuhmer et al., 1989)
Noxiustoxin	**NxTX**	*Centruroides noxius*	Scorpion	Kv1.2, 1.3	(Grissmer et al., 1994)
Stichodactyla toxin	**ShK**	*Stichodactyla helianthus*.	Sea anemone	Kv1.1, 1.2, 1.3, 1.4, 1.6,	(Kalman et al., 1998; Middleton et al., 2003; Suarez-Kurtz et al., 1999)
Tityustoxin Kα	**TsTX-Kα**	*Tityus serrulatus*	Scorpion	Kv1.2, 1.3	(Hopkins, 1998; Rodrigues et al., 2003)

Table 2.2 │ Details of toxins known to block Kv1 channels

there are some functional residues in the C-terminal of the DTX_I molecule (Katoh et al., 2000). The study went on to examine the possibility of the toxin possessing a functional diad or triad of residues crucial for channel binding, as have been discovered in sea anemone and scorpion toxins (Honma and Shiomi, 2006). Two putative triads were identified; Lys19/Tyr17/Trp37 and Lys5/28/29 (**Fig. 2.5c**). Conversely, binding of αDTX (the DTX_I angusticeps homologue, see **Table 2.1**) only depends on residues at the N terminus for binding, with those in the β-hairpin (the location of the DTX_I Lys19/Tyr17/Trp37 triad) being unimportant. In fact, three residue differences between αDTX and DTX_I at positions 18, 34 and 36 result in large changes in the electrostatic potential of the domain. Thus, the more acidic residues surrounding Lys19 of αDTX are suggested to disturb interactions between it and negatively charged residues of the K^+ channel pore (Katoh et al., 2000). It had been suggested that the fact that DTX_k has two areas of residues vital for binding (in the β-hairpin and the 3_{10}-helix) compared with only one for αDTX (those at the N-terminus and not the β-hairpin) could be responsible for the very selective nature of DTX_k (blocking only Kv1.1 channels) compared to αDTX (inhibits Kv1.1, 1.2 and 1.6), as a larger proportion of the toxin molecule interacts with the channel pore therefore requiring a higher degree of pore sequence specificity (**Table 2.2**) (Gasparini et al., 1998; Wang et al., 1999a). However, if DTX_I does in fact have two binding triads, this does not translate into α subunit specificity as DTX_I inhibits Kv1.1 and 1.2 channels (Table 2.2). It could though account for the higher binding affinity to rat brain membranes of DTX_I over αDTX (Katoh et al., 2000).

A study of the energetic and structural interactions between δDTX and the *Shaker* K^+ channel, with the pore region mutated to resemble that of Kv1.1 (Imredy and MacKinnon, 2000) found that a triangular patch of 7 amino acids formed the interaction surface of the toxin. In agreement with results gathered for subfamily member DTX_k, the vital residues for δDTX binding are in the 3_{10}-helix and the β-hairpin (Imredy and MacKinnon, 2000). The authors propose that the asymmetric ligand binds off-centre to the pore, interacting predominantly with the turret region of one α subunit and contacting the 2 adjacent subunits, therefore, not interacting with all 4 subunits equally (see **Fig. 2.6** for schematic). Assuming that a single toxin molecule binds per channel, the result is 4 possible orientations involving different combinations of the channel forming subunits. Such an interaction would render a

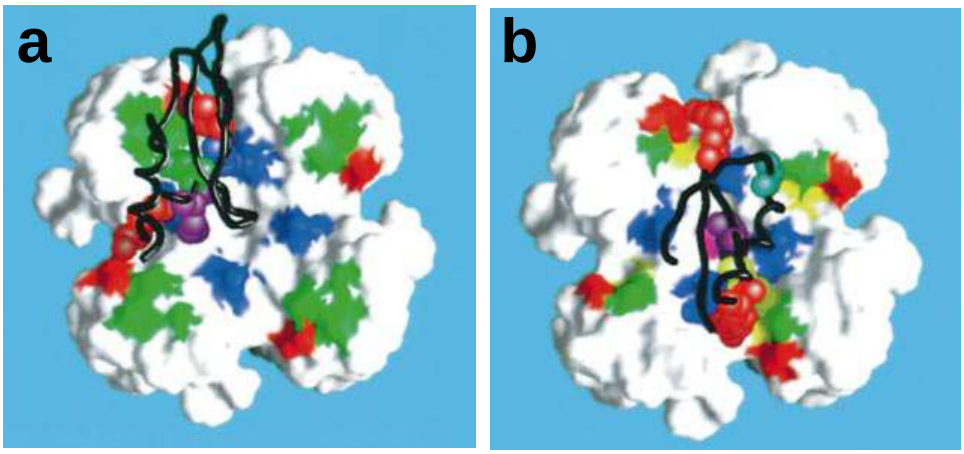

Figure 2.6 | Hypothetical binding orientation of snake and scorpion toxins. **a**, δDTX bound to the mutant Shaker K^+ channel. The channel is shown looking directly down the pore from the extracellular side. Lys6 of δDTX is shown in purple. **b**, Binding orientation of agitoxin 2 on the K^+ channel based on mutant cycle analysis of its interaction with the Shaker channel (MacKinnon et al., 1998; Ranganathan et al., 1996). The channel is in the same orientation as in **a**. The purple residue on AgiTX-2 is Lys27 which interacts with the external K^+ binding site of the channel and, thus, acts as a "plug"' in the pore (Park and Miller, 1992; Ranganathan et al., 1996). The toxin backbones are shown as a black line. Taken

channel with bound DTX not completely, physically blocked, conveniently explaining the residual flow of current through certain channels even in the presence of very high toxin doses. The authors put forward 2 possible explanations for the mechanism of inhibition of the channels; that the positively charged toxin acts as a K^+ repellent or, more likely, that a DTX molecule attached to a turret results in a more rigid pore structure which could then negatively influence the flow of ions (Imredy and MacKinnon, 2000).

2.7.2 Scorpion toxins Scorpion toxins that inhibit K^+ channel activity have homologous primary amino acid sequences (Garcia et al., 2001; Garcia et al., 1998). There have been at least 26 subfamilies identified as of 2008 (α-KTx_{1-26}) (Shijin et al., 2008), with the isolation

of scorpion toxins being a very active field [some examples include: (Abbas et al., 2008; Abdel-Mottaleb et al., 2008; Corzo et al., 2008; Shijin et al., 2008; Srairi-Abid et al., 2008). These peptides are 30-40 amino acids in length, with 3 or 4 disulphide bridges which link 3 anti-parallel β strands with an α helical region (see **Table 2.3** for the sequences of some toxin examples). This results in a very compact structure where all the residues are in solution, with the exception of the cysteines which are buried in the peptide (**Fig. 2.7**) (Garcia et al., 2001; Garcia et al., 1998). On the whole, scorpion toxins are less specific than DTXs as they inhibit other families of Kv channels besides Kv1 such as Ca^{2+}-activated (K_{Ca}) channels [e.g. Charybdotoxin (ChTX), and NxTX] (some examples are listed in **Table 4.4**). Although divided into sub-families based on sequence homology, toxins across these sub-families inhibit Kv1 channels e.g. ChTX (α-KTx_1), NxTX (α-KTx_2) and the agitoxins (AgiTXs) (α-KTx_3) (Hopkins et al., 1996).

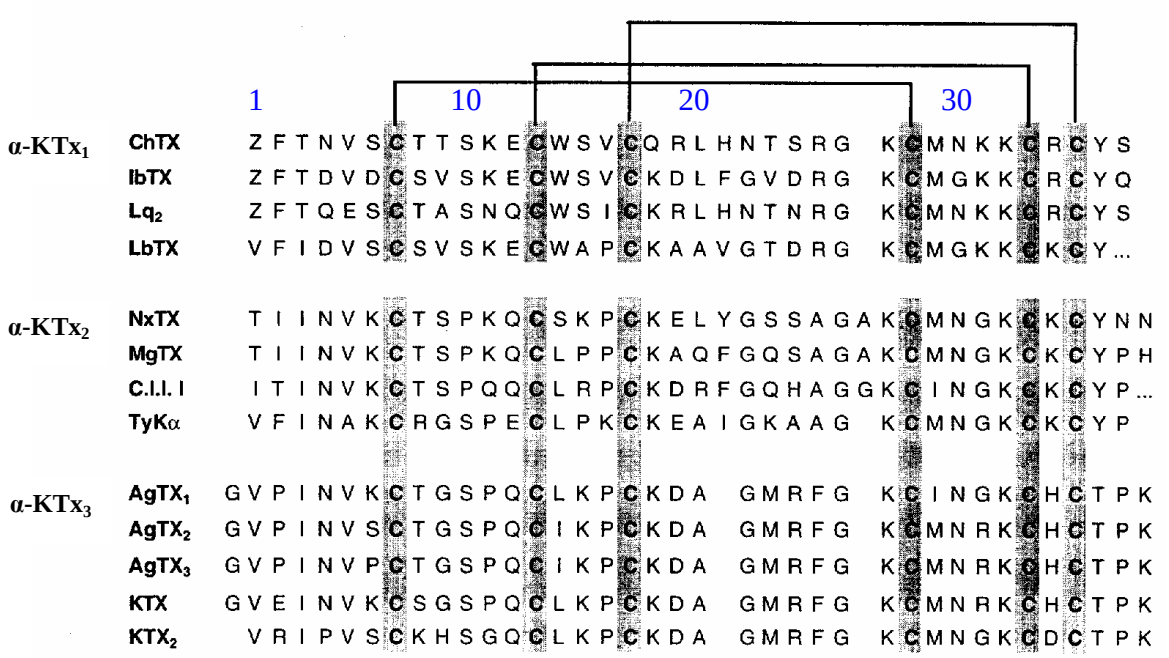

Table 2.3 | Comparison of the amino acid sequences of various scorpion toxins, aligned with respect to the 6 cysteine residues (bold). The position of the disulphide bonds is indicated. ChTX – carybdotoxin, IbTX – iberiotoxin, Lq2 – *L. quinquestriatus* toxin 2, LbTX – limbatustoxin, NxTX – noxiustoxin, MgTX – margatoxin, C.l.l. I - *C. limpidus limpidus* toxin I, TyKα – tityustoxin-Kα, $AgTX_1$ – agitoxin 1, $AgTX_2$ – agitoxin 2, $AgTX_3$ – agitoxin 3, KTX – kaliotoxin, KTX_2 – kaliotoxin 2. Taken from (Garcia et al., 1998)

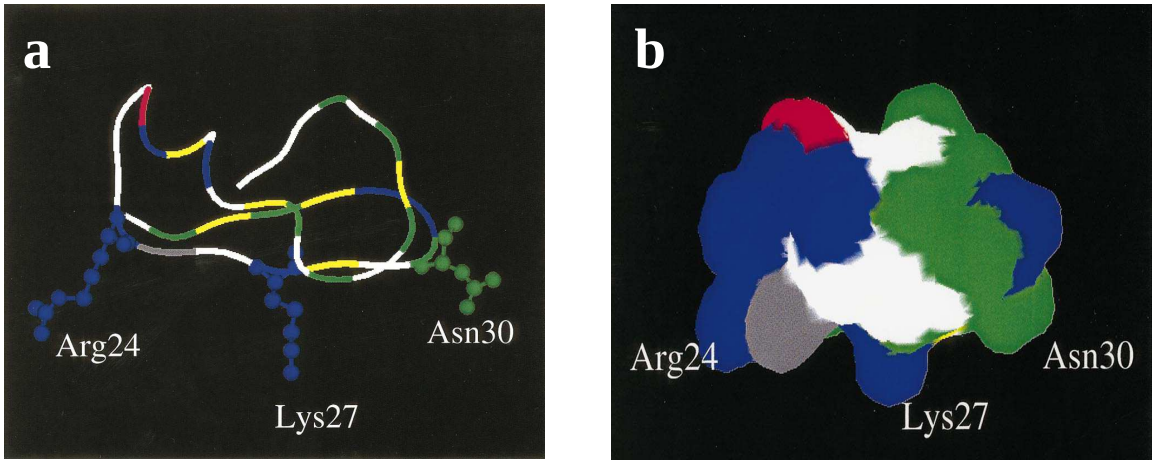

Fig 2.7 | Backbone and three-dimensional structures of agitoxin-2. Structure showing side chains that are vital for binding to the *Shaker* channel; a, backbone structure and b, three-dimensional structure. Colours represent residues with the following properties: white, hydrophobic; green, polar; red, negatively charged; blue positively charged; gray, aromatic; yellow, cysteine. Taken from (Garcia et al., 2001).

Like the dendrotoxins, several scorpion toxins also block Kv1.1, 1.2 and 1.6 though, interestingly, several also target Kv1.3 [e.g. margatoxin (MgTX)] (Hopkins et al., 1996). Subunit sensitivities for some of these toxins are given in **Table 2.2**. While DTXs and scorpion toxins interact with many of the same amino acids on Kv1 channels (Imredy and MacKinnon, 2000), they bind in slightly different places. Scorpion toxin binding, like DTX, is governed by electrostatic interactions between negative residues of the channel and positive residues of the toxin, the lysine at position 27 having been identified as crucial for binding of several toxins including ChTX and AgiTX-2 (**Fig. 2.7**) (Garcia et al., 2001). The positively charged side chain of the residue lies physically close to the K^+ binding site in the ion conduction pore and, therefore, its location in the toxin/channel complex is near the centre of symmetry in the tetrameric channel structure (Garcia et al., 2001). Therefore, scorpion toxins bind in the centre of the pore and physically "plug" it, compared with the off-centre interaction of DTXs. AgiTX-2, for example, fits between the channel turrets competing for the K^+ binding site, thereby, obstructing the pore (Imredy and MacKinnon,

2000) (see schematic **Fig. 2.6**). Indeed, the size of the residue at position 425 of the *Shaker* channel can sterically prevent peptides from reaching their binding site (Garcia et al., 2001).

2.7.3 Sea anemone toxins These are rich sources of both voltage-gated Na^+ and K^+ channel toxins (Honma and Shiomi, 2006). The Kv1 channel blockers include Stichodactyla toxin, ShK, isolated from the Caribbean sea anemone, *Stichodactyla helianthus,* BgK from *Bunodosoma granulifera* and HmK from *Heteractis magnifica*. They are 35 – 37 amino acids long with 3 conserved disulphide bridges; 3-35, 12-28 and 17-32. Amino acids serine at position 20, lysine at 22 and tyrosine at 23 are completely conserved in all sea anemone Kv1 blockers. They are vital for the binding of ShK to both rat brain membranes and Kv1.1, 1.2, 1.3 and 1.6. The lysine and tyrosine residues have been identified as having particular importance, similar to the dyad found in scorpion toxins (e.g. lysine 27 and tyrosine 36 for ChTX). Despite a different molecular scaffold, the dyads of both scorpion and sea anemone toxins superimpose in the three-dimensional structures (Honma and Shiomi, 2006). ShK, like scorpion toxins, binds centrally to the outer vestibule of channels, plugging the pore (Lewis and Garcia, 2003).

2.8 Classical K^+ channel blockers

Tetraethylammonium (TEA) and 4-aminopyridine (4-AP) block various families of K^+ channels and many Kv1 α subunits are sensitive to them. TEA is a quarternary ammonium cation consisting of four ethyl groups attached to a central nitrogen atom (**Fig. 2.8a**). While it can bind to both intra- and extracellular sites of a K^+ channel (Lenaeus et al., 2005), in these experiments it was applied externally. An aromatic amino acid residue at the equivalent of position 449 of the *Shaker* channel is required for extracellular channel block by TEA (MacKinnon and Yellen, 1990), and all four subunits of a channel make an energetic contribution to the binding of a molecule of TEA (Heginbotham and MacKinnon, 1992; Kavanaugh et al., 1992). 4-AP is a small molecule (**Fig. 2.8b**) that requires membrane depolarization, i.e. open channels, to block. For a channel to become unblocked, depolarization is again required demonstrating that 4-AP becomes trapped in closed channels (Armstrong and Loboda, 2001; Choquet and Korn, 1992).

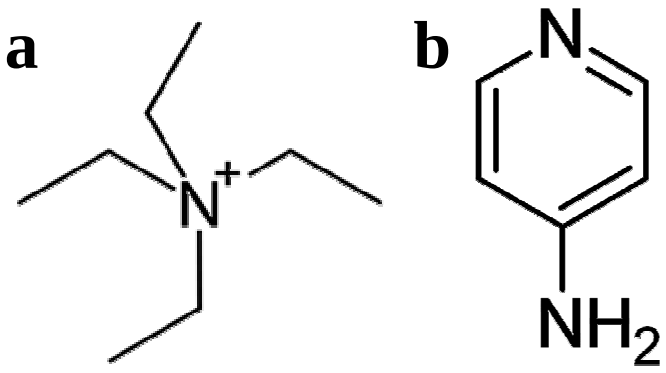

Figure 2.8 | Structures of the classical K+ channel blockers tetraethylammonium (**a**) and 4-aminopyridine (**b**)

While 4-AP does not block channels from the outside, it can block when applied extracellulary therefore it must cross the cell membrane. The difference between the extra (lower) and intracellular (higher) pH of a cell is a key factor in the potency of 4-AP. Therefore it is likely that the molecule crosses the membrane in an unionised form, and blocks the channel from the inside once it is re-ionised .(Choquet and Korn, 1992).

2.9 Investigation of relevant channels

While expression of Kv1 α subunit genes (with or without the accompanying β subunits) yields distinct voltage-dependent K^+ currents, the biophysical and pharmacological properties of these channels rarely matches those of native K^+ currents recorded from neurons. This highlights the need to establish the subunit compositions of authentic neuronal Kv1 channels so that insight into channel structure and function can be obtained from the biophysical and pharmacological properties of exact, recombinantly reconstructed channels (Dolly and Parcej, 1996). This is especially important given that mutations of these channels are implicated in various channelopathies such as Episodic Ataxia 1, some epilepsies and even Multiple Sclerosis (Lehmann-Horn and Jurkat-Rott, 1999; Manganas et al., 2001; Zuberi et al., 1999), and the development of successful therapeutics depends on the availability of an authentic target for drug development. The theoretically possible

number of channels that could be produced from homo- and hetero-tetrameric combinations of the 6 α subunit genes alone is manifold. However, only a subset of the potential oligomers have been identified (Coleman et al., 1999; Koschak et al., 1998; Scott et al., 1994a; Shamotienko et al., 1997), most of which are heteromers, suggesting that these combinations may confer properties suited to the role of a channel at a particular location. This emphasises the importance of studying physiologically-relevant channels unlike numerous studies performed solely on homomeric Kv1 channels [e.g. (Garcia et al., 1994; Grissmer et al., 1994; Hopkins, 1998; Stuhmer et al., 1989)].

As isolating native channels from mammalian brain is not a practical approach for supplying adequate material for investigation of blockers, development of recombinant technology to produce physiologically relevant channels (detailed later in Chapter 6) is a vital step for continued exploration of these proteins.

2.10 Potential utilisation of the specific inhibition of Kv1 channels by peptide toxins

The value of peptide toxins as blockers of Kv1 channels has already been demonstrated, through the use of DTXs and scorpion toxins to purify channels from native tissue and determine their specific subunit compositions (Koch et al., 1997; Koschak et al., 1998; Wang et al., 1999b). Additionally, scorpion toxins have been used to determine the pore region of channels (MacKinnon and Miller, 1989). It is these venom-isolated peptide toxins that currently offer the best hope for brain heteromer-specific Kv1 blockers. Understanding their interactions with physiologically-relevant oligomers, in contrast to the homomers more usually studied, will aid in the pharmacological profiling of Kv1 channels. Finding and/or developing blockers specific for defined heteromers would prove particularly useful in assigning a molecular basis for K^+ currents recorded from neurons. Perhaps most importantly, there is potential for such molecules to contribute to future therapeutics.

There are features of these toxins that in all likelihood would prohibit them from being directly used in a clinical situation. For example, such peptides do not cross the blood-brain barrier, their bioavailability would preclude oral administration requiring instead intravenous, intramuscular or subcutaneous administration, and they are likely to trigger immune responses (Lewis and Garcia, 2003). However, using the toxins as templates to design small molecules that mimic their action could achieve the hetero-oligomeric specific

inhibition required, targeting localised channel populations which would surely decrease adverse side effects.

2.11 Rb^+ efflux assay for high-throughput screening of specific blockers for Kv1 hetero-tetramers

Large scale profiling of a library of peptide toxins requires not only a convenient source of native-like targets but also a suitable system for determining channel/toxin interactions.

Typically, electrophysiological recordings are the gold standard for ion channel measurements; these are very accurate but incredibly time consuming and, as such, not suitable for screening. Ion channel activity has previously been quantified by flux assays. In the case of K^+ channels with equal conductivity for Rb^+, inhibitors have been tested for blockade of the efflux of radioactive $^{85}Rb^+$. However, the use of such high-energy radioisotopes for large scale screens would not be favourable due to their associated hazards, especially in large quantities. Moreover, the expense of the isotope, as well as its disposal, is of major concern.

As an alternative, a high-throughput, non-radioactive Rb^+ efflux assay has previously been described (Terstappen, 1999). Cells expressing the channel of interest are loaded with Rb^+ and its release upon K^+ depolarisation, in the presence and absence of inhibitors, quantified by atomic absorption spectroscopy (AAS). The 96-well format of this assay makes it very attractive for screening applications. The potential for automation of the assay was considered, but analysis of AAS samples was thought to be a limiting step (Terstappen, 1999). Modifying conventional atomic absorption spectrometers to cope with the smaller samples volumes provided by a microplate format, coupled with attached auto-samplers has allowed AAS to become a high-throughput technique (Ford et al., 2002). This is, therefore, a very practical assay for screening large numbers of compounds in the search for blockers of native-like Kv1 channels composed of specific combinations of α subunits.

2.12 Aims of this study

Many peptide toxins have been shown to block Kv1 channels, mostly through investigation of recombinant homomeric channels as it is the α subunit composition that confers sensitivity to these blockers (Grissmer et al., 1994; Gutman et al., 2005), and the expression

of α subunit cDNAs alone forms active channels (Scott et al., 1994b). In the main, Kv1 channels from mammalian brain are composed of heteromeric combinations of α subunits (Shamotienko et al., 1997). As different compounds require contributions from various subunits for binding (Akhtar et al., 2002; Heginbotham and MacKinnon, 1992), it is possible that screening heteromeric channels will identify toxins with effects unpredictable from looking at parental monomers alone. Such inhibitors could act as useful tools for characterising and distinguishing the specific oligomers responsible for K^+ currents recorded in neurons. Given the many advantages of the Rb^+ efflux assay for high-throughput screening of K^+ channel inhibitors, it was highly desirable to establish and optimise this technique for determining their effects on concatenated α subunit combinations, expressed in mammalian cells. Automation of the efflux assay would expand the scope to screen numerous potential blockers against all the available heteromeric channels. Electrophysiological recordings and radio-labelled toxin binding experiments could confirm results obtained by this newly-established assay and provide functional characterisation of such expressed channels. In this way, the effects of many toxins on heteromeric channels could be analysed, for the first time, and toxins selective for such channels identified.

Ultimately this research aimed to express channels with compositions mimicking those elucidated from mammalian brain, and to characterise them according to their biophysical and pharmacological properties. Recreation of such native-like tetramers would provide authentic targets for development of future therapeutics.

Chapter 3
Materials and Methods

3.1 Materials

Restriction enzymes were purchased from New England Biolabs, Klenow DNA polymerase from Epicentre Biotechnologies, SP6 polymerase and RNase inhibitor from Roche, pSFV plasmid, pCR-blunt plasmid, DH5α competent cells, SOC medium and Lipofectamine 2000 transfection reagent from Invitrogen; 0.5% trypsin/EDTA, L-glutamate, ab/am solution, Geneticin, Opti-MEM medium and sterile PBS (for tissue culture) were bought from Gibco. HiSpeed plasmid purification kits and Polyfect were from Qiagen. pβUT2 was a gift from A. Rodaway, Kings College, London, pIRES2-EGFP plasmid was from Clontech and Kv1.X sequences in pAKS plasmid were a gift from Prof. O. Pongs. Calbiochem supplied MOWIOL. Protein molecular weight markers were purchased from Biorad. Mouse monoclonal anti-Kv1.2 antibody was generated against K^+ channels purified from bovine brain (Muniz et al., 1992), Kv1.2 antibody directed against external epitopes was a gift from Prof. J.S. Trimmer; Kv1.3 and Kv1.6 antibodies were from Santa Cruz and Abcam, respectively, and all AF conjugated secondary antibodies from Molecular Probes. Kv1.2 (clone K14/16), Kv1.4 (clone 13/31) and Kv1.1 (clone 20/78) antibodies for immuno-labelling total channel populations were bought from Neuromab. α and δDTX and DTX_k were isolated from the venoms of *Dendroaspis angusticeps* and *polylepis*, respectively (Dolly, 1992). 4-AP and TEA were purchased from Lancaster Synthesis, Shk and Tityustoxin-Kα (TsTX-Kα) from Peptides International; all other toxins tested from Alomone Labs. ^{125}Iodine was from Aim Research Company, Rb^+ standard for atomic absorption spectroscopy from Acro Organics and BCA (bicinchoninic acid) assay kit from Pierce. All other chemicals including tissue culture reagents were from Sigma.

3.2 Molecular biology procedures

3.2.1 Generation of Kv1.1-1.2 cRNA Kv1.1-1.2–pSFV1 cRNA was prepared by Dr. O. Shamotienko. DNA, as described previously (Akhtar et al., 2002), was linearised with Spe1 restrictase and used to generate capped cRNA with SP6 polymerase. This entailed

incubating 15 µg of DNA and 20 µl of SP6 polymerase plus 15 µl of RNase inhibitor in a total volume of 500 µl at 37°C for 1.5 h, before adding another 10 µl of the enzyme and continuing the incubation for 1.5 h. The resultant cRNA (~3.25 mg/ml) was stored in aliquots as an ethanol precipitate at -80°C; for reconstitution, the samples were centrifuged, ethanol removed and the pellet dissolved in sterile PBS.

3.2.2 Preparation of Kv1.1-1.2 and 1.6-1.2 pIRES2-EGFP constructs These were made by Dr O. Shamotienko as described in (Sokolov et al., 2007), including Kv1.1, 1.2 and 1.6 monomers. pIRES2-EGFP plasmid contains an internal ribosomal entry site (IRES), from the encephalomyocarditis virus (ECMV), between a multiple cloning site (MCS) and an EGFP cloning region. This allows both the gene of interest (cloned into the MCS) and EGFP to be translated from the same mRNA strand. EGFP is a variant of wild-type green fluorescent protein (GFP), optimised for brighter fluorescence and enhanced expression in mammalian cells; expression simplifies the monitoring of transfection efficiency, channel expression and selecting cells for electrophysiological recordings.

Kv1.1-1.2 Spe I and BamH I restrictases were used simultaneously to digest Kv1.1-1.2 pSFV (Akhtar et al., 2002) followed by blunting of the 5'-overhangs of the product with Klenow DNA polymerase. pIRES2-EGFP was digested with Bgl II and Sma I and similar blunting of the 5'-ends was again performed. Both the digested insert and plasmid were purified by agarose gel electrophoresis, and the 1.1-1.2 insert was ligated into the pIRES2-EGFP plasmid. Restriction mapping with Nhe I and Pst I was used to check the orientation of the insert once DNA had been prepared from single colonies of transformed DH5α cells. DNA was then purified on a larger scale using a HiSpeed plasmid purification kit.

Kv1.6-1.2 In preparation for assembling the Kv1.6-1.2 pIRES2-EGFP plasmid, the following forward and reverse primers were used to amplify Kv1.6 and 1.2 constituents from pAKS plasmid: Kv1.6 – forward, TCG A<u>CT CGA G</u>CC GCC ACC ATG AGA TCG GAG AAA TCC C and reverse, TCG A<u>GG ATC C</u>GA CCT CCG TGA GCA TTC TTT TC (without a stop codon) and Kv1.2 – forward, CGA <u>CTC GAG</u> ATG ACA GTG GCT ACC GGA G and reverse, TCG A<u>GG ATC C</u>TC AGA CAT CAG TTA AC, with Xho I and BamH I restriction sites underlined on the forward and reverse primers, respectively.

The PCR reaction was as follows: 2 min denaturation followed by 22 cycles of: 94°C, 30 s; 55°C, 45 s; 75°C, 2 min. Following agarose gel electrophoresis purification, PCR products were cloned into pβUT2 plasmid after both were digested with Xho I and BamH I. Next, Kv1.6 pβUT2 was incubated with BamH I and the 5'-overhangs blunted, as above with Klenow DNA polymerase. EcoR I was then used to remove the 3'-untranslated region (UTR) flanking the pβUT2 MCS (Akhtar et al., 2002). To remove the Kv1.2 insert with its 5' and 3' UTRs, the Kv1.2 pβUT2 plasmid was incubated with Hind III and 5'-overhangs were blunted followed by digestion with EcoR I. After purification, the Kv1.6 pβUT2 plasmid and Kv1.2 insert were ligated yielding the Kv1.6-1.2 pβUT2 plasmid, with the Kv1.6 and 1.2 connected by the 5'-UTR. Confirmation that monomeric constituents were in the same open reading frame (ORF) was achieved using a forward primer based on the 3'-region of Kv1.6 and the reverse based on the 5'-region of Kv1.2. In order to subclone Kv1.6-1.2 into pIRES2-EGFP, the 2 plasmids were incubated with Hind III and Xho I, respectively, followed by blunt ending of 5'-overhangs, and digestion with EcoR I. The insert and plasmid were purified and semi-directionally cloned, and Kv1.6-1.2 pIRES2-EGFP formed; DNA was prepared from single colonies of transformed DH5α cells, using a Qiagen plasmid purification kit.

3.2.3 Cassette cloning system This was developed as described in (Shamotienko et al., 2008), by Dr O. Shamotienko, Dr J. Wang and Prof J. O. Dolly. Dr O. Shamotienko and Dr M. Bodeker prepared the constructs. A modified pβUT2 plasmid was the source of a proven inter-subunit linker as above and in (Akhtar et al., 2002).

3.2.3a PCR amplification of Kv1.X–constituents Rat Kv1.1-, 1.2-, 1.3-, 1.4- and 1.6-pAKS plasmids were used as PCR templates; their amplification was achieved using the primers detailed in **Table 3.1** which incorporated Xba I and Xho I restriction sites at the 5' and 3' ends, respectively. The conditions for amplification using Pfx high fidelity polymerase were: initial denaturation, 95°C for 2 min, then 22 cycles of amplification with each cycle comprising denaturation, 94°C for 30 s, annealing at 58°C for 45 s and elongation at 72°C for 2 min. PCR-products were purified by electrophoresis on agarose gel and cloned into the 'intermediate' pCR-blunt plasmid; competent DH5α cells were transformed with the

Rat Kv1 α Subunits	Forward primer (with Xba I site underlined)	Reverse primer (-STOP)* (with Xho I site underlined)
Kv1.1	G TCTAGA AT GAC GGT GAT GTCAGG GGA GAATGC	G CTCGAG AA CAT CGG TCA GGA GCT TGC TCT TAT TAAC
Kv1.2	GTCTAGAATGACAGTGGCTACCGGAGA C CCAGTGG	G CTCGAG GA CAT CAG TTA ACA TTT TGG TAATAT TCAC*
Kv1.3	GTCTAGAATGACCGTGGTGCCCGGGG AC CACCTG	GCTCGAGGACATCAGTGAATATCTTTTT GATGTTGACAC
Kv1.4	GTCTAGAATGGAGGTGGCAATGGTGAG TGCC	GCTCGAGGACACATCAGTCTCCACAGC CTTTGCATTAG
Kv1.6	GTCTAGAATGAGATCGGAGAAATCCCT TACGC	GCTCGAGGAGACCTCCGTGAGCATTCT TTTCTCTGC
Subunit domain in pIRES2 plasmids (with restriction site)	Forward primer (restriction site underlined)	Reverse primer (restriction site underlined)
I (Nhe I – Bgl II)	AGCTAGCAGAATAAACGCTCAACTTTG GCAGATC	GAGATCTCCAGATCCGGTACCAGATCG ATCTCGAC
II (Bgl II – EcoR I)	GAGATCTAGAATAAACGCTCAACTTTGG CAGATC	CGAATTCCCAGATCCGGTACCAGATCG ATCTCGAC
III (EcoR I – Sal I)	CGAATTCAGAATAAACGCTCAACTTTGG CAGATC	AGTCGACCCAGATCCGGTACCAGATCG ATCTCGAC
IV (Sal I – BamH I)	AGTCGACAGAATAAACGCTCAACTTTG GCAGATC	AGGATCCCCAGATCCGGTACCAGATCG ATCTCGAC

* Reverse primer for Kv1.2 (+STOP): G CTCGAG TT ATC AGA CAT CAG TTA ACA TTT TGG TAA TAT TCAC

Table 3.1│ Cassette cloning primers. **Upper panel:** specific primers used for amplification of Kv1.X subunits, with Xba I and Xho I sites on forward and reverse primers, respectively, to facilitate subsequent cloning into pβUT2. Only Kv1.2 was engineered with two STOP codons. **Lower panel:** UTR specific primers for amplifying rat Kv1 subunits, incorporating linker sequences from pβUT2 and restriction sites allowing position-dependent cloning of individual subunits (with flanking linker) into corresponding domain positions within the pIRES2 MCS. The UTR-specific primers differed only by domain–specific flanking restriction sites.

ligated products. DNA was prepared on a large scale from positive clones; after digestion with Xho I and Xba I, inserts were purified by agarose gel electrophoresis and subcloned into pβUT2, using Xho I and Xba I sites.

3.2.3b Modification of pβUT2 plasmid and cloning of Kv1.X inserts with flanking half-linkers Sal I, BamH I and Bg1 II sites of the MCS of pβUT2 plasmid were eliminated by sequential in-filling to prevent their interference with subsequent assembly of oligomeric constructs into pIRES2-EGFP or-DsRed plasmids. Purified Kv1.X inserts were ligated into mutated pβUT2 plasmid and positive clones identified by digestion with Xba I and Xho I enzymes. These acted as templates for the subsequent PCR. The forward and reverse primers used were based not on the Kv1.X genes but on the first (up to the Xba I site) and last (downstream of Xho I site) 30 nucleotides of the UTRs of the *Xenopus* β-globin gene flanking the MCS of pβUT2 (**Table 3.1**). Restriction sites introduced during this PCR allowed positional cloning into the pIRES2-EGFP or-DsRed mammalian expression vectors (see later). PCR amplification was performed under the same conditions as before; single bands of the expected size were purified by agarose gel electrophoresis, cloned into pCR-blunt plasmid and assembled into the pIRES plasmids. All constructs were verified by DNA sequencing.

3.2.3c Assembly of Kv1.X tetrameric constructs Paired sites for Nhe I/Bgl II, Bgl II/EcoR I, Eco RI/Sal I, and Sal I/BamH I, respectively, were used to individually sub-clone the genes from pCR-blunt into domains I to IV of pIRES2-EGFP or -DsRed. In the same way, dimeric combinations of channels could be constructed, by sub-cloning only 2 Kv1.X genes into the pIRES2 vectors with the ORF still maintained. In these instances, positions 3 and 4 were occupied. Correct positioning of all the constructs in pIRES2 plasmids were confirmed by restriction analysis. Concatenated Kv1 channel constructs were expressed in HEK-293 (HEK) cells (except where stated) and experiments performed 48 h after transfection.

3.2.4 Transforming competent cells Competent *E. coli* DH5α cells, stored at -80°C, were thawed on ice and 50 µl aliquoted into pre-cooled tubes containing the required DNA.

Following a 30 min incubation of the cells and DNA on ice at 4°C, they were heat shocked with 20 s in a water bath at 42°C, then returned to ice for a further 20 min; 950 μl of SOC medium was added and the mixture transferred to a larger tube for incubation in a shaker incubator for 90 min at 220 rpm and 37°C. The resultant culture (100 μl) was spread on a kanamycin (50 μg/ml) plate and cultured overnight at 37°C. If individual colonies were not visible, a second kanamycin plate was streaked from the first as DNA preparation requires individual colonies.

3.2.5 Preparation of DNA This was prepared using HiSpeed plasmid purification kits (midi and maxi), according to the manufacturer's instructions. A single colony was picked from plate previously streaked with transformed bacteria and cultured in 50 μg/ml kanamycin LB medium (5 ml) for 8 h at 37°C and 300 rpm. Once this starter culture had begun to grow (i.e. the medium had become cloudy), it was used to inoculate a 200 ml culture (also containing 50 μg/ml kanamycin in LB medium) which was grown overnight under the same conditions. The following day, bacteria were pelleted by centrifugation at 6000 g for 15 min at 4°C. The pellet was resuspended in buffer P1 followed by addition of the alkaline lysis buffer P2, thorough mixing, and a 5 min incubation. Buffer P3 was then added, neutralising the mixture and precipitating genomic DNA, proteins and cell debris. The lysate was incubated in a QIAfilter cartridge for 10 min, during which time a HiSpeed tip was equilibrated using Buffer QBT. The cell lysate was then filtered into the prepared tip and the resultant cleared lysate left to pass through the tip, before washing with Buffer QC. DNA collected in the HiSpeed tip was then eluted with buffer QF, precipitated with isopropanol and put through a QIAprecipitator which collects the DNA. Ethanol (70%) was passed through the precipitator to wash the DNA following which air was pushed through twice to remove any ethanol left over. Finally, the DNA was eluted in TE buffer.

3.3 Cell culture techniques

3.3.1 Mammalian cell lines CHO, HEK and COS-7 (COS) cells were maintained in Dulbecco's Modified Eagle's Medium (DMEM), supplemented with 10% FCS, ab/am solution and L-glutamate, as adherent cultures in a 5% CO_2 incubator at 37°C. Once cells had grown to 80% confluency, they were harvested by trypsinisation and re-plated.

Trypsinisation was performed following removal of culture medium and 2 PBS washes of the cell layer; 0.5% trypsin/EDTA solution was then added for approximately 5 min. Once the cells were detached, supplemented DMEM was added resulting in inactivation of the trypsin by the serum in the medium, which contains trypsin inhibitors. Cells were then processed as required.

3.3.2. Electroporation of cells with cRNA (used for expression of the Kv1.1-1.2 channel in CHO cells) An 80% confluent 75 cm^2 flask was harvested and washed twice by centrifugation at 160 g for 5 min followed by re-suspension in sterile PBS. After the final wash, cells were resuspended in 0.8 ml PBS containing 75 µg cRNA. This mixture was transferred to a 0.4 cm electroporation cuvette and 2 pulses of 850 V, with a capacitance of 25 uF, were applied. After 1 min, the cells were diluted in supplemented DMEM and plated as necessary. Cells were then kept in a 5% CO_2 incubator at 37°C for 24 h.

3.3.3 Polyfect transfection of cells Cell densities and quantities of DNA, Polyfect and medium were determined from the Handbook supplied by the manufacturer. HEK cells were plated in the required flasks one day prior to transfection such that they were 50% confluent. DNA was diluted in non-supplemented DMEM, mixed well and Polyfect then added. The mixture was left for 10 min for complex formation to occur during which time growth medium was replaced on the plated HEK cells. Once the incubation time had elapsed, supplemented DMEM was added to the DNA/Polyfect mixture, and the total volume transferred to the cells with gentle swirling to ensure even distribution of the complexes. Cells were then incubated at 37°C, 5% CO_2 for 48 h to allow gene expression.

3.3.4 Transfection of cells using Lipofectamine 2000 HEK cells plated one day previously, in the appropriate culture vessel at a density of approximately 40%, were used for transfections. DNA, Lipofectamine 2000 and medium volumes for the various size culture flasks are given in the manufacturer's instructions. Quantities for a 75 cm^2 flask are given in brackets. DNA (30 µg) and Lipofectamine 2000 (75 µl) were separately diluted with Opti-MEM (1.9 ml) and left for 5 min, following which they were combined and incubated at room temperature for a further 20 min. During this time, growth medium was removed

from the cells to be transfected and following 2 washes with non-supplemented DMEM to remove any traces of serum or antibiotics, an appropriate amount (19 ml) of the same medium was returned to the cells. Following the 20 min incubation, the DNA/Lipofectamine 2000 mixture was also added. Cells were replaced at 37°C, 5% CO_2 overnight. The following day, medium was replaced with supplemented DMEM and cells were re-plated if necessary. When expression levels were not sufficient for functional analysis of channels, the DNA concentration was doubled without altering any other parameters.

3.3.5 Lipofectamine 2000 COS cell transfection for K^+ channel surface labelling COS cells used for surface immuno-staining experiments were plated on poly-l-lysine coated 22x22 mm coverslips in 35 mm dishes at a density of ~8% in 2 ml supplemented DMEM one day prior to transfection. In this instance, 1 μg DNA and 1 μl Lipofectamine 2000 were used for each dish, each diluted with 50 μl Opti-MEM. Once the DNA and transfection reagent had been mixed and incubated for 20 min, COS cells were placed in 0.5 ml of serum-free DMEM after 2 washes in the same. The DNA/Lipofectamine 2000 mixture was added and the cells were incubated at 37°C, 5% CO_2 for 4 h following which medium was replaced with supplemented DMEM and the cells were incubated for a further 2 days.

3.3.6 Establishing Kv1 expressing stable cell lines To prepare HEK cell lines stably expressing Kv1 channels, cells were transfected with the relevant pIRES2-EGFP construct using Polyfect; 48 h post transfection, Geneticin was added to the culture medium at a final concentration of 1 mg/ml. Once the non-transfected cells had died and become detached (approx 2 – 3 weeks) and the surviving cells were growing at a healthy rate, they were re-plated in 24-well plates at a density of 1 cell/well. EGFP expression of the growing cells was monitored via fluorescent microscopy and stock cultures were produced from the brightest colonies.

3.4 Monitoring expression of recombinant channels

3.4.1 Immuno-staining of K^+ channel proteins expressed in CHO cells Following electroporation, CHO cells were plated onto sterile coverslips and incubated in DMEM (as

above) for 24 h. Coverslips were washed three times with PBS before the cells were fixed with 4% PFA (in the same buffer) for 15 min. Following 3 PBS washes, samples were quenched with 50 mM NH_4Cl/PBS for 15 min, and washed again. Permeabilisation was with 0.1% TX-100/PBS for 5 min and another 3 washes followed. The cells were then incubated with a mouse monoclonal antibody specific for Kv1.2 α subunit, diluted in 5% FCS/PBS for 4 h at room temperature. Three further PBS washes followed, before incubation for 2 h at room temperature with goat anti-mouse IgG-conjugated to AF 488 diluted 1:1500 in 5% FCS/PBS, washing and staining with DAPI for 5 min. After a final wash step, coverslips were mounted onto slides with MOWIOL and, once dried, viewed with an Olympus 1X71 microscope using filters appropriate for the fluorophores employed. Control experiments were also performed omitting secondary antibody and, in some cases, untransfected cells were similarly treated to provide a further control.

3.4.2 Immuno-fluorescent labelling of surface Kv1 channels COS cells plated on poly-l-lysine coverslips in 35 mm dished and transfected 2 days previously with Lipofectamine 2000 were processed as described in (Manganas and Trimmer, 2000) with some minor modifications (see Appendix A for buffer compositions). Medium was removed from cells and replaced with 1 ml ice-cold 3% PFA/PBS for 30 min at 4°C. Following 3x5 min washes with chilled PBS, cells were blocked in Tris-buffered milk (blotto) for 30 min. This was followed by incubation with primary antibodies directed against an ecto-domain of Kv1.2, for 2 h at room temperature (10 μg/ml purified IgG in blotto – 750 μl/dish). After 3x20 min washes with blotto, cells were permeabilised with 0.1% TX-100/blotto for 30 min at room temperature, then incubated with a second cytoplasmically-directed primary antibody (used at 10 μg/ml in the same buffer), for 1 h at room temperature. Secondary antibody incubation followed 3x10 min washes in 0.1% TX-100/blotto. These AF conjugated antibodies were used at 1:1500 dilutions, in 0.1% TX-100/blotto, for 45 – 60 min at room temperature. The requisite secondary antibodies for both primaries were combined in a single incubation and where DAPI staining of nuclei was required, it too was included in this step (0.005 μg/ml). Washing with 0.1% TX-100/PBS was the final step before coverslips were mounted on slides, sealed with nail varnish and kept at -20°C overnight. Slides were viewed as detailed above. All primary antibodies were re-used for

further experiments. For controls, primary antibodies were omitted. As fluorescent protein genes are present in the pIRES plasmids used for channel expression, their fluorescence was also viewed to ensure it did not interfere with signals from antibodies.

3.4.3 Western blot analysis SDS-PAGE and Western blotting were performed as described in Section A. Briefly, transiently- and stably-expressing cells were harvested with 0.5 mM PBS/EDTA instead of trypsin/EDTA. Detached cells were resuspended in PBS and after centrifugation the resultant pellet was dissolved in 1xLDS sample buffer (~4 mg/ml protein), heated to 80°C for 10 min, and passed through a 25 G needle. Samples were then run on 4-12% pre-cast gels and following transfer, membranes were developed with Kv1 α subunit-specific primary antibodies, secondaries conjugated to HRP and SuperSignal West Pico Luminol/Enhancer substrate solution.

3.4.4 Biotinylation of surface targeted, expressed channels These experiments were performed by Dr O. Shamotienko. For biotinylation of surface proteins, an aqueous solution (17 µl) of sulphosuccinimydyl-6-(biotin-amido) hexanoate (60 mg/ml) was added to 0.3 ml of cell suspension (5 mg protein/ml) and incubated at 22°C for 1 h. Excess reagent was quenched and removed by 3 washes with PBS containing 100 mM glycine before resuspending the cells in PBS and extracting with 2% TX-100 for 1 h at 4°C. After centrifugation (300 000 g for 1 h), the supernatant was diluted 3-fold and an aliquot (1 ml) incubated at 4°C overnight with a 50% slurry of streptavidin-agarose CL-4B. Loosely-bound unwanted proteins were removed by 3 washes with PBS/0.4 M NaCl and the immobilised proteins dissolved in sample buffer (2x). The resultant samples were subjected to SDS-PAGE and Western blotting with antibodies specific for Kv1.1 or 1.2 (Shamotienko et al., 1999).

3.5 Pharmacological analysis of recombinant Kv1 channels using a Rb^+ efflux assay

3.5.1 Assessment of known K^+ channel blockers on Kv1.1-1.2 channels transiently expressed in CHO cells Rb^+ efflux experiments were performed as described in (Terstappen, 1999), with some modifications (see Appendix B for buffer compositions). Cells electroporated with Kv1.1-1.2-pSFV cRNA were plated in 96-well plates at a density of

50,000 cells/well, in 100 µl of DMEM. The following day, Rb^+ loading was achieved by replacement of culture medium with 300 µl of buffer containing 5.4 mM Rb^+ for 4 h. Extracellular Rb^+ was removed by washing in 25 mM HEPES wash buffer (pH 7.4) using a Biotek 405 *cw* plate washer. Stimulation buffer containing 75 mM K^+ (100 µl) was then applied to cells for 3 min to activate expressed channels. To measure basal (unstimulated) release, some cells were incubated with the wash buffer (containing 0.1 mM K^+), also for 3 min. An aliquot (75 µl) of the supernatants were collected following the stimulation period, after which cells were washed again before being lysed with 100 µl 1% TX-100 for 10 min; 75 µl of lysate was collected and all samples were diluted with 300 µl of ionization prevention (IP) buffer. The supernatant and lysate samples were analysed by AAS, using a Thermo Solaar S4 atomic absorption spectrometer, attached to a Gilson 222XL auto-sampler for loading the samples. Rb^+ concentration was automatically determined from defined standards. The amounts of basal and stimulated release, that is Rb^+ concentration in the supernatants, were expressed as % of total (supernatant + lysate) Rb^+ content.

To ascertain the optimum time required for Rb^+ loading, medium on transfected cells was replaced with the appropriate buffer at various time intervals. Once the incubation time had elapsed, the test plate was washed and 100 µl 1% TX-100 added for 10 min; lysates (75 µl) were collected, diluted and analysed as described above. The optimum concentration of K^+ required to activate the expressed channels was also determined by measuring supernatant [Rb^+] after exposure to stimulation buffer with varying [K^+] ([NaCl] was altered to maintain the isomolar balance). To show that Rb^+ release was indeed due to expressed channels, untransfected CHO cells and those electroporated in the absence of cRNA were similarly analysed. Substances tested for channel blocking ability were either added to the stimulation buffer (4-AP and TEA) or included with the cells for the final hour of Rb^+ loading (αDTX). For experiments on channel blockers, results were expressed as % evoked release ± S.E.M. relative to that for the drug-free control; the evoked increment was calculated by subtracting basal from the stimulated release value. For all experiments, at least eight wells were assayed for every condition and measurements repeated with 3 different batches of electroporated cells.

3.5.2 Characterisation of the pharmacological profiles of Kv1 channels expressed in HEK cells, using a modified Rb^+ efflux assay Alterations to the assay described above were made to suit HEK rather than CHO cells used initially, and to improve application of peptide toxins. Buffer compositions are those used routinely for such cells by Xention Ltd. (Cambridge, UK). HEK cells stably expressing channels and/or those transiently transfected using Lipofectamine 2000, were plated in poly-D-lysine coated 96-well plates (Biocoat, BD Falcon), at a density of 50,000 cells/well in a final volume of 100 µl of culture medium (1 day post transfection for transients). The following day, cells were loaded for 4 h with Rb^+ by replacement of medium with 150 µl of Rb^+ loading buffer, and experiments performed as previously described; however, slightly modified wash and stimulation buffers (see Appendix C for compositions) were employed, and stimulation time for Rb^+ efflux was increased from 3 to 5 min.

Toxins were tested for blocking ability by addition to the cells of 50 µl of a 2x concentration (diluted in 0.01% bovine serum albumin (BSA)/modified wash buffer), following washing. After a 10 min incubation, cells were stimulated with 50 µl 150 mM K^+ modified stimulation buffer (isomolar replacement of NaCl with KCl) resulting in a final concentration of toxin and 75 mM K^+. The assay was continued as previously described. For experiments involving 4-AP and TEA, they were included directly in the stimulation buffer (or in wash buffer for some measurements) as described above. Control wells were included in each experiment for measurement of basal or unchallenged stimulated release. Samples were diluted with 275 µl I.P. buffer before being analysed by AAS as detailed above. Fractional inhibition of evoked Rb^+ release is plotted ± S.E.M., n = >16 wells from measurements made on at least 2 different days. Details of all compounds screened are given in **Tables 2.2** and **4.3**.

3.6 Electrophysiological recordings and data analysis

3.6.1 Analysis of K^+ current evoked from Kv1.1-1.2 channels expressed in CHO (performed by Dr M. Sokolov) K^+ currents were recorded from CHO cells electroporated with Kv1.1-1.2-pSFV cRNA in voltage-clamp, whole cell mode (Hamill et al., 1981). Cells were plated on glass coverslips immediately after transfection, and currents recorded the next day. The extracellular solution contained (in mM): 150 NaCl, 5 KCl, 1.8 $CaC1_2$, 1 $MgCl_2$, 10

HEPES, 5 NaOH, and 10 D-glucose, adjusted to pH 7.4 with HCl. Patch pipettes were pulled from thin-walled borosilicate glass capillaries (1.5 mm OD, 1.2 mm ID); pipette resistance was typically between 2 and 5 MΩ. No compensation was made for series resistance (ranged from 3-7 MΩ). Patch pipettes were filled with a solution containing (in mM) 70 KCl, 70 K-gluconate, 1 $MgC1_2$, 5 EGTA, 10 HEPES, and 10 D-glucose, adjusted to pH 7.4 with KOH. The osmolarity of all extra- and intra-cellular solutions were in the range of 320 ± 7 mOsm. The liquid junction potential was not corrected. The currents were filtered at 1 kHz, and sampled at 5 kHz (or 1 kHz for 60 s pulse). Recordings were made at room temperature (22-24^{o}C), using a HEKA EPC10 amplifier and Pulse software. Pharmacological experiments were performed by applying drugs directly to the recording chamber. Currents were recorded in response to repetitive pulses (200 ms, +40 mV); when stabilised, drugs were applied and the amplitudes obtained for 10-20 pulses averaged, final values for each concentration being taken from at least 3 cells.

3.6.2 Electrophysiological recordings and data analysis from HEK cells stably expressing Kv1.1-1.2 and 1.6-1.2 (described in (Sokolov et al., 2007) and performed by Dr M. Sokolov)

After obtaining stable expression of K^+ channels in HEK cells, K^+ currents were recorded as described above, with some modifications. Currents were filtered at 1 kHz, and sampled at 4 kHz (with the exception of 60 s pulses, which were sampled at 50 Hz). P/4 leak subtraction was used. The membrane holding potential was -60 mV. To determine voltage dependency of activation kinetics after a pre-conditioning pulse to -110 mV for 300 ms, a series of depolarisation steps (400 ms duration) from -60 to +50 mV were applied in 10 mV increments. Current amplitudes corresponding to 40-90% of the maximum were fitted with a single exponential function. Conductance-voltage (G-V) relations were determined from averaged current after 200-300 ms of activation, normalised relative to the K^+ driving force by assuming a reversal potential of -75 mV (measured reversal potential was between -70 and -80 mV). Kinetics of K^+ current deactivation were measured after a 50 ms step to +40 mV. Inactivation was evaluated during 60 s depolarisation steps to +40 mV. To determine steady-state inactivation, cells were maintained at +20 mV for 40 s, followed by 1 s steps to the indicated voltage to remove inactivation, and then stepped to +40 mV to determine the

extent of K^+ current remaining. Time constants were determined by fitting currents with single or double exponential functions of the form:

$$I = A_0 + A_1 \exp(-t/\tau_1) + A_2 \exp(-t/\tau_2) \quad (1)$$

where A_0, A_1 and A_2 are amplitude coefficients, τ_1 and τ_2 time constants.

The voltage-dependence of deactivation was fitted by the equation:

$$\tau = A \exp(-zFE/2.303RT) \quad (2)$$

where A is an amplitude coefficient, z elementary charge, F Faraday's constant, E membrane potential, R gas constant, and T temperature.

Steady steady-state inactivation and conductance-voltage relationships were fitted by a Boltzmann equation of the form:

$$G = G_{max} \{1 + \exp[(V_{½} - V)/k]\}^{-1}. \quad (3)$$

Drugs were applied directly to the recording chamber and current amplitudes measured from the average of 10-20 pulses (200 ms, +20 mV), after current levels stabilised. All data shown are mean ± S.E.M. (n>3); where not shown, error bars fall within the data point.

3.6.3 Characterisation of K^+ currents elicited from hetero-tetramers (described in (Shamotienko et al., 2008) and performed by Dr H. Shaban and Dr J.T. Sack) Membrane currents were measured in whole-cell voltage-clamp mode, as outlined in (Sokolov et al., 2007), except where specified. Borosilicate patch pipettes were filled with an internal solution (in mM): 90 KCl, 50 KF, 30 KOH, 10 EGTA, 20 HEPES, pH 7.4. The extracellular bath solution contained (in mM) 135 choline chloride, 20 KOH, 1.8 $CaCl_2$, 1 $MgCl_2$, and 40 HEPES, pH 7.4. Just prior to use, 0.01% (w/v) BSA was added; silanised pipette tips and tubes were used for handling toxins. Solutions were exchanged by continuous flow with a peristaltic pump or a Cellectricon Dynaflow-16 system. Series resistance compensation was applied to minimise the voltage error (<10 mV). Correction was made for a calculated liquid junction potential of +8.4 mV. Membrane holding potential was -100 mV. Leak subtraction was used to isolate K^+ current. Analogue traces were filtered at 5 kHz, and sampled at 50 kHz. Non-linear fitting was carried out with equations described previously (Sack and Aldrich, 2006). Data are reported as mean ± S.E.M.; n values refer to number of individual cells tested.

3.7 ^{125}I-αdendrotoxin binding studies

For all experiments involving ^{125}I-αDTX, HEK cells transfected with the relevant construct 48 h previously using Lipofectamine 2000 were harvested with 0.5 mM PBS/EDTA instead of trypsin. Once cells were dislodged from the flask, they were resuspended in PBS and centrifuged as described (see above). Silanised plasticware was also used to minimise toxin absorption.

3.7.1 Iodination of αdendrotoxin Toxin was radiolabelled as previously described (Dolly, 1992) using the chloramine-T method; 0.98 mg/ml αDTX (10 µl), buffer A (5 µl), 1 mCi Na^{125}I (10 µl) and 1 mg/ml chloramine-T (5 µl) were combined for 60 s, then the reaction quenched with 970 µl buffer B. At this stage 2x 10 µl aliquots were removed and diluted with 990 µl buffer D, for determination of the specific activity. The rest of the reaction mixture was loaded onto a column containing 2 ml CM-sepharose CL6B resin. After the column was washed with 20 ml buffer B (including washings from the reaction tube) to remove free ^{125}I, the labelled toxin was eluted with buffer C (10 ml). Fractions (1 ml) were collected and those containing the radio-labelled toxin determined with a Geiger counter. Aliquots removed for determination of specific activity were incubated on ice for 20 min with 250 µl 40% TCA and 740 µl 1% BSA, with mixing. The pellet resulting from centrifugation at 10,000 g for 5 min was washed with 10% TCA and counted in a γ-counter. Specific activity was 200 Ci/mmol.

Buffer A – 0.4 M sodium phosphate, pH 7.4

Buffer B – 10 mM sodium phosphate, pH 7.4 and 0.02% (w/v) TX-100

Buffer C – buffer B + 0.6 M NaCl

Buffer D – buffer B + 2% (w/v) sodium metabisulphite

3.7.2 Saturable binding of ^{125}I-αdendrotoxin to various Kv1 channels and its displacement by unlabelled toxins Cells suspended in binding buffer (150 mM NaCl, 5 mM KCl, 1 mM $SrCl_2$, 50 mM imidazole-HCl, 1% BSA, pH 7.5) were incubated for 1 h at room temperature in a total volume of 200 µl, with increasing concentrations of ^{125}I-αDTX (0.5-10 nM) in the presence or absence of 1 µM unlabelled αDTX. Aliquots (90 µl) of the reaction mixture were filtered through Whatman GF/B filters followed by three washes (0.5 ml each) with ice-cold TBS-buffer (150 mM NaCl, 5mM KCl, 50 mM Tris-HCl, pH 7.5).

For displacement experiments, suspended cells were incubated with 2.5 nM ^{125}I-αDTX, with and without increasing concentrations of various unlabelled toxins. Radioactivity remaining on washed filters was measured with a γ-counter and resultant data analysed, using Graph Pad Prism software. K_D and Bmax values were obtained from fitting the saturable binding data with a one site binding equation; $Y = Bmax.X/K_D+X$, where X is [ligand] and Y is specific binding. K_i values for the peptide toxins investigated were calculated as described in Chapter 5.

3.7.3 Determination of protein concentrations in cell suspensions

The concentration of protein in toxin binding samples (in the absence of added BSA) was determined using a BCA assay. It is a detergent compatible method based on the reduction of Cu^{2+} to Cu^{1+} by protein in an alkaline environment. A Cu^{1+} ion then chelates with 2 BCA molecules producing a complex that absorbs strongly at 562 nm. BSA standards as well as reagent A (sodium carbonate, sodium bicarbonate, bicinchoninic acid and sodium tartrate in 0.1M NaOH) and reagent B (4% cupric sulphate) are provided in the kit.

Samples of cell suspensions in binding buffer were adjusted to 1% TX-100 to solubilise proteins and the same buffer containing 1% TX-100 was used to make up BSA standards and, also, served as the blank; 50 parts reagent A and 1 part reagent B, comprised the working reagent, 200 µl of which was used to dilute 25 µl of standards, samples and blank, in a microplate. After mixing for 30 s, the covered plate was incubated at 37°C for 30 min. After cooling to room temperature, absorbance was measured at 562 nm. Protein concentrations of the samples were determined from a standard curve produced from absorbance readings of the standards after correction for the blank.

Chapter 4

Expression in mammalian cells of 2 concatemers of brain Kv1 channel α subunits give similar K^+ currents but yield pharmacologically distinguishable heteromers: assessment of their suitability for screening of inhibitors

4.1 Overview

Synthesis and assembly of Kv1 channels is controlled to yield a limited variety of channels as demonstrated by Shamotienko et al (Shamotienko et al., 1997). Presumably, properties of these specific channel combinations are suited to different roles according to neuron type or location. Channels purified from mammalian brain are predominantly heteromeric in composition (Wang et al., 1999b); therefore, it is necessary to characterise oligomers with these defined α subunit combinations and stoichiometries. Such heteromeric channels contain different proportions of Kv1 α subunits, with Kv1.2 being the most prevalent, followed by Kv1.1 (Scott et al., 1994a). Kv1.1 subunits always occur with Kv1.2 (Shamotienko et al., 1997), with heteromers consisting of these subunits alone present in several areas of human brain; cerebral cortical grey matter, cerebral white matter and spinal cord (Coleman et al., 1999).

In a previous study (Akhtar et al., 2002), a Kv1.1-1.2 construct was prepared using a linker from the *Xenopus* β-globin gene and expressed in *Xenopus* oocytes. Although it gave an outward, non-inactivating K^+ current whose voltage-dependency of activation differed from those of the parental homomers, its other electrophysiological and pharmacological properties were not determined. Also to avoid any peculiarities with the amphibian host, it was desirable to fully characterise this channel when expressed in mammalian cells. Thus, the tandem-linked Kv1.1-1.2 construct was co-expressed with the β2 subunit in BHK cells using a Semliki Forest virus (SFV) and found to produce a hetero-oligomer of the expected size, indicative of the assembly of two Kv1.1-1.2 dimers (Akhtar et al., 2002). High-affinity binding of ^{125}I-labelled αDTX or DTX_k observed with the intact cells demonstrated correct folding and assembly of the two dimeric constituents to form a tetrameric channel containg

two Kv1.1 and two 1.2 subunits in the plasma membrane (Tytgat et al., 1995), but its functionality was not analysed electrophysiologically.

The aims of this study were to profile the biophysical and pharmacological properties of this Kv1.1-1.2 containing channel expressed in CHO cells [due to their low content of endogenous outward K^+ currents (Yu and Kerchner, 1998)], in order to establish its utility as a prototypic, authentic target for future screening of drugs capable of selectively inhibiting particular subtypes. For this purpose, it was not necessary to co-express auxiliary β subunits as in the previous study (Akhtar et al., 2002) because the determinants for external binding of channel blockers are provided by the α subunits (Doyle et al., 1998). However, biophysical properties could be affected by the absence of β subunits and therefore, eventually, constructs consisting of 4 α and 4 β subunits will be desirable for such drug development strategies. The transfection procedure was simplified for expressing the K^+ channel; cells were electroporated with cRNA prepared using the SFV expression plasmid (pSFV1) that contained the inserted Kv1.1-1.2 gene (Akhtar et al., 2002), rather than using the more time consuming preparation of SFV particles for transfecting the cells. Optimisation of the simple, fast and convenient Rb^+ efflux assay allowed functional analysis of various ion channel blockers on the expressed protein. To validate the results, comparisons were made with those obtained from electrophysiological recordings.

Following success with this approach, it was extended to other constructs. First, however, modifications to the expression system were required to yield a longer lasting and larger quantity of channel-expressing cells, compared to the short-lived and finite number of cells provided by electroporation with cRNA described above. To this end, the Kv1.1-1.2-pSFV1 construct was subcloned into pIRES2-EGFP and a stable cell line developed using HEK cells. Kv1.6 is the third most abundant α subunit in brain, like Kv1.1 is found complexed with Kv1.2 (Scott et al., 1994a) and in the limited number of instances where subunit stoichiometries of neuronal Kv1 tetramers have been identified unambiguously, there is evidence of a swap of Kv1.1 with Kv1.6. That is, a Kv1.1 subunit is interchanged with Kv1.6 in channels containing the requisite Kv1.2, along with Kv1.3 and 1.4 subunits (Coleman et al., 1999; Shamotienko et al., 1997). The functional consequences of this single subunit swap are, therefore, of interest. Kv1.2 and 1.6 have also been detected

together in auditory neurons from the trapezoid body of Kv1.1 knockout mice (Brew et al., 2003). Taking these factors into account, the next channel chosen for study was one containing Kv1.6 and 1.2 subunits; hence, a Kv1.6-1.2-pIRES2-EGFP construct was prepared and a stably expressing HEK cell line developed. The biophysical and pharmacological profiles of these channels were ascertained by electrophysiological recordings, Rb^+ efflux and radiolabelled toxin displacement. Importantly, a ligand capable of distinguishing Kv1.1-12 and Kv1.6-1.2 containing channels was identified. These findings have been published (Sokolov et al., 2007).

Having optimised the Rb^+ efflux assay for profiling the pharmacology of concatenated K^+ channels in CHO cells, the establishment of 2 cell lines stably expressing channels containing Kv1.1-1.2 and Kv1.6-1.2 provided a ready supply of recombinant channels of the defined subunit composition. This facilitated further exploitation of the Rb^+ flux assay by its automation. The technology not only allowed the screening of a range of peptide toxins in the search for further blockers that distinguish these 2 channels, but also allowed exploration of the possibility of using Rb^+ efflux for more detailed measurements of inhibitory constants.

4.2 Optimised expression of Kv1.1-1.2 containing channels resulted in assembly in functional form on the plasmalemma of CHO cells

The effect of altering various electroporation parameters on the percentage of cells expressing Kv1.1-1.2 was investigated (**Table 4.1**). Following electroporation with cRNA containing the Kv1.1-1.2 gene in pSFV, cells were plated on sterile coverslips, 24 h later fixed and labelled with a monoclonal antibody specific for Kv1.2 (Muniz et al., 1992) to asses channel expression (**Fig. 4.1a-c**). The number of labelled cells was compared with the total number of cells in the same field (as determined by DAPI staining of their nuclei) to give the fraction expressing K^+ channels (**Table 4.1**, **Fig. 4.1a**). Two pulses of 850 V with capacitance of 25 µF and 75 µg of RNA was decided upon as these conditions resulted in ~50% of cells being transfected, a level of expression sufficient for Rb^+ efflux experiments and electrophysiological analysis. The specificity of Kv1.2 labelling was confirmed by experiments conducted either on untransfected cells or by omission of the primary antibody when labelling transfected cells (**Fig. 4.1c**); neither of these conditions gave a fluorescent

signal. **Fig. 4.1b** demonstrates the 2 distinct staining patterns observed: uniform staining throughout the cell, and punctate staining at the plasma membrane with the majority of fluorescence concentrated in the perinuclear region.

Electroporation conditions					**% Transfected cells**
RNA (μg)	Volts	C (μF)	No. of pulses	Path length (cm)	
30	210	25	2	0.1	18
45	600	50	3	0.4	27
45	300	800	1	0.4	35
75	420	25	2	0.2	39
75	850	25	2	0.4	47
120	850	25	2	0.4	59
180	850	25	2	0.4	66

Table 4.1│ Influence of electroporation conditions on expression of Kv1.1-1.2 containing channels in CHO cells.

It was established that storing cRNA at -80°C for >8 weeks was not detrimental to transfection efficiency (**Fig. 4.2a**). There was a decrease in the % of cells expressing Kv1.1-1.2 48 h post transfection compared with 24 h (**Fig. 4.2a**); therefore, all experiments were performed 1 day after cells were electroporated.

Having confirmed the presence of the required protein expressed in transfected cells, it was desirable to verify the integrity of the channel on the plasmalemma. This was achieved by labelling the surface proteins with a reactive biotin conjugate, affinity-separation of the biotinylated derivatives from a detergent-solubilised extract on streptavidin resin, followed by SDS-PAGE and Western blotting. The isolated surface K^+ channel showed one protein band with Mr ~120 kDa that was recognised by antibodies specific for Kv1.1 or Kv1.2 α subunits, and corresponds to the size of the dimer (**Fig. 4.1d**). A notable absence of smaller proteins is indicative of the channel in its membrane-bound state containing only intact Kv1.1-1.2 protein, where two copies make up the pharmacologically-active oligomer, demonstrated by experiments further on. Samples of total protein that were biotinylated similarly but not fractionated, gave a broad band of Mr ~ 60 kDa reactive with both antibodies, in addition to the larger protein of Mr ~ 120 kDa (**Fig. 4.1d**). The smaller band is approximately the size of one α subunit and may be a result of cleavage of the dimeric

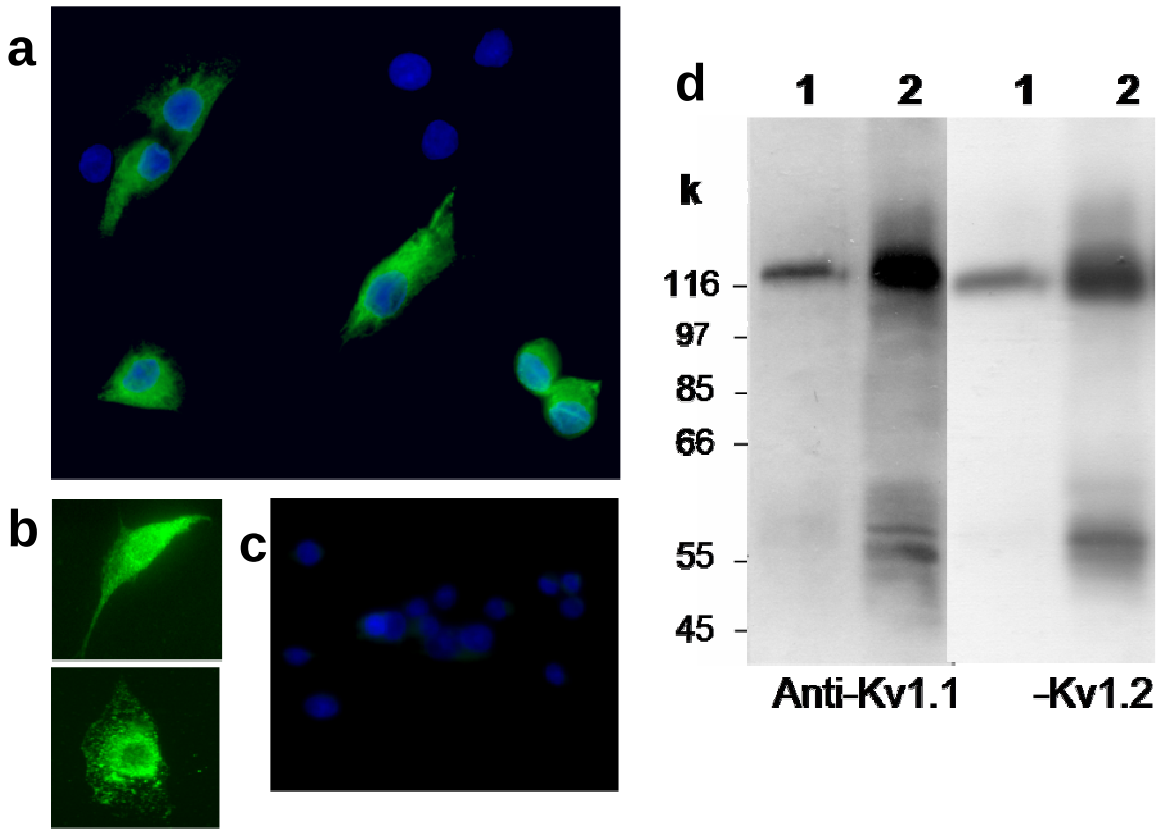

Figure 4.1 | Expression of Kv1.1-1.2 containing channels: fluorescence microscopy and biotinylation of surface proteins reveal expression of the recombinant K^+ channel and targeting to the plasmalemma of CHO cells. Cells electroporated with cRNA encoding the Kv1.1-1.2 protein were fixed 24 h post-transfection, permeabilised and labelled with a monoclonal antibody specific for Kv1.2 α subunit. Bound IgG was visualised with anti-species IgG conjugated to AF 488 (green) (**a**,**b**). **a**, Cell nuclei were stained with DAPI (blue) to demonstrate transfection efficiency (see Materials and Methods). **b**, Two patterns of labelling were observed: uniform throughout the cell (top), and punctate staining at the plasma membrane with a concentration of the signal in the perinuclear region (bottom). Omission of the primary antibody resulted in absence of the signal (**c**). **d**, Transfected cells were solubilised with TX-100 after biotinylation of the surface proteins and the soluble extract incubated with streptavidin-agarose resin. Immobilised proteins were subjected to SDS-PAGE and Western blotting, utilising antibodies specific for Kv1.1 or 1.2. Lanes: 1, eluate from the streptavidin-agarose resin; 2, total cell lysate. A single band of Mr ~ 120 kDa, representing intact Kv1.1-1.2 dimer was observed for the K^+ channels from the surface of biotinylated cells whereas components of lower molecular weight also occurred in the total protein sample.

protein but as it is not present in the surface expressed channels it will not impact on functional studies. Thus, the presence on the plasmalemma of an assembled oligomer (composed of a pair of dimers – see 4.5) was demonstrated and expression optimised to allow functional characterisation of the surface expressed channel.

4.3 Effects of known Kv1 channel blockers on Kv1.1-1.2 expressed in CHO cells determined using a high-throughput Rb^+ efflux assay

Experiments were performed to measure the effect of various Kv1 channel inhibitors on Rb^+ efflux through the expressed channels. The investigation also established the suitability of these transfected cells for employment in a high-throughput assay which can be used for screening compounds in search of novel pharmacological agents against these expressed targets of pre-defined composition. The necessary time for Rb^+ loading was found to be 3 h, as beyond this time the concentration of Rb^+ in cells stopped increasing (**Fig. 4.2b**). Likewise, 75 and 100 mM K^+ evoked the greatest release of Rb^+ via the activated recombinant channels (**Fig. 4.2c**), and the lower effective amount was chosen for all experiments going forward. In control experiments, basal and stimulated release of Rb^+ were measured from untransfected as well as transfected CHO cells. Low levels of Rb^+ were released from untransfected cells under both conditions, similar to basal release from transfected cells, the corresponding stimulated Rb^+ release being at least twice that from these cells (**Fig. 4.2d**). This 2:1 ratio of stimulated to basal release was applied as a necessary criterion for all subsequent experiments [as advised by personnel at Xention Ltd. (Cambridge, UK), where the assay is used for high-throughput screening]. A further control was included to exclude that electroporation of cells (in the absence of cRNA) affected their ability to retain Rb^+ under both basal and stimulating conditions (**Fig. 4.2d**). 4-AP, TEA and αDTX were all shown to inhibit evoked Rb^+ efflux (**Fig. 4.3a-c**); 4-AP inhibited release with an IC_{50} roughly estimated at 0.5 mM (**Fig. 4.3a**). TEA also reduced Rb^+ efflux though to a lesser extent than 4-AP; the very high, maximum dose (50 mM) used gave only a 50% reduction in release (**Fig. 4.3b**). αDTX blocked Rb^+ efflux at nanomolar concentrations (**Fig. 4.3c**) as was expected, with an extrapolated IC_{50} of ~ 2nM. Basal efflux was not affected by the test compounds (**Fig. 4.3d**) – that is, basal release from cells was the same in both the presence and absence of the test compound. The experiments were

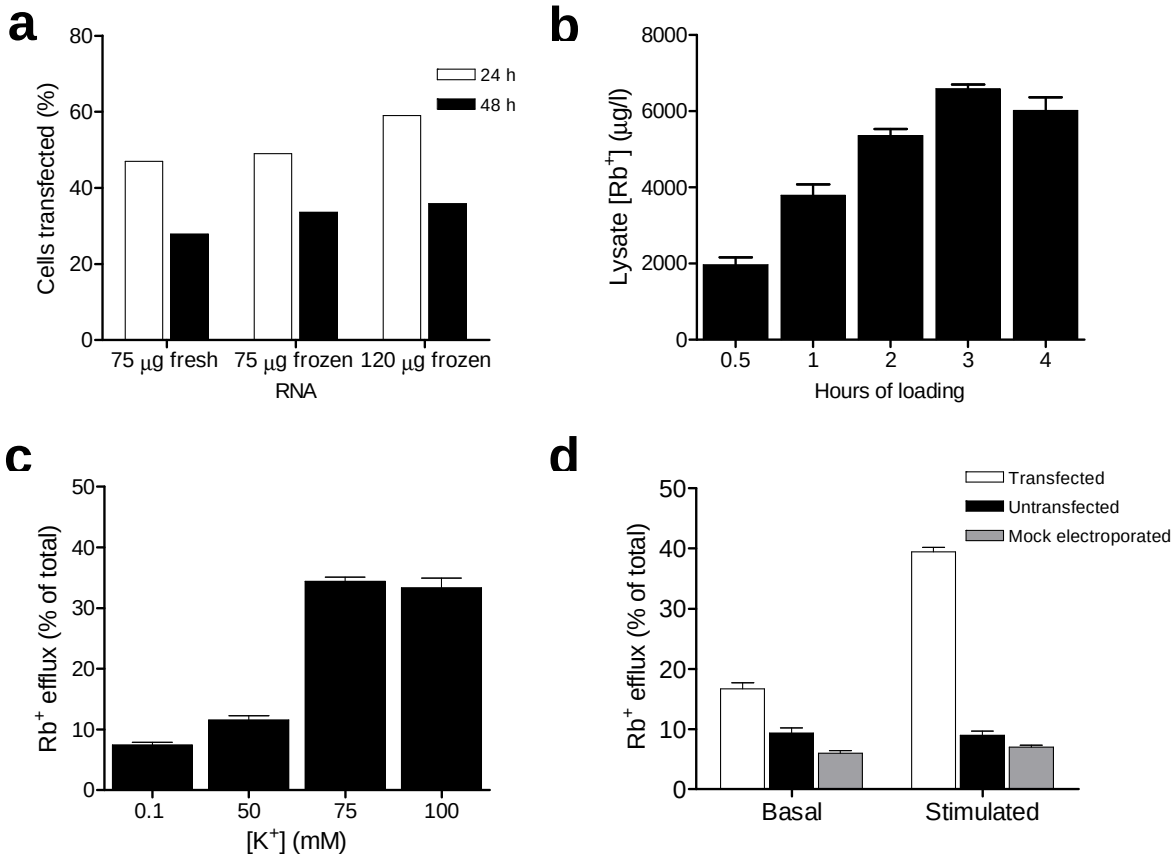

Figure 4.2 | Optimisation of channel expression and Rb^+ efflux conditions. **a**, Comparison of transfection efficiency with freshly prepared cRNA and that stored at -80°C for >8 weeks at 24 and 48 h post transfection was assessed as described in Results. **b**, [Rb^+] in cell lysates (µg/l) was analysed after various loading times (mean ± S.E.M.; n=>12. **c**, Both supernatant and lysates were measured following channel activation with various concentrations of K^+, and Rb^+ efflux expressed as % total Rb^+ in the cells (i.e. content in supernatants and lysates; mean ± S.E.M.; n=≥19). **d**, Transfected, untransfected and mock electroporated CHO cells were loaded with Rb^+ and release was measured under basal and stimulating conditions (3 min with 75 mM K^+), using AAS (see Materials and Methods). Supernatant Rb^+ levels are expressed relative to the total as mean ± S.E.M.; n=15.

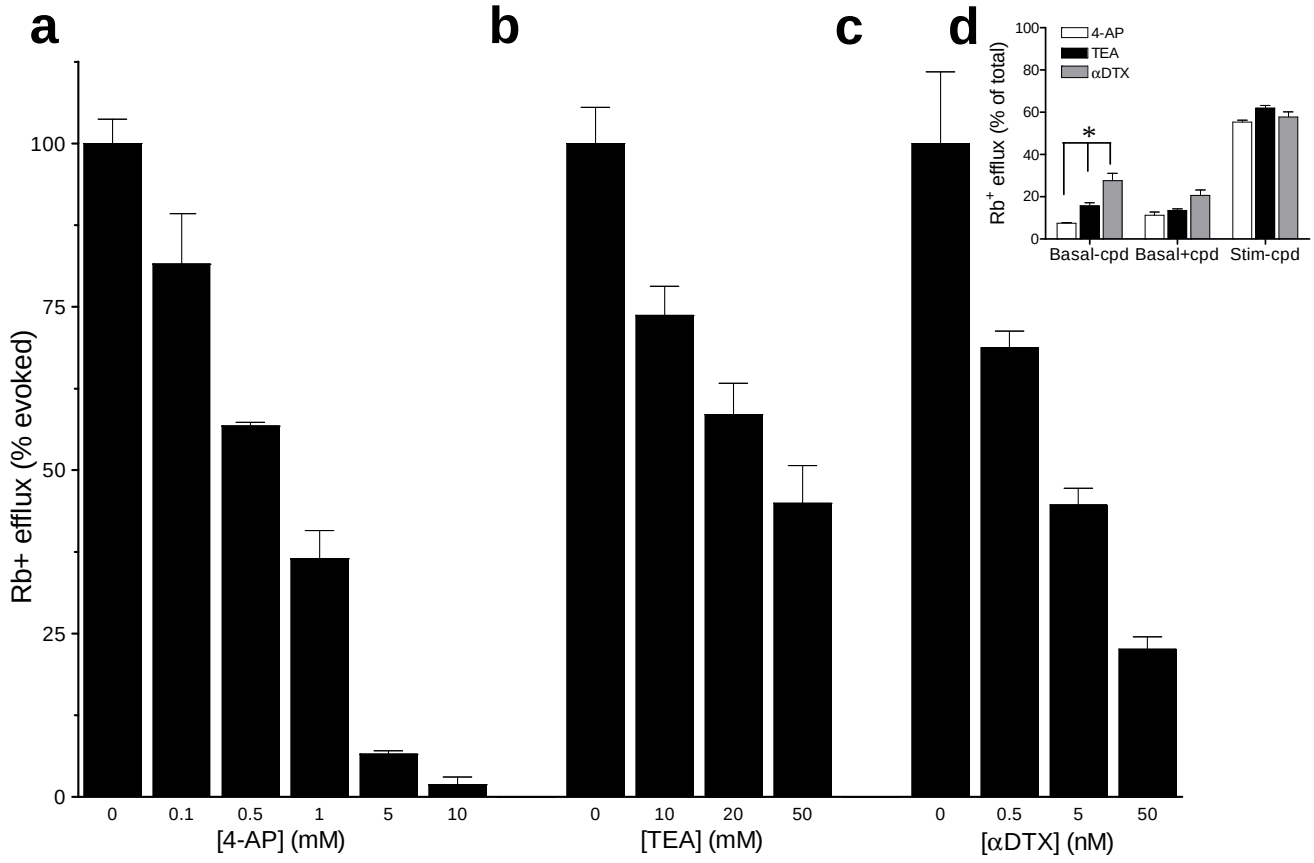

Figure 4.3 | Sensitivity of Kv1.1-1.2 containing channels expressed in CHO cells to various channel blockers as measured by the Rb^+ assay. Rb^+ efflux from transfected cells used for drug testing was calculated as described in Materials and Methods, and subtraction of values for basal release from those for stimulation gave the evoked increment for each set of cells. The quantities of evoked Rb^+ release measured in the presence of 4-AP, TEA or αDTX were plotted (mean ± S.E.M.; n=≥24) relative to the requisite normalised control. 4-AP or TEA was added to the stimulation buffer (**a** and **b**) whereas αDTX was included in the Rb^+ loading buffer (**c**). While basal efflux was unaffected by the test compounds (**d**), it differed significantly (in the absence of compounds) between different batches of transfected cells (*), as measured by one-way ANOVA (p=0.0001).

performed on different days using different batches of cells and consequently there were significant differences in the amount of basal release measured between different compounds (**Fig. 4.3d**). However, as basal release of Rb^+ was measured for each batch of cells and only experiments where the stimulated Rb^+ release was at least twice the basal release were used, this variability in the measurements was accounted for.

4.4 Comparison of the susceptibilities of this expressed K^+ channel to 4-aminopyridine, tetraethylammonium and αdendrotoxin as revealed by electrophysiological recordings and Rb^+ efflux

A fraction of the K^+ current (I_K) produced by this channel proved very sensitive to 4-AP, with a concentration of just 20 μM already exhibiting significant inhibition of the evoked I_K, and 0.1 mM giving a reduction of 40% compared with the normalised control (**Fig. 4.4a**). However, a component of the current appears to be insensitive to 4-AP as at 10 mM, 45% of I_K remained. In comparison, at this concentration, evoked release of Rb^+ was almost completely inhibited. Sensitivity of this I_K to TEA was markedly reduced compared with 4-AP, as 3 mM TEA did not reduce the current significantly. The highest concentration used (20 mM) inhibited current by only 34% (**Fig. 4.4b**), a value which correlates well with Rb^+ efflux results where the same dose reduced evoked Rb^+ release by 42%. Electrophysiological recordings revealed αDTX to be more potent at blocking I_K than Rb^+ efflux (**Fig. 4.4c**), with 80% inhibition requiring 10 and 50 nM, respectively.

4.5 Surface expression of concatenated Kv1 channels stably expressed in HEK cells to a level adequate for functional analysis

Initial experiments on COS, BHK and CHO cells transiently-transfected with Kv1.1-1.2-pIRES2-EGFP vector showed a protein corresponding in size to the dimer together with smaller immuno-reactive bands (data not shown), whereas HEK cells were devoid of such fragments (see below). This advantageous feature of HEK cells was exploited for successfully creating stable cell lines expressing intact dimer-containing channels. After 2-3 weeks in geneticin-containing medium, practically all of the surviving cells (~5-10% of the original number plated) transfected with Kv1.1-1.2- or Kv1.6-1.2-pIRES2-EGFP showed green EGFP fluorescence, which allowed subsequent cell clones to be selected and

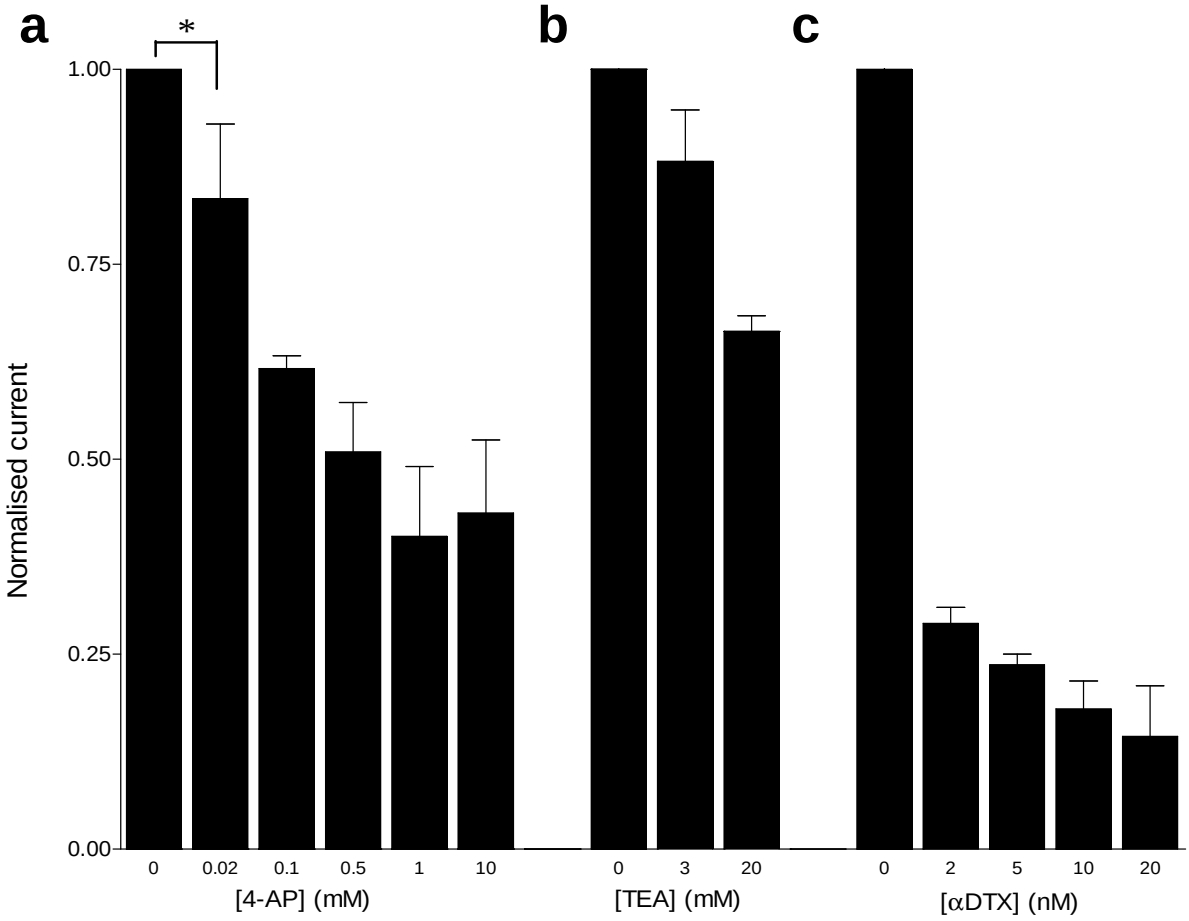

Figure 4.4 | Inhibition of K^+ currents from Kv1.1-1.2 containing channels. Electrophysiological recordings were performed to compare the effect of K^+ channel blockers on this recombinantly-expressed channel with that measured by Rb^+ efflux. K^+ currents were elicited in transfected CHO cells with 200 ms depolarising pulses (to +40 mV); the amplitudes recorded from 10-20 pulses before and after drug application were averaged and normalised. Each point is the mean of 3–6 (**a**) and 2–3 values (**b**,**c**) ± S.E.M. 4-AP inhibits the K^+ current from the Kv1.1-1.2 containing channels significantly at the lowest concentration tested, 0.02 mM 4-AP (*, p=0.0049, measured by an unpaired t-test).

propagated. SDS-PAGE and Western blotting revealed a band of Mr ~120 kDa, recognised in these cells by respective anti-Kv1.1, Kv1.2 and Kv1.6 antibodies. It is noteworthy that there is an absence of smaller bands corresponding to the size (~ 60 kDa) observed for the monomeric constituents (**Fig. 4.5**). Cell lines chosen for preparing stocks suspensions gave satisfactory levels of ^{125}I-αDTX binding (ranged from 0.08 – 0.15 pmoles/mg protein); such surface expression of channels is adequate for electrophysiological and Rb^+ efflux measurements.

4.6 Kv1.1-1.2 and Kv1.6-1.2 channels exhibit similar electrophysiological properties, yet are differentiated from their monomeric constituents by their half-activation voltages

Patch-clamp whole-cell recordings from HEK cells stably expressing the Kv1.6-1.2 or Kv1.1-1.2 containing channels gave sigmoidally-activating currents, typically of 1-7 nA amplitude, following a depolarisation step from -110 mV to +50 mV (**Fig. 4.6a**). Likewise, deactivation of the I_K was found to be similar for both channels. At -40 mV, current deactivation occurred incompletely with a time constant of about 20 ms; with more negative potentials, the speed of decay increased with a voltage dependence equivalent to 1.2 elementary charges traversing the transmembrane voltage drop (**Fig. 4.6b**). This voltage dependence is similar to that of the *Shaker* Kv1 channel (Zagotta et al., 1994).

To quantify the activation kinetics of these channels, K^+ current rise was fitted by a mono-exponential function (see section **3.6.2**, equation 1). Activation rates are similar for Kv1.6-1.2 and Kv1.1-1.2 (**Fig. 4.6c**), giving time constants (τ) at 0 mV of approximately 10 ms (**Table 4.2**), and accelerating with increasing command voltage. Also similar to the *Shaker* channel, the steepness of voltage dependence of activation varied with different voltage ranges and could not be fitted by equation (2) (see Materials and Methods) as a simple elementary charge movement (**Fig. 4.6c**). Conductance-voltage relations were generated by plotting the conductances obtained at different voltages (**Fig. 4.6d**). This revealed that the two channel heteromers activate slightly differently; their half-maximal activation potentials are separated by 7 mV, though their slopes are identical (**Table 4.2**). No significant inactivation of the K^+ currents from either Kv1.6-1.2 or Kv1.1-1.2 could be detected within 400 ms of depolarisation to +50 mV (**Fig. 4.7**); however, a prolonged step revealed slow inactivation of each channel (**Fig. 4.7a**). Inactivating currents could be fitted

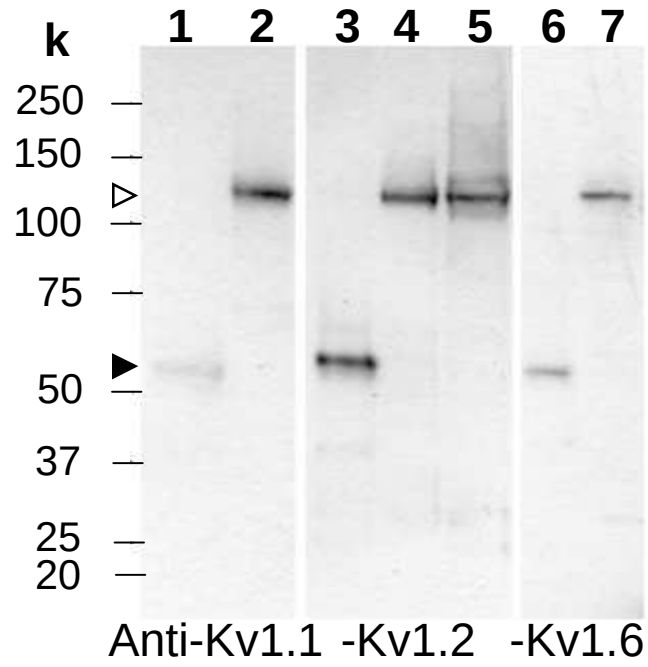

Figure 4.5 | Expression of Kv1.1-1.2 or Kv1.6-1.2 containing channels and monomers in HEK cells via pIRES2-EGFP vectors. Western blotting results confirm the correct sizes and subunit compositions. Suspensions of HEK cells stably- and transiently-expressing the dimeric and monomeric channels, respectively, were subjected to SDS-PAGE, and stained with antibodies specific for Kv1.1, Kv1.2 or Kv1.6 using ECL regents (see Materials and Methods). Lanes: 1, Kv1.1 monomer; 2,4 Kv1.1-1.2 dimer; 3, Kv1.2 monomer; 5,7 Kv1.6-1.2 dimer and 6, Kv1.6 monomer. Sizes of the standard markers used are indicated. Note that each dimer gave the expected size (▷), with an absence of any bands corresponding to the mobility of the monomers (►).

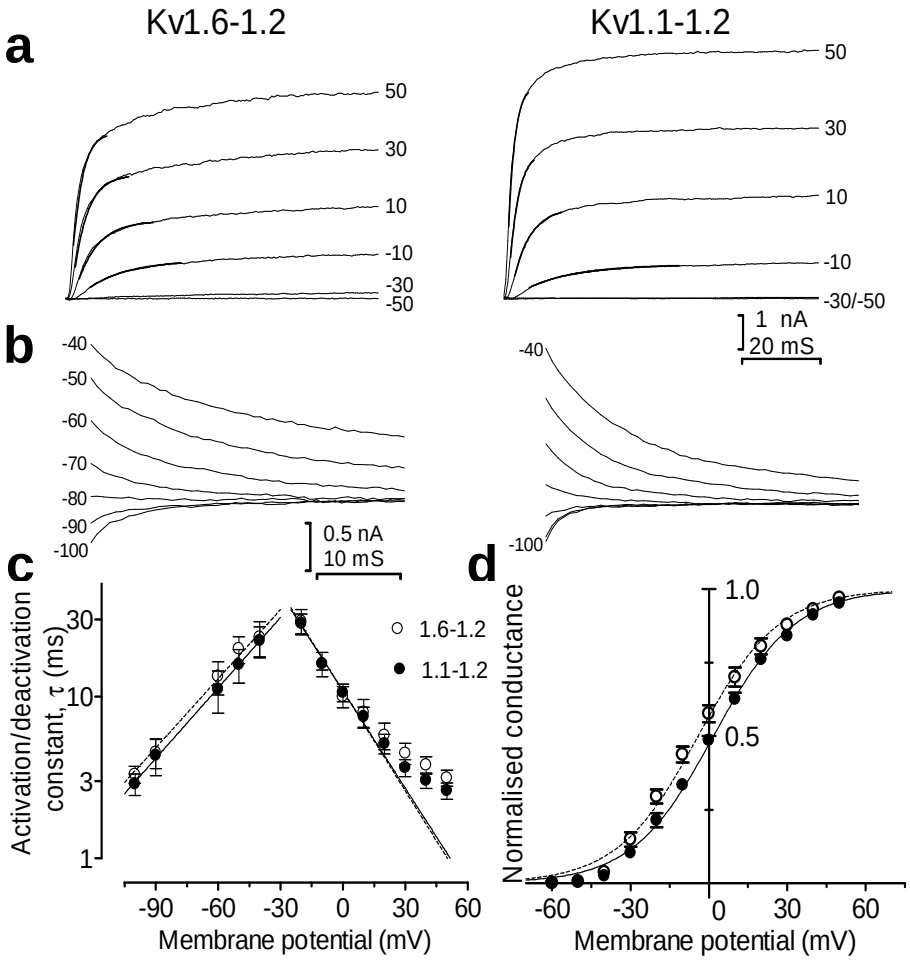

Figure 4.6 | Voltage dependence for activation and deactivation of Kv1.1-1.2 and 1.6-1.2 containing channels stably expressed in HEK cells. **a**, Typical K^+ current recorded from Kv1.6-1.2 and Kv1.1-1.2 containing channels during an I–V protocol (depolarising voltage steps of 400 ms from -60 to +50 mV in 10 mV increments; records of the initial 80 ms from every second trace are shown). Thick lines overlapping the current traces resulted from fitting the data with a mono-exponential function. Note: current traces at -30 and -50 mV overlap for Kv1.1-1.2. **b**, Deactivation observed after returning membrane potential from +40 mV to the various voltages specified. Scale bars apply to both channel traces (**a**,**b**). **c**, Activation and deactivation kinetics determined by fitting current traces with a mono-exponential function. The dashed and continuous lines resulted from fitting equation (2) (see Materials and Methods) to the calculated τ values for Kv1.6-1.2 and Kv1.1-1.2, respectively. Activation time constants at voltages from -20 to +10 mV were used for fitting; data for both channels deviate from fits at positive voltages. **d**, Conductances at various command potentials were normalised and fitted with a Boltzmann equation (3); dashed and continuous lines represent the fitted results for Kv1.6-1.2 and Kv1.1-1.2, respectively (overlapping for deactivation). A significant difference in the $V_{½}$ values for activation was revealed with two-tailed Mann-Whitney U test ($p < 0.03$). Error bars show S.E.M.

with a double exponential function, revealing similar inactivation constants (**Table 4.2**). On average, at the end of a 60 s depolarisation step to 40 mV, currents had inactivated by more than 80% (**Table 4.2**). On examining the influence of voltage on inactivation of the currents with a steady-state inactivation protocol (**Fig. 4.7b,c**), membrane potentials more negative than -60 mV were found to be required to remove inactivation from either channel (**Fig. 4.7d**).

As replacing Kv1.6 with Kv1.1 in a heteromeric channel caused a detectable negative shift in its half-activation voltage (see above), a basis for this was sought by studying the parental homo-tetrameric channels. Thus, the conductance-voltage relationship of each monomer was determined using pIRES2-EGFP constructs expressed in HEK cells (**Fig. 4.8**). The Kv1.1 homomeric channel showed half-activations at -24 mV, Kv1.6 at -15 mV and Kv1.2 at 7.2 mV. While Kv1.6 homo-tetramers activate at more positive voltages than those made from Kv1.1, replacing Kv1.1 with Kv1.6 in a concatenated construct caused the resultant channel to activate at more negative voltages. This indicates that the gating differences between Kv1.6 and Kv1.1 are more complex than a simple alteration in the midpoint of voltage sensor activation.

HEK stable cell lines	Activation		Deactivation τ (ms)		Inactivation (step to +40 mV; 60 s)		Steady-state inactivation
	$V_{½}$ (mV); k	τ (ms) at +0; 20; 50 mV	at –100 mV	at –40 mV	% of I	τ_1; τ_2 (s)	$V_{½}$ (mV)
Kv1.1-1.2	-0.7 ± 1.6; 17 ± 1; (n=9)	10.6 ± 1.3; 5.1 ± 0.7; 2.6 ± 0.3; (n=6)	2.9 ± 0.4 (n=6)	22.2 ± 4.9	82.4 ± 3.6 (n=6)	1.6 ± 0.2; 13.2 ± 2	-95.7 ± 0.9; (n=5)
Kv1.6-1.2	-7.3 ± 2.3; * 17 ± 0.5; (n=7)	10 ± 1.5; 5.8 ± 1.1; 3.1 ± 0.4; (n=5)	3.3 ± 0.4 (n=4)	23.3 ± 5.7	82.5 ± 2.6 (n=4)	2.4 ± 0.7; 20 ± 6	-92.5 ± 2.1; (n=6)

Table 4.2 | Electrophysiological properties determined for Kv1.1-1.2 and Kv1.6-1.2 channels

* significant difference ($p < 0.03$, Mann-Whitney *U* test)

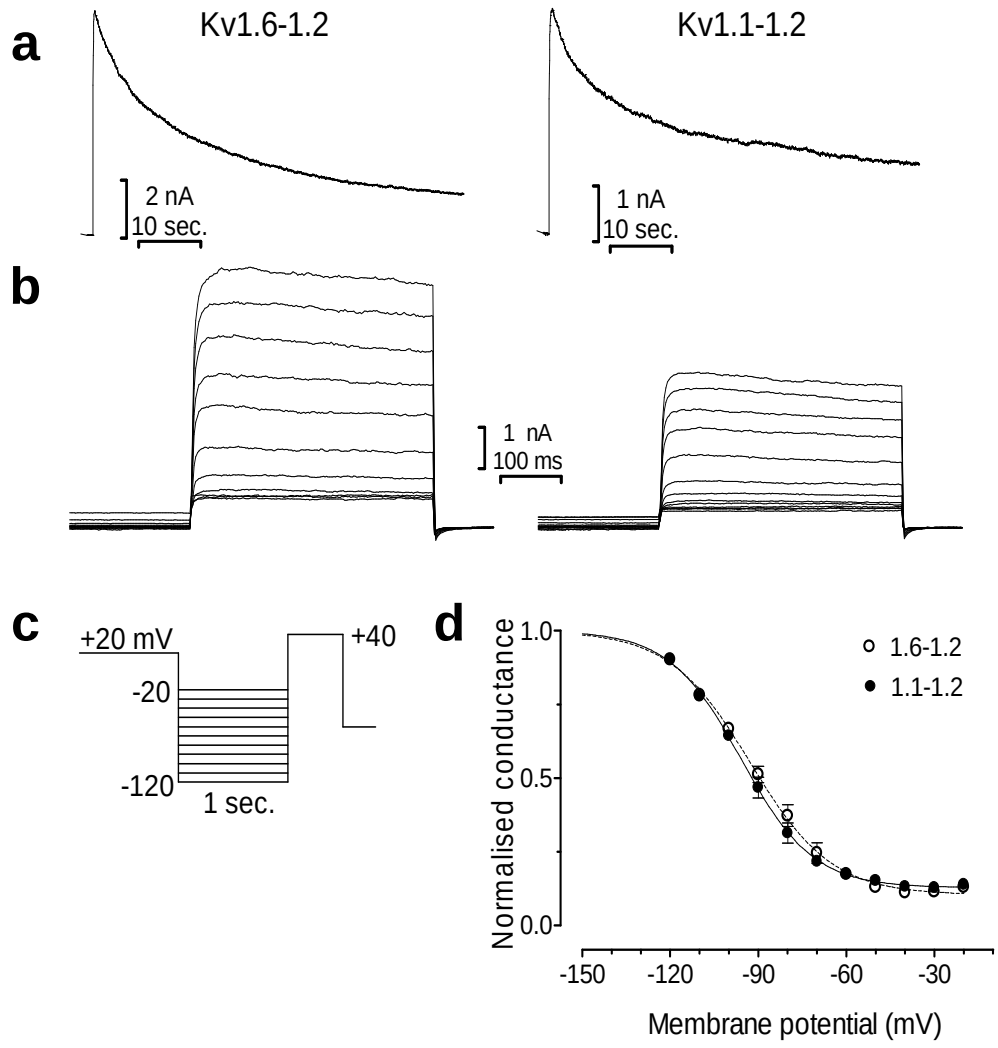

Figure 4.7| Inactivation properties of K^+ currents resulting from Kv1.1-1.2 and 1.6-1.2 channels stably expressed in HEK cells. **a**, K^+ currents show the development of slow inactivation in response to a 60 s depolarisation pulse to +40 mV. **b**, Shows steady-state inactivation. **c**, Cells were held at +20 mV for 40 s to allow channels to undergo significant inactivation, then subjected to pre-conditioning pulses of different negative potentials, followed by a test pulse to +40 mV. Scale bars apply to both channel traces. **d**, Conductances resulting from the test pulse were plotted against membrane potentials of the pre-pulse; the data fitted with a Boltzmann function are shown as dashed and continuous lines for Kv1.6-1.2 and Kv1.1-1.2, respectively.

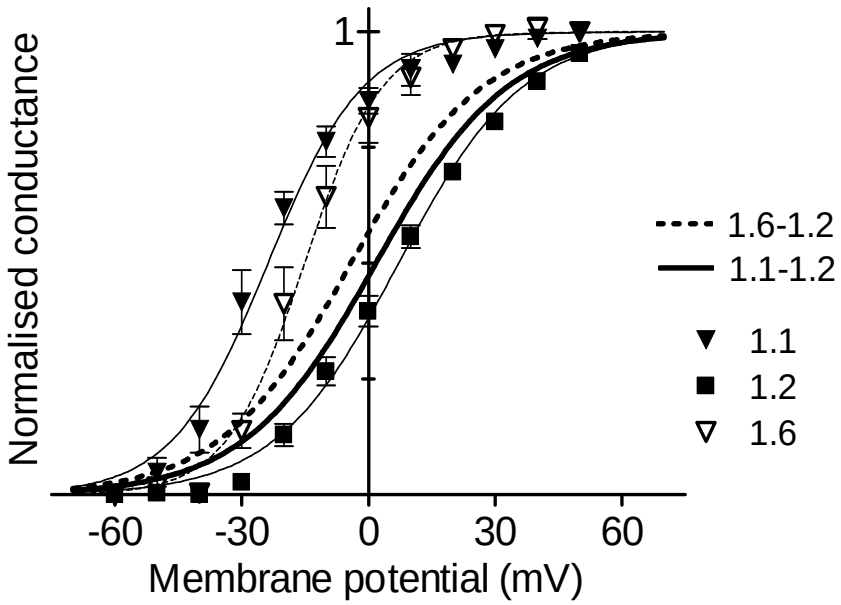

Figure 4.8│ Voltage dependency of activation of homomeric K^+ channels transiently expressed in HEK cells. G-V plots of homomeric channels formed by Kv1.1, 1.2 or 1.6 after transient expressed in HEK cells. Conductance values were fitted with a Boltzmann function, equation (3) (see Materials and Methods). The resultant values for half-activation (in mV) and slope were as follows; Kv1.1: -24 ± 1, 11 ± 1 (n=5); Kv1.2: 7.2 ± 0.6, 15 ± 0.5 (n=6) and Kv1.6: -15 ± 1, 9 ± 1 (n=4). The curves shown for Kv1.6-1.2 and 1.1-1.2 channels are fitted plots taken from **Fig. 4.6d**.

4.7 Channels composed of Kv1.6-1.2 and Kv1.1-1.2 can be distinguished by their susceptibilities to inhibitors

Different homo-tetrameric Kv1 channels differ to varying extents in their sensitivity to pharmacological agents; therefore, the long-term goal of this work is to develop a pharmacopoeia capable of identifying different heteromeric Kv1 subtypes. A first step along this path is to find ligands that can distinguish between hetero-tetramers that vary in some, but not all, α subunits.

External TEA proved less effective in blocking the K^+ current produced by Kv1.6-1.2 than Kv1.1-1.2 (**Fig. 4.9a**). All four K^+ channel subunits are known to make an energetic contribution to the binding of a single TEA molecule at the external mouth of the conduction pore (Heginbotham and MacKinnon, 1992; Kavanaugh et al., 1992). Hence, the sensitivity observed is in the expected rank order, as Kv1.1 homo-tetramers are more sensitive to TEA than those containing Kv1.6. In contrast, 4-AP, another classical blocker of Kv1 channels, failed to distinguish between the channels made from Kv1.6-1.2 or Kv1.1-1.2 (**Fig. 4.9b**), consistent with very similar 4-AP sensitivities of the parental homomers (Grupe et al., 1990; Stuhmer et al., 1989). αDTX binds to homo-tetramers of all the Kv1 subunits studied herein (Grupe et al., 1990; Stuhmer et al., 1989) and, accordingly, inhibited the K^+ currents mediated by Kv1.6-1.2 or Kv1.1-1.2 channels (**Fig. 4.9c**) [c.f. Rb^+ flux, (**Fig. 4.10c**) and ^{125}I αDTX binding (**Fig. 4.11**)]. By this electrophysiological measurement αDTX is significantly more effective on Kv1.6-1.2 than Kv1.1-1.2, but despite the significance of the difference it is insufficient to make this toxin a distinguishing ligand. On the other hand, DTX_k proved effective in this regard. DTX_k is known to block any Kv1.1-containing channel in oocytes (Akhtar et al., 2002). Whereas the Kv1.6-1.2, 1.6 or 1.2 channels proved virtually resistant to DTX_k, it inhibited Kv1.1-1.2 or 1.1 (**Fig. 4.9d**) and, thus, the latter toxin can successfully discern the swap of Kv1.6 for Kv1.1 in a heteromeric K^+ channel.

Experiments were performed to measure the effects of the same compounds on evoked release of Rb^+ from the same stable HEK cell lines. The resultant data is plotted as fractional inhibition of Rb^+ release instead of percentage evoked Rb^+ efflux used elsewhere in the chapter and thesis, to allow easy comparison with the similarly plotted, corresponding electrophysiology data (**Fig. 4.9** and **4.10**), as published in (Sokolov et al.,

2007). Thus, in keeping with the paper layout the electrophysiology data has been discussed first in the equivalent sections of this chapter (**4.6 and 4.7**).

Comparable to results obtained electrophysiologically, TEA preferentially blocked depolarisation-elicited efflux of Rb^+ through Kv1.1-1.2 containing channels (**Fig. 4.10a**) compared with Kv1.6-1.2, with data for the HEK expressed Kv1.1-1.2 channels corresponding to that recorded for TEA inhibition of the same channels expressed in CHO cells (**Fig. 4.3**). While the effect of 4-AP on the two channels was significantly different at 1 and 10 mM, Kv1.1-1.2 was more inhibited at 1 mM and less at 10 mM (**Fig 4.10b**), demonstrating again that 4-AP does not distinguish these two heteromers produced from α subunits with very similar sensitivities to 4-AP (Grupe et al., 1990; Stuhmer et al., 1989). αDTX displayed similar efficacy towards both heteromers (**Fig. 4.10c**), hence the slightly, yet significant, enhanced sensitivity of Kv1.6-1.2 compared with Kv1.1-1.2 containing channels to αDTX as measured electrophysiologically was not replicated confirming that this toxin is not a distinguishing ligand. Importantly, the ability of DTX_k to discriminate between the heteromers studied was confirmed by Rb^+ efflux experiments, where strong inhibition of evoked Rb^+ release through Kv1.1-1.2 containing channels was in stark contrast to the minimal reduction in supernatant Rb^+ concentrations observed in wells containing channels made up of Kv1.6-1.2 subunits (**Fig. 4.10d**). Although some studies have reported lower potencies for inhibitors when measured by Rb^+ efflux than electrophysiological recordings (Middleton et al., 2003), this is likely due to the different conditions used elsewhere because under the comparable conditions herein both methods gave similar results. Individual cells are selected when making electrophysiological recordings whereas Rb^+ efflux data results from a whole population of cells. Where results do differ slightly (e.g. αDTX) this distinction between the 2 assays is likely the reason. It is also important to note that channels stably expressed in HEK cells gave more similar results with the two methods used than those transiently expressed in CHO cells, likely due to a more uniform population of channels. In the case of the peptide toxins, the risk of adherence to plasticware was also addressed by silanisation of all relevant assay materials. Overall, correspondence to the electrophysiological data again validates the Rb^+ efflux method to screen K^+ channel hetero-multimers for specific ligands.

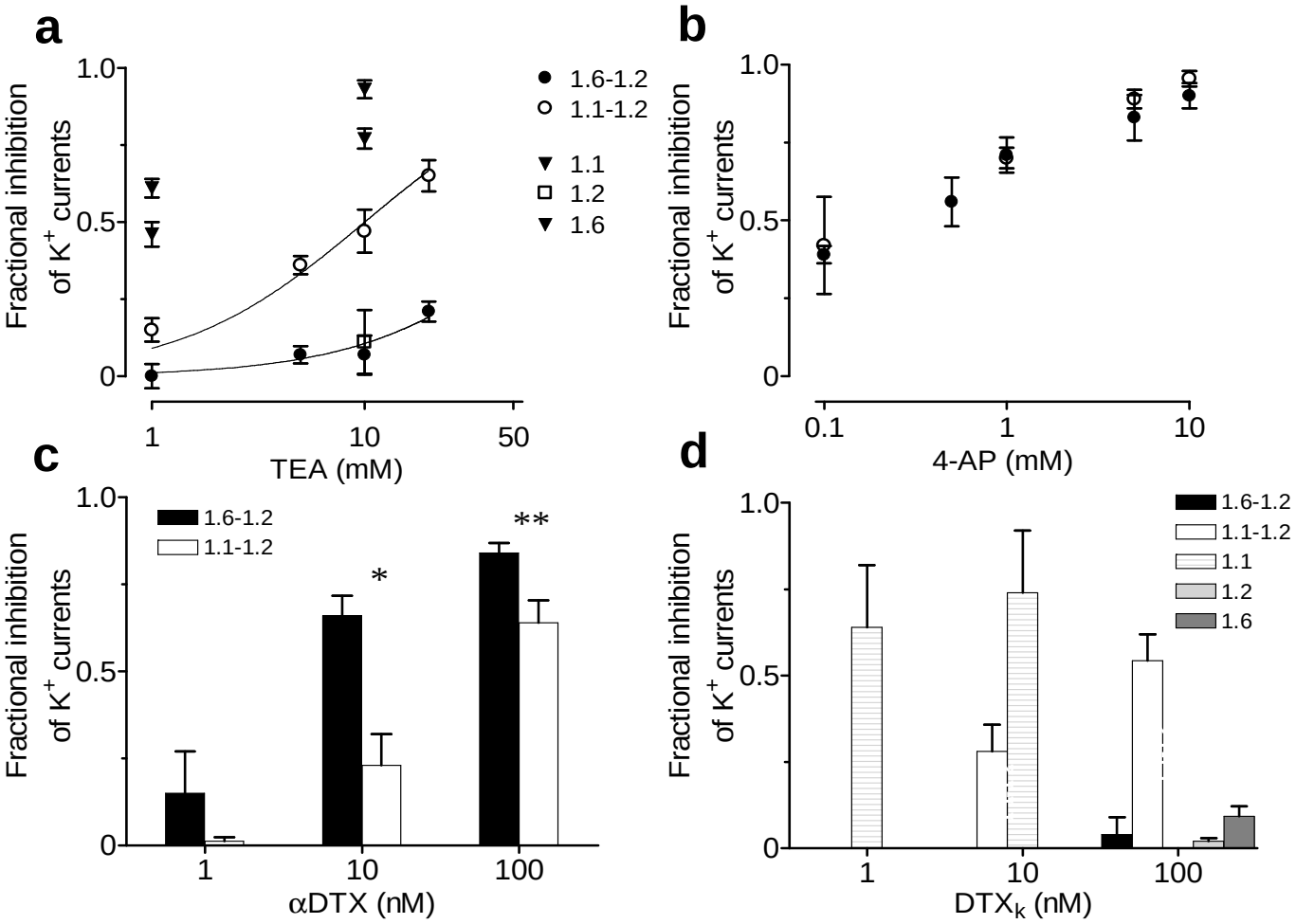

Figure 4.9 | Pharmacological distinction of Kv1.1-1.2 and 1.6-1.2 containing channels through inhibition of their K^+ currents. Channels were expressed in HEK cells using Kv1.6-1.2, Kv1.1-1.2 or their individual constituent subunits. Currents were evoked by depolarising pulses (to +40 mV or +20 mV for 4-AP; 200 ms); the amplitudes recorded from 10-20 pulses before and after drug application (**a**, TEA; **b**, 4-AP; **c**, αDTX; **d**, DTX_k) were averaged and normalised. The resultant values for fractional inhibition of the K^+ currents are presented (mean ± S.E.M) with at least 3 cells tested for every drug concentration. Lines on the TEA panel show results fitted with a Langmuir isotherm (**a**). The difference in inhibition of the two channels by αDTX is significant at both 10 (*, p=0.016) and 100 nM (**, p=0.048), but not at 1 nM (**c**).

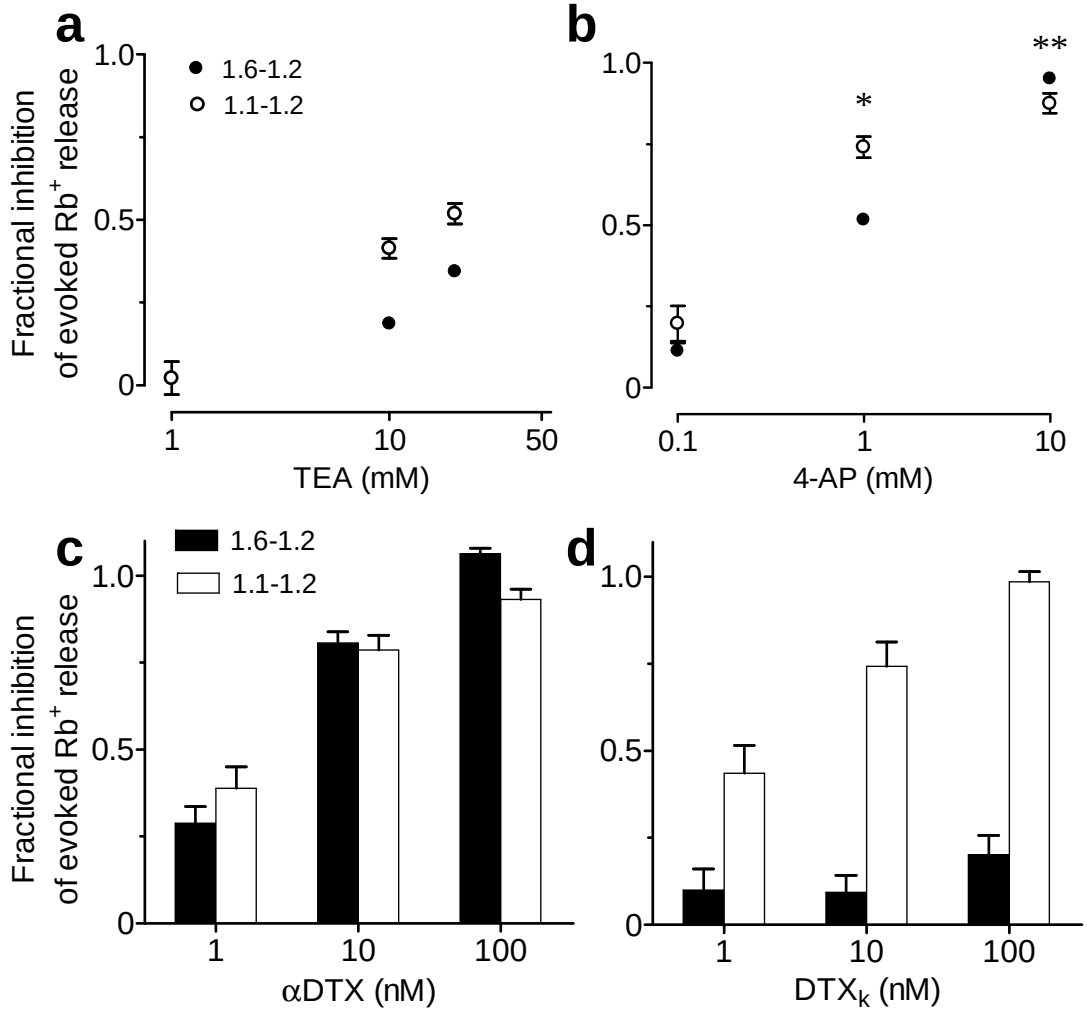

Figure 4.10 | Pharmacological inhibition of evoked Rb^+ release from HEK cells expressing Kv1.1-1.2 or Kv1.6-1.2 containing channels. After loading transfected cells with Rb^+, basal and stimulated release were measured in the presence and absence of blockers (**a**,TEA; **b**,4-AP; **c**,αDTX and **d**,DTX_k). Evoked increments were normalised and plotted ± S.E.M. [n = >16; in **a** and **b**, error bars fall within the data point for 1.1-1.2 and in **a**, the 1 mM value for Kv1.6-1.2 is obscured by that of Kv1.1-1.2]. In **b**, the effect of 4-AP on the channels differs significantly at 1 (*, p=<0.0001) and 10 (**, p=0.0256) mM, as measured by an unpaired t-test. Basal efflux (as % of total) from untransfected cells and those expressing Kv1.6-1.2 or 1.1-1.2 was 17.9 ± 0.9%, 8.9 ± 0.3% and 15.4 ± 1.3%, respectively. The slight decrease in unstimulated release from transfected cells is likely due to expressed K^+ channels lowering the resting potential of the cells, thereby, reducing the outward driving force for Rb^+. Stimulated Rb^+ efflux for Kv1.6-1.2 and Kv1.1-1.2 were 69.2 ± 1.0% and 49.4 ± 2.1%, compared to 18.2 ± 0.6% for untransfected cells.

The ability of DTX_k to discriminate between these two channels was further confirmed by displacement with unlabelled αDTX or DTX_k of ^{125}I-αDTX bound to intact cells. In the case of Kv1.1-1.2 channels, both αDTX and DTX_k displaced the labelled toxin with the displacement curve for DTX_k closely following that for αDTX (**Fig. 4.11a**). ^{125}I-αDTX bound to the Kv1.6-1.2 containing channels was affected by unlabelled αDTX in a similar way to the Kv1.1-1.2 channels demonstrating a similar binding of the toxin to the two heteromers as demonstrated by electrophysiological and Rb^+ efflux measurements (**Fig. 4.11b**). However with Kv1.6-1.2 channels, DTX_k gave only feeble competition of ^{125}I-αDTX binding with the highest concentration used displacing less than half of the bound toxin (**Fig. 4.11b**). This much weaker affinity of Kv1.6-1.2 for DTX_k (at least 200-fold) is consistent with the known requirement for the presence of at least 1 Kv1.1 subunit for avid binding, and accords with its inability to block K^+ current or Rb^+ efflux through this channel.

In summary, both of these channels share susceptibility to 4-AP and αDTX but replacement of Kv1.1 by Kv1.6 results in the loss of sensitivity to TEA and DTX_k; thus, use of such ligands on neuronal preparations may allow pharmacological discernment of heteromeric channels with particular subunit compositions.

4.8 Automation of the Rb^+ efflux assay

This was automated using the set up shown in **Fig. 4.12**. Each individual component can be programmed from the central computer (**Fig. 4.12g**) through individual software drivers which allow various protocols to be written for each component. CLARA software is used to link all the processes together into a complete assay cycle which can be repeated as many times as there are cell plates for analysis. Cell and compound plates, empty assay plates and racks of tips start in the Twister II plate racks (**Fig. 4.12d**). A deep well plate containing wash and stimulation buffers and a reservoir containing lysis buffer are placed on the Sciclone ALH 500 (**Fig. 4.12a**). On commencement of the assay cycle, the plate washer (**Fig. 4.12e**) and multidrop (**Fig. 4.12f**) are initialised, tips moved to the Sciclone and loaded onto the 96-well head, a compound plate is also moved to the Sciclone and a cell plate moved to the plate washer and washed – all using the Twister II Robotic arm (**Fig. 4.12c**).

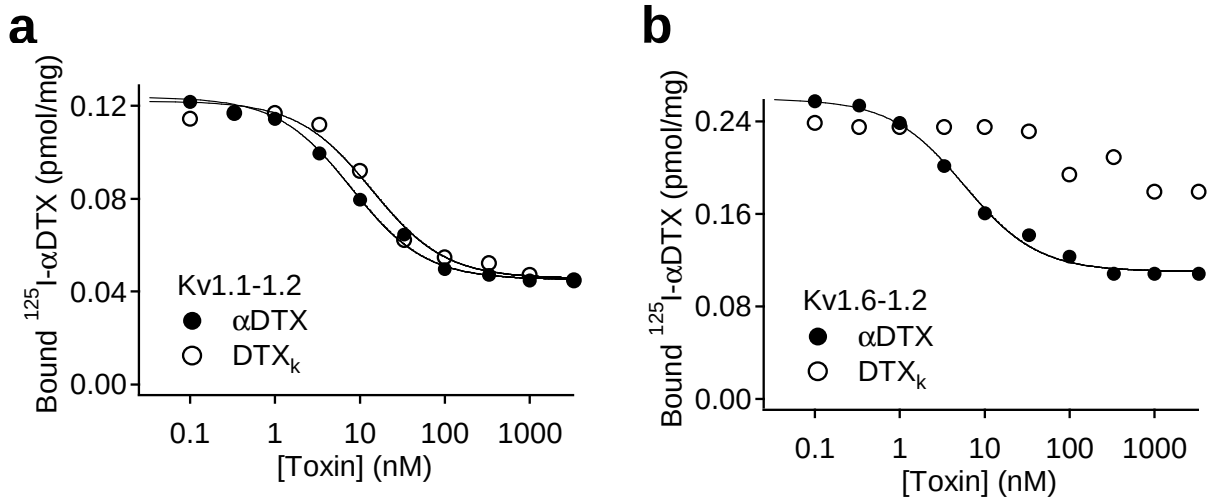

Figure 4.11 | Differential displacement by dendrotoxin$_k$ of ^{125}I-αdendrotoxin bound to Kv1.1-1.2 and 1.6-1.2 containing channels. HEK cells stably expressing Kv1.1-1.2 (**a**) or Kv1.6-1.2 (**b**) were incubated with a saturable concentration (2.5 nM) of ^{125}I-αDTX and the indicated concentration of unlabelled αDTX or DTX$_k$. Data points are the mean of triplicate measurements (see Materials and Methods). Curves represent a Langmuir isotherm fit to the data. IC$_{50}$ values from these fits were for αDTX: Kv1.1-1.2, 8.0 nM, Kv1.6-1.2, 5.7 nM and for DTX$_k$: Kv1.1-1.2, 13.8 nM; Kv1.6-1.2, >3300 nM. The content of sites was calculated by subtracting non-saturable binding of ^{125}I-αDTX remaining after displacement by unlabelled αDTX from cells stably expressing Kv1.1-1.2 and Kv.1.6-1.2, which represented 37 and 42% of the respective totals, to yield values of 0.08 and 0.15 pmoles/mg of total cell protein. It is notable that the higher content of sites obtained for the cells expressing Kv1.6-1.2 than Kv1.1-1.2 channels underlies the larger stimulated Rb^+ efflux from the former.

The cell plate is returned to the Sciclone and compound added. During the compound incubation time, the tips on the 96-well head are changed, an assay plate is
brought to the Sciclone and the compound plate is disposed of (**Fig. 4.12h**). Wash or stimulation buffers are then added to the cell plate and, once the stimulation period has elapsed, the supernatants from the cell plate are transferred to the empty assay plate, the cell plate is moved to the washer, washed and returned to the Sciclone; tips are changed again and the lysis buffer is added. During lysis, the supernatant assay plate is moved to the multidrop, the contents diluted and returned to the plate racks. A second empty plate is moved to the Sciclone. Once lysates are collected, the second assay plate is diluted with the multidrop and it plus the cell plate are returned to the plate racks and the used tips removed. The cycle is then repeated for the prescribed number of cell plates. The tips for the 96-well head are provided in racks containing 384 tips. Therefore, once 4 sets of tips have been used the empty rack is placed in the waste, by being dropped through a hole in the table to the waste bin below, and a fresh tip box moved from the plate racks. There is an area on the Sciclone through which the used tips are dropped and collected in a container underneath (obscured by the plate racks in **Fig. 4.12**).

4.9 Screening of a small library revealed many additional inhibitors of Kv1.1-1.2 and 1.6-1.2 containing channels but none that could distinguish them like dendrotoxin$_k$

The capacity of the automated Rb^+ efflux assay was utilised for screening a small library of potential K^+ channel blockers. For the purposes of the screen, these were divided into compounds known to block Kv1 containing channels (all peptide toxins), see **Table 2.2** for details, and those that block other families of K^+ channels (**Table 4.3**). In keeping with the screening protocols used in industry (e.g. at Xention Ltd., Cambridge, UK) a single concentration was employed for (nearly) all the toxins, for the initial screen. The peptide toxins to be screened inhibit channels that are sensitive to them in the low-sub nanomolar range, depending on the channel expression system and assays used. Thus, a concentration of 10 nM was chosen with the expectation that Rb^+ efflux through sensitive channels would be substantially inhibited clearly revealing insensitive channels. The only exception was MCD peptide. While the published effective doses also differ (**Table 2.2**, references), they tend to be considerably higher than those for the other peptide toxins investigated, hence a

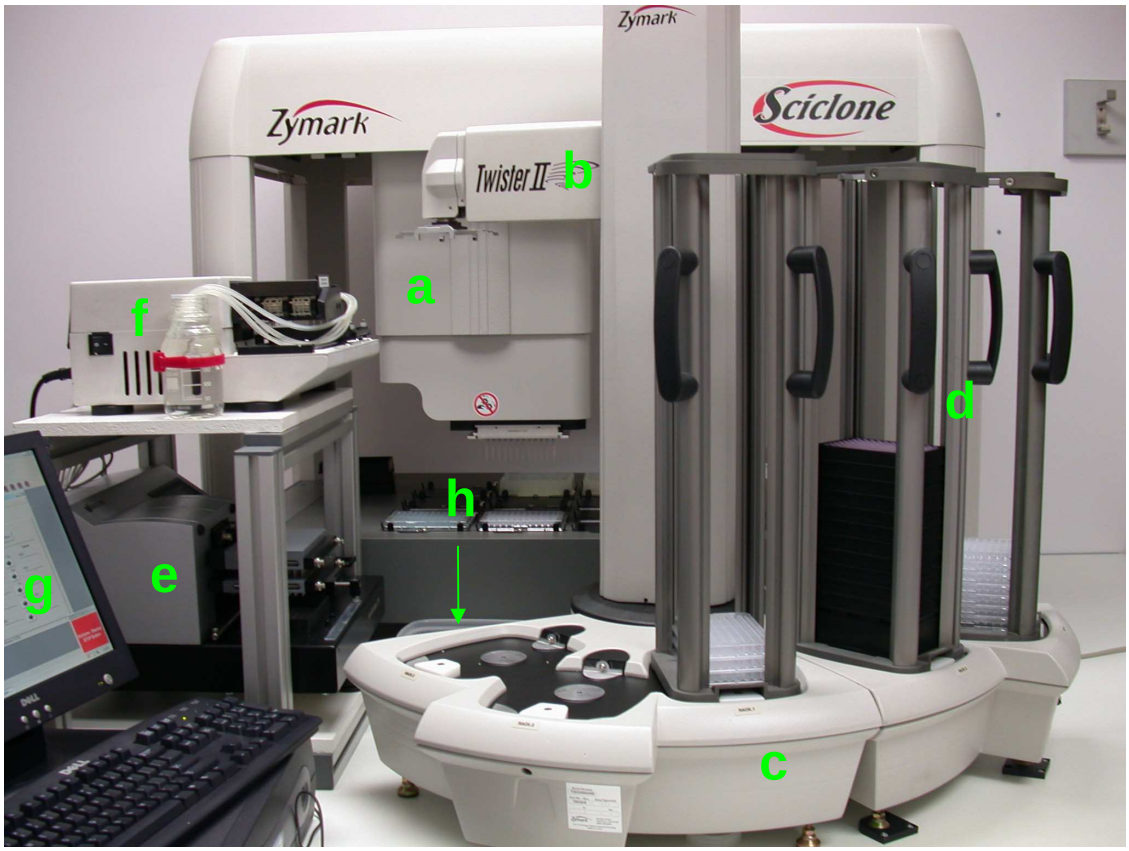

Figure 4.12 | Robotic system used for automation of the Rb^+ efflux assay. The system is composed of a Sciclone ALH 500 automated liquid handling system (**a**) and a Zymark Twister II microplate handler (**c**) with robotic arm (**b**) and plate racks (**d**). A Biotek ELX 405 *cw* plate washer (**e**) designed for washing plates containing cells was used for all washing steps. All large volume dilution steps were performed by a Thermo Scientific Multidrop 384 (**f**). Clara Software, with the appropriate drivers for each component, was used to run the system (**g**). Waste is disposed of through a hole in the table under which is a bin (**h**).

concentration of 100 nM was chosen. With a few exceptions, all of the Kv1 inhibitors blocked both the heteromers used in this study (**Fig. 4.13**). As with previous experiments (**Fig 4.10**), DTX_k discriminated between the two channels. δDTX, the *Dendroaspis angusticeps* homologue of DTX_k differentially inhibited the channels and two-way ANOVA analysis of the effect of DTX_k and δDTX on the two heteromers revealed that there is a significant difference between the reaction of both the channels to both the toxins ($p=0.0022$). Despite the significant difference in inhibition of the channels by δDTX, the fact that the toxin blocks Rb^+ efflux through both channels by more than 50% makes it an inappropriate distinguishing ligand (**Fig. 4.13**). Hence the startling specificity of DTX_k is revealed. Reports published previously have shown β and γDTX to inhibit Kv1.1 and 1.2 homomers expressed in *Xenopus* oocytes (Hopkins et al., 1996), a result not replicated in this study. This could be as a result of differences between the amphibian and mammalian expression systems, though more likely is due to discrepancies between the purification and identification of these toxins from the native venom.

Inhibitors active against other families of K^+ channels did not attenuate Rb^+ efflux through the Kv1.1-1.2 and 1.6-1.2 containing channels tested (**Fig 4.14**), further reassurance for the reliability of the assay. This was with the exception of Lq2 (**Fig. 4.14a**) which blocks the inward-rectifier K^+ channel, ROMK1 but also Kv1 channels (Lu and MacKinnon, 1997). As with the Kv1 channel blockers, 10 nM was used as the screening concentration unless available information on inhibition of the target channel type revealed the inhibitor to be less potent, in which case 100 nM was used.

It is important to note that there is some scatter in the efflux data obtained from the screen performed. Firstly, a number of compounds block Rb^+ efflux resulting in levels less than those in unstimulated wells (**Fig. 4.13**, e.g. MgTX and ShK). Secondly, in some cases, the supernatant concentration of Rb^+ is not exactly 100% with toxins that do not inhibit the test channel (**Fig. 4.13,** e.g. DTX_k on Kv1.6-1.2). Finally, there are instances of Rb^+ release being greater than the concentrations measured from unchallenged, stimulated cells (**Fig. 4.14**, e.g. BeKm I and E4031). As an added control for each 96-well plate of cells tested, 8 wells were treated with 10 mM 4-AP to ensure that stimulated release was inhibited. There was a large amount of scatter in this result also, typically ranging from -10% – +10% of normalised evoked efflux (data not shown). As all effux data is normalised to evoked

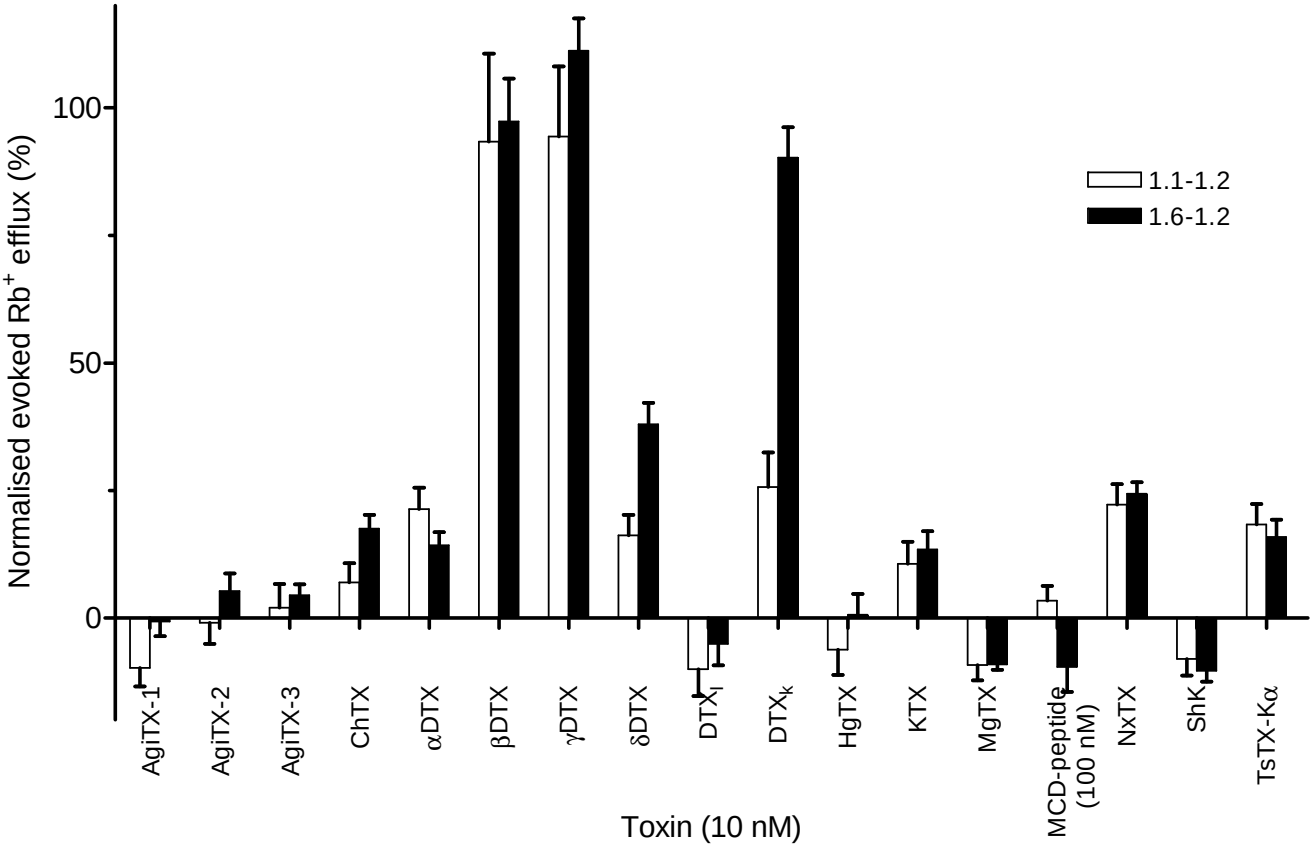

Figure 4.13 | Effect of various peptide toxins on Rb^+ efflux through recombinant Kv1.1-1.2 and 1.6-1.2 channels stably expressed in HEK cells. Rb^+ efflux experiments were performed, as described in Materials and Methods, to asses the activity of various peptide toxins (with know activity against Kv1 channels) towards these defined heteromeric channels. Results are expressed as mean ± S.E.M. (n=≥16). Two-way ANOVA analysis of the effect of δDTX and DTX_k on both channels found that the channels were inhibited differently by the toxins and each toxin had a different effect (p=<0.0001 in both cases). Test concentrations used were derived from effective doses previously published (see section **4.9**). **Table 2.2** gives details of the toxins used and Kv1 homomers they are active against.

Name	Type	Source	Sensitive K^+ channel type	Refs
Aa1	Peptide toxin	*Androctonus australis* (scorpion)	*Shaker* B (A-type) K^+ channels (IC_{50} 4.5μM)	(Pisciotta et al., 1998)
Apamin	Peptide toxin	*Apis mellifera* (honey bee)	Small conductance (SK), Ca^{2+}-activated K^+ channels (IC_{50} SK1 3.3 nM, SK2 83 pM)	(Blatz and Magleby, 1986; Strobaek et al., 2000)
BDS-I	Peptide toxin	*Anemonia sulcata* (sea anemone)	Rapidly inactivating (I_A) Kv3.4 K^+ channels (IC_{50} 47 nM)	(Diochot et al., 1998)
BDS-II	Peptide toxin	*Anemonia sulcata* (sea anemone)	Rapidly inactivating (I_A) Kv3.4 K^+ channels (IC_{50} 56 nM)	(Diochot et al., 1998)
BeKm-I	Peptide toxin	*Buthus eupeus* (scorpion)	ERG1 K^+ channels (IC_{50} 3.3 nM)	(Korolkova et al., 2001)
E-4031	Methane-sulfonanilide	class III antiarrhythmic drug	Voltage gated (HERG) K^+ channels (IC_{50} 7.7 nM)	(Zhou et al., 1998)
Ergtoxin	Peptide toxin	*Centruroides noxius* (scorpion)	ERG1 K^+ channels	(Scaloni et al., 2000)
Iberiotoxin	Peptide toxin	*Buthus tamulus* (scorpion)	High conductance, Ca^{2+}-activated K^+ channels (IC_{50} 250 pM)	(Galvez et al., 1990)
Lq2	Peptide toxin	*Leiurus quinquestriatus var. hebraeus* (scorpion)	Voltage- and Ca^{2+}-activated and Inward rectifier K_{ir} 1 (ROMK1) K^+ channels	(Lu and MacKinnon, 1997; Lucchesi et al., 1989)
Maurotoxin	Peptide toxin	*Maurus palmatus* (scorpion)	Voltage- and Ca^{2+}-activated K^+ channels	(Castle et al., 2003)
Paxilline	Tremorgenic alkaloid mycotoxin	*Penicillium paxilline* (fungus)	High conductance (MAXI-K), Ca^{2+}-activated K^+ channels	(Knaus et al., 1994)
Penitrem A	Fungal neurotoxin	*Aspergillus, Claviceps, Penicillium* species (fungi)	High conductance (MAXI-K), Ca^{2+}-activated K^+ channels	(Knaus et al., 1994)
Scyllatoxin	Peptide toxin	*Leiurus quinquestriatus var. hebraeus* (scorpion)	Small conductance (SK), Ca^{2+}-activated K^+ channels (IC_{50} SK1 80 nM, SK2 287 pM)	(Strobaek et al., 2000)
Slotoxin	Peptide toxin	*Centruroides noxius* (scorpion)	High conductance (MAXI-K), Ca^{2+}-activated K^+ channels (K_d 1.5 nM)	(Garcia-Valdes et al., 2001)
Tamapin	Peptide toxin	*Mesobuthus tamalus* (scorpion)	Small conductance (SK), Ca^{2+}-activated K^+ channels (IC_{50} 24 pM)	(Pedarzani et al., 2002)
Tertiapin	Peptide toxin	*Apis mellifera* (honey bee)	Inward rectifier (GIRK, K_i 8.6 nM and ROMK1, 2.0 nM) K^+ channels	(Jin and Lu, 1998)
Tertiapin Q	Peptide toxin	*Apis mellifera* (honey bee)	Inward rectifier (GIRK) and Ca^{2+}-activated (BK) K^+ channels (IC_{50}	(Jin and Lu, 1998; Kanjhan

Table 4.3 | Details of compounds known to block various K^+ channel families

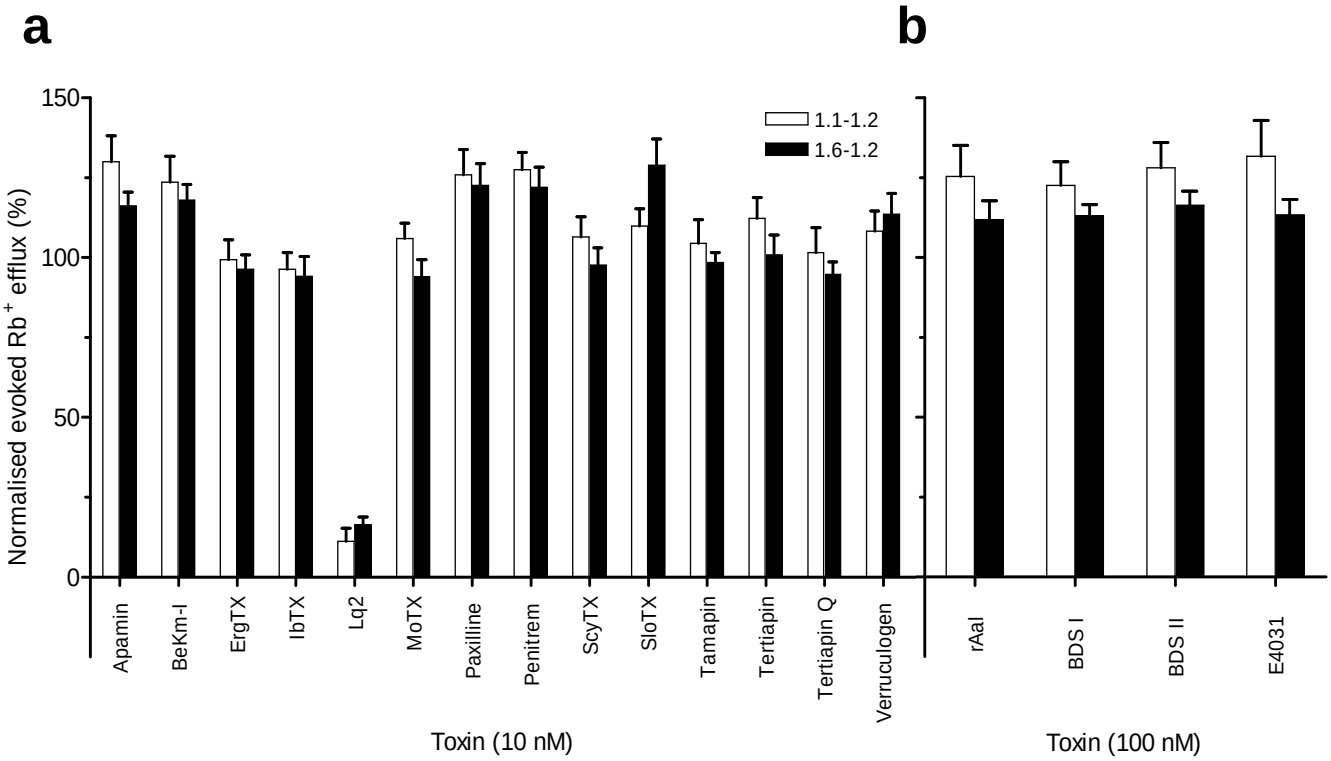

Figure 4.14 | Blockers with activity against various families of K^+ channels do not inhibit Rb^+ efflux through Kv1.1-1.2 or 1.6-1.2 containing channels. Details of the compounds studied are given in **Table 4.3**. Doses of 10 nM (**a**) or 100 nM (**b**) were determined from published concentrations used when these molecules were applied to the channel type they are active against. Data plotted is mean ± S.E.M., n≥16. Lq2 was the one exception that did block.

release calculated from just 16 wells - 8 unstimulated and 8 stimulated - it is not surprising that there is some scatter. Increasing the number of wells used for each condition should minimise this, but the number of wells used for such controls much be balanced with the number of compounds to be tested in each experiment. As the purpose of an initial screen is to establish only if a compound inhibits a specific channel or not, the quality of the data achieved herein is sufficient to support such conclusions.

4.10 Assessment of the suitability and accuracy of Rb^+ efflux for determining inhibitory constants of blockers

Having ascertained that at a fixed concentration, 10 nM, a number of peptide toxins block both channels used in this study, the IC_{50} values were determined for some of the more potent inhibitors [AgiTXs, ChTX (with Lq2 included for comparison), MgTX and ShK]. Inhibition of evoked Rb^+ efflux in the presence of various concentrations of each toxin (0.025–10 nM) was plotted using GraphPad Prism and the % evoked release remaining was fit with the Hill equation. IC_{50} values and Hill coefficients of the resultant slopes were determined from the line fit. Results obtained with the 2 channels were remarkably similar (**Fig 4.15a-e** and **Table 4.4**). All 3 AgiTXs inhibited K^+ elicited Rb^+ efflux with similar potencies; IC_{50} values were in the low nanomolar range with AgiTX-1 being the most potent and AgiTX-2 the least, with all values within a 10-fold concentration range. ChTX and Lq2 blocked the channels with potencies comparable to the AgiTXs. While Lq2 was more potent than ChTX, the difference was not sufficient to distinguish them. While none of these toxins proved able to distinguish the heteromers, these experiments demonstrate the suitability of Rb^+ efflux for the determination of inhibitory constants of toxins that block in the nanomolar range, thereby, offering a much faster alternative to the more labour intensive electrophysiology techniques. The Hill coefficient values are close to 1 (**Table 4.4**), demonstrating the expected independent binding of the toxin to the channel.

For some toxins though, the lowest concentrations used were already blocking both channels and Hill coefficient values were greater than 1 (**Fig. 4.16** and **Table 4.4**). MgTX and ShK potently inhibited Rb^+ efflux through both the Kv1.1-1.2 and 1.6-1.2 containing channels with IC_{50}s in the picomolar range. A minimum number of cells must be used in each well for Rb^+ efflux to give a sufficient signal:noise ratio. In the case of these very

potent toxins, the smallest possible cell number could still be too high for the number of toxin molecules in a µl volume of a picomolar solution, based on the following estimated calculations:

- ~8 nA current/cell x 1 pA predicted current/channel (Gutman et al., 2003a) = 8,000 channels/cell
- *100,000 cells/well x 8,000 channels/cell = 800 million channels /well
- 1.3 femtomole channel/well in **80 µl solution = 16 pM channel concentration

(* 50,000 cells/well left overnight; therefore, assume each cell divides once, ** 50 µl of compound added to well, plus a small amount of wash buffer remaining in each well)

Toxin is added to cells for 10 min and even assuming that all toxin molecules are available for binding to the channels where there is a small or no excess of toxin, an infinitely longer incubation time would be required for such a process to occur.

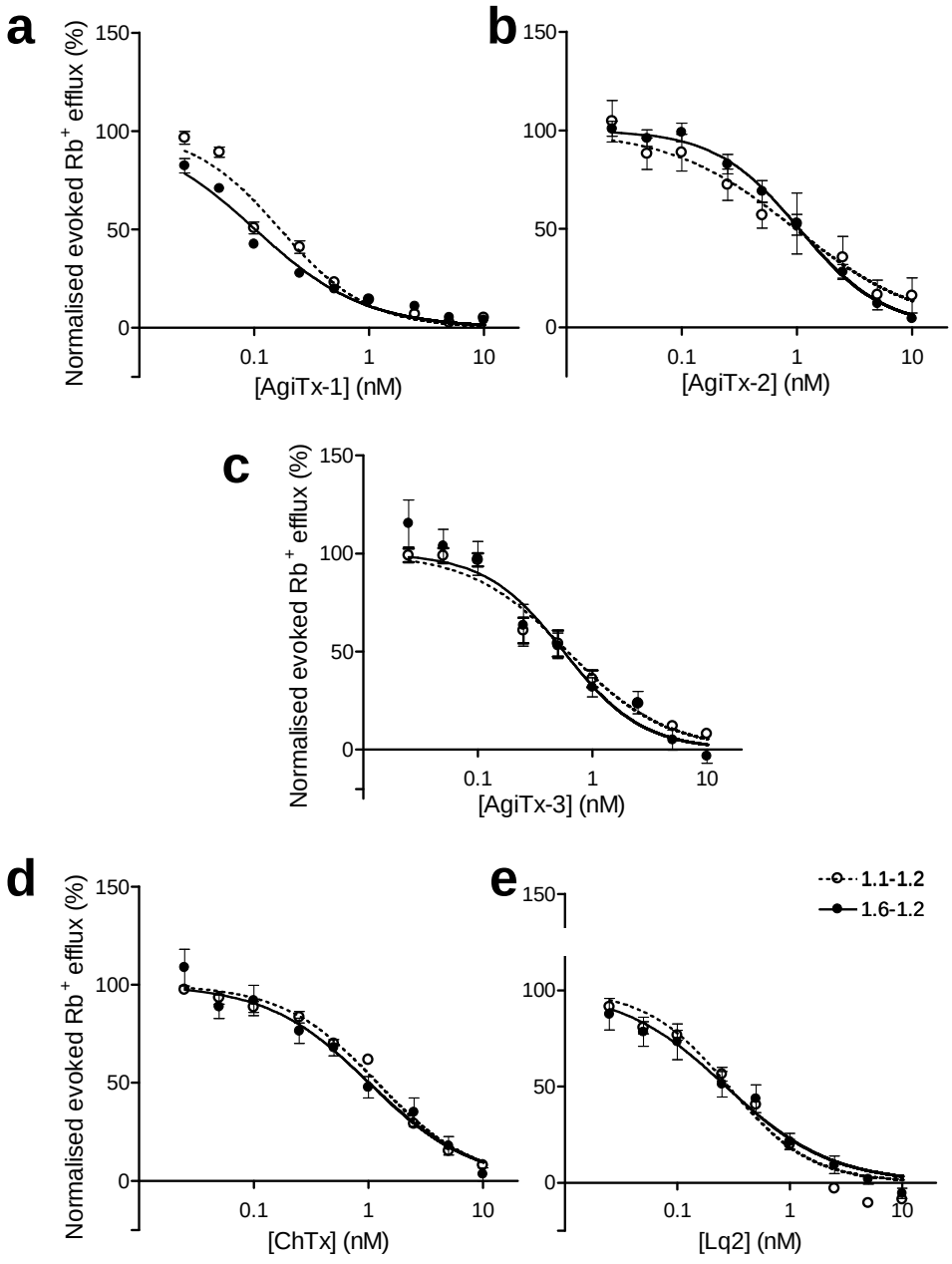

Figure 4.15 | Concentration response curves showing the effects of various toxins on Kv1.1-1.2 and 1.6-1.2 containing channels, as measured by Rb^+ efflux. Curves were fit using a Hill plot allowing an unconstrained Hill slope. IC_{50} and Hill coefficients are shown in **Table 4.4**; values plotted are an average of n >16 ± S.E.M.

Toxin	Kv1.1-1.2		Kv1.6-1.2	
	IC_{50} (nM)	Hill	IC_{50} (nM)	Hill
AgiTX-1	0.10	1.1	0.15	0.9
AgiTX-2	1.06	1.2	0.98	0.8
AgiTX-3	0.59	1.0	0.39	1.2
ChTX	1.2	1.0	1.0	1.0
Lq2	0.17	1.2	0.32	0.9
MgTX	0.01	1.3	0.01	1.3
ShK	0.006	1.3	$3.1x10^{-6}$	2.0

Table 4.4 | IC_{50} and Hill coefficient values determined by Rb^+ efflux for several toxins' inhibition of Kv1.1-1.2 and 1.6-1.2 containing channels

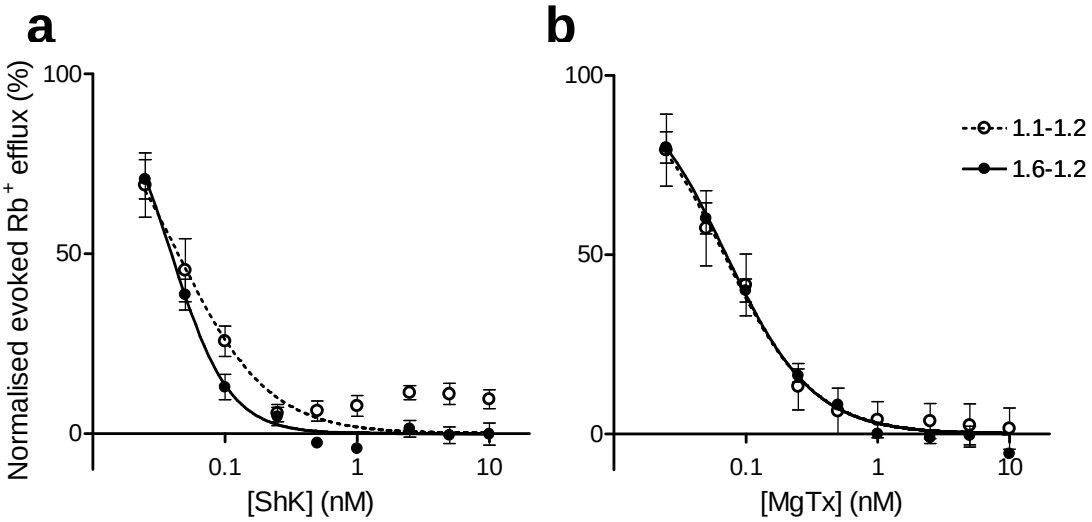

Figure 4.16 | Toxins that block Kv1.1-1.2 and 1.6-1.2 containing channels in the sub-nanomolar range are too potent for accurate determination of inhibitory constants by the Rb^+ efflux assay. Values plotted are an average of n >16 ± S.E.M. See **Table 4.4** for IC_{50} and Hill coefficient values.

4.11 Discussion

4.11.1 Kv1.1-1.2 containing channels expressed in CHO cells are susceptible to various blockers as measured electrophysiologically and by Rb^+ efflux

To develop inhibitors of therapeutic value, it is necessary to determine the functional properties of Kv1 channels in neurons, as related to their structures. These channels are present in neurons as oligomers of 4 α subunits (Parcej et al., 1992), in most instances as a combination of more than 1 α subunit type (Shamotienko et al., 1997). It is, therefore, necessary to study such physiologically-relevant heteromers in order to identify their individual characteristics and profiles as distinct from the homomers usually studied e.g. (Grissmer et al., 1994; Gutman et al., 2005). Given that Kv1.2 and Kv1.1 are the most prevalent α subunits in brain (Scott et al., 1994a), Kv1.1 is always associated with Kv1.2 (Shamotienko et al., 1997) and channels composed of only Kv1.1 and Kv1.2 α subunits have been identified in human brain (Coleman et al., 1999), this channel was chosen for study. Furthermore, several mutations have been reported in the Kv1.1 gene from patients with channelopathies (Lehmann-Horn and Jurkat-Rott, 1999). Recreation of this naturally-occurring heteromer was achieved through linkage of the α subunit genes as described previously (Akhtar et al., 2002). cRNA generated from the Kv1.1-1.2-pSFV1 plasmid was electroporated into CHO cells, resulting in good transfection efficiency and surface expressed channels; this was demonstrated by immuno-staining with an antibody specific for Kv1.2 (Muniz et al., 1992) and biotinylation followed by Western blotting of the surface-expressed channels. Electroporation conditions were optimised such that ~50% of cells were transfected, this being sufficient expression for electrophysiological recordings, enabling functional characterisation of these mammalian-expressed channels, experiments not conducted in the earlier study (Akhtar et al., 2002). The channel expression level was also such that Rb^+ efflux experiments could be conducted. The Rb^+ efflux assay as described by (Terstappen, 1999) is non-radioactive, high capacity (due to the 96-well plate format) and capable of functional analysis of both native and recombinant channels. It allows robust and reproducible characterisation of ion channel modulating compounds. Employment of this assay for use with recombinant heteromeric channels offers a convenient method in the search for specific blockers, especially in comparison to labour intensive and costly electrophysiology techniques. In this study, the assay was optimised

for use with the Kv1.1-1.2 expressing CHO cells and the effects of various inhibitors were measured and compared to those obtained from electrophysiological recordings.

The recombinant channel generally behaved as expected in response to blockers. However, there were some minor differences observed between the assay systems. 4-AP (10 mM) gave a more complete block of Rb^+ efflux than K^+ current, presumably due to dissimilar experimental conditions used, based on the reasoning detailed in (Armstrong and Loboda, 2001). For example, the membrane potential was discharged with 75 mM K^+ rather than by the more extensive depolarisation used electrophysiologically. Incomplete block as measured by the latter has been attributed to the use of very negative holding potentials and a partial relief of inhibition by large depolarisation (Armstrong and Loboda, 2001). Conversely, low concentrations of 4-AP (<1 mM) inhibited I_K more than Rb^+ efflux, perhaps due to a reduced effectiveness of this compound in the presence of Rb^+ compared to K^+ (Kirsch et al., 1986).

The inhibition by TEA of Rb^+ efflux resembles that seen electrophysiologically. In both instances, the expressed channel showed low susceptibility to TEA, with 20 mM giving only ~40% inhibition; this is likely due to the presence of 2 TEA-insensitive Kv1.2 subunits (Gutman et al., 2005). While αDTX blocked the K^+ current potently and almost completely as would be expected from the sensitivities of Kv1.1 and 1.2 homomeric channels to the toxin (Grissmer et al., 1994), equivalent levels of blockade required higher concentrations in the flux assay. This could be due to restricted diffusion of the toxin to cells, but as the cell number in each well was balanced between maintaining a monolayer while still providing sufficient channels for Rb^+ efflux measurements, this possibility should be minimised. Perhaps, more likely, the effect is due to the adherence of some toxin to the cell plate and other plastics used during the course of the assay.

Despite these limited discrepancies, this study has confirmed that Rb^+ efflux can be used to determine the pharmacological profiles of recombinant K^+ channels of defined subunit composition expressed in mammalian cells. The ability to investigate several blockers in a single experiment, conferred by the 96-well format, is particularly attractive for pharmacological applications. This, coupled with the recombinant technology validated herein for creating Kv1 channels of specific α subunit composition, should facilitate research into the pharmacological characteristics of native channels, thereby, revealing

heteromer-specific blockers. However, given the short useful life-span of the electroporated CHO cells (24 h) and the large numbers of cells that would be required for screening even a minimal library of potential blockers, a larger source of channels and longer lasting cells were necessary for harnessing the full potential of this technology.

4.11.2 Heteromers composed of Kv1.1-1.2 and 1.6-1.2 stably expressed in HEK cells provide a plentiful source of channels for extensive biophysical and pharmacological characterisation

To this end, stable cell lines were developed expressing Kv1.1-1.2 and 1.6-1.2 containing channels. The resultant channels, composed of the 3 most prevalent Kv1 subunits in brain, were profiled and revealed similar biophysical properties. There was, however, a change in activation when Kv1.1 was substituted with Kv1.6, resulting in Kv1.6-1.2 containing channels activating at somewhat more negative potentials. As Kv1.6 monomers activated at more positive potentials than Kv1.1, this result is unexpected. It illustrates the point that assumptions cannot be made as to the properties of heteromeric channels based on those of homomers. The pharmacology of these channels was of particular interest given the ultimate aim of this research - to find specific blockers of hetero-tetrameric combinations of Kv1 α subunits. Therefore, the effects of TEA, 4-AP, αDTX and DTX_k were investigated. 4-AP and αDTX had similar effects on both channels, consistent with the published effects of these blockers on the parental Kv1.1, 1.2 and 1.6 homomeric channels (Gutman et al., 2005; Harvey, 1997). TEA was less effective at blocking Kv1.6-1.2 than Kv1.1-1.2 containing channels as expected given the increased susceptibility of Kv1.1 subunits compared with Kv1.6. When measured electrophysiologically, this difference was sufficient to distinguish the 2 channels. However, while Rb^+ efflux results revealed a difference in sensitivities, it was not as pronounced as found with the former. DTX_k proved to be the most effective discriminating ligand, from both electrophysiological recordings and Rb^+ efflux results. Furthermore, while DTX_k displaced ^{125}I-αDTX from Kv1.1-1.2 containing channels, this was not the case with those containing Kv1.6-1.2. This data clearly establishes the distinguishing properties of DTX_k. Taken together, these results demonstrate the unique properties of the 2 heteromeric channels studied and emphasise the

importance of investigating K^+ channels composed of α subunit combinations mimicking those found in neuronal channels.

The agreement between Rb^+ efflux and the more conventional electrophysiology results demonstrated with HEK-expressed channels, and the provision of large numbers of channels with this expression system, led to automation of the assay resulting in a truly high-throughput screening system. Such added capacity was utilised to perform a small scale screen of some blockers known to inhibit some Kv1 and other families of K^+ channels. Examination of the Kv1 α subunits sensitivities of the known Kv1 blockers demonstrated some predictability for effects on Kv1.1-1.2 and Kv1.6-1.2 containing channels. However, despite previously reported action of β and γDTX on both Kv1.1 and Kv1.2 homomers expressed in oocytes, no inhibition was seen herein. While differences in post-translational modifications between amphibian and mammalian expression systems could contribute to this, or inconsistencies in the identification of these toxins when purified from venom, this discrepancy demonstrates yet again the importance of studying physiologically-relevant heteromeric channels and not extrapolating from homomers. Inhibitors that block other families of K^+ channels did not affect the Kv1 channels used in this study. In this case Lq2, a blocker of ROMK1 channels (Lu and MacKinnon, 1997), was an exception. However, Lq2 is purified from the same venom of ChTX and has close sequence homology, differing at only 8 positions (Lucchesi et al., 1989). It is, therefore, not surprising that both these toxins exhibit similar effects on the expressed channels.

Having performed a successful screen, the quantitative potential of Rb^+ efflux was deciphered by examining inhibitory constants from concentration response measurements. While toxins that block at picomolar concentrations are too potent for such measurements, requiring instead electrophysiological analysis, toxins that block these channels with IC_{50} values in the nanomolar range are ideal for such analysis. The outcome demonstrates the value of Rb^+ efflux as a means of decreasing the number of samples to be tested using more time consuming techniques, and its potential for quantitative analysis in some situations. This validated approach can now be applied to more Kv1 constructs to determine pharmacological profiles and garner further information in the search for heteromer-specific ligands.

Chapter 5

Comparison of the pharmacological profiles of channels composed of a Kv1.X-1.2 series of dimers

5.1 Overview

In the search for blockers with specificity for neuronally-expressed Kv1 channel heteromers, it is important to understand the influence of combinations of α subunits within tetramers, on their inhibitory activities. To achieve this, Kv1.1-1.2, 1.2-1.2, 1.3-1.2, 1.4-1.2 and 1.6-1.2 containing channels were expressed in HEK cells, their surface targeting confirmed by immuno-fluorescence and pharmacological profiles determined using Rb^+ efflux. Saturable binding of ^{125}I-αDTX to cells expressing the recombinant proteins further established the presence of intact channels on the plasmalemma; abilities of various other toxins to antagonise the binding of the radioactive probe were found to be comparable with Rb^+ efflux results.

This study explored the effects of heteromeric combinations of α subunits on blockade of channels by various peptide toxins, results that cannot be determined solely by examining the previously reported interactions of relevant parental homomers with the requisite inhibitor. It is clear that a heteromeric channel consisting of some toxin-sensitive subunits cannot be assumed to be inhibited by that compound. Indeed, the presence of some insensitive subunits in a heteromer can reduce or prevent inhibition despite inclusion in the channel of subunits sensitive to the toxin in question. Identifying the effects of heteromeric α subunit compositions on peptide toxin inhibition is an important step in the design of blockers specific for oligomeric channel subtypes.

5.2 Plasma membrane targeting of Kv1.X-1.2 containing channels revealed by immuno-staining

COS cells transfected with Kv1.X-1.2-pIRES2-EGFP plasmids, prepared using the cassette cloning system (see Materials and Methods and Chapter 6), were labelled with IgGs specific to external epitopes of Kv1.2 (Tiffany et al., 2000) (**Fig. 5.1** left hand panels).

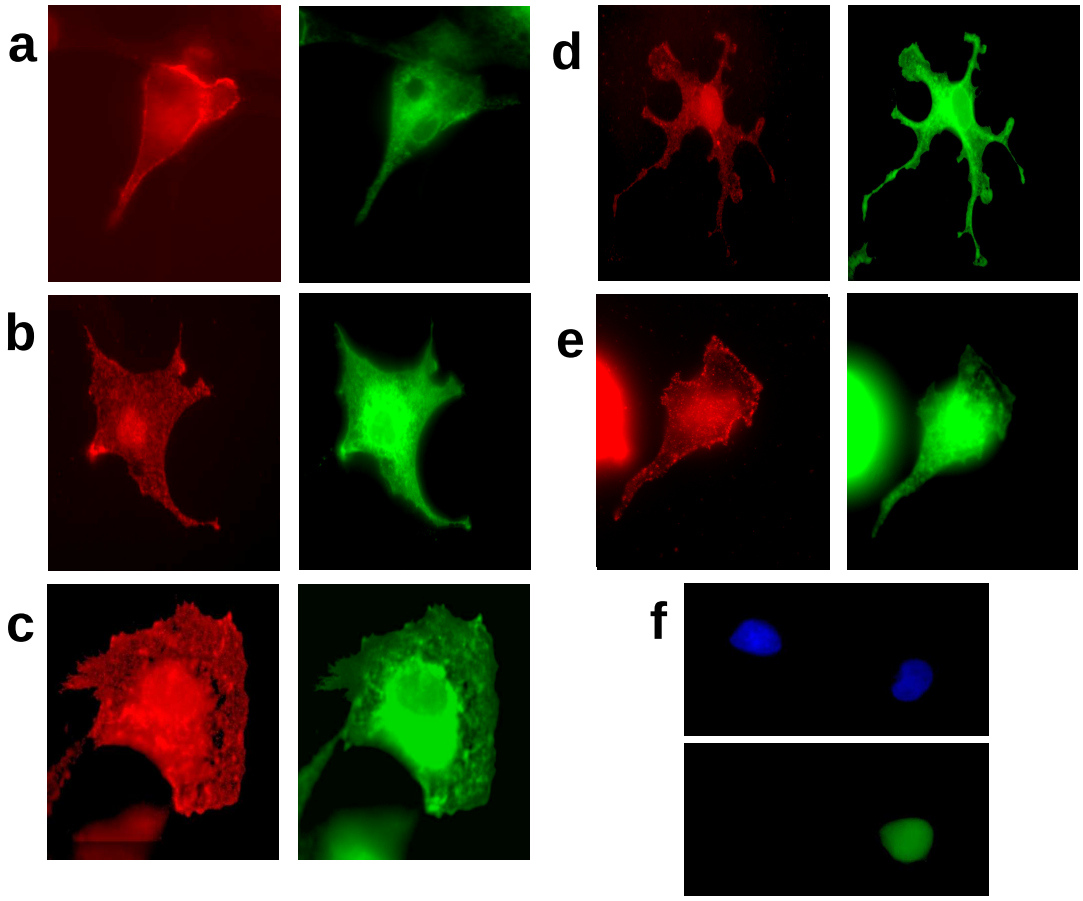

Figure 5.1| Fluorescent micrographs showing surface expression of channels containing 5 different Kv1.X-1.2 dimers. COS cells, transfected with Kv1.1-1.2- (**a**), Kv1.2-1.2- (**b**), Kv1.3-1.2- (**c**), Kv1.4-1.2- (**d**) or Kv1.6-1.2-pIRES2-EGFP (**e**) were double labelled using an antibody reactive with external epitopes of Kv1.2 (Tiffany et al., 2000) (left panels) and a monoclonal antibody specific for an intracellular epitope of Kv1.2 (right panels). The surface labelling visualised (red) was distinguished from the total (green) using anti-species IgGs coupled to AF 594 or 488, respectively (**a-e**). **f**, Only background signals were seen upon omission of primary antibodies, representing the signal resulting from EGFP expression in transfected cells. Top panel shows DAPI stained nuclei, the bottom panel, EGFP signal from a transfected cell. With these exposure conditions, the EGFP fluorescence visible is concentrated mainly around the nucleus of the cell and clearly does not interfere with the specific signals resulting from antibody labelling.

After cell permeabilisation, a monoclonal Kv1.2 antibody directed against a cytoplasmic domain was used to label the total channel population (**Fig. 5.1** right hand panels). Secondary antibodies conjugated to AF 594 and 488, respectively, were used. Despite a large population of internal channels for each construct, a significant proportion of each of the channels was targeted to the cell surface. Different patterns of staining resulted from the 2 antibodies used. While surface channels are labelled all over the plasma membrane, in the total field there is a strong signal from the internal channels, concentrated around the nucleus. Omission of the primary antibodies resulted in an absence of signals at this exposure, and in doing so revealed the EGFP signal due to the pIRES2-EGFP constructs (**Fig. 5.1f**). This result shows clearly that such fluorescence does not interfere with the antibody labelling.

5.3 Saturable binding of ^{125}I-αdendrotoxin demonstrates that the surface expressed channels are correctly assembled

Suspensions of cells expressing the Kv1.X-1.2 constructs were incubated with increasing concentrations of iodinated toxin in the presence and absence of unlabelled αDTX. Subtraction of the non-specific binding from the total generated the saturable component. Thus, ^{125}I-αDTX was shown to bind to the channels tested in a saturable manner (**Fig. 5.2**), evidence that correctly folded and assembled tetrameric channels are present on the cell surface (Tytgat et al., 1995). The K_D and B_{max} values for the five constructs are listed in **Table 5.1**. The K_D value (0.6 nM) obtained for Kv1.1-1.2 containing channels (**Fig. 5.2a**) was comparable with results previously obtained for concatenated Kv1.1 and 1.2 subunits (0.5 nM) (Akhtar et al., 2002). Kv1.6-1.2 containing channels behaved similarly (K_D = 0.6 nM), as might be expected due to the presence of 4 αDTX-sensitive α subunits (**Fig. 5.2e**). Surprisingly, toxin interaction with Kv1.2-1.2 heteromers resulted in a higher K_D (1.7 nM), perhaps as a result of the transient nature of the channel expression (**Fig. 5.2b**). The K_D of 5 nM for Kv1.3-1.2 containing channels could be attributed to the presence of αDTX insensitive Kv1.3 subunits in the channels (**Fig. 5.2c**). Likewise, this was also the case for Kv1.4-1.2 containing channels (K_D = 4.3 nM) (**Fig 5.2d**). The presence of a positively charged lysine residue in the pore region of the 1.4 subunits obviously electrostatically reduces the toxin's affinity. The low unsaturable binding levels are likely due to enhanced

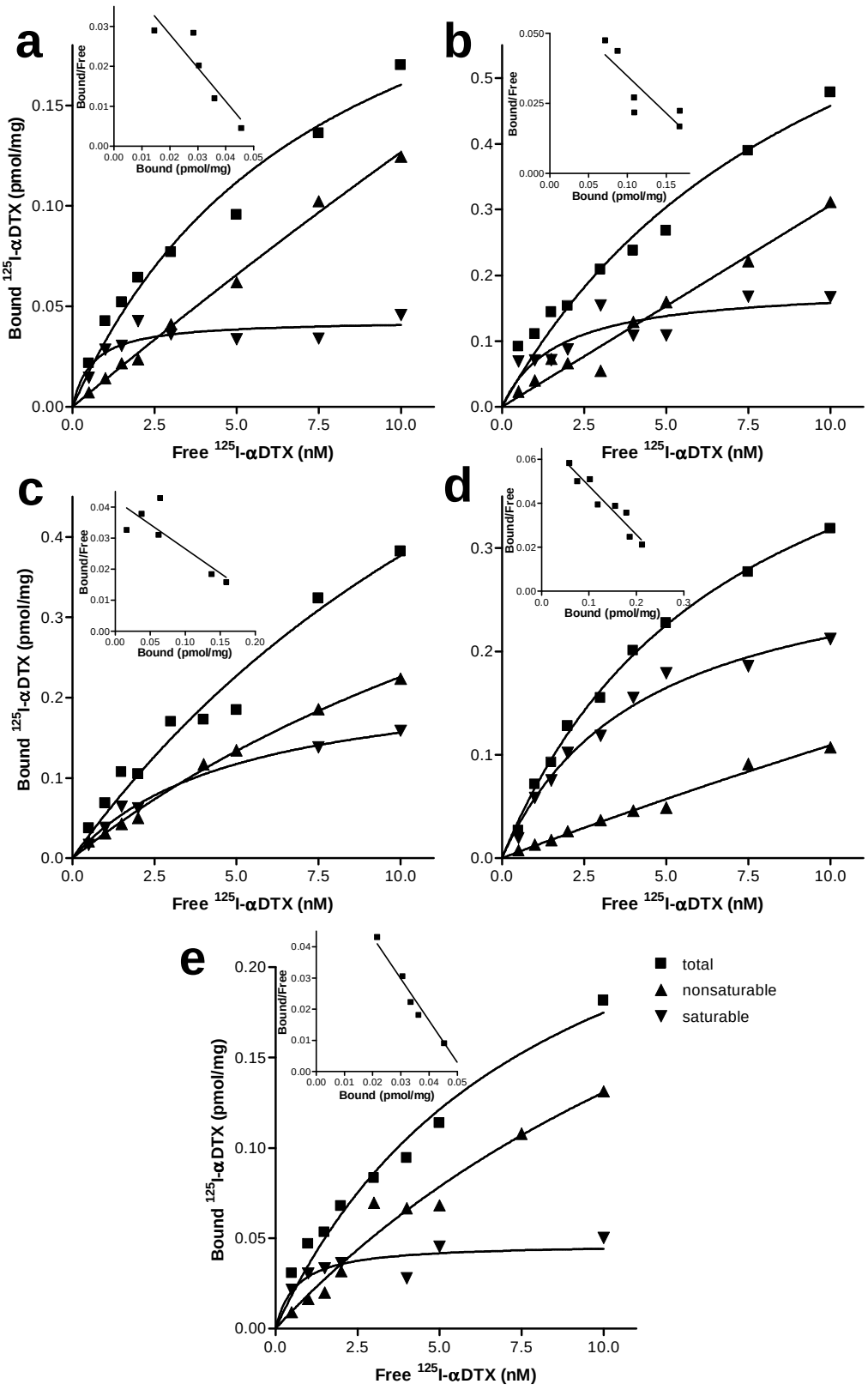
a
b
c
d
e
Bound ^{125}I-αDTX (pmol/mg)
Free ^{125}I-αDTX (nM)
Bound/Free
Bound (pmol/mg)
total
nonsaturable
saturable

Figure 5.2 | Saturable binding of ^{125}I-αdendrotoxin to intact HEK cells transfected with various heteromeric Kv1 channel constructs. **a**, Stably expressed Kv1.1-1.2 containing channels, **b**, **c** and **d**, transiently expressed Kv1.2-1.2, 1.3-1.2 and 1.4-1.2 containing channels respectively. **e**, Kv1.6-1.2 heteromers stably expressed. Total binding (resulting from increasing concentrations of ^{125}I-αDTX) was quantified with a filtration assay; non-saturable binding was measured in the presence of 1 μM unlabelled αDTX; substraction of the 2 values yields the saturable component. Insets show a Scatchard plot of the saturable binding. Data was analysed using GraphPad Prism nonlinear regression to yield K_D values.

Channel	K_D (nM)	B_{max} (pmol/mg)
Kv1.1-1.2	0.6	0.04
Kv1.2-1.2	1.7	0.2
Kv1.3-1.2	5.0	0.2
Kv1.4-1.2	4.3	0.3
Kv1.6-1.2	0.6	0.05

Table 5.1 | K_D and B_{max} values for saturable binding of ^{125}I-αdendrotoxin to HEK cells expressing Kv1.X-1.2 containing channels

surface expression of these channels, imbued by the presence of Kv1.4 subunits (Manganas and Trimmer, 2000). This is supported by a higher B_{max} value than the other constructs (**Table 5.1**). It should be noted that both Kv1.2-1.2 and Kv1.3-1.2 channels had a much higher level of surface expressed channels, presumably due to the larger quantities of DNA required to achieve saturable toxin binding when expressing these constructs compared with Kv1.1-1.2 and 1.6-1.2 containing channels.

5.4 Effects of various Kv1 inhibitors on the functionality of Kv1.X-1.2 heteromeric channels cannot be predicted from inhibition of their parental homomers

Rb^+ efflux experiments were performed on HEK cells transiently transfected with Kv1.2-1.2- and 1.3-1.2-pIRES2-EGFP and a stable cell line expressing Kv1.4-1.2-pIRES2-EGFP. The 3 constructs were prepared by the modular cloning described in Materials and Methods and Chapter 6. Stable cell lines expressing Kv1.2-1.2 and 1.3-1.2 containing channels were also developed but the level of expression was insufficient to give an adequate signal:noise ratio in the Rb^+ efflux assay. The effects of peptide toxin inhibitors with known activity on Kv1 channels (**Table 2.2**) were investigated and combined with results obtained previously for Kv1.1-1.2 and 1.6-1.2 containing channels (**Fig. 4.3, 4.13, 4.14**) but this screen also included ShK-Dap^{22}, a derivative of the sea anemone toxin ShK, described in (Kalman et al., 1998; Middleton et al., 2003). β and γDTX failed to inhibit flux through any of the recombinant channels at the concentration tested despite the presence of Kv1.2 subunits, contrary to their previously attributed activity on Kv1.1 and 1.2 containing channels (Hopkins et al., 1996). DTX_k, which only blocks channels containing Kv1.1 (Akhtar et al., 2002), inhibited Rb^+ efflux only through Kv1.1-1.2. Notably, its homologue δDTX from *Dendroaspis angusticeps* behaved similarly, not attenuating Rb^+ release through Kv1.2-1.2, 1.3-1.2 or 1.4-1.2 containing channels. However, in contrast to DTX_k, it blocked Kv1.6-1.2 channels significantly more ($p<0.0001$). Both these toxins were isolated from venom in-house and are very pure, giving single peaks on ion-exchange and reverse phase chromatography. Although the peptide sequences of these toxins differ in only 3 places (**Table 2.1**), these residues are on the channel-binding face of the toxin and this clearly has a marked effect on the activity (Harvey, 1997; Imredy and MacKinnon, 2000).

Literature to date reports kaliotoxin (KTX) to have inhibitory activity on I_K through channels possessing Kv1.1 or 1.3 (Grissmer et al., 1994). The inhibition of Rb^+ efflux through Kv1.1-1.2 and 1.3-1.2 containing channels in this screen is, therefore, to be expected; however, efflux via Kv1.6-1.2 was also reduced. Given that Kv1.2-1.2 is not similarly affected, it can be presumed that this effect is due to Kv1.6 subunits being sensitive to this toxin, an observation not previously recorded. However, it would be worthwhile to try higher concentrations of KTX on Kv1.2-1.2 containing channels to ascertain if the small amount of block seen in these measurements is real or more likely due

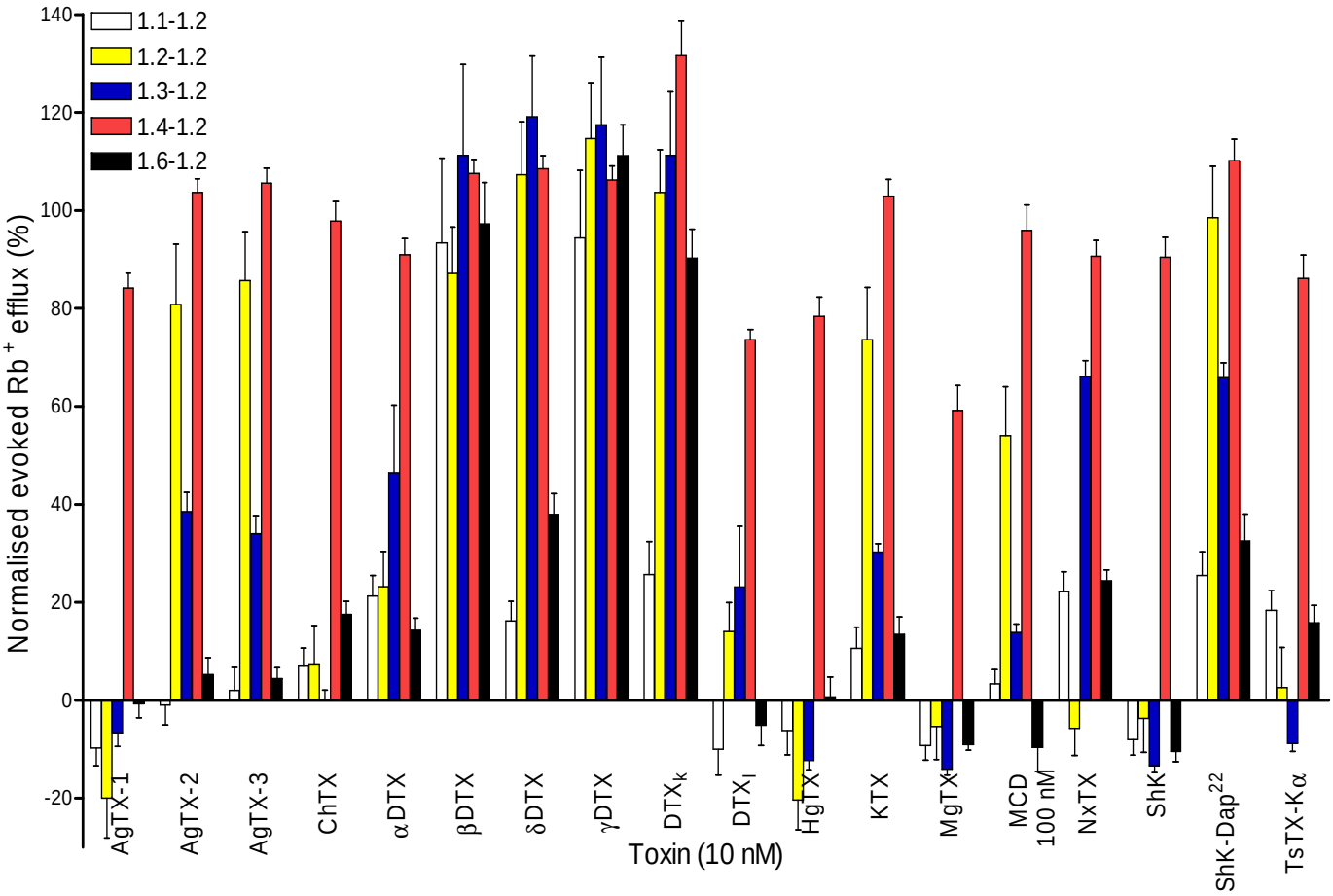

Figure 5.3 | Inhibition of Rb^+ efflux through channels made up from the Kv1.X-1.2 dimer series expressed in HEK cells. The effects of various peptide toxin blockers of Kv1 channels on Rb^+ efflux from HEK cells expressing Kv1.1-1.2-, Kv1.2-1.2-, Kv1.3-1.2-, Kv1.4-1.2- and Kv1.6-1.2-pIRES2-EGFP constructs, were quantified by AAS. Evoked (stimulated-basal) efflux was normalised to that for an unchallenged control and data plotted as average (n = 16) ± S.E.M., with measurements performed on at least 2 different days. All toxins were tested at 10 nM with the exception of MCD peptide where a 100 nM dose was used - in line with previously reported effective doses (Grissmer et al., 1994). Rb^+ efflux through Kv1.6-1.2 containing channels was inhibited significantly more by δDTX compared with DTX_k ($p<0.001$) as measured by an unpaired t-test.

to data scatter; experiments not performed herein due to the large amounts of toxin required and the associated expense. The other toxins tested inhibited channels in accordance with known α subunit sensitivies with the exception of the toxins described in-depth in the coming sections. Across all the toxins tested, Kv1.4-1.2 containing channels gave unusual results. While in most cases the presence of insensitive subunits does not prevent channel inhibition, this is not the case for Kv1.4-1.2 containing channels. Kv1.4 homomers are not blocked by any known peptide toxin (see below) and their presence in a heteromeric channel appears to greatly reduce or prevent blockade of the sensitive subunits. TsTX-Kα is a potent blocker of Kv1.2 channels (Hopkins, 1998) [as well as Kv1.3 (Rodrigues et al., 2003)] but while it inhibited all the other Kv1.X-1.2 containing channels, it proved relatively ineffective towards Kv1.4-1.2, blocking less that 20% of the Rb^+ efflux. This effect is seen with all toxins tested including ShK which was once reported to block Kv1.4 channels (Kalman et al., 1998) although that result has not been replicated elsewhere. Prevention of expected channel inhibition by the presence of Kv1.4 is less pronounced with some toxins e.g. MgTX, HgTX and DTX_I. Further investigations are necessary to determine the extent to which the binding of these toxins are affected by the presence of Kv1.4 subunits. Overall though, it appears that Kv1.4 subunits act, to a greater or lesser extent, in a "repulsive" manner in the inhibitory actions of toxins on heteromeric channels.

5.5 Inhibitors of other families of K^+ channels do not inhibit these Kv1 channels, with a few exceptions

In the main, the K^+ channel inhibitors used in this screen (see **Table 4.3** for details) did not attenuate Rb^+ efflux (**Fig. 5.4a,b**). As observed in other screening experiments there was some scatter in the data (see Chapter 4), in many cases with Rb^+ concentrations in supernatants being higher than in the unchallenged control wells; this resulted in evoked release greater than 100%. Generally, this was more pronounced for transiently-expressed channels, reinforcing the notion that this is likely due to data variability rather than measured channel modulatory effects of the compounds in question. However in some more extreme cases, e.g. Penitrem on Kv1.2-1.2, the potential of channel opening activity could be investigated. As was observed with Kv1.1-1.2 and 1.6-1.2 containing channels (**Fig. 4.14**), Lq2 blocked other members of the Kv1.X-1.2 family with the exception of

Kv1.4-1.2 (**Fig. 5.4a**) where less than 20% inhibition of Rb^+ efflux was observed. This corresponds to the actions of the related ChTX, raising the assumption that these toxins target the same Kv1 α subunits. Given that the 2 toxins are isolated from the same venom and have significant sequence homology differing at only 8 positions (Lucchesi et al., 1989), this is not unlikely. Experiments on Kv1.4-1.2 containing channels with ChTX and Lq2 using a range of concentrations, would determine if Lq2 more potently inhibits Kv1.4 containing channels – a result suggested from this initial screening data. Maurotoxin (MoTX) is a potent blocker of the intermediate-conductance Ca^{2+}-activated K^+ channel, hIKCa1 (Visan et al., 2004), but there have also been reports of its ability to block Kv1.1, 1.2 and 1.3 homomers (Kharrat et al., 1996). This toxin was initially screened against Kv1.1-1.2 and 1.6-1.2 containing channels (**Fig. 4.14**). However, no inhibition of Rb^+ efflux was observed, even in the case of Kv1.1-1.2 where only reportedly sensitive subunits were present in the channel. The same result was observed with Kv1.3-1.2 containing channels and, not surprisingly, Kv1.4-1.2. However, Rb^+ efflux was attenuated through channels consisting of only Kv1.2 subunits (Kv1.2-1.2), highlighting the sometimes unexpected interaction between peptide toxins and heteromeric Kv1 channels.

5.6 Screening agitoxins against the Kv1.X-1.2 series reveals previously unknown sensitivities of Kv1 α subunits

Three AgiTXs have been isolated from the venom of the scorpion *Leiurus quinquestriatus var. hebraeus* (Garcia et al., 1994). To date, AgiTXs -1 and -2 have been shown to be active on Kv1.1, 1.3 and 1.6 and AgiTX-3 inhibits Kv1.3 channels (Cayabyab et al., 2000; Garcia et al., 1994; Suarez-Kurtz et al., 1999). In this study, AgiTX-1 inhibited Rb^+ efflux through Kv1.2-1.2 containing channels (**Fig. 5.5a**). Given that this is a homomeric Kv1.2 channel, the result suggests that the toxin also has activity against Kv1.2 subunits. This was not the case for AgiTXs 2 and 3 which did considerably inhibit Rb^+ efflux through the Kv1.2-1.2 channels. While there appears to be some decrease in Rb^+ efflux through Kv1.2-1.2 channels with these toxins, this is likely due to data scatter as the channel is transiently expressed and the error bars are considerable. Likewise, AgiTX-3 was shown to have the same effects as AgiTX-2 on the heteromeric channels investigated, implying the same

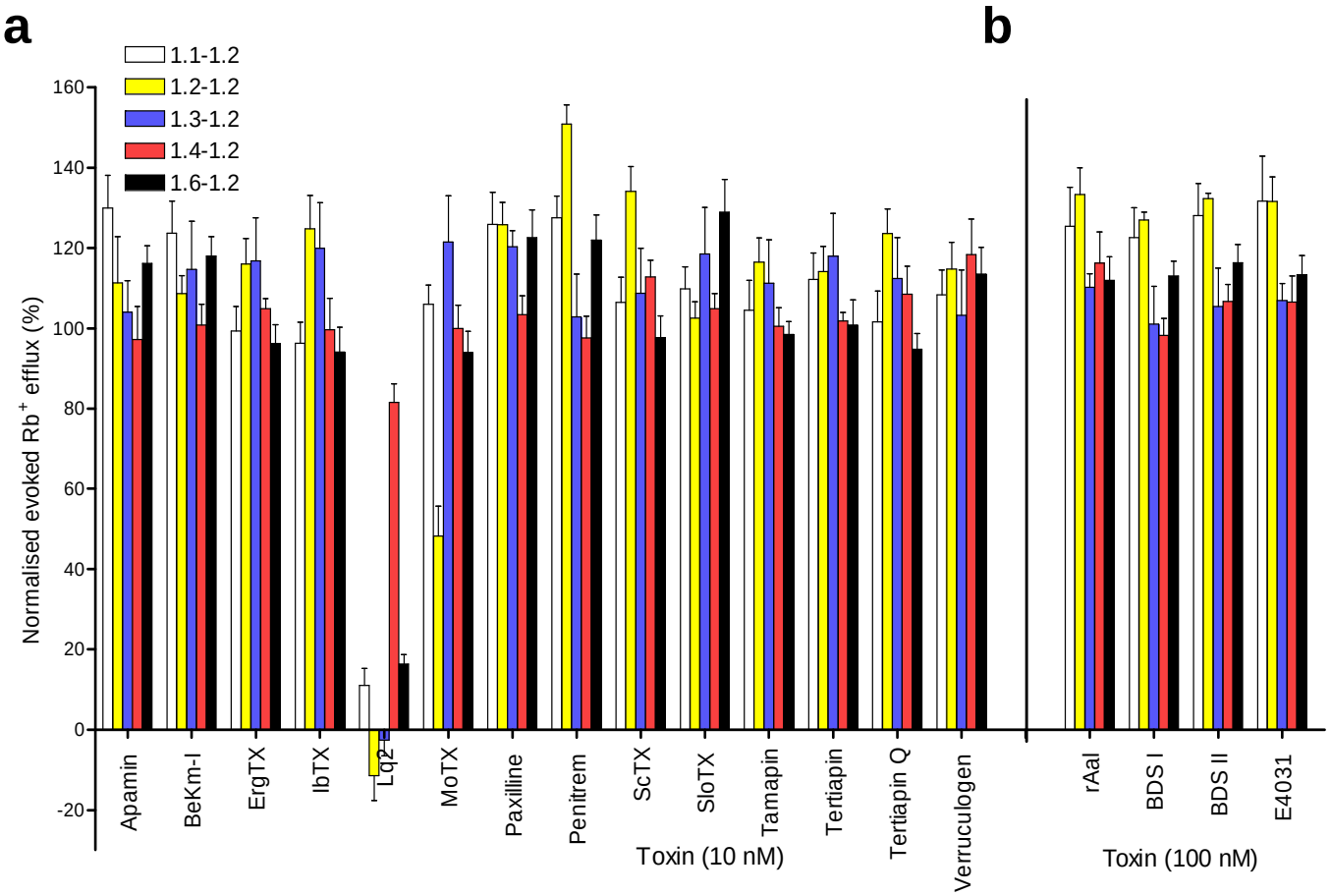

Figure 5.4 | Effects of various blockers of other K^+ channel families on Rb^+ efflux through the Kv1.X-1.2 channels. MoTX was found to be an interesting blocker of Kv1.2-1.2. Evoked Rb^+ release in the presence of 10 nM (**a**) or 100 nM (**b**) test compound (detailed in **Table 4.3**), was normalised to unchallenged efflux. Data plotted are average (n = 16) ± S.E.M.

range of α subunit targets (**Fig. 5.5a**). It is clear that the presence of Kv1.4 subunits in the heteromers examined proves repulsive to these toxins, as there was no inhibition of Rb^+ efflux by AgiTX-2 or -3 through Kv1.4-1.2 containing channels. In the presence of AgiTX-1, flux was inhibited by ~20%. While this is possibly due to scatter in the data, it could also be a result of a limited effect of this toxin imbued by its action on the Kv1.2 subunits in the channel. As these results were obtained with just a single concentration of the respective toxins (10 nM), ^{125}I-αDTX displacement experiments were performed to further evaluate this result (**Fig. 5.5b**). Inhibitory constants (K_i) of the various peptide toxins investigated were calculated according to the equation: $K_i = (IC_{50})/\{1+ [L^*]/K_D\}$, where the IC_{50} value was taken from the sigmoidal concentration-response curves for the displacement of ^{125}I-αDTX, drawn and analysed using GraphPad Prism and [L*] is concentration of radioactive ligand, in this case 2.5 nM. K_i values are listed in the figure legend and in **Table 5.2**. Kv1.1-1.2 and 1.6-1.2 containing channels are most potently blocked by all 3 AgiTXs, with K_is less than 1 nM. Though Kv1.3-1.2 heteromers were less sensitive to the toxins, they were still inhibited in the low nanomolar range. While knowledge of the interaction of these toxins with channels possessing various α subunits was expanded, these toxins do not fulfil the criterion set for this search; that is ability to distinguish the heteromers examined.

5.7 Noxiustoxin gives a similar displacement of ^{125}I-αdendrotoxin from Kv1.2-1.2 and 1.3-1.2 containing channels in contrast to Rb^+ efflux results

NxTX has been shown to block Kv1.2 and Kv1.3 elicited I_Ks with a K_D of 2 and 1 nM, respectively (Grissmer et al., 1994). However in this study, while Rb^+ efflux through Kv1.2-1.2 channels was inhibited completely by 10 nM toxin, the same was not the case for Kv1.3-1.2 containing channels, where only 35% block was observed (**Fig. 5.6a**). As both homomeric channels have very similar sensitivities to NxTX, this result was unexpected and, therefore, ^{125}I-αDTX displacement experiments were performed and inhibitory constants determined (**Fig. 5.6b**). Under these experimental conditions, however, the toxin potency was virtually identical for both channels (Kv1.2-1.2, K_i = 0.1 nM; Kv1.3-1.2, K_i = 0.2 nM, see **Table 5.2**).

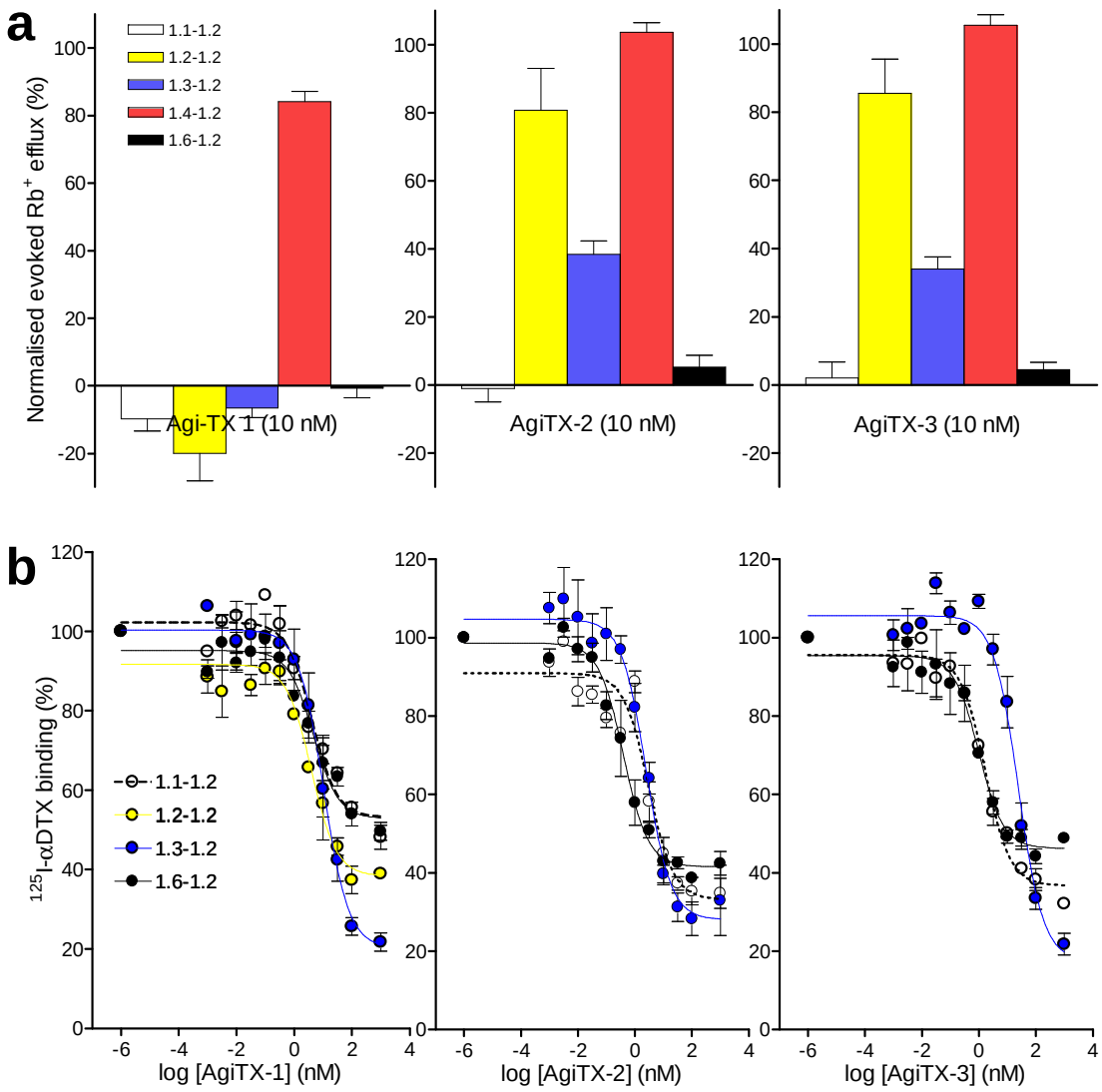

Figure 5.5 | Comparison of the influences of agitoxins on the series of Kv1.X-1.2 containing channels expressed in HEK cells. Results obtained for the inhibition of Rb^+ efflux (**a**) (taken from **Fig. 5.3**), were confirmed by displacement of bound ^{125}I-αDTX (**b**). **b**, Averages (n = 4) are plotted ± S.D. K_is are as follows, for AgiTX-1: 1.1-1.2 (0.8 nM), 1.2-1.2 (1.6 nM), 1.3-1.2 (6.9 nM), 1.6-1.2 (0.9 nM); for AgiTX-2: 1.1-1.2 (0.6 nM), 1.3-1.2 (1.6 nM), 1.6-1.2 (0.1 nM) and for AgiTX-3: 1.1-1.2 (0.3 nM), 1.3-1.2 (16.2 nM), 1.6-1.2 (0.2 nM).

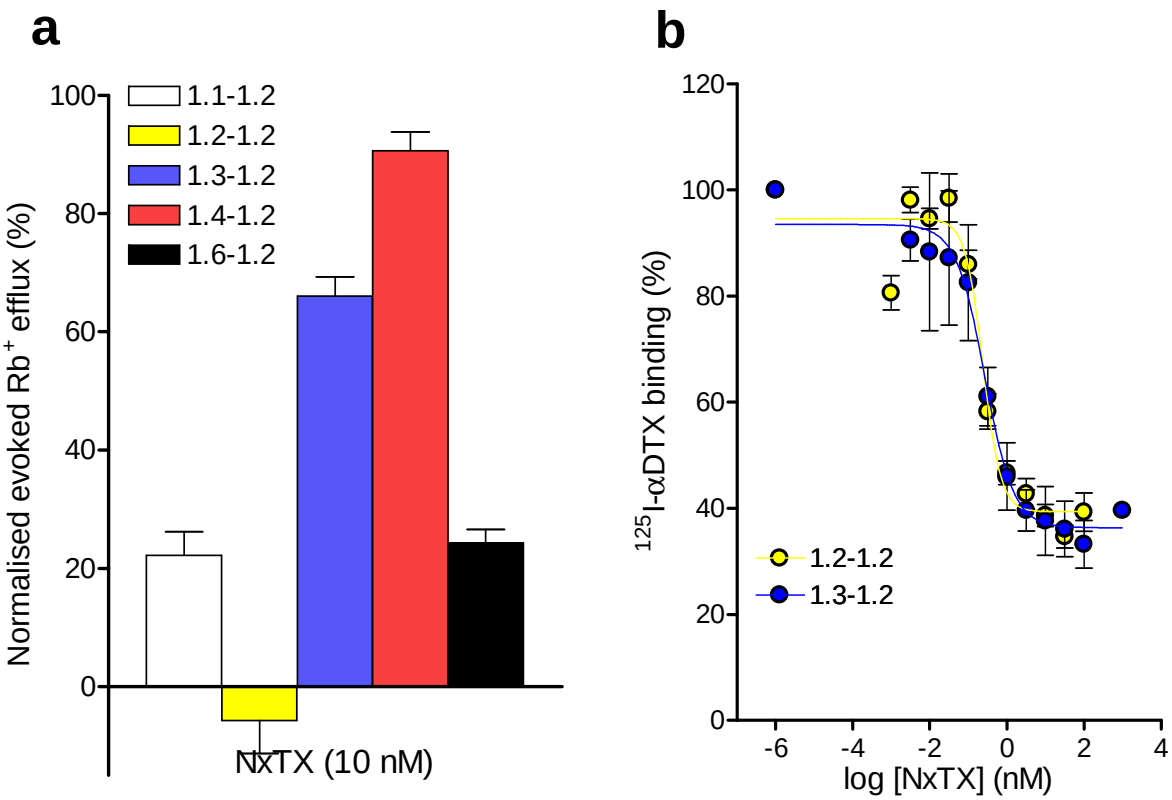

Figure 5.6 | Contrary to Rb^+ efflux results, noxiustoxin inhibits ^{125}I-αdendrotoxin binding to Kv1.2-1.2 and 1.3-1.2 containing channels with very similar potency. While blockade of evoked Rb^+ release through Kv1.3-1.2 channels was only 35% compared with 100% for 1.2-1.2 (**a**), displacement of ^{125}I-αDTX by the toxin from both channels was almost identical (**b**). Toxin displacement data is plotted as mean ± S.D., n = 4.

	Kv1.1-1.2	Kv1.2-1.2	Kv1.3-1.2	Kv1.4-1.2	Kv1.6-1.2
Agitoxin-1	0.8	1.6	6.9		0.9
Agitoxin-2	0.6		1.6		0.1
Agitoxin-3	0.3		16.6		0.2
Noxiustoxin		0.1	0.2		
ShK-Dap^{22}	2.3				38.0
Maurotoxin		0.9	0.1		
αdendrotoxin				1.9	
Hongotoxin				0.8	
Margatoxin				0.6	

Table 5.2 | K_i values (nM) for the displacement of ^{125}I-αdendrotoxin from various Kv1.X-1.2 containing channels expressed on the surface of HEK cells

5.8 ShK and its derivative ShK-Dap^{22} have different potencies and selectivities for channels comprising the Kv1.X-1.2 series

As described above (**Fig. 5.7a**), 10 nM ShK gave a 100% inhibition of Rb^+ efflux through all Kv1.X-1.2 channels with the exception of Kv1.4-1.2, due presumably to the presence of "inhibitory" Kv1.4 subunits. While the derivative ShK-Dap^{22} blocked Kv1.1-1.2, 1.3-1.2 and 1.6-1.2 containing channels (**Fig. 5.7b**), it showed a reduced potency compared with wild type ShK at the same concentration. This was expected given the results from previous studies (Kalman et al., 1998; Middleton et al., 2003). Both toxins failed to significantly block Rb^+ efflux through Kv1.4-1.2 containing channels (**Fig 5.7a,b**), suggesting that these toxins are also "repelled" by the presence of Kv1.4 subunits in a channel. Once again, the small (~10%) reduction of flux seen with ShK on these channels (**Fig. 5.7a**) could be due to data scatter or the presence of Kv1.2 subunits, which ShK inhibits. Most interestingly, ShK-Dap^{22} did not attenuate evoked Rb^+ release (**Fig. 5.7b**) from Kv1.2-1.2 channels in agreement with published data showing the low affinity of Kv1.2 homomers to this toxin (Middleton et al., 2003). This result was confirmed by its inability to displace ^{125}I-αDTX bound to the same channels (**Fig. 5.7c**). This was not the case for displacement of ^{125}I-αDTX from Kv1.1-1.2 or 1.6-1.2 containing channels, though the potency of the toxin was

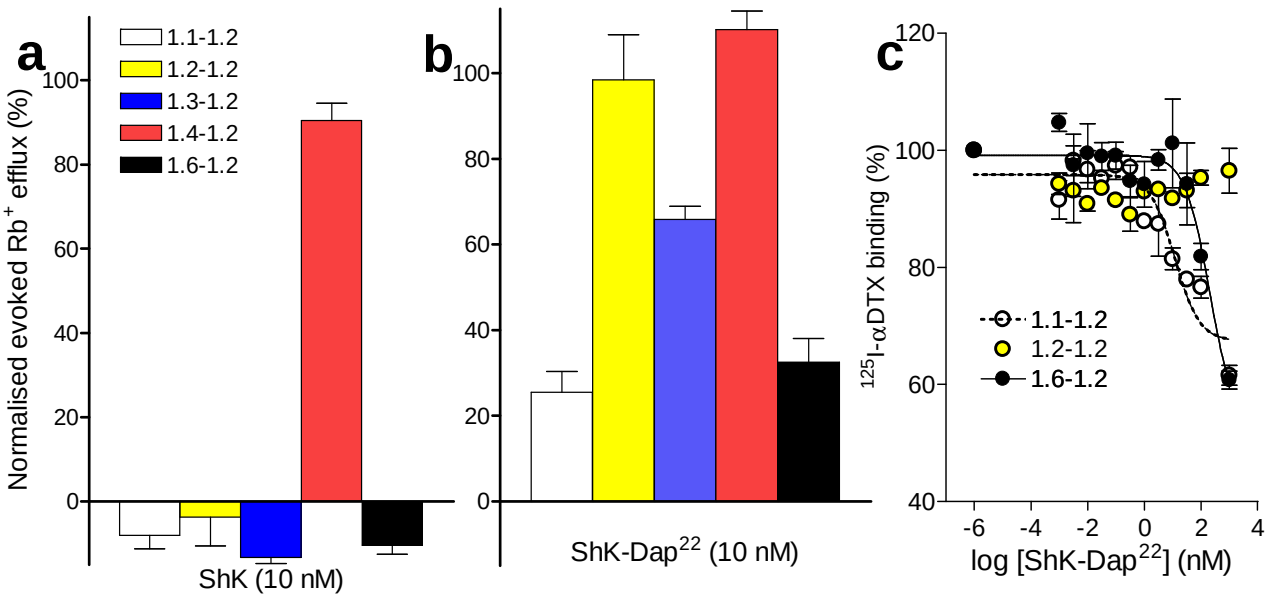

Figure 5.7 | ShK-Dap^{22} is less potent but more selective than the wild type ShK. The different potencies and selectivities of ShK and ShK-Dap^{22} were measured by inhibition of Rb^+ efflux through Kv1.X-1.2 containing channels (**a** and **b**; data from **Fig. 5.3**). The selectivity of ShK-Dap^{22} is confirmed with ^{125}I-αDTX displacement experiments (**c**). Average values are plotted ± S.D.; n = 4.

less than has been seen with other peptide toxins (K_i = 2.3 and 38.0 nM for Kv1.1-1.2 and 1.6-1.2 containing channels respectively, **Table 5.2**), resulting in large amounts of non-displaceable binding even with 1 µM ShK-Dap^{22} (**Fig. 5.7c**). Taken together this data demonstrates the lower potency of the ShK derivative, but its selectivity for Kv1.1-1.2 (and to a lesser extent Kv1.6-1.2) containing channels over Kv1.2 homomers is in agreement with previous reports (Middleton et al., 2003).

5.9 Maurotoxin is distinct from other venom-derived peptide toxins studied herein in its effects on heteromeric compared to homomeric channels

Given reports that MoTX inhibits I_K through Kv1.1, 1.2 and 1.3 channels expressed in *Xenopus* oocytes (Kharrat et al., 1996), it was surprising that only Rb^+ efflux through

Kv1.2-1.2 and not Kv1.1-1.2 and 1.3-1.2 channels was inhibited by this toxin, as 4 sensitive subunits are present in the latter (**Fig. 5.4a/5.8a**). Displacement by 1 μM MoTX of ^{125}I-αDTX bound to these channels was quantified to asses this result (**Fig. 5.8b**). As expected, this very large dose of toxin did not displace appreciable amounts of labelled αDTX from Kv1.1-1.2 (or Kv1.6-1.2) containing channels. However, this was not the case for those containing Kv1.3-1.2 (and 1.2-1.2 as expected from the Rb^+ efflux results). Therefore, experiments were performed to compare the K_is of displacement (**Fig. 5.8c**). While MoTX more potently displaced ^{125}I-αDTX from Kv1.3-1.2 compared with Kv1.2-1.2 containing channels, there was less than a 10-fold difference between them (Kv1.2-1.2, 0.9 nM and

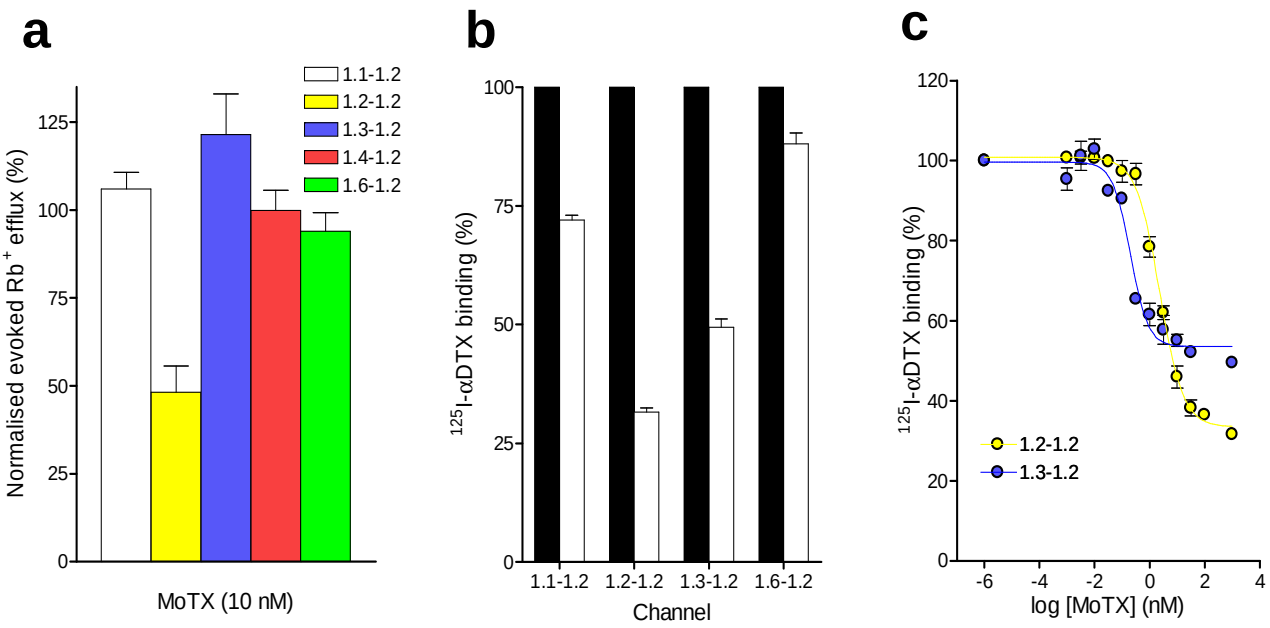

Figure 5.8 | Inhibition by maurotoxin of Kv1.2 containing heteromeric channels is influenced by the presence of other subunits. Rb^+ efflux data shows MoTX blocks Kv1.2 homomeric channels and not those containing Kv1.2 with other subunits (**a** – taken from **Fig. 5.4**). **b**, An excess (1 μM) of MoTX (□) does not substantaially displace ^{125}I-αDTX (■) bound to the Kv1.1-1.2 and 1.6-1.2 containing channels (mean ± S.D., n = 4). K_i values for Kv1.2-1.2 and 1.3-1.2, the 2 MoTX sensitive channels, were compared (0.9 and 0.1 nM respectively); averages are plotted ± S.D., n=4 (**c**).

Kv1.3-1.2, 0.1 nM, **Table 5.2**). Furthermore, the total amount of radio-labelled toxin displaced for Kv1.3-1.2 heteromers was limited, with high levels of non-displaceable binding remaining. Taken together, this data demonstrates that MoTX inhibition of heteromeric combinations of channels differs from that of other Kv1 blockers examined.

5.10 αdendrotoxin does not attenuate Rb^+ efflux through the Kv1.4-1.2 channel, but the expressed protein binds ^{125}I-αdendrotoxin and this is displaced by several toxins

Despite the lack of substantial inhibition of Kv1.4-1.2 containing channels by various Kv1.2 inhibiting toxins in Rb^+ efflux experiments, ^{125}I-αDTX bound saturably to this channel with low levels of non-specific binding (**Fig. 5.2d,**). In the presence of some toxins (HgTX and MgTX), however, there did appear to be some reduction in Rb^+ efflux, found to be statistically significant (**Fig. 5.9**). To test the consistency of these results, displacement of ^{125}I-αDTX by these toxins was quantified (**Fig. 5.9b**). The resultant K_i values reflect the degree of inhibition of Rb^+ efflux (in nM; αDTX, 1.9; HgTX, 0.8; MgTX, 0.6, **Table 5.2**). These results not only demonstrate the possibility of using αDTX as a radio-ligand for Kv1.4 containing channels when sensitive subunits are present, but also suggest that MgTX and HgTX may have some properties that render them less susceptible to "repulsion" by Kv1.4 than other peptide toxins examined.

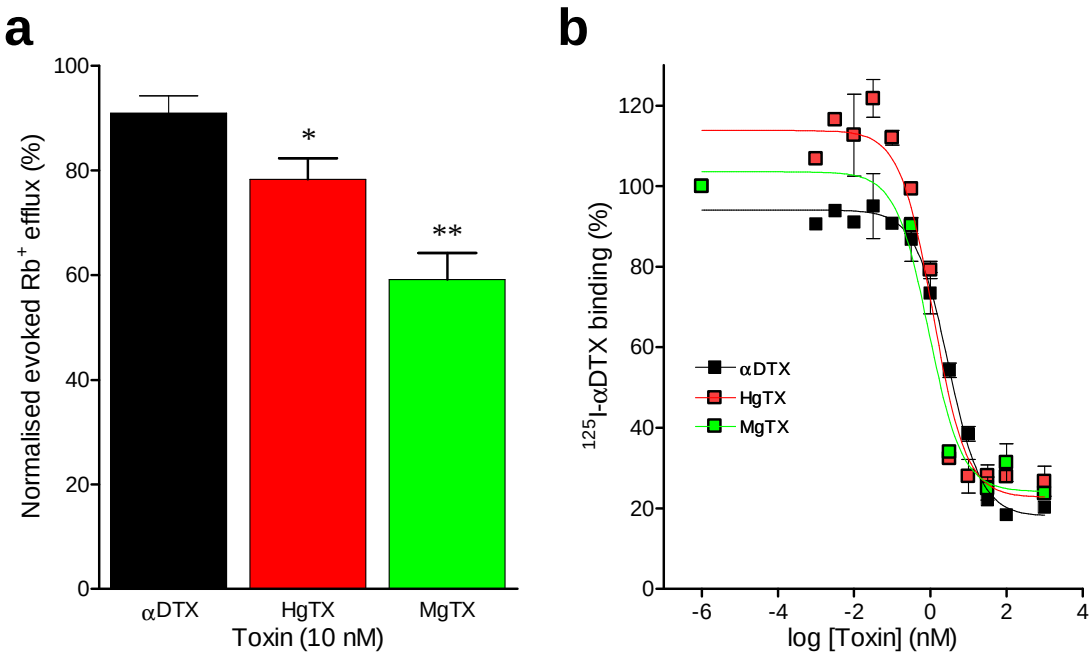

Figure 5.9| Comparison of ^{125}I-αdendrotoxin displacement from Kv1.4-1.2 containing channels by 3 peptide toxins. Kv1.4-1.2 containing channels proved insensitive to several Kv1.2 blocking toxin when measured by Rb^+ efflux (**a**). Increased inhibition of Rb^+ efflux by both HgTX and MgTX was statistically significant compared with block by αDTX; HgTX, p=0.0216 (*), MgTX, p=0.0001 (**), as measured by an unpaired t-test. **b**, Displacement of radio-labelled αDTX by the same unlabelled, HgTX and MgTX are expressed as averages (n = 4) ± S.D.

5.11 Discussion

Potential future therapeutics for the treatment of the many conditions involving hypo-excitability of subtypes of Kv1 channels require absolute specificity for their target, given the wide expression of these channels. As the majority of Kv1 channels isolated from mammalian brain are heteromeric combinations of α subunits, it is these channel compositions that need to be mimicked when considering targets for drug screening. Understanding the interaction of blockers with heteromeric as opposed to homomeric channel combinations, provides necessary insights for the design of these important inhibitors.

Kv1.2 is the most prevalent subunit in brain (Scott et al., 1994a) and is present in most heteromers whose compositions have been determined (Coleman et al., 1999; Shamotienko et al., 1997). Therefore, different subunits were combined with it, to produce the interesting Kv1.X-1.2 series. The cassette cloning system described in Chapter 6 and (Shamotienko et al., 2008) was used to make the constructs (Kv1.2-1.2, 1.3-1.2 and 1.4-1.2) which had not been investigated in previous studies. The extensive characterisation of channels resulting from these constructs confirms the efficacy of the modular cloning system for expressing constructs with any number of positions filled, as the constructs used here had only 2 positions filled and expressed functional channels, confirming that the ORF was maintained.

In an attempt to understand the interactions of the peptide toxins used in this study with heteromeric channels, screening of numerous Kv1 blocking peptide toxins was performed using a Rb^+ efflux assay. Inhibition of Rb^+ efflux was monitored in channels composed of subunits not previously shown to be sensitive to the toxins in question. In this way, the study served to increase the number of Kv1 α subunits known to be susceptible to some of the inhibitors screened. Of course, this assumes that sensitivities of homomeric Kv1.X channels can be extrapolated from results achieved with heteromeric combinations of Kv1 α subunits. While such conclusions are likely correct, it is important that the same assumptions are not made to predict heteromer pharmacology from examining homomeric combinations of channels alone. Nevertheless, in this study further target subunits for the AgiTXs, KTX and the ChTX homologue Lq2 have been putatively identified.

The “repulsive” effect of the Kv1.4 subunit on peptide toxin binding to channels containing it was also clearly demonstrated. That is, Rb^+ efflux through the Kv1.4-1.2 containing

channels was reduced to a far lesser extent than the other channels examined. Based on results obtained from the other members of the Kv1.X-1.2 series, toxins with activity against Kv1.2 subunits including but not limited to αDTX, ChTX, ShK and TsTX-Kα, would have been expected to block Rb^+ efflux. However, this was not the case as these toxins (10 nM) inhibited release by no more than 20%. Interestingly, some toxins did have a more pronounced effect and these were investigated further. When performing ^{125}I-αDTX binding experiments on the Kv1.X-1.2 containing channel series, Kv1.4-1.2 was also included despite the fact that αDTX did not inhibit flux. Surprisingly, the ^{125}I-αDTX bound specifically (K_D=4.3 nM) to the expressed channel, albeit with reduced affinity. This allowed displacement experiments to be performed confirming the Rb^+ efflux result that MgTX and HgTX have some inhibitory activity towards this channel. The interaction of αDTX as measured with Rb^+ efflux compared to toxin displacement experiments is surprising. Perhaps, the presence of Kv1.4 subunits increases the time required for toxin binding and, therefore, the 10 min toxin incubation used for Rb^+ efflux experiments is not sufficient but the 1 h incubation time used for radio-labelled toxin experiments is. An interesting next step is to see if the "repulsive" effect of Kv1.4 is altered in relation to the number of subunits present in a channel.

Importantly, there were several instances where the specificity of a toxin for a particular heteromer could not be predicted from published sensitivities of the relevant parental homomers. The selectivity of the ShK derivative ShK-Dap[22] for Kv1.1 and 1.2 containing heteromeric channels compared with either of the homomers, as previously reported (Middleton et al., 2003), was reproduced in this study for Kv1.1-1.2 compared with Kv1.2-1.2 containing channels (i.e. Kv1.2) homomers. Most surprising and truly unique though, was MoTX. Only Rb^+ efflux through Kv1.2-1.2 channels was blocked despite the fact that Kv1.1 and 1.3 subunits have also been shown to be sensitive to this toxin (Kharrat et al., 1996). Kv1.2 is the most sensitive of the 3 subunits, perhaps explaining why Rb^+ efflux through channels composed solely of this subunit (the Kv1.2-1.2 heteromers) was blocked. While of the remaining subunits, previously published data (Kharrat et al., 1996) suggests I_K through Kv1.1 is more sensitive to block by MoTX than K^+ current through Kv1.3 channels, when ^{125}I-αDTX displacement experiments were performed the opposite result was obtained. That is, while toxin binding to Kv1.1-1.2 was very poorly displaced by

MoTX, the toxin was more effective on Kv1.3-1.2 containing channels. The unusual features of this toxin certainly warrant further investigation. Perhaps it is more effective on homomeric as compared with heteromeric combinations of channels. Identification of the structures and residues responsible for this surprising selectivity could provide vital information for the manipulation of other more promiscuous but potent blockers.

Chapter 6

Concatenating tetramers of Kv1 α subunits to mimic those expressed neuronally unveils novel K^+ channel characteristics of authentic therapeutic targets

6.1 Overview

Many ion-channels, receptors, transporters and enzymes are heteromeric proteins, some of which are composed of structurally-related subunits. In most cases, specific channel subtypes or combinations are localised to particular tissues (Coleman et al., 1999), presumably to fulfill a defined function imbued by such controlled composition. When looking for new therapeutics, development of blockers specific for such localised oligomers should decrease side effects. The versatile and novel methodology described herein for concatenating subunits allows expression and functional characterisation of such proteins, providing native-like targets for drug screening.

This technology was developed for the study of hetero-tetrameric Kv1 channels with subunit compositions mimicking those identified in mammalian brain (Coleman et al., 1999; Koch et al., 1997; Koschak et al., 1998; Shamotienko et al., 1997). Functional analysis of such recombinant channels facilitated determination of the characteristic profiles of these channels which can be used to elucidate the molecular entities responsible for K^+ currents recorded from neurons.

This chapter describes the generation of 4 concatenated tetrameric combinations of Kv1 α subunits. Initially, three of these channels were extensively characterised and shown to traffic to the surface of HEK cells and yield functionally uniform channels whose K^+ currents could be distinguished by inactivation profiles and responses to selective blockers. This work has been submitted for publication in (Shamotienko et al., 2008). Experiments further investigating the effect of various toxins on Kv1.4 containing channels, begun in the previous chapter, involved the use of a fourth tetrameric channel.

6.2 The modular cloning system

This was designed to prepare concatenated constructs of Kv1.X genes, encoding any pre-determined stoichiometry and composition of α subunits. It involved linking constituents in the same ORF, using a proven inter-subunit linker originating from the *Xenopus* β-globin gene (Akhtar et al., 2002), making this approach potentially applicable to any multi-protein complex.

6.2.1 Generation and engineering of a bank of α subunit genes Initial PCR of Kv1.1, 1.2, 1.3 and 1.6 DNAs yielded single bands of the expected molecular mass of 1.5 kbp with Kv1.4 giving a larger size of 2.0 kbp. Amplified products were individually cloned into the polylinker of pβUT2 situated between the 5' and 3' UTRs of the *Xenopus* β-globin gene. Subsequent amplification of individual subunits within pβUT2 was carried out using primers designed against these flanking UTRs (**Table 3.1**); additionally, pairs of restriction sites were introduced to allow positional cloning of individual subunits (with flanking UTR elements) into the MCS of the pIRES expression plasmids (**Fig. 6.1a**). The first gene of each tetramer was inserted as domain I between Nhe I and Bgl II sites, with cloning being achieved using UTR-specific primers that encompass their sequences. Similarly, cloning of each of the constituent sequences into the remaining three domains could be accomplished, utilising the requisite pairs of restriction sites (**Fig. 6.1a**). Unlike the genes in domains I-III, the occupant of the last slot contained two stop codons. Thus, all four groups of UTR-specific primers differed only by domain–specific flanking restriction sites. Since each half-linker contained 30 nucleotides plus 3 (after assembly) for restriction sites, each two neighbouring subunits in the assembled oligomers (regardless of their domain) were separated by 78 nucleotides, including 6 each for Xba I and Xho I sites. Each product from the second round of PCR showed single DNA bands of the expected sizes when subjected to agarose electrophoresis.

6.2.2 Domain-specific assembly of gene cassettes into pIRES plasmids and expression of concatenated Kv1 channels Assembly of cassettes containing α subunit genes can be started from any of the 4 cloning domains. Similarly, any constituent can be cut-out and replaced

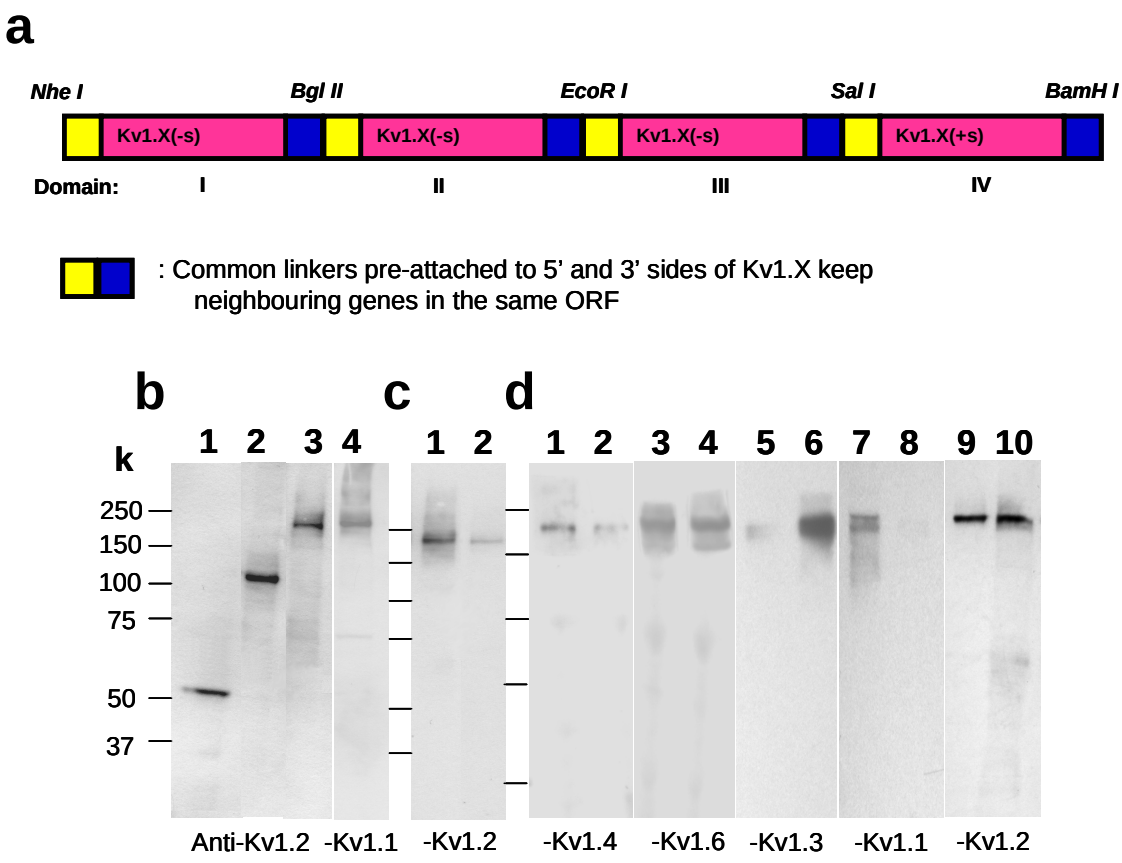

Figure 6.1| Concatenation of Kv1.X genes, expression and surface targeting in HEK cells of intact tetrameric Kv1 channels. **a**, Schematic - attachment to Kv1 genes of half-linkers and restriction sites for assembly of concatemers in pIRES2-EGFP or -DsRed. UTRs of *Xenopus* β globin gene and restriction sites for the enzymes specified were added to the ends of the Kv1.X inserts by PCR to allow position-specific cloning into the plasmids. Complete linkers form during the assembly of concatemers retaining all the sequences in the same ORF. **b**, HEK cells were transfected with pIRES2 reporter plasmids containing the Kv1 inserts specified and after 48 h subjected to SDS-PAGE followed by Western blotting with the antibodies specified, and visualisation using ECL reagents. Samples from cells transfected with pIRES2-EGFP containing the following constructs are shown in lanes: 1, Kv1.2; 2 Kv1.2-1.2; 3 & 4, Kv1.1-1.1-1.2-1.2. **c**, Biotinylation of surface proteins. Lanes: 2, surface biotinylated and affinity-isolated Kv1.1-1.1-1.2-1.2; 1, total protein from the non-biotinylated cells. **d**, Western blots of cells transfected with tetrameric constructs in pIRES2-DsRed; Kv1.4-1.6-1.1-1.2, (lanes 1, 3, 5, 7, 9), Kv1.4-1.6-1.3-1.2 (lanes 2, 4, 6, 8, 10). Lysates prepared from untransfected cells showed no reactivity against the antibodies used for the blotting (data not shown). Mobilities of standard proteins are indicated (**b-d**).

with another desirable Kv1.X gene; in fact, the structures of all the constructs were easily verified by restriction mapping (**Fig. 6.2**). For convenience, assembly was started at domain IV by incorporating the Kv1.2 gene (+ stop codons) into pIRES2-EGFP; upon expression, this gave a band with a Mr ~ 60-65 kDa, as revealed by SDS-PAGE and Western blotting (**Fig. 6.1b**), a size expected for this partially-glycosylated subunit. A homo-dimeric expressed protein with a Mr ~ 120 kDa (**Fig. 6.1b**) resulted from placing Kv1.2 (-stop codon) into domain III of the plasmid. Insertion of Kv1.1 (- stop codon) into domain II of Kv1.2-1.2, followed by incorporation of Kv1.1 (-stop codon) into domain I produced a full Kv1.X tetramer. After expression, this yielded a protein of Mr ~ 240 kDa detected by antibodies specific for Kv1.1 and 1.2 (**Fig. 6.1b**). Likewise, direct immuno-blotting of lysates from HEK cells transfected with pIRES2-DsRed containing Kv1.4-1.6-1.1-1.2 or Kv1.4-1.6-1.3-1.2 visualised a major band in each case corresponding to Mr ~ 240 kDa, when probed with antibodies specific for each of the constituent subunits (**Fig. 6.1d**). Some immuno-blots detected double bands corresponding, perhaps, to glycosylated forms characteristic of Kv1.4-containing channels (Shi and Trimmer, 1999). The successful generation of 3 hetero-tetrameric channels (the fourth is described later) exemplifies the usefulness of this strategy for assembling multi-component constructs which, in turn, allowed new structure-activity studies.

6.3 Intact and active tetrameric channels are targeted to the plasma membrane of HEK cells

For utilising recombinant Kv1 channels as targets for future drug screening, it was important to establish whether the concatenated oligomers traffic intact to the plasma membrane in active form when expressed in mammalian cells. Labelling of COS cells expressing Kv1.1-1.1-1.2-1.2 with IgGs specific for external epitopes of Kv1.2, followed by fluorescent microscopy, demonstrated clear staining on the cell surface (**Fig. 6.3a,b** – left hand panels). When the same cells were then permeabilised and incubated with a monoclonal antibody specific for a cytosolic epitope of Kv1.2, all the channels became stained (**Fig. 6.3a**). Repeating this with a monoclonal antibody specific for an intracellular epitope of Kv1.1 confirmed the presence of both subunits in the expressed channels

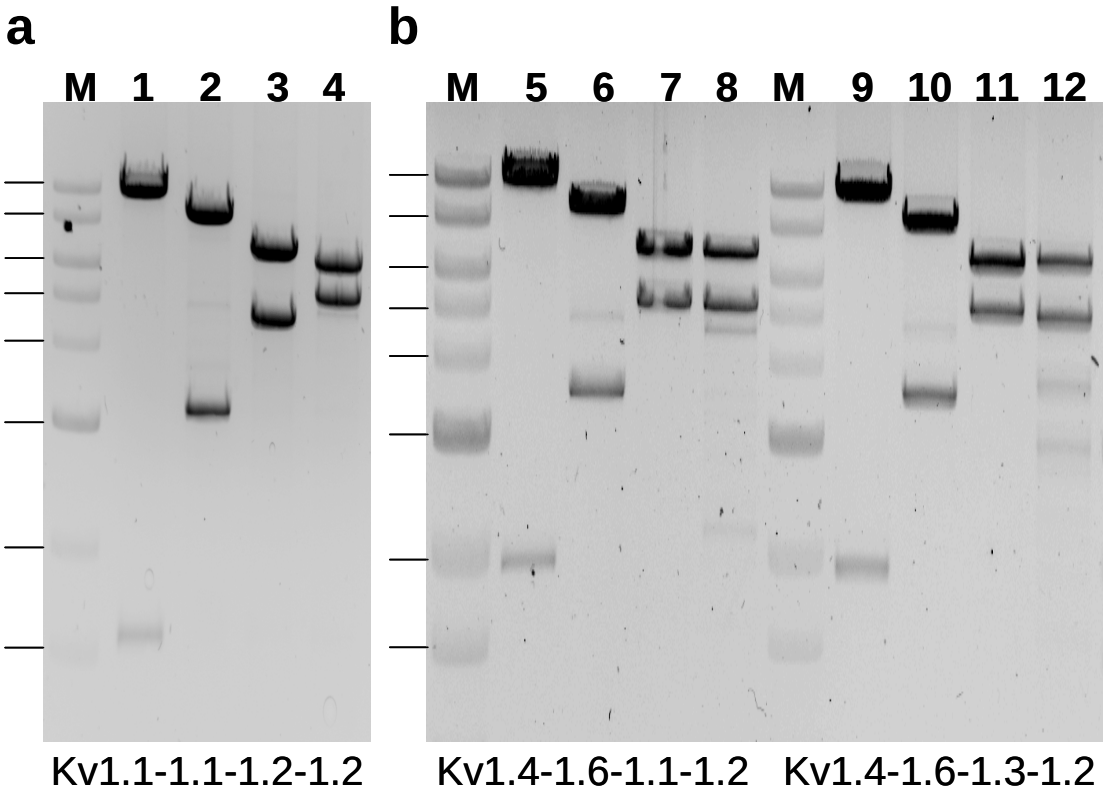

Figure 6.2│Restriction mapping of Kv1.X tetrameric constructs and intermediates formed during the concatenation. **a**, Sequential release from pIRES2-EGFP Kv1.1-1.1-1.2-1.2 of Kv1.1, Kv1.1-1.1, Kv1.1-1.1-1.2 or Kv1.1-1.1-1.2-1.2 inserts by digestion with Nhe l and Bgl II, EcoR I, Sal I or BamH I, as seen in lanes 1-4 from an agarose (1%) gel electrophoretogram. **b**, Sequential release of Kv1.4, Kv1.4-1.6, Kv1.4-1.6-1.1 or Kv1.4-1.6-1.1-1.2 inserts from the final pIRES2-DsRed Kv1.4-1.6-1.1.-1.2, and, Kv1.4, Kv1.4-1.6, Kv1.4-1.6-1.3 or Kv1.4-1.6-1.3-1.2 inserts from Kv1.4-1.6-1.3-1.2-pIRES2-DsRed by digestion with Nhe l and Bgl II, EcoR I, Sal I or BamH I, as seen in lanes 5-8 and 9-12 respectively also from an agarose (1%) gel electrophoretogram. M, kbp markers, from the top; 10.0, 8.0, 6.0, 5.0, 4.0, 3.0, 2.0, 1.5, (in **a** and **b**). Note tetramer band is larger than vector band in lanes 4, 8 and 12.

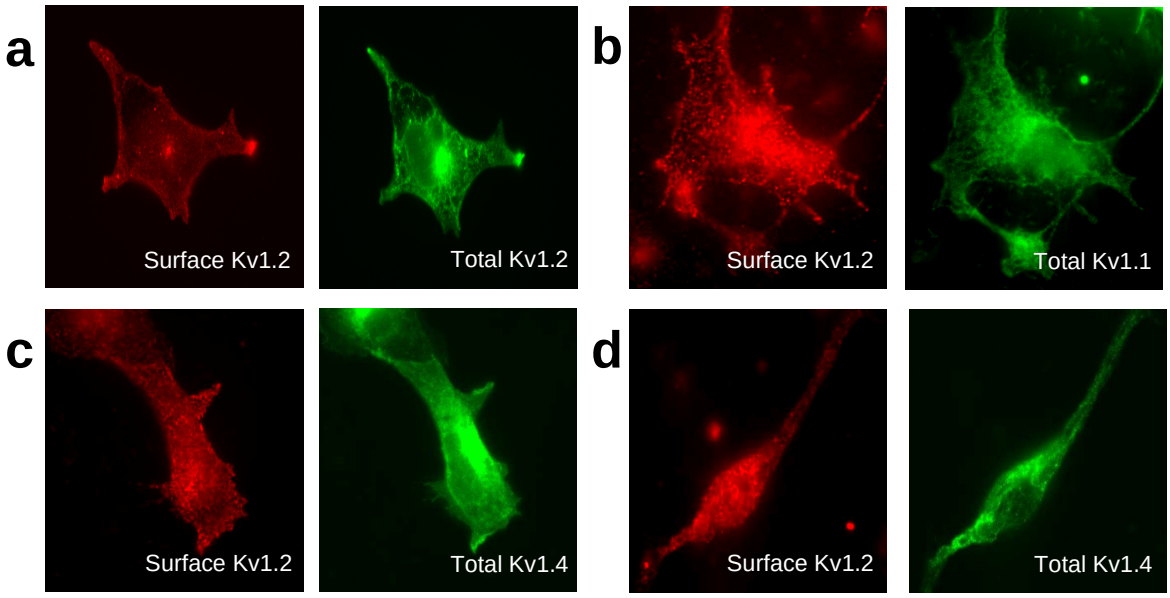

Figure 6.3 | Surface expression of 3 hetero-tetrameric Kv1 channels in COS cells. 48 h post transfection with Kv1.1-1.1-1.2-1.2-pIRES2-EGFP (**a,b**), Kv1.4-1.6-1.1-1.2- (**c**) or Kv1.4-1.6-1.3-1.2-pIRES2-DsRed (**d**), COS cells were labelled using an antibody reactive with external epitopes of Kv1.2 (Tiffany et al., 2000), visualised with anti-rabbit AF 594 (left panels). Following permeabilisation of the same cells, monoclonal antibodies specific for intracellular epitopes of Kv1.2 (**a**), 1.1 (**b**) or Kv1.4 (**c,d**) and anti-mouse AF 488 (right panels) were used to reveal the total channel population. Only background signals were seen upon omitting the primary antibodies; in the case of pIRES2-DsRed constructs (**c,d**), no background fluorescent signal from the DsRed was visible under these conditions.

(**Fig. 6.3b**). As the majority of staining occurred intracellularly in each case (**Fig. 6.3a.b)**, it was necessary to biochemically analyse the minority of channels on the surface to ascertain whether their protein profile differed from that of the total population (**Fig. 6.1b,c**). This was accomplished by biotinylation of the surface components in intact transfected HEK cells. Precipitation of the solubilised biotinylated proteins with streptavidin agarose, SDS-PAGE and Western blotting revealed that only the intact tetrameric channel (Kv1.1-1.1-1.2-1.2) was expressed on the surface (**Fig. 6.1c**). With the other two hetero-tetramers used in this study, surface expression was also demonstrated by fluorescent microscopy (**Fig. 6.3c,d**). Evidence for a correctly-folded and assembled tetrameric channel on the plasmalemma was provided by the avid binding of αDTX to the intact cells (**Fig. 6.4a**). Intact HEK cells expressing Kv1.1-1.1-1.2-1.2 displayed saturable interaction with ^{125}I-labelled αDTX (K_D = 0.74 nM); in view of this affinity corresponding to that (0.5 nM) previously reported for channels composed of tandem-linked Kv1.1-1.2 in (Akhtar et al., 2002) and in Chapter 5 (0.6 nM), binding is not affected by this concatenation. The content of sites (0.13 pmoles/mg protein) (**Fig. 6.4a**) reflects a similar level of expression of tetramer compared to that observed for cells stably expressing dimeric constructs (Sokolov et al., 2007). This is considerably lower than the 1.22 pmoles/mg observed for the same combination of subunits in a previous study (Akhtar et al., 2002), however in that instance the construct was expressed via electroporation with viral particles and co-expressed with Kvβ2.1 which both increase the surface expression of channels. Saturable interaction of ^{125}I-αDTX with cells expressing Kv1.4-containing constructs, Kv1.4-1.6-1.1-1.2 or Kv1.4-1.6-1.3-1.2, could not be reliably detected by this method with minimal specific binding observed (**Fig. 6.4d**), consistent with a rapid dissociation observed for αDTX from Kv1.4-containing channels (see below). This is surprising, however, given the measurable binding of the toxin to Kv(1.4-1.2)$_2$ described in Chapter 5.

6.4 Hetero-tetrameric constructs express uniform populations of Kv1 channels

Functional properties of concatenated Kv1 heteromers were examined by whole-cell voltage-clamped recordings from transfected HEK cells. The resultant currents indicated proper assembly of the recombinant channels. Kv1.1-1.1-1.2-1.2 gave an I_K consistent with a single population of channels; depolarising voltage steps from a holding potential of -100

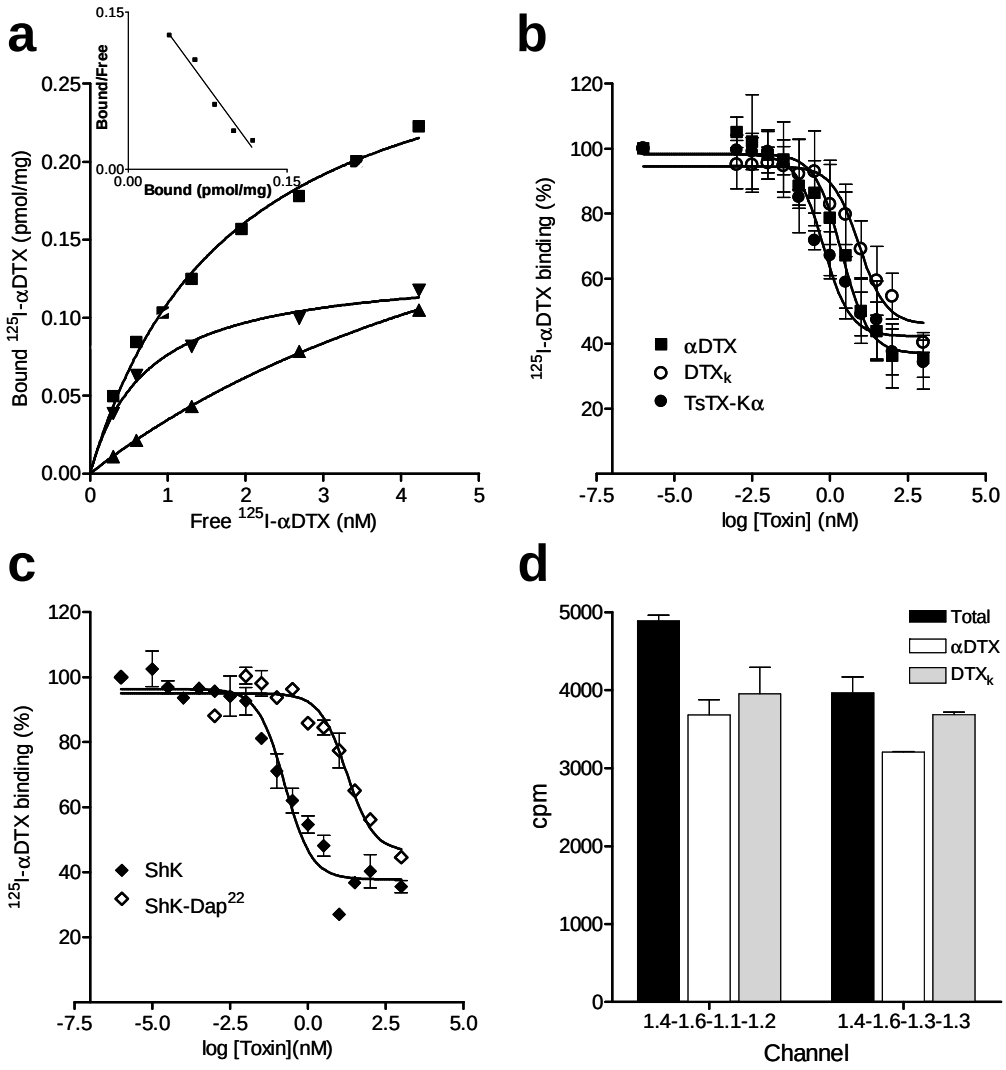

Figure 6.4| Radiolabelled αdendrotoxin binding to tetrameric channels expressed on HEK cells. Saturable binding (▼) of ^{125}I-αDTX to intact HEK cells, expressing Kv1.1-1.1-1.2-1.2, quantified with a filtration assay (**a**); relatively low values were recorded for non-saturable (▲) binding compared with the total (■). Inset shows a Scatchard plot of the saturable binding. **b**, Competition of 2.5 nM ^{125}I-αDTX binding (mean ± SD; n = 4) to transfected cells as in (**a**) by αDTX, DTX$_k$ or TsTX-Kα. **c**, Representative plot showing the relative potencies of ShK and ShK-Dap^{22} in antagonising 2.5 nM ^{125}I-αDTX binding to the K^+ channels as in (**b**). **d**, Binding of 2.5 nM ^{125}I-αDTX to cells expressing Kv1.4-1.6-1.1-1.2 or Kv1.4-1.6-1.3-1.2 was measured in the absence (total, ■) and presence (αDTX, □; DTX$_k$ ■) of 1 μM competing unlabelled toxins (mean ± SD; n = 4). Very little specific binding was observed, probably due to the fast dissociation of the radio-ligand from these channels.

mV triggered outward delayed-rectifying I_K typical of Kv1 channels. Sigmoidally-shaped activation currents were observed which could be fit by the power of a single exponential function (**Fig. 6.5a, Table 6.1**), indicative of channels undergoing multiple conformational transitions at similar rates before their opening (Hodgkin and Huxley, 1952). The observed slow inactivation of I_K (**Fig. 6.5b**) accords with a lack of an N-type, fast inactivation domain (Jan and Jan, 1997). Upon return to negative voltage, I_K decayed with a mono-exponential time-course (**Fig. 6.5c, Table 6.1**), again, consistent with a uniform population of underlying channels. Activation-gating accelerated as the voltage step was increased, and at values positive to +20 mV increased with a voltage dependence of 0.24 elementary charges (**Fig. 6.5d**). Likewise, upon release of membrane potentials to less than -60 mV,

	Kv1.1-1.1-1.2-1.2	Kv1.4-1.6-1.1-1.2	Kv1.4-1.6-1.3-1.2
τ-Activation at 0 mV (ms)	1.9 ± 0.1 (n=3)	1.5 ± 0.1 (n=5)	1.8 ± 0.1 (n=7)
τ-Inactivation at 0 mV, fast (ms)	540 ± 20 (n=5)	45 ± 8 (n=7)	47 ± 0.1 (n=5)
τ-Inactivation at 0 mV, slow (ms)	6200 ± 500 (n=5)	260 ± 20 (n=7)	270 ± 6 (n=5)
$V_{½}$ (mV)	-12 ± 1 (n=13)	-19 ± 0.8 (n=10)	-23 ± 0.6 (n=10)
Slope (*k*) (mV)	15 ± 0.8 (n=13)	11 ± 0.7 (n=10)	10 ± 0.5 (n=10)

Table 6.1 | Biophysical and pharmacological properties of 3 hetero-tetrameric K^+ channels.
Values for activation and inactivation were calculated by fitting power and double-exponential functions, respectively. Values for $V_{½}$ and slope *k* were calculated from Boltzmann equation fitting of the g_k–V relations from peak outward currents.

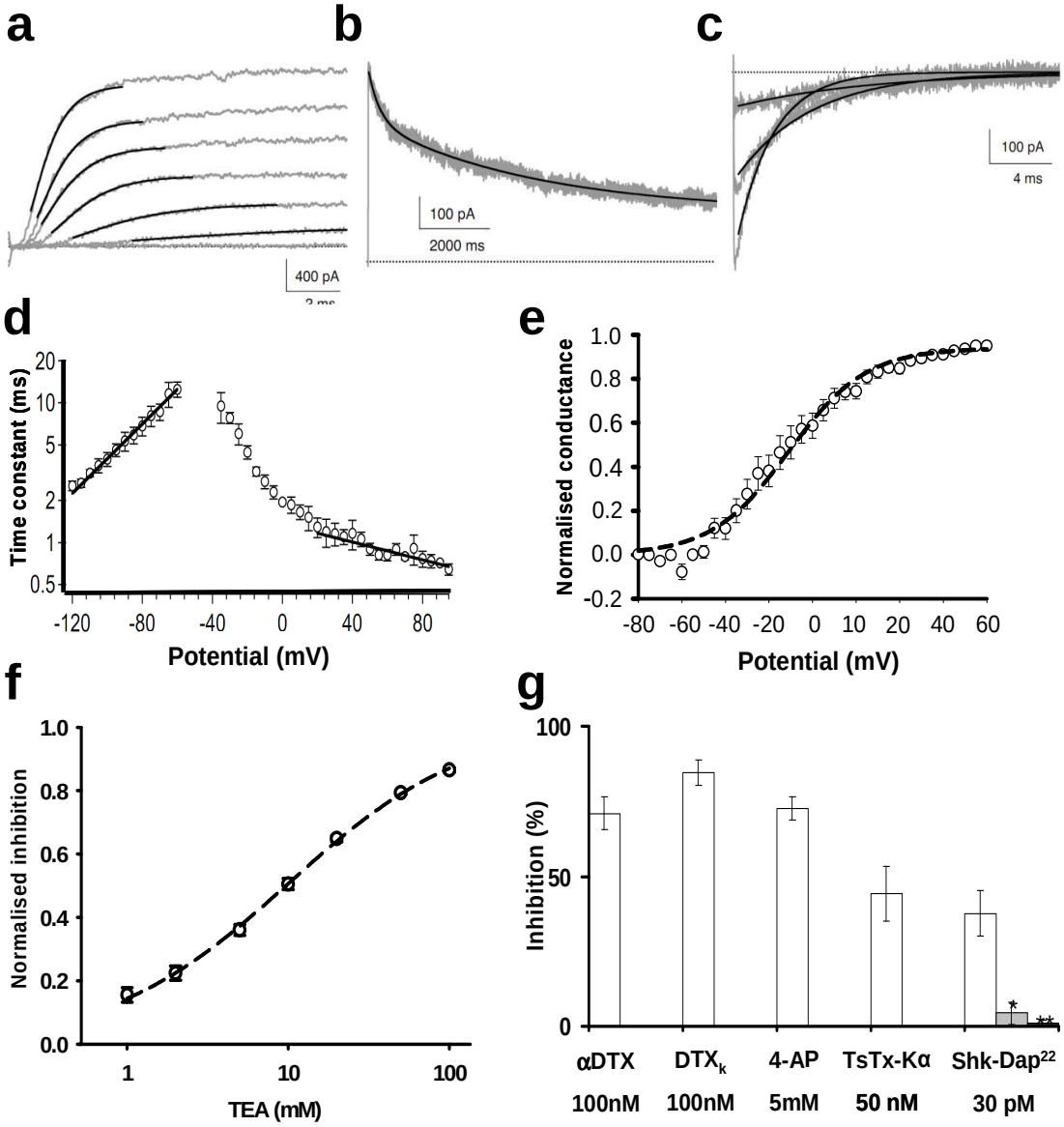

Figure 6.5| Kv1.1-1.1-1.2-1.2 construct expresses functionally uniform channels on HEK cells. **a**, K^+ currents (I_K) in response to depolarising steps (grey traces) from -40 to 80 mV in 20 mV increments fit with the power of an exponential function (black lines). **b**, Inactivation of I_K during a pulse to 0 mV (grey traces), fit with a double exponential function (black line). **c**, Deactivation of I_K at -80, -100 or -120 mV (grey traces) after 50 ms at +60 mV, fit with mono-exponential functions (black lines). **d**, Time constants (n=3) associated with activation (>-50 mV) or deactivation (<-50 mV); lines are fits of exponential functions. **e**, Conductance-voltage relationship of outward K^+ peak currents (n=15) after 100 ms at indicated voltage; dashed line is a Boltzmann fit. **f**, Concentration dependence of TEA inhibition of I_K (n=4) during voltage steps to +60 mV for 50 ms. Inhibition in each cell was normalised (○) to a saturating value of a

fit with Langmuir isotherm (dashed line). **g**, Reduction by various agents of I_K from Kv1.1-1.1-1.2-1.2 (open bar), homomeric Kv1.1 (grey bar) or Kv1.2 (black bar) during voltage steps to +60 mV for 50 ms ($n \geq 5$). ShK-Dap^{22} measurements were conducted in a solution used previously (Sokolov et al., 2007). Greater inhibition by ShK-Dap^{22} of the hetero-tetramer compared to the homomers was statistically significant [Kv1.1, p=0.01 (*); Kv1.2, p=0.001 (**) – measured by a Student's t-test].

the deactivation became progressively faster with a voltage dependence of -0.81 elementary charges. Analysis of the steady-state conductance-voltage relation (g_K-V) revealed a conductance profile well-fitted by a single Boltzmann function (**Fig. 6.5e**), with an activation midpoint and slope (**Table 6.1**) intermediate to those for homomers of the parental Kv1.1 or Kv1.2 subunits (Sokolov et al., 2007).

6.5 Biophysical profiles and susceptibilities to inhibitors can be used to distinguish these heteromeric channels

The sensitivities of I_K to various blockers were examined. TEA, a characterised K^+ channel blocker, binds just external to the K^+ conduction pore with all 4 subunits contributing to this interaction (Lenaeus et al., 2005). The TEA dose-response of I_K from Kv1.1-1.1-1.2-1.2 was well fit by a Langmuir binding isotherm (**Fig. 6.5f)** giving a dissociation constant of 8.4 mM, a value intermediate to that of Kv1.1 and 1.2 homo-tetramers (Sokolov et al., 2007). Similarly αDTX, DTX_k, 4-AP, TsTX-Kα and ShK-Dap^{22} inhibited this I_K (**Fig. 6.5g**), in accord with their known interactions with Kv1.1- and 1.2-containing channels (Middleton et al., 2003; Sokolov et al., 2007). Congruently, ^{125}I-αDTX was readily displaced from this channel by DTX_k, αDTX, TsTX-Kα (**Fig. 6.4b**) (K_is = 2.0, 0.6 and 0.1 nM, respectively) or ShK-Dap^{22} (**Fig. 6.4c**). The greater potency of ShK than its derivative ShK-Dap^{22} (K_i = 0.04 compared with 4.0 nM) is consistent with their abilities to inhibit homomeric Kv1 channels (Middleton et al., 2003), and the results obtained in Chapter 5 for the displacement of radio-labelled αDTX by ShK-Dap^{22} from Kv1.1-1.2 heteromers (2.3 nM). A reported pattern (Middleton et al., 2003) of ShK-Dap^{22} binding to Kv1.1/1.2 concatemers was indicative of a mixture of channels being expressed; in contrast, displacement herein of ^{125}I-αDTX from Kv1.1-1.1-1.2-1.2 indicates that this concatemer is

more uniform (**Fig. 6.4c**). One subpopulation of Kv1.1/1.2 hetero-tetramers is known to bind ShK-Dap^{22} with an unexpectedly high affinity (Middleton et al., 2003). Accordingly, 30 pM ShK-Dap^{22} substantially blocked I_K from Kv1.1-1.1-1.2-1.2 yet proved ineffective at this low concentration against either Kv1.1 or 1.2 homomers (**Fig. 6.5g**), mirroring the displacement by this toxin of ^{125}I-αDTX bound to Kv1.1-1.2 and Kv1.2-1.2 containing channels (see Chapter 5). This pronounced selectivity for the hetero-oligomer illustrates the potential utility of ShK-Dap^{22} in differentiating K^+ currents.

Unlike Kv1.1-1.1-1.2-1.2, I_K mediated by Kv1.4-1.6-1.1-1.2 and Kv1.4-1.6-1.3-1.2 channels displayed fast inactivation over tens of ms (**Fig. 6.6a-c, Table 6.1**) imbued by the free N-terminus of the leading Kv1.4 subunit (Rettig et al., 1994). Surprisingly, this rapid decay occurred in the presence of one Kv1.6 subunit, which possesses a domain known to disallow N-type fast inactivation in heteromers containing Kv1.4 (Roeper et al., 1998). It is possible that the functionality of this domain was attenuated due to its N-terminus being constrained in the second concatenated domain. Analysis of the currents elicited by depolarising voltage steps revealed similar g_K-V relations for these channels (**Fig. 6.6d, Table 6.1**), well fitted by a single Boltzmann function, consistent with a uniform population of expressed channels. The dose responses for inhibition of these two channels by TEA showed somewhat different sensitivities (**Fig. 6.6e**); both sets of data were well-described by a Hill slope of 1 with K_D values for Kv1.4-1.6-1.1-1.2 and Kv1.4-1.6-1.3-1.2 of 36 and 78 mM, respectively. Despite Kv1.3 and 1.4 homo-tetramers being insensitive to αDTX (Stuhmer et al., 1989), these heteromeric channels retained some sensitivity to 100 nM of this toxin with 78% block (± 5%; n = 8) of I_K from Kv1.4-1.6-1.1-1.2 and 70% block (± 2%; n = 9) of I_K from Kv1.4-1.6-1.3-1.2. However, these 2 currents recovered rapidly upon toxin washout with respective $\tau_{dissociation}$ values of 12 s (± 3; n = 4) and 9 s (± 2; n = 8). Notably, DTX_k discriminated between the two Kv1.4 containing tetramers even though the sole difference between them is the replacement of Kv1.1 with Kv1.3 in domain III. Consistent with the exclusive inhibition by DTX_k of channels containing Kv1.1 (Akhtar et al., 2002), its inclusion was shown to greatly enhance susceptibility of I_K to this toxin (**Fig. 6.6a,b,f**). Indeed, DTX_k at low concentrations (≤ 10 nM) almost exclusively blocked I_K mediated via the Kv1.1-containing tetramer while, at 100 nM, this toxin gave only partial

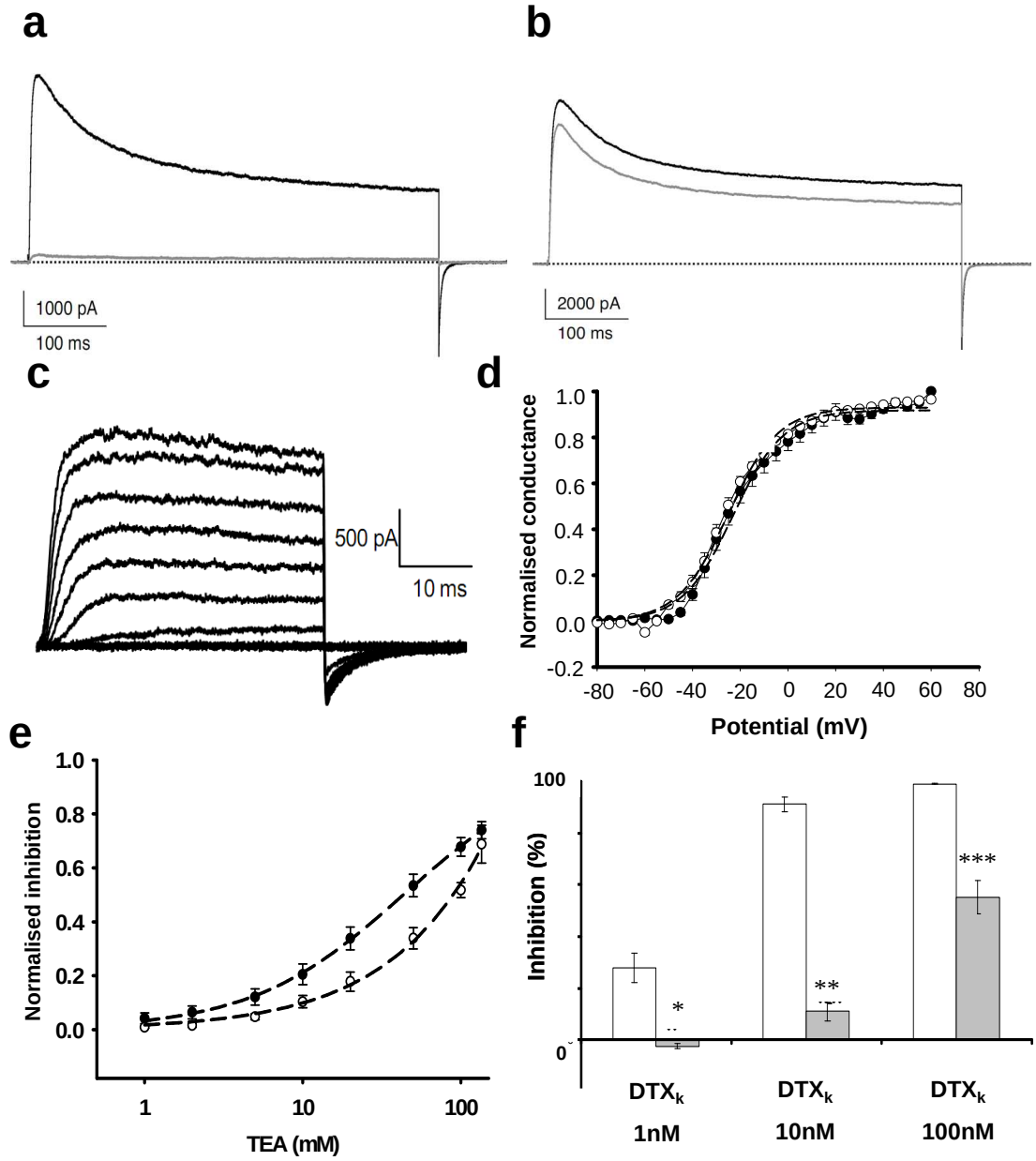

Figure 6.6 | Similar Kv1.4-containing hetero-tetrameric channels are distinguishable by dendrotoxin$_k$ and tetraethylammonium. **a** and **b**, The effect of 10 nM DTX$_k$ on I_K from Kv1.4-1.6-1.1-1.2 and Kv1.4-1.6-1.3-1.2 induced by 500 ms voltage steps from -100 to 0 mV. Control trace in black; drug effect in gray. **c**, Representative current traces of Kv1.4-1.6-1.1-1.2 in response to depolarising steps from -100 to +80 mV in 20 mV increments; for clarity, similar data from Kv1.4-1.6-1.3-1.2 is not shown. **d**, g_k-V relations assembled from peak outward currents from Kv1.4-1.6-1.1-1.2 (●) and Kv1.4-1.6-1.3-1.2 (○). **e**, Concentration dependence for TEA inhibition of I_K from Kv1.4-1.6-1.1-1.2 (●) or Kv1.4-1.6-1.3-1.2 (○) assayed by pulses to

0 mV (n=5) and fit by the Langmuir isotherm as in **Fig 6.5f**. **f**, Inhibition by 3 DTX_k concentrations of I_K from Kv1.4-1.6-1.1-1.2 (open bar) or Kv1.4-1.6-1.3-1.2 (grey bars), assayed at ≤ 0 mV showed a significant sensitivity difference, measured by a Student's t-tet [1 nM, p=0.00029 (*); 10 nM, p=0.0002 (**); 100 nM, p=0.00034 (***)].

inhibition of I_K from Kv1.1-free hetero-oligomer (**Fig. 6.6f**). Hence, DTX_k can clearly differentiate between these otherwise indistinguishable channel subtypes.

6.6 Increasing the number of Kv1.4 α subunits in a channel heightens the resistance to inhibition by peptide toxins

A fourth tetramer, Kv1.4-1.2-1.2-1.2, was also expressed to provide a comparison with $Kv(1.4\text{-}1.2)_2$ in examining the effect of the number of Kv1.4 subunits on a channel's pharmacology. HEK cells were transiently transfected with Kv1.4-1.2-1.2-1.2-pIRES2-EGFP using Lipofectamine 2000, and for $Kv(1.4\text{-}1.2)_2$ channels, a HEK stable cell line was used. Inhibition of Rb^+ efflux through these 2 channels was quantified in the presence of several concentrations of various toxins (**Fig. 6.7**). In earlier studies (see Chapter 5), Kv1.4-1.2 containing channels were found to be virtually insensitive to most toxins at 10 nM.

Therefore, the dose of toxins used for these experiments was increased. KTX, which blocks neither Kv1.4 nor Kv1.2 homomers was also used to ensure that any attenuation of Rb^+ efflux observed was not due to non-specific effects resulting from high toxin doses. As was expected, neither channel was blocked by 500 nM of this toxin (**Fig. 6.7**). As αDTX, HgTX and MgTX have been most extensively characterised on Kv1.4-1.2 channels in experiments so far (Chapter 5), they were tested here. Also included was the *Dendroaspis polylepis* homologue of αDTX, DTX_I. In all cases, channels containing only 1 copy of Kv1.4 were more sensitive to inhibition than those containing 2, the extent of which varied depending on the toxin used (**Fig. 6.7**). Consistent with MgTX and HgTX being the most potent blockers of Kv1.4-1.2 channels, they also inhibited Kv1.4-1.2-1.2-1.2 to a greater extent. Most interesting was the difference between the homologues αDTX and DTX_I. At 10 nM, αDTX had little effect on Rb^+ efflux through either channel, whereas at this concentration, DTX_I clearly distinguished them. A ten-fold increase in concentration of this toxin saw any

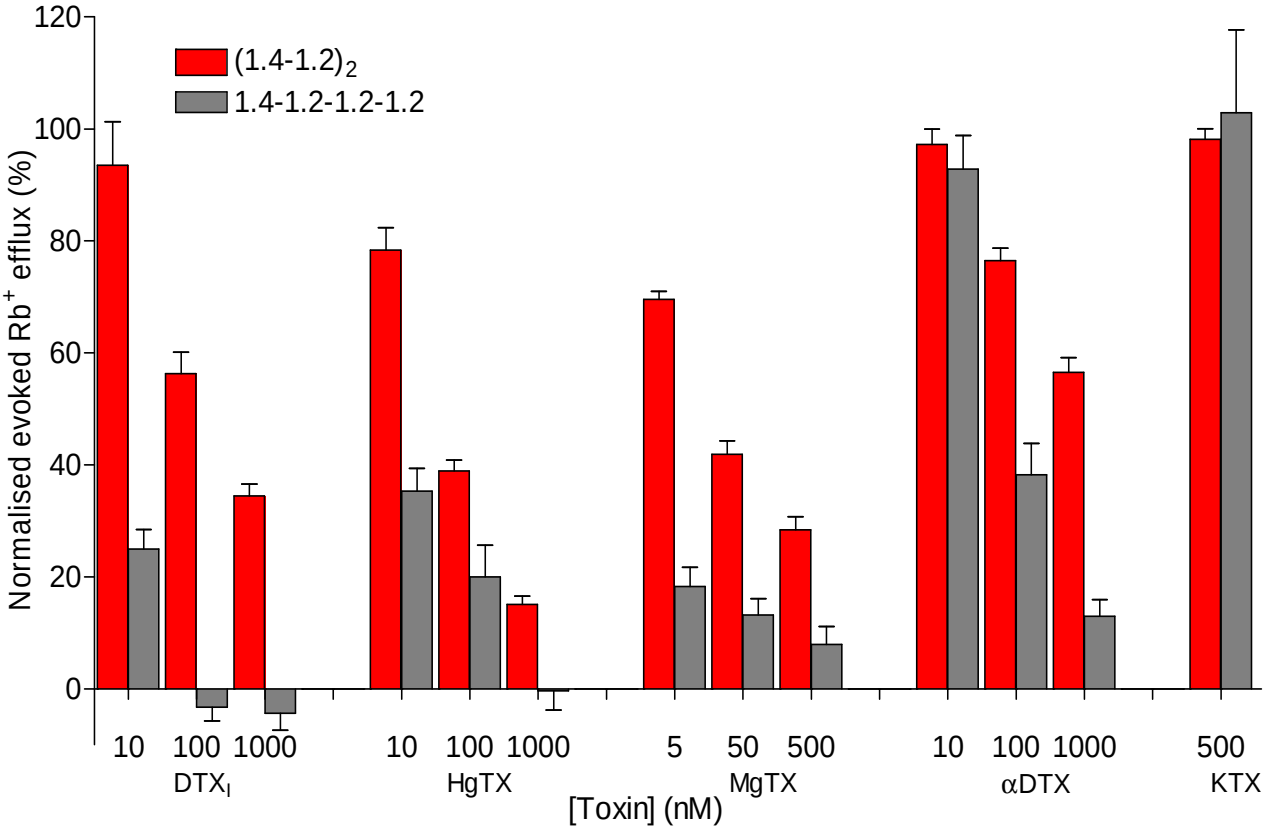

Figure 6.7 | A comparison of the effect of Kv1.4 subunits on the inhibition of Rb^+ efflux through Kv1.4- and 1.2-containing channels by various peptide toxins. Averages (n=16) are plotted ± S.E.M. KTX, which is unable to block either Kv1.4 or Kv1.2 is included to ensure that attenuation of evoked Rb^+ efflux by high concentrations of other toxins is specific.

"repulsive" effect of Kv1.4 abolished with the channel containing only 1 copy; complete block was observed - a result not achieved by MgTX nor HgTX. While electrophysiological refinement of these results will be needed, it appears that toxins are affected differently both by the presence of Kv1.4 and the number of subunits. It could be argued that differences observed between the 2 channels could be as much a result of an increase in the sensitive Kv1.2 subunits, as a decrease in "repulsive" Kv1.4. However, a demonstration previously that the presence of only 1 sensitive subunit in a channel confers near maximal activity of DTX_k (Akhtar et al., 2002), makes this unlikely.

6.7 Discussion

A long-term aim of re-creating native Kv channel heteromers is to understand their pharmacology and, eventually, develop drugs to aid identification of subtypes *in vivo*; control of α subunit stoichiometry is crucial for this. The extensive validation of 3 'native-like' Kv1 heteromers demonstrated that the concatenation can generate uniform populations of channels, allowing measurement of their biophysical and pharmacological parameters for the first time. The successful expression of these representative channels, containing combinations of 5 neuronally-predominant α subunits, highlights that this technology should be able to recreate any subtype of the numerous K^+ channel families found in various tissues (Gutman et al., 2003b). As extensive future developments are required to generate these Kv1 channels associated with the requisite β subunit partners (Rettig et al., 1994; Shamotienko et al., 1997), criteria adopted herein for the purpose of subtype identification rely largely on pharmacological characteristics known to be unaffected by these cytoplasmically-located auxiliary proteins.

It was clearly demonstrated here that the properties of hetero-tetramers are not necessarily predictable from the parental homo-tetramers; by showing that Kv1.1-1.1-1.2-1.2 displays greater susceptibility to ShK-Dap^{22} than the respective homomers. Despite the fact that the selectivity of peptide toxins for heteromeric channels has been largely unknown, these toxins have been widely used to dissect native currents. For example, Kv1.1 and 1.2 subunits have been shown to have a role in μ opioid receptor-mediated inhibition of GABAergic inputs into basolateral amygdala neurons (Finnegan et al., 2006). αDTX, DTX_k and TsTX-Kα inhibited the effect of the μ opioid receptor agonist D-Ala2, N-MePhe4, Gly-

ol-enkephalin (DAMGO), on miniature inhibitory post synaptic currents, decreasing their frequency (Finnegan et al., 2006). Given that all 3 toxins proved effective, it seems likely that they are acting on Kv1 hetero-tetramers containing at least one Kv1.1 and one Kv1.2 α subunit.

Although Kv1.4 and Kv1.3 homo-tetramers are insensitive to αDTX and DTX_k (Grissmer et al., 1994; Hopkins, 1998), the native-like heteromers containing these subunits were found to be blocked by either toxin, provided subunit(s) from sensitive homomers were present. This newly-revealed pharmacology makes Kv1.4-containing heteromers candidates for native, rapidly-inactivating DTX-sensitive currents, such as those found to shape the action potentials in the axon initial segment of layer 5 pyramidal neurons (Kole et al., 2007), or the low-threshold I_K of the medial nucleus of the trapezoid body of the calyx of Held (Dodson et al., 2002). In particular, similar biophysical and pharmacological properties make Kv1.4-1.6-1.1-1.2 a candidate to shape temporal precision in octopus cells of the mammalian cochlear nucleus (Dolganiuc et al., 2000). Improved interpretation of these and other attempts to establish the molecular identity of native channels will be greatly aided by empirical determination of the pharmacology of physiologically-relevant heteromers, a process initiated by the advances achieved here.

Examining the pharmacological influence of Kv1.4 subunits in heteromeric channels (in this and Chapter 5) revealed MgTX and HgTX to be more potent than the other toxins investigated on Kv1.4-1.2 containing channels. However, at low (10 nM) doses on Kv1.4-1.2-1.2-1.2 channels, DTX_I was as effective as MgTX and HgTX and more so at higher concentrations. While Kv1 blockers isolated from scorpion toxins (including MgTX and HgTX) inhibit channels by physically occluding the pore, the DTXs are hypothesised to bind off-centre, interacting predominantly with 3 subunits (Imredy and MacKinnon, 2000). This could be an advantageous feature for DTXs when blocking channels containing only 1 Kv1.4 subunit, as this “repulsive” element could be avoided, perhaps explaining the potent block of Kv1.4-1.2-1.2-1.2 by DTX_I. However, αDTX did not have the same effect suggesting that the nature of DTX binding to Kv1 channels is not the sole factor. That said, proportionally the αDTX elicited attenuation of Rb^+ efflux through Kv1.4-1.2-1.2-1.2 was more so than Kv1.4-1.2 with increased toxin concentration. While DTX_I and αDTX, differ by only five residues, studies to date have shown that three of these changes occur in a

region important for DTX_I binding to channels [see **Table 2.1**, **Fig. 2.5**, (Katoh et al., 2000; Wang et al., 1999a)]. While this is used explain the increased binding of DTX_I to rat brain membranes compared with αDTX, it does not explain the potency of DTX_I binding to channels containing one Kv1.4 subunit. Presumably, the smaller the area that contacts with a channel, the easier it would be to avoid the repellent lysine residue present in Kv1.4 subunits. Future site-directed mutagenesis studies of the DTX_I Lys19/Tyr/17/Trp37 triad of residues would be necessary to determine whether this extra binding site is in fact responsible for the enhanced inhibition of Kv1.4-1.2-1.2-1.2 channels by DTX_I. The construction of concatemers consisting of one Kv1.4 subunit and various combinations of other α subunits would answer questions as to the role of other subunits in this enhanced inhibition.

The new cassette cloning methodology described in this Chapter allows quick and easy generation of constructs to address technical questions, such as the influence of the number of Kv1.4 subunits in a channel on peptide toxin binding, as examined here with the expression of a fourth tetramer. It is now possible to design and produce a series of constructs which would allow specific questions to be answered, thereby, increasing understanding of the interactions of brain Kv1 channels with their inhibitors. Furthermore, this technology could be applied to examine the biophysical properties of such channels, for example investigating the effect on inactivation kinetics, of various combinations of Kv1.4 and 1.6 subunits in heteromers.

To date, no neuronal currents produced by heteromeric Kv1 channels have had their underlying subunit compositions unambiguously identified. The large number of selective Kv1 toxins now available, in combination with this new concatenation technology, provides a route towards that long-sought goal. Here, the successful expression of tetrameric combinations of 5 α subunits, and trafficking to the surface as single proteins such that their distinguishing characteristics were measurable, represents a major first step. Moreover, these recombinant channels now serve as authentic drug targets for therapeutics to control neuronal excitability and synaptic transmission.

Chapter 7
General Conclusions

Developing tools for studying Kv1 channels, and finding inhibitors of therapeutic value, require determination of the functional properties of structurally-defined channels. The necessity for investigating neuronally-occurring heteromeric α subunit combinations is clearly demonstrated in this study. Recombinant expression of oligomers with the requisite defined stoichiometry requires concatenation of α subunit genes. Such channels provide authentic targets for drug discovery, and heteromer-specific blockers can be used for elucidating the molecular basis of neuronal K^+ currents.

In this study, expression of Kv1.1-1.2 α subunit containing channels via electroporation of CHO cells with cRNA prepared from pSFV1-Kv1.1-1.2 provided the necessary proof of concept for such an approach. Previous studies had demonstrated that when expressing such dimeric constructs 2 copies of the resultant protein combine to form a tetrameric channel of the expected size (Akhtar et al., 2002). Binding of radio-labelled αDTX to the channels in this study further confirms the tetrameric assembly, as 4 α subunits are required for binding of the toxin (Tytgat et al., 1995). The most selective blockers identified, thus far, for the Kv1 channel family are pore-blocking peptide toxins isolated from venoms. As these bind to the external surface of channels provided by α subunits, the internally-acting auxiliary β subunits which do not affect the pharmacological properties were not included. Expression levels of surface targeted, intact proteins in mammalian cells proved adequate for functional characterisation of the resultant channels via electrophysiological recordings, experiments not performed in the previous study (Akhtar et al., 2002). A source of recombinant channels for setting up and optimising a non-radioactive Rb^+ efflux assay was also provided by this method. Results achieved with this and the more time-consuming electrophysiological protocols were generally in agreement but with some inconsistencies likely due to inherent differences in the assays (see below). Despite this, both assays identified the blocking ability of the same compounds.

Development of HEK cell lines stably expressing the Kv1.1-1.2 construct and other Kv1.X-1.2 containing channels provided a more convenient and plentiful source of targets for screening potential inhibitors. Initially, biophysical and pharmacological properties of Kv1.1-1.2 and 1.6-1.2 containing channels were compared identifying DTX_k as a distinguishing ligand. With more similar protocols employed, and a more consistent source of channels provided by stable cell lines, there was greater consistency between the data from electrophysiological and Rb^+ efflux assays (see below). The improved source of recombinant channels, coupled with further Rb^+ efflux assay validation, facilitated the setting-up of an automated system for Rb^+ efflux measurements of these and the other Kv1.X-1.2 containing channels resulting in a truly high-throughput assay platform.

When designing protocols for high-throughput screening measurements, several factors must be taken into consideration depending on the experiment priorities. The purpose of such a screen is to test as many compounds as possible in the search for inhibitors and, in doing so, only analyse promising leads by more time-consuming methods. To achieve this aim, the protocol employed must be balanced between getting maximum information on a particular compound, with the possibility of missing potential blockers but having a more time/cost effective assay and, therefore, screening more compounds. With these considerations in mind, a single concentration of toxin was applied initially in this study, determined from previously established effective ranges. In some instances, this may have resulted in distinguishing toxins not being identified but in these cases the degree of distinction is likely not sufficient for future therapeutic consideration. For example, some toxins may block all channels at the selected dose, but distinguish between them at much lower concentrations. The considerations detailed above were also taken into account when dealing with variations in the data obtained. In an initial screen, a yes or no answer is required as to whether the test compound inhibits the channel in question. Some scatter in the data is acceptable as long as this decisive outcome can be achieved. Therefore, the numbers of wells used in the plate for control and each toxin are chosen on this basis. Increasing the number of wells for each condition should reduce data scatter but that will reduce the quantity of compounds that can be screened per plate. The use of stable cell lines for these experiments gave more consistent results with smaller error bars, thereby,

reducing the scatter in the data. Having performed the initial screen, the automated assay can be exploited further both to clarify any unusual results and to obtain additional information about channel inhibition by the compounds in question. In this study, the Rb^+ efflux assay was validated for determining inhibitory constants for interesting blockers, information which can confirm their discrimination of different channels, refining the pool of toxins chosen for further analysis. Likewise, the action of toxins that appeared to inhibit Kv1.4 containing channels was confirmed simply by increasing the number of concentrations of toxin tested (the cost of toxin is prohibitive for full dose response curves).

In the main, results achieved from Rb^+ efflux experiments were consistent with those determined by electrophysiological and radio-labelled toxin binding techniques. There were some exceptions which are important to note and address. In experiments conducted with CHO cells, differences existed in the sensitivities measured by the various methods for the Kv1.1-1.2 containing channels when inhibited by 4-AP and αDTX. While Rb^+ efflux through these channels was almost completely blocked by 4-AP I_K was not, with a component of the current seemingly insensitive. Some possible reasons for this are addressed in the Chapter 4 Discussion. Reassuringly, these dissimilarities were not evident upon repeating these experiments with channels stably expressed in HEK cells. Likewise, discrepancies in sensitivity of the CHO-expressed channel to αDTX when measured by the 2 techniques were not evident in the HEK expressed channels. Use of BSA in solutions and silanised plastic for Rb^+ efflux experiments in HEK cells may have reduced adherence of the toxin to plasticware used, thereby increasing the amount available for binding to the channels. There were also some differences between Rb^+ efflux and radio-labelled toxin results. For example, MoTX did not block Rb^+ efflux through Kv1.3-1.2 channels but did displace ^{125}I-αDTX bound to the same channels; NxTX displaced the labelled toxin bound to both Kv1.2-1.2 and 1.3-1.2 with same efficacy but Rb^+ flux through the latter was inhibited to a much lesser extent. Displacement but not inhibition of flux by a toxin could be attributed to the use of higher concentrations in the former but this does not explain the observed binding of ^{125}I-αDTX to Kv1.4-1.2 containing channels where little flux inhibition was achieved, even at increased concentrations, or the fact that the same labelled toxin did not bind specifically to tetramers containing just 1 copy of Kv1.4 (Kv1.4-1.6-1.1-1.2 and

Kv1.4-1.6-1.3-1.2). While it is possible that the longer incubation with toxin in the displacement experiments compared with the flux assay could help to overcome the "repulsive" action of Kv1.4 subunits, the lack of binding to channels containing only 1 copy of this subunit is confusing. Given the increased size of the tetrameric construct compared with that of the dimer and the subsequent reduction in expression levels (data not shown), it is possible that there was not sufficient channel expression to bind appreciable amounts of toxin. The fast dissociation constant of the unlabelled toxin from these channels, as measured electrophysiologically, could also contribute but this would be expected to be a factor when measuring binding to the channels made from dimers, evidence of which was not clear from the results obtained.

The pharmacological characterisation of 5 Kv1.X-1.2 containing oligomers was an important step in elucidating the interactions of peptide toxins with heteromeric rather than homomeric channels. The Rb^+ efflux data obtained from experiments performed with many peptide toxins on this channel series, gave some insight into the contribution to toxin inhibition of the various α subunits within the channel. It is, thus, deduced that the composite subunits can be termed necessary, permissive or repulsive. In many instances, the presence of only one copy of a subunit with sensitivity for a toxin will result in block of the channel; such subunits are deemed "necessary". Also, in the majority of cases, any other α subunits in the channel that are insensitive to the toxin in question do not have a negative effect on the block, and, therefore, could be described as "permissive". One exception to this is Kv1.4. No known toxins inhibit Kv1.4 monomers. Furthermore, the presence of even one copy of this subunit in a channel can negate the effects of three sensitive or "necessary" subunits. Thus, in such instances Kv1.4 can be termed "repulsive". It was also revealed that the peptide toxins investigated can behave in an unexpected fashion highlighting the importance of screening heteromeric combinations of α subunits. MoTX for example, has been shown to inhibit I_K from Kv1.2, and to a lesser extent 1.1 and 1.3 homomers expressed in *Xenopus* oocytes (Kharrat et al., 1996). It could, therefore, be hypothesised that at least one of these three subunits would be "necessary" in a heteromer, that any Kv1.6 subunits present would be "permissive" and presumably any Kv1.4 subunits, "repulsive". However, MoTX blocked Rb^+ efflux through Kv1.2 homo-tetramers only and

did not inhibit Kv1.1-1.2 or 1.3-1.2 containing channels despite the presence of 2 pairs of sensitive subunits in each. This could be attributed to potency. However, in radio-ligand displacement studies, MoTX displaced ^{125}I-αDTX from Kv1.3-1.2 containing channels (albeit with high levels of non-specific binding remaining) as well as channels containing only Kv1.2 subunits, but not channels composed of two copies of Kv1.1-1.2. This suggests that the toxin may be more sensitive to homomeric combinations of channels. An important next step would be to investigate inhibition by MoTX of Kv1.1 and 1.3 homomers in the same assay to confirm the homomeric selectivity of the toxin. Taken together this demonstrates, again, the necessity of working with physiologically relevant α subunit combinations when studying the interactions between channels and their inhibitors.

While concatenating 2 α subunit genes provides channels composed of two copies of each subunit, many heteromers isolated from mammalian brain are composed of three or four different α subunits. The next step in studying native-like Kv1 channels, therefore, was the concatenation and expression of four α subunit genes in a single construct. The cassette cloning system described herein is a simple and convenient system for achieving this goal. Its modular nature allows easy swapping of one or more subunits, potentially with those found to be mutated in diseased states, and the strategy of holding all the domains in the same ORF means constructs can be expressed with any number of the positions filled – demonstrated by expression of some of the dimeric channels. The tetramers produced to date were biophysically and pharmacologically characterised and proved distinguishable based on the resultant profiles. For the first time, these novel properties allowed putative definition of the molecular basis of several K^+ currents recorded from neurons (see Chapter 6 Discussion). Profiling of more native combinations will no doubt aid in this task.

This thesis sought to define the pharmacology of heteromeric Kv1 channels mimicking those in mammalian brain, to progress towards the ultimate goal of finding specific blockers of channels as a source of potential therapeutics. Selective inhibition of channel subtypes would also lead to a better understanding of their role in neurons. To date the inhibitory activites of peptide toxins have been studied mainly on homomeric Kv1 channels. It was therefore necessary to understand the interaction of these blockers with channels

composed of heteromeric combinations of α subunits. Recombinant expression of various dimeric combinations of α subunits provided a source of channels and a Rb^+ efflux assay was validated for the quantitive and qualitative analysis of the pharmacological properties of the proteins. Generation of stable cell lines and automation of the Rb^+ efflux assay made large scale screening of potential blockers a possibility. Following proof of concept studies, the pharmacology of the Kv1.X-1.2 dimer series was extensively characterised. This process increased the known number of Kv1 α subunits sensitive to some of the toxins investigated. Furthermore, the contributions of the various subunits in a channel to toxin inhibition were described and toxins identified that did not fit the pattern. Identification of the features responsible for these unusual characteristics could prove useful in the design of heteromer-specific blockers. Development of a modular cloning system for the expression of all four α subunits of a Kv1 heteromer allows the expression of any neuronally isolated channel, thereby providing an invaluable range of authentic targets for the development of therapeutics. Characterisation of the biophysical and pharmacological profiles of three such channels allowed putative identification of the α subunit combinations responsible for recorded neuronal currents, an important step forward in K^+ channel research.

Going forward, this novel cloning system must be exploited fully to produce a range of targets for further studies. While investigation of externally binding pore blocking peptides only requires the expression of α subunit genes, it is desirable to improve the recombinant technology to express the associated β subunits, thereby fully recreating native channels. The development of stably expressing cell lines would allow the employment of more, high throughput techniques such as automated patch-clamp (Qpatch) for biophysical and pharmacological profiling. In continuing the work described herein the first step would be to use the new cloning system to produce constructs that once expressed as stable cells lines could be used to answer questions raised in this thesis. Investigating the interaction of Kv1 homomers (especially Kv1.1 and 1.3) with MoTX, would confirm or reject the hypothesis that MoTX preferentially inhibits channels composed of homomeric rather than heteromeric combinations of subunits. In a similar way, constructs containing one Kv1.4 subunit and various combinations of other subunits could be used to examine the influence of subunits other than Kv1.4 on the inhibition of Kv1.4 containing channels by, for

example, HgTX, MgTX, αDTX and DTX_I. With as many constructs as possible expressed stably, the scope for the techniques that can be used to profile them is increased.

Site-directed mutagenesis is a logical next step to build on the information gained during the course of this study. A possible approach for investigating the potency of DTX_I on channels containing one Kv1.4 subunit is given in the discussion of Chapter 6. When profiling the pharmacology of the Kv1.X-1.2 series of dimers the most unexpected results came from MoTX. This was the one toxin that does not fit with the "necessary", "permissive" and "repulsive" model for predicting the pharmacology of Kv1 channels composed of heteromeric combinations of α subunits. Scorpion toxins that block ion channels contain three or four disulphide bridges with most K^+ channel blockers containing three. The position of these bonds is highly conserved: for three disulphide-bridged toxins; C1-C4, C2-C5, C3-C6 and for four bridged toxins; C1-C5, C2-C6, C3-C7, C4-C8. However, MoTX not only has 4 disulphide bridges but they are also in different places; C1-C5, C2-C6, C3-C4 and C7-C8. This results in the α helix being connected to different strands of the β-sheet instead of the same strand. This affects the position of some residues and therefore could affect the pharmacological properties of the toxin (Fajloun et al., 2000). While mutagenesis studies to return the disulphide bridges to the conserved positions resulted in less potent inhibition of Kv1.2 and 1.3 homomers (Fajloun et al., 2000), there is no evidence as to the effect this would have on heteromeric combinations of channels. Perhaps the altered bridging is what confers the toxin with its unusual pharmacological profile and similar alterations to other more potent but less selective blockers could result in greater selectivity perhaps combined with enhanced potency. The high-throughput assay described in this thesis together with the cloning strategy for the quick and easy assembly of tetrameric combinations of α subunits will allow the screening of large numbers of mutants against many combinations of Kv1 channels. While a peptide toxin is unikely to be used in a clinical situation, it could act as a template for the design of a small molecule with the same key functional groups. Alternatively, the channel expression and screening technologies described herein could be used to search compound libraries from a variety of sources in the search for lead compounds for future therapeutics.

References

Abbas N, Belghazi M, Abdel-Mottaleb Y, Tytgat J, Bougis PE and Martin-Eauclaire MF (2008) A new Kaliotoxin selective towards Kv1.3 and Kv1.2 but not Kv1.1 channels expressed in oocytes. *Biochem Biophys Res Commun* **376**(3):525-530.

Abdel-Mottaleb Y, Vandendriessche T, Clynen E, Landuyt B, Jalali A, Vatanpour H, Schoofs L and Tytgat J (2008) OdK2, a Kv1.3 channel-selective toxin from the venom of the Iranian scorpion Odonthobuthus doriae. *Toxicon* **51**(8):1424-1430.

Akhtar S, Shamotienko O, Papakosta M, Ali F and Dolly JO (2002) Characteristics of brain Kv1 channels tailored to mimic native counterparts by tandem linkage of alpha subunits: implications for K+ channelopathies. *J Biol Chem* **277**(19):16376-16382.

Aoki KR (2001) Pharmacology and immunology of botulinum toxin serotypes. *J Neurol* 248 Suppl 1:3-10.

Armstrong CM and Loboda A (2001) A model for 4-aminopyridine action on K channels: similarities to tetraethylammonium ion action. *Biophys J* **81**(2):895-904.

Beeton C, Wulff H, Singh S, Botsko S, Crossley G, Gutman GA, Cahalan MD, Pennington M and Chandy KG (2003) A novel fluorescent toxin to detect and investigate Kv1.3 channel up-regulation in chronically activated T lymphocytes. *J Biol Chem* **278**(11):9928-9937.

Benishin CG, Sorensen RG, Brown WE, Krueger BK and Blaustein MP (1988) Four polypeptide components of green mamba venom selectively block certain potassium channels in rat brain synaptosomes. *Mol Pharmacol* **34**(2):152-159.

Black AR, Donegan CM, Denny BJ and Dolly JO (1988) Solubilization and physical characterization of acceptors for dendrotoxin and beta-bungarotoxin from synaptic membranes of rat brain. *Biochemistry* **27**(18):6814-6820.

Blatz AL and Magleby KL (1986) Single apamin-blocked Ca-activated K+ channels of small conductance in cultured rat skeletal muscle. *Nature* **323**(6090):718-720.

Brew HM, Hallows JL and Tempel BL (2003) Hyperexcitability and reduced low threshold potassium currents in auditory neurons of mice lacking the channel subunit Kv1.1. *J Physiol* **548**(Pt 1):1-20.

Carbone E, Wanke E, Prestipino G, Possani LD and Maelicke A (1982) Selective blockage of voltage-dependent K+ channels by a novel scorpion toxin. *Nature* **296**(5852):90-91.

Castle NA, London DO, Creech C, Fajloun Z, Stocker JW and Sabatier JM (2003) Maurotoxin: a potent inhibitor of intermediate conductance Ca2+-activated potassium channels. *Mol Pharmacol* **63**(2):409-418.

Cayabyab FS, Khanna R, Jones OT and Schlichter LC (2000) Suppression of the rat microglia Kv1.3 current by src-family tyrosine kinases and oxygen/glucose deprivation. *Eur J Neurosci* **12**(6):1949-1960.

Chai Y, Huang X, Cong B, Liu S, Chen K, Li G and Gaisano HY (2006) Involvement of VAMP-2 in exocytosis of IL-1 beta in turbot (Scophthalmus maximus) leukocytes after Vibrio anguillarum infection. *Biochem Biophys Res Commun* **342**(2):509-513.

Choquet D and Korn H (1992) Mechanism of 4-aminopyridine action on voltage-gated potassium channels in lymphocytes. *J Gen Physiol* **99**(2):217-240.

Coleman SK, Newcombe J, Pryke J and Dolly JO (1999) Subunit composition of Kv1 channels in human CNS. *J Neurochem* **73**(2):849-858.

Corzo G, Papp F, Varga Z, Barraza O, Espino-Solis PG, Rodriguez de la Vega RC, Gaspar R, Panyi G and Possani LD (2008) A selective blocker of Kv1.2 and Kv1.3 potassium channels from the venom of the scorpion Centruroides suffusus suffusus. *Biochem Pharmacol* **76**(9):1142-1154.

Diochot S, Schweitz H, Beress L and Lazdunski M (1998) Sea anemone peptides with a specific blocking activity against the fast inactivating potassium channel Kv3.4. *J Biol Chem* **273**(12):6744-6749.

Dodson PD, Barker MC and Forsythe ID (2002) Two heteromeric Kv1 potassium channels differentially regulate action potential firing. *J Neurosci* **22**(16):6953-6961.

Dolganiuc A, Stavaru C, Anghel M, Baltaru D, Georgescu E and Olinescu A (2000) The migratory and phagocytic activity of polymorphonuclear leukocytes in rheumatoid arthritis and osteoarthritis patients. *Roum Arch Microbiol Immunol* **59**(1-2):43-53.

Dolly JO (1992) Polypeptide neurotoxins as probes for certain voltage-dependent K+ channels., in *Receptor-Ligand Interactions: a Practical Approach* (Hulme EC ed) pp 37–61, IRL Press, Oxford.

Dolly JO (2005) Molecular definition of neuronal targets for novel neurotherapeutics: SNAREs and Kv1 channels. *Neurotoxicology* **26**(5):753-760.

Dolly JO and Aoki KR (2006) The structure and mode of action of different botulinum toxins. *Eur J Neurol* **13 Suppl 4**:1-9.

Dolly JO and Parcej DN (1996) Molecular properties of voltage-gated K+ channels. *J Bioenerg Biomembr* **28**(3):231-253.

Doyle DA, Morais Cabral J, Pfuetzner RA, Kuo A, Gulbis JM, Cohen SL, Chait BT and MacKinnon R (1998) The structure of the potassium channel: molecular basis of K+ conduction and selectivity. *Science* **280**(5360):69-77.

Fajloun Z, Ferrat G, Carlier E, Fathallah M, Lecomte C, Sandoz G, di Luccio E, Mabrouk K, Legros C, Darbon H, Rochat H, Sabatier JM and De Waard M (2000) Synthesis, 1H NMR structure, and activity of a three-disulfide-bridged maurotoxin analog designed to restore the consensus motif of scorpion toxins. *J Biol Chem* **275**(18):13605-13612.

Feldmann M, Brennan FM, Foxwell BM, Taylor PC, Williams RO and Maini RN (2005) Anti-TNF therapy: where have we got to in 2005? *J Autoimmun* **25 Suppl**:26-28.

Feng D, Flaumenhaft R, Bandeira-Melo C, Weller P and Dvorak A (2001) Ultrastructural localization of vesicle-associated membrane protein(s) to specialized membrane structures in human pericytes, vascular smooth muscle cells, endothelial cells, neutrophils, and eosinophils. *J Histochem Cytochem* **49**(3):293-304.

Finnegan TF, Chen SR and Pan HL (2006) Mu opioid receptor activation inhibits GABAergic inputs to basolateral amygdala neurons through Kv1.1/1.2 channels. *J Neurophysiol* **95**(4):2032-2041.

Ford JW, Stevens EB, Treherne JM, Packer J and Bushfield M (2002) Potassium channels: gene family, therapeutic relevance, high-throughput screening technologies and drug discovery. *Prog Drug Res* **58**:133-168.

Fox DA (1997) The role of T cells in the immunopathogenesis of rheumatoid arthritis: new perspectives. *Arthritis Rheum* **40**(4):598-609.

Freidin M and Kessler JA (1991) Cytokine regulation of substance P expression in sympathetic neurons. *Proc Natl Acad Sci U S A* **88**(8):3200-3203.

Galvez A, Gimenez-Gallego G, Reuben JP, Roy-Contancin L, Feigenbaum P, Kaczorowski GJ and Garcia ML (1990) Purification and characterization of a unique, potent, peptidyl probe for the high conductance calcium-activated potassium channel from venom of the scorpion Buthus tamulus. *J Biol Chem* **265**(19):11083-11090.

Garcia-Calvo M, Leonard RJ, Novick J, Stevens SP, Schmalhofer W, Kaczorowski GJ and Garcia ML (1993) Purification, characterization, and biosynthesis of margatoxin, a component of Centruroides margaritatus venom that selectively inhibits voltage-dependent potassium channels. *J Biol Chem* **268**(25):18866-18874.

Garcia-Valdes J, Zamudio FZ, Toro L and Possani LD (2001) Slotoxin, alphaKTx1.11, a new scorpion peptide blocker of MaxiK channels that differentiates between alpha and alpha+beta (beta1 or beta4) complexes. *FEBS Lett* **505**(3):369-373.

Garcia ML, Gao Y, McManus OB and Kaczorowski GJ (2001) Potassium channels: from scorpion venoms to high-resolution structure. *Toxicon* **39**(6):739-748.

Garcia ML, Garcia-Calvo M, Hidalgo P, Lee A and MacKinnon R (1994) Purification and characterization of three inhibitors of voltage-dependent K+ channels from Leiurus quinquestriatus var. hebraeus venom. *Biochemistry* **33**(22):6834-6839.

Garcia ML, Hanner M and Kaczorowski GJ (1998) Scorpion toxins: tools for studying K+ channels. *Toxicon* **36**(11):1641-1650.

Gasparini S, Danse JM, Lecoq A, Pinkasfeld S, Zinn-Justin S, Young LC, de Medeiros CC, Rowan EG, Harvey AL and Menez A (1998) Delineation of the functional site of alpha-dendrotoxin. The functional topographies of dendrotoxins are different but share a conserved core with those of other Kv1 potassium channel-blocking toxins. *J Biol Chem* **273**(39):25393-25403.

Grimsholm O, Rantapaa-Dahlqvist S and Forsgren S (2005) Levels of gastrin-releasing peptide and substance P in synovial fluid and serum correlate with levels of cytokines in rheumatoid arthritis. *Arthritis Res Ther* **7**(3):R416-426.

Grissmer S, Nguyen AN, Aiyar J, Hanson DC, Mather RJ, Gutman GA, Karmilowicz MJ, Auperin DD and Chandy KG (1994) Pharmacological characterization of five cloned voltage-gated K+ channels, types Kv1.1, 1.2, 1.3, 1.5, and 3.1, stably expressed in mammalian cell lines. *Mol Pharmacol* **45**(6):1227-1234.

Grupe A, Schroter KH, Ruppersberg JP, Stocker M, Drewes T, Beckh S and Pongs O (1990) Cloning and expression of a human voltage-gated potassium channel. A novel member of the RCK potassium channel family. *Embo J* **9**(6):1749-1756.

Gutman GA, Chandy KG, Adelman JP, Aiyar J, Bayliss DA, Clapham DE, Covarriubias M, Desir GV, Furuichi K, Ganetzky B, Garcia ML, Grissmer S, Jan LY, Karschin A, Kim D, Kuperschmidt S, Kurachi Y, Lazdunski M, Lesage F, Lester HA, McKinnon D, Nichols CG, O'Kelly I, Robbins J, Robertson GA, Rudy B, Sanguinetti M, Seino S, Stuehmer W, Tamkun MM, Vandenberg CA, Wei A, Wulff H and Wymore RS (2003a) International Union of Pharmacology. XLI. Compendium of voltage-gated ion channels: potassium channels. *Pharmacol Rev* **55**(4):583-586.

Gutman GA, Chandy KG, Adelman JP, Aiyar J, Bayliss DA, Clapham DE, Covarriubias M, Desir GV, Furuichi K, Ganetzky B, Garcia ML, Grissmer S, Jan LY, Karschin A, Kim D, Kuperschmidt S, Kurachi Y, Lazdunski M, Lesage F, Lester HA, McKinnon D, Nichols CG, O'Kelly I, Robbins J, Robertson GA, Rudy B, Sanguinetti M, Seino S, Stuehmer W, Tamkun MM, Vandenberg CA, Wei A, Wulff H and Wymore RS (2003b) International Union of Pharmacology. XLI. Compendium of voltage-gated ion channels: potassium channels. *Pharmacol Rev* **55**(4):583-586.

Gutman GA, Chandy KG, Grissmer S, Lazdunski M, McKinnon D, Pardo LA, Robertson GA, Rudy B, Sanguinetti MC, Stuhmer W and Wang X (2005) International Union of Pharmacology. LIII. Nomenclature and molecular relationships of voltage-gated potassium channels. *Pharmacol Rev* **57**(4):473-508.

Halliwell JV, Othman IB, Pelchen-Matthews A and Dolly JO (1986) Central action of dendrotoxin: selective reduction of a transient K conductance in hippocampus and binding to localized acceptors. *Proc Natl Acad Sci U S A* **83**(2):493-497.

Hamill OP, Marty A, Neher E, Sakmann B and Sigworth FJ (1981) Improved patch-clamp techniques for high-resolution current recording from cells and cell-free membrane patches. *Pflugers Arch* **391**(2):85-100.

Harvey AL (1997) Recent studies on dendrotoxins and potassium ion channels. *Gen Pharmacol* **28**(1):7-12.

Heginbotham L and MacKinnon R (1992) The aromatic binding site for tetraethylammonium ion on potassium channels. *Neuron* **8**(3):483-491.

Helyes Z, Pinter E, Nemeth J, Sandor K, Elekes K, Szabo A, Pozsgai G, Keszthelyi D, Kereskai L, Engstrom M, Wurster S and Szolcsanyi J (2006) Effects of the somatostatin receptor subtype 4 selective agonist J-2156 on sensory neuropeptide release and inflammatory reactions in rodents. *Br J Pharmacol* **149**(4):405-415.

Hodgkin AL and Huxley AF (1952) A quantitative description of membrane current and its application to conduction and excitation in nerve. *J Physiol* **117**(4):500-544.

Honma T and Shiomi K (2006) Peptide toxins in sea anemones: structural and functional aspects. *Mar Biotechnol (NY)* **8**(1):1-10.

Hopkins WF (1998) Toxin and subunit specificity of blocking affinity of three peptide toxins for heteromultimeric, voltage-gated potassium channels expressed in Xenopus oocytes. *J Pharmacol Exp Ther* **285**(3):1051-1060.

Hopkins WF, Miller JL and Miljanich GP (1996) Voltage-gated Potassium Channel Inhibitors. *Current Pharmaceutical Design* **2**(4):389-396.

Humeau Y, Doussau F, Grant NJ and Poulain B (2000) How botulinum and tetanus neurotoxins block neurotransmitter release. *Biochimie* **82**(5):427-446.

Imamura K, Spriggs D, Ohno T and Kufe D (1989) Effects of botulinum toxin type D on secretion of tumor necrosis factor from human monocytes. *Mol Cell Biol* **9**(5):2239-2243.

Imredy JP, Chen C and MacKinnon R (1998) A snake toxin inhibitor of inward rectifier potassium channel ROMK1. *Biochemistry* **37**(42):14867-14874.

Imredy JP and MacKinnon R (2000) Energetic and structural interactions between delta-dendrotoxin and a voltage-gated potassium channel. *J Mol Biol* **296**(5):1283-1294.

Jahn R and Scheller RH (2006) SNAREs--engines for membrane fusion. *Nat Rev Mol Cell Biol* **7**(9):631-643.

Jan LY and Jan YN (1992) Structural elements involved in specific K+ channel functions. *Annu Rev Physiol* **54**:537-555.

Jan LY and Jan YN (1997) Cloned potassium channels from eukaryotes and prokaryotes. *Annu Rev Neurosci* **20**:91-123.

Ji RR, Kohno T, Moore KA and Woolf CJ (2003) Central sensitization and LTP: do pain and memory share similar mechanisms? *Trends Neurosci* **26**(12):696-705.

Jin W and Lu Z (1998) A novel high-affinity inhibitor for inward-rectifier K+ channels. *Biochemistry* **37**(38):13291-13299.

Kalman K, Pennington MW, Lanigan MD, Nguyen A, Rauer H, Mahnir V, Paschetto K, Kem WR, Grissmer S, Gutman GA, Christian EP, Cahalan MD, Norton RS and Chandy KG (1998) ShK-Dap22, a potent Kv1.3-specific immunosuppressive polypeptide. *J Biol Chem* **273**(49):32697-32707.

Kaneyama K, Segami N, Sun W, Sato J and Fujimura K (2005) Analysis of tumor necrosis factor-alpha, interleukin-6, interleukin-1beta, soluble tumor necrosis factor receptors I and II, interleukin-6 soluble receptor, interleukin-1 soluble receptor type II, interleukin-1 receptor antagonist, and protein in the synovial fluid of patients with temporomandibular joint disorders. *Oral Surg Oral Med Oral Pathol Oral Radiol Endod* **99**(3):276-284.

Kanjhan R, Coulson EJ, Adams DJ and Bellingham MC (2005) Tertiapin-Q blocks recombinant and native large conductance K+ channels in a use-dependent manner. *J Pharmacol Exp Ther* **314**(3):1353-1361.

Kasama T, Kobayashi K, Yajima N, Shiozawa F, Yoda Y, Takeuchi HT, Mori Y, Negishi M, Ide H and Adachi M (2000) Expression of vascular endothelial growth factor by synovial fluid neutrophils in rheumatoid arthritis (RA). *Clin Exp Immunol* **121**(3):533-538.

Katoh E, Nishio H, Inui T, Nishiuchi Y, Kimura T, Sakakibara S and Yamazaki T (2000) Structural basis for the biological activity of dendrotoxin-I, a potent potassium channel blocker. *Biopolymers* **54**(1):44-57.

Kavanaugh MP, Hurst RS, Yakel J, Varnum MD, Adelman JP and North RA (1992) Multiple subunits of a voltage-dependent potassium channel contribute to the binding site for tetraethylammonium. *Neuron* **8**(3):493-497.

Kay J and Calabrese L (2004) The role of interleukin-1 in the pathogenesis of rheumatoid arthritis. *Rheumatology (Oxford)* **43 Suppl 3**:iii2-iii9.

Keeble JE and Brain SD (2004) A role for substance P in arthritis? *Neurosci Lett* **361**(1-3):176-179.

Kharrat R, Mabrouk K, Crest M, Darbon H, Oughideni R, Martin-Eauclaire MF, Jacquet G, el Ayeb M, Van Rietschoten J, Rochat H and Sabatier JM (1996) Chemical synthesis and characterization of maurotoxin, a short scorpion toxin with four disulfide bridges that acts on K+ channels. *Eur J Biochem* **242**(3):491-498.

Kirsch GE, Yeh JZ and Oxford GS (1986) Modulation of aminopyridine block of potassium currents in squid axon. *Biophys J* **50**(4):637-644.

Knaus HG, McManus OB, Lee SH, Schmalhofer WA, Garcia-Calvo M, Helms LM, Sanchez M, Giangiacomo K, Reuben JP, Smith AB, 3rd and et al. (1994) Tremorgenic indole alkaloids potently inhibit smooth muscle high-conductance calcium-activated potassium channels. *Biochemistry* **33**(19):5819-5828.

Koch RO, Wanner SG, Koschak A, Hanner M, Schwarzer C, Kaczorowski GJ, Slaughter RS, Garcia ML and Knaus HG (1997) Complex subunit assembly of neuronal voltage-gated K+ channels. Basis for high-affinity toxin interactions and pharmacology. *J Biol Chem* **272**(44):27577-27581.

Kole MH, Letzkus JJ and Stuart GJ (2007) Axon initial segment Kv1 channels control axonal action potential waveform and synaptic efficacy. *Neuron* **55**(4):633-647.

Kontny E, Wojtecka LE, Rell-Bakalarska K, Dziewczopolski W, Maslinski W and Maslinski S (2002) Impaired generation of taurine chloramine by synovial fluid neutrophils of rheumatoid arthritis patients. *Amino Acids* **23**(4):415-418.

Korolkova YV, Kozlov SA, Lipkin AV, Pluzhnikov KA, Hadley JK, Filippov AK, Brown DA, Angelo K, Strobaek D, Jespersen T, Olesen SP, Jensen BS and Grishin EV (2001) An ERG channel inhibitor from the scorpion Buthus eupeus. *J Biol Chem* **276**(13):9868-9876.

Koschak A, Bugianesi RM, Mitterdorfer J, Kaczorowski GJ, Garcia ML and Knaus HG (1998) Subunit composition of brain voltage-gated potassium channels determined by hongotoxin-1, a novel peptide derived from Centruroides limbatus venom. *J Biol Chem* **273**(5):2639-2644.

Lehmann-Horn F and Jurkat-Rott K (1999) Voltage-gated ion channels and hereditary disease. *Physiol Rev* **79**(4):1317-1372.

Leicher T, Bahring R, Isbrandt D and Pongs O (1998) Coexpression of the KCNA3B gene product with Kv1.5 leads to a novel A-type potassium channel. *J Biol Chem* **273**(52):35095-35101.

Lenaeus MJ, Vamvouka M, Focia PJ and Gross A (2005) Structural basis of TEA blockade in a model potassium channel. *Nat Struct Mol Biol* **12**(5):454-459.

Lewis RJ and Garcia ML (2003) Therapeutic potential of venom peptides. *Nat Rev Drug Discov* **2**(10):790-802.

Li Y, Um SY and McDonald TV (2006) Voltage-gated potassium channels: regulation by accessory subunits. *Neuroscientist* **12**(3):199-210.

Long SB, Campbell EB and Mackinnon R (2005a) Crystal structure of a mammalian voltage-dependent Shaker family K+ channel. *Science* **309**(5736):897-903.

Long SB, Campbell EB and Mackinnon R (2005b) Voltage sensor of Kv1.2: structural basis of electromechanical coupling. *Science* **309**(5736):903-908.

Lu Z and MacKinnon R (1997) Purification, characterization, and synthesis of an inward-rectifier K+ channel inhibitor from scorpion venom. *Biochemistry* **36**(23):6936-6940.

Lucchesi K, Ravindran A, Young H and Moczydlowski E (1989) Analysis of the blocking activity of charybdotoxin homologs and iodinated derivatives against Ca2+-activated K+ channels. *J Membr Biol* **109**(3):269-281.

MacKinnon R (1991) New insights into the structure and function of potassium channels. *Curr Opin Neurobiol* **1**(1):14-19.

MacKinnon R (2003) Potassium channels. *FEBS Lett* **555**(1):62-65.

MacKinnon R, Cohen SL, Kuo A, Lee A and Chait BT (1998) Structural conservation in prokaryotic and eukaryotic potassium channels. *Science* **280**(5360):106-109.

MacKinnon R and Miller C (1989) Mutant potassium channels with altered binding of charybdotoxin, a pore-blocking peptide inhibitor. *Science* **245**(4924):1382-1385.

MacKinnon R and Yellen G (1990) Mutations affecting TEA blockade and ion permeation in voltage-activated K+ channels. *Science* **250**(4978):276-279.

Mahanthappa NK and Patterson PH (1998) Culturing Mammalian Sympathoadrenal Derivatives, in *Culturing Nerve Cells* (Banker G and Goslin K eds) pp 289-316, MIT Press, Cambridge, MA

Mahowald ML, Singh JA and Dykstra D (2006) Long term effects of intra-articular botulinum toxin A for refractory joint pain. *Neurotox Res* **9**(2-3):179-188.

Manganas LN, Akhtar S, Antonucci DE, Campomanes CR, Dolly JO and Trimmer JS (2001) Episodic ataxia type-1 mutations in the Kv1.1 potassium channel display distinct folding and intracellular trafficking properties. *J Biol Chem* **276**(52):49427-49434.

Manganas LN and Trimmer JS (2000) Subunit composition determines Kv1 potassium channel surface expression. *J Biol Chem* **275**(38):29685-29693.

Martin-Martin B, Nabokina SM, Blasi J, Lazo PA and Mollinedo F (2000) Involvement of SNAP-23 and syntaxin 6 in human neutrophil exocytosis. *Blood* **96**(7):2574-2583.

McInnes IB, Leung BP, Harnett M, Gracie JA, Liew FY and Harnett W (2003) A novel therapeutic approach targeting articular inflammation using the filarial nematode-derived phosphorylcholine-containing glycoprotein ES-62. *J Immunol* **171**(4):2127-2133.

McInnes IB and Liew FY (1998) Interleukin 15: a proinflammatory role in rheumatoid arthritis synovitis. *Immunol Today* **19**(2):75-79.

McInnes IB and Schett G (2007) Cytokines in the pathogenesis of rheumatoid arthritis. *Nat Rev Immunol* **7**(6):429-442.

Middleton RE, Sanchez M, Linde AR, Bugianesi RM, Dai G, Felix JP, Koprak SL, Staruch MJ, Bruguera M, Cox R, Ghosh A, Hwang J, Jones S, Kohler M, Slaughter RS, McManus OB, Kaczorowski GJ and Garcia ML (2003) Substitution of a single residue in Stichodactyla helianthus peptide, ShK-Dap22, reveals a novel pharmacological profile. *Biochemistry* **42**(46):13698-13707.

Mollinedo F, Borregaard N and Boxer LA (1999) Novel trends in neutrophil structure, function and development. *Immunol Today* **20**(12):535-537.

Muniz ZM, Parcej DN and Dolly JO (1992) Characterization of monoclonal antibodies against voltage-dependent K+ channels raised using alpha-dendrotoxin acceptors purified from bovine brain. *Biochemistry* **31**(49):12297-12303.

Murray RZ, Kay JG, Sangermani DG and Stow JL (2005a) A role for the phagosome in cytokine secretion. *Science* **310**(5753):1492-1495.

Murray RZ, Wylie FG, Khromykh T, Hume DA and Stow JL (2005b) Syntaxin 6 and Vti1b form a novel SNARE complex, which is up-regulated in activated macrophages to facilitate exocytosis of tumor necrosis Factor-alpha. *J Biol Chem* **280**(11):10478-10483.

Nishimoto N and Kishimoto T (2004) Inhibition of IL-6 for the treatment of inflammatory diseases. *Curr Opin Pharmacol* **4**(4):386-391.

Orlova EV, Papakosta M, Booy FP, van Heel M and Dolly JO (2003) Voltage-gated K+ channel from mammalian brain: 3D structure at 18A of the complete (alpha)4(beta)4 complex. *J Mol Biol* **326**(4):1005-1012.

Pagan JK, Wylie FG, Joseph S, Widberg C, Bryant NJ, James DE and Stow JL (2003) The t-SNARE syntaxin 4 is regulated during macrophage activation to function in membrane traffic and cytokine secretion. *Curr Biol* **13**(2):156-160.

Panyi G, Sheng Z and Deutsch C (1995) C-type inactivation of a voltage-gated K+ channel occurs by a cooperative mechanism. *Biophys J* **69**(3):896-903.

Papazian DM, Schwarz TL, Tempel BL, Jan YN and Jan LY (1987) Cloning of genomic and complementary DNA from Shaker, a putative potassium channel gene from Drosophila. *Science* **237**(4816):749-753.

Parcej DN, Scott VE and Dolly JO (1992) Oligomeric properties of alpha-dendrotoxin-sensitive potassium ion channels purified from bovine brain. *Biochemistry* **31**(45):11084-11088.

Park CS and Miller C (1992) Mapping function to structure in a channel-blocking peptide: electrostatic mutants of charybdotoxin. *Biochemistry* **31**(34):7749-7755.

Patterson PH (1994) Leukemia inhibitory factor, a cytokine at the interface between neurobiology and immunology. *Proc Natl Acad Sci U S A* **91**(17):7833-7835.

Pedarzani P, D'Hoedt D, Doorty KB, Wadsworth JD, Joseph JS, Jeyaseelan K, Kini RM, Gadre SV, Sapatnekar SM, Stocker M and Strong PN (2002) Tamapin, a venom peptide from the Indian red scorpion (Mesobuthus tamulus) that targets small conductance Ca2+-activated K+ channels and afterhyperpolarization currents in central neurons. *J Biol Chem* **277**(48):46101-46109.

Pisciotta M, Ottolia M, Possani LD and Prestipino G (1998) A novel toxin form the scorpion Androctonus australis blocks Shaker K+ channels expressed in Xenopus oocytes. *Biochem Biophys Res Commun* **242**(2):287-291.

Pitzurra L, Rossetto O, Chimienti AR, Blasi E and Bistoni F (1996) Tetanus toxin-sensitive VAMP-related proteins are present in murine macrophages. *Cell Immunol* **169**(1):113-116.

Pongs O (1992) Structural basis of voltage-gated K+ channel pharmacology. *Trends Pharmacol Sci* **13**(9):359-365.

Pongs O, Kecskemethy N, Muller R, Krah-Jentgens I, Baumann A, Kiltz HH, Canal I, Llamazares S and Ferrus A (1988) Shaker encodes a family of putative potassium channel proteins in the nervous system of Drosophila. *Embo J* **7**(4):1087-1096.

Ranganathan R, Lewis JH and MacKinnon R (1996) Spatial localization of the K+ channel selectivity filter by mutant cycle-based structure analysis. *Neuron* **16**(1):131-139.

Rehm H and Lazdunski M (1988) Purification and subunit structure of a putative K+-channel protein identified by its binding properties for dendrotoxin I. *Proc Natl Acad Sci U S A* **85**(13):4919-4923.

Rettig J, Heinemann SH, Wunder F, Lorra C, Parcej DN, Dolly JO and Pongs O (1994) Inactivation properties of voltage-gated K+ channels altered by presence of beta-subunit. *Nature* **369**(6478):289-294.

Rizo J and Sudhof TC (1998) Mechanics of membrane fusion. *Nat Struct Biol* **5**(10):839-842.

Rodrigues AR, Arantes EC, Monje F, Stuhmer W and Varanda WA (2003) Tityustoxin-K(alpha) blockade of the voltage-gated potassium channel Kv1.3. *Br J Pharmacol* **139**(6):1180-1186.

Roeper J, Sewing S, Zhang Y, Sommer T, Wanner SG and Pongs O (1998) NIP domain prevents N-type inactivation in voltage-gated potassium channels. *Nature* **391**(6665):390-393.

Rudy B (1988) Diversity and ubiquity of K channels. *Neuroscience* **25**(3):729-749.

Sack JT and Aldrich RW (2006) Binding of a gating modifier toxin induces intersubunit cooperativity early in the Shaker K channel's activation pathway. *J Gen Physiol* **128**(1):119-132.

Scaloni A, Bottiglieri C, Ferrara L, Corona M, Gurrola GB, Batista C, Wanke E and Possani LD (2000) Disulfide bridges of ergtoxin, a member of a new sub-family of peptide blockers of the ether-a-go-go-related K+ channel. *FEBS Lett* **479**(3):156-157.

Scott VE, Muniz ZM, Sewing S, Lichtinghagen R, Parcej DN, Pongs O and Dolly JO (1994a) Antibodies specific for distinct Kv subunits unveil a heterooligomeric basis for subtypes of alpha-dendrotoxin-sensitive K+ channels in bovine brain. *Biochemistry* **33**(7):1617-1623.

Scott VE, Rettig J, Parcej DN, Keen JN, Findlay JB, Pongs O and Dolly JO (1994b) Primary structure of a beta subunit of alpha-dendrotoxin-sensitive K+ channels from bovine brain. *Proc Natl Acad Sci U S A* **91**(5):1637-1641.

Shadiack AM, Hart RP, Carlson CD and Jonakait GM (1993) Interleukin-1 induces substance P in sympathetic ganglia through the induction of leukemia inhibitory factor (LIF). *J Neurosci* **13**(6):2601-2609.

Shamotienko O, Akhtar S, Sidera C, Meunier FA, Ink B, Weir M and Dolly JO (1999) Recreation of neuronal Kv1 channel oligomers by expression in mammalian cells using Semliki Forest virus. *Biochemistry* **38**(51):16766-16776.

Shamotienko O, Shaban H, Ní Dhochartaigh S, Bodeker M, Wang J, Dolly JO and Sack JT (2008) Concatenating Kv1 αsubunits unveils novel channel characteristics of promising therapuetic targets. *Publication Pending.*

Shamotienko OG, Parcej DN and Dolly JO (1997) Subunit combinations defined for K+ channel Kv1 subtypes in synaptic membranes from bovine brain. *Biochemistry* **36**(27):8195-8201.

Shi G and Trimmer JS (1999) Differential asparagine-linked glycosylation of voltage-gated K+ channels in mammalian brain and in transfected cells. *J Membr Biol* **168**(3):265-273.

Shijin Y, Hong Y, Yibao M, Zongyun C, Han S, Yingliang W, Zhijian C and Wenxin L (2008) Characterization of a new Kv1.3 channel-specific blocker, J123, from the scorpion Buthus martensii Karsch. *Peptides* **29**(9):1514-1520.

Sitges M, Possani LD and Bayon A (1986) Noxiustoxin, a short-chain toxin from the Mexican scorpion Centruroides noxius, induces transmitter release by blocking K+ permeability. *J Neurosci* **6**(6):1570-1574.

Smith KJ, Felts PA and John GR (2000) Effects of 4-aminopyridine on demyelinated axons, synapses and muscle tension. *Brain* **123 (Pt 1)**:171-184.

Smith LA, Reid PF, Wang FC, Parcej DN, Schmidt JJ, Olson MA and Dolly JO (1997) Site-directed mutagenesis of dendrotoxin K reveals amino acids critical for its interaction with neuronal K+ channels. *Biochemistry* **36**(25):7690-7696.

Sokolov MV, Shamotienko O, Dhochartaigh SN, Sack JT and Dolly JO (2007) Concatemers of brain Kv1 channel alpha subunits that give similar K(+) currents yield pharmacologically distinguishable heteromers. *Neuropharmacology*.

Srairi-Abid N, Shahbazzadeh D, Chatti I, Mlayah-Bellalouna S, Mejdoub H, Borchani L, Benkhalifa R, Akbari A and El Ayeb M (2008) Hemitoxin, the first potassium channel toxin from the venom of the Iranian scorpion Hemiscorpius lepturus. *Febs J* **275**(18):4641-4650.

Strobaek D, Jorgensen TD, Christophersen P, Ahring PK and Olesen SP (2000) Pharmacological characterization of small-conductance Ca(2+)-activated K(+) channels stably expressed in HEK 293 cells. *Br J Pharmacol* **129**(5):991-999.

Stuhmer W, Ruppersberg JP, Schroter KH, Sakmann B, Stocker M, Giese KP, Perschke A, Baumann A and Pongs O (1989) Molecular basis of functional diversity of voltage-gated potassium channels in mammalian brain. *Embo J* **8**(11):3235-3244.

Suarez-Kurtz G, Vianna-Jorge R, Pereira BF, Garcia ML and Kaczorowski GJ (1999) Peptidyl inhibitors of shaker-type Kv1 channels elicit twitches in guinea pig ileum by blocking kv1.1 at enteric nervous system and enhancing acetylcholine release. *J Pharmacol Exp Ther* **289**(3):1517-1522.

Swaminathan P, Hariharan M, Murali R and Singh CU (1996) Molecular structure, conformational analysis, and structure-activity studies of Dendrotoxin and its homologues using molecular mechanics and molecular dynamics techniques. *J Med Chem* **39**(11):2141-2155.

Tapper H, Furuya W and Grinstein S (2002) Localized exocytosis of primary (lysosomal) granules during phagocytosis: role of Ca2+-dependent tyrosine phosphorylation and microtubules. *J Immunol* **168**(10):5287-5296.

Terstappen GC (1999) Functional analysis of native and recombinant ion channels using a high-capacity nonradioactive rubidium efflux assay. *Anal Biochem* **272**(2):149-155.

Tiffany AM, Manganas LN, Kim E, Hsueh YP, Sheng M and Trimmer JS (2000) PSD-95 and SAP97 exhibit distinct mechanisms for regulating K(+) channel surface expression and clustering. *J Cell Biol* **148**(1):147-158.

Tytgat J, Debont T, Carmeliet E and Daenens P (1995) The alpha-dendrotoxin footprint on a mammalian potassium channel. *J Biol Chem* **270**(42):24776-24781.

Visan V, Fajloun Z, Sabatier JM and Grissmer S (2004) Mapping of maurotoxin binding sites on hKv1.2, hKv1.3, and hIKCa1 channels. *Mol Pharmacol* **66**(5):1103-1112.

Wang FC, Bell N, Reid P, Smith LA, McIntosh P, Robertson B and Dolly JO (1999a) Identification of residues in dendrotoxin K responsible for its discrimination between neuronal K+ channels containing Kv1.1 and 1.2 alpha subunits. *Eur J Biochem* **263**(1):222-229.

Wang FC, Parcej DN and Dolly JO (1999b) alpha subunit compositions of Kv1.1-containing K+ channel subtypes fractionated from rat brain using dendrotoxins. *Eur J Biochem* **263**(1):230-237.

Wei A, Covarrubias M, Butler A, Baker K, Pak M and Salkoff L (1990) K+ current diversity is produced by an extended gene family conserved in Drosophila and mouse. *Science* **248**(4955):599-603.

Westacott CI and Sharif M (1996) Cytokines in osteoarthritis: mediators or markers of joint destruction? *Semin Arthritis Rheum* **25**(4):254-272.

Xu J, Yu W, Jan YN, Jan LY and Li M (1995) Assembly of voltage-gated potassium channels. Conserved hydrophilic motifs determine subfamily-specific interactions between the alpha-subunits. *J Biol Chem* **270**(42):24761-24768.

Yu SP and Kerchner GA (1998) Endogenous voltage-gated potassium channels in human embryonic kidney (HEK293) cells. *J Neurosci Res* **52**(5):612-617.

Zagotta WN, Hoshi T, Dittman J and Aldrich RW (1994) Shaker potassium channel gating. II: Transitions in the activation pathway. *J Gen Physiol* **103**(2):279-319.

Zhou Y, Morais-Cabral JH, Kaufman A and MacKinnon R (2001) Chemistry of ion coordination and hydration revealed by a K+ channel-Fab complex at 2.0 A resolution. *Nature* **414**(6859):43-48.

Zhou Z, Gong Q, Ye B, Fan Z, Makielski JC, Robertson GA and January CT (1998) Properties of HERG channels stably expressed in HEK 293 cells studied at physiological temperature. *Biophys J* **74**(1):230-241.

Zuberi SM, Eunson LH, Spauschus A, De Silva R, Tolmie J, Wood NW, McWilliam RC, Stephenson JB, Kullmann DM and Hanna MG (1999) A novel mutation in the human voltage-gated potassium channel gene (Kv1.1) associates with episodic ataxia type 1 and sometimes with partial epilepsy. *Brain* **122 (Pt 5)**:817-825.

Appendix A: Composition of buffers for K^+ channel surface labelling

PBS

138 mM NaCl
26.7 mM KCl
14.7 mM KH_2PO_4
81 mM Na_2HPO_4

pH 7.4

Blotto

10 mM Tris - pH 8.0
0.15 M NaCl
4% non-fat milk powder

Mounting Medium

p-Phenylenediamine (10 mg/ml) in PBS, pH 9.0, diluted 1:10 in glycerol, mixed in the dark, aliquoted and stored at -20°C.

Appendix B: Composition of buffers for the Rb^+ flux assay when using CHO cells

Rb^+ Loading Buffer

5.4 mM RbCl
150 mM NaCl
2 mM $CaCl_2$
0.8 mM NaH_2PO_4
1 mM $MgCl_2$
5 mM Glucose
25 mM Hepes

pH 7.4

25 mM Hepes Wash Buffer

0.1 mM KCl
155.3 mM NaCl
2 mM $CaCl_2$
0.8 mM NaH_2PO_4
1 mM $MgCl_2$
5 mM Glucose
25 mM Hepes

pH 7.4

75 mM K^+ Stimulation Buffer

75 mM KCl
80.4 mM NaCl
2 mM $CaCl_2$
0.8 mM NaH_2PO_4
1 mM $MgCl_2$
5 mM Glucose
25 mM Hepes

pH 7.4

Ionization Prevention Buffer

1 % HNO_3
0.1% CsCl

Appendix C: Composition of buffers for the Rb^+ flux assay when using HEK cells

Modified Wash Buffer

0.1 mM KCl
149.9 mM NaCl
2 mM $CaCl_2$
1 mM $MgSO_4$
5 mM Glucose
10 mM Hepes

pH 7.4

Modified Stimulation Buffer

75 mM NaCl
75 mM KCl
2 mM $CaCl_2$
1 mM $MgSO_4$
5 mM Glucose
10 mM Hepes

pH 7.4

150 mM K^+ Modified Stimulation Buffer

150 mM KCl
0 mM NaCl
2 mM $CaCl_2$
1 mM $MgSO_4$
5 mM Glucose
10 mM Hepes

pH 7.4

Ionization Prevention Buffer

0.1 % CsCl